Institut für Geowissenschaften
Mathematisch-Naturwissenschaftliche Fakultät
Universität Potsdam

MAFIC MAGMATISM IN THE EASTERN CORDILLERA AND PUTUMAYO BASIN, COLOMBIA: CAUSES AND CONSEQUENCES

Dissertation

zur Erlangung des akademischen Grades
Doktor der Naturwissenschaften
"*doctor rerum naturalium*"
eingereicht an der
Mathematisch-Naturwissenschaftlichen Fakultät
der Universität Potsdam

von
Dipl.-Geol. Mónica Fernanda Vásquez Parra
Geb. 25.03.1977 in Bogota, D.C, Kolumbien

Potsdam, im Januar 2007

"El Señor te cuidará en el hogar y en el camino, desde ahora y para siempre"

Salmo 121:8

ABSTRACT

The Eastern Cordillera of Colombia is mainly composed of sedimentary rocks deposited since early Mesozoic times. Magmatic rocks are scarce. They are represented only by a few locally restricted occurrences of dykes and sills of mafic composition presumably emplaced in the Cretaceous and of volcanic rocks of Neogene age. This work is focused on the study of the Cretaceous magmatism with the intention to understand the processes causing the genesis of these rocks and their significance in the regional tectonic setting of the Northern Andes.

The magmatic rocks cut the Cretaceous sedimentary succession of black shales and marlstones that crop out in both flanks of the Eastern Cordillera. The studied rocks were classified as gabbros (Cáceres, Pacho, Rodrigoque), tonalites (Cáceres, La Corona), hornblende gabbros (La Corona), pyroxene-hornblende gabbros (Pacho, La Corona, Rodrigoque, Pajarito), and pyroxene-hornblendites (Pajarito). The gabbroic samples are mainly composed of plagioclase, clinopyroxene, and/or green to brown hornblende, whereas the tonalitic rocks are mainly composed of plagioclase and quartz. The samples are highly variable in crystal sizes from fine- to coarse-grained. Accessory minerals such as biotite, titanite and zircon are present. Some samples are characterized by moderate to strong alteration, and show the presence of epidote, actinolite and chlorite.

Major and trace element compositions of the rocks as well as the rock-forming minerals show significant differences in the geochemical and petrological characteristics for the different localities, suggesting that this magmatism does not result from a single melting process. The wide compositional spectrum of trace elements in the intrusions is characteristic for different degrees of mantle melting and enrichment of incompatible elements. MORB- and OIB-like compositions suggest at least two different sources of magma with tholeiitic and alkaline affinity, respectively. Evidence of slab-derived fluids can be recognized in the western part of the basin reflected in higher Ba/Nb and Sr/P ratios and also in the Sr radiogenic isotope ratios, which is possible a consequence of metasomatism in the mantle due to processes related to the presence of a previously subducted slab. The trace element patterns evidence an extensional setting in the Cretaceous basin producing a continental rift.

Electron microprobe analyses (EMPA) of the major elements and synchrotron radiation micro-X-ray fluorescence (μ-SRXRF) analyses of the trace element composition of the early crystallized minerals of the intrusions (clinopyroxenes and amphiboles) reflect the same dual character that has been found in the bulk-rock analyses. Despite the observed alteration of the rocks, the mineral composition shows evidences for an enriched and a relative depleted magma source. Even the normalization of the trace element concentrations of clinopyroxenes and amphiboles to the whole rock nearly follows the pattern predicted by published partition coefficients, suggesting that the alteration did not change the original trace element compositions of the investigated minerals.

Sr-Nd-Pb isotope data reveal a large isotopic variation but still suggest an initial origin of the magmas in the mantle. Samples have moderate to highly radiogenic compositions of $^{143}Nd/^{144}Nd$ and

high $^{87}Sr/^{86}Sr$ ratios and follow a trend towards enriched mantle compositions, like the local South American Paleozoic crust. The melts experienced variable degrees of contamination by sediments, crust, and seawater. The age corrected Pb isotope ratios show two separated groups of samples. This suggests that the chemical composition of the mantle below the Northern Andes has been modified by the interaction with other components resulting in a heterogeneous combination of materials of diverse origins.

Although previous K/Ar age dating have shown that the magmatism took place in the Cretaceous, the high error of the analyses and the altered nature of the investigated minerals did preclude reliable interpretations. In the present work $^{40}Ar/^{39}Ar$ dating was carried out. The results show a prolonged history of magmatism during the Cretaceous over more than 60 Ma, from ~136 to ~74 Ma (Hauterivian to Campanian).

Pre-Cretaceous rifting phases occurred in the Triassic-Jurassic for the western part of the basin and in the Paleozoic for the eastern part. Those previous rifting phases are decisive mechanisms controlling the localization and composition of the Cretaceous magmatism. Therefore, it is the structural position and not the age of the intrusions which preconditions the kind of magmatism and the degree of melting. The divergences on ages are the consequence of the segmentation of the basin in several sub-basins which stretching, thermal evolution and subsidence rate evolved independently.

The first hypothesis formulated at the beginning of this investigation was that the Cretaceous gabbroic intrusions identified in northern Ecuador could be correlated with the intrusions described in the Eastern Cordillera. The mafic occurrences should mark the location of the most subsiding places of the large Cretaceous basin in northern South America. For this reason, the gabbroic intrusions cutting the Cretaceous succession in the Putumayo Basin, southern Colombia, were investigated. The results of the studies were quite unexpected. The petrologic and geochemical character of the magmatic rocks indicates subduction-related magmatism. K/Ar dating of amphibole yields a Late Miocene to Pliocene age (6.1 ± 0.7 Ma) for the igneous event in the basin. Although there is no correlation between this magmatic event and the Cretaceous magmatic event, the data obtained has significant tectonic and economic implications. The emplacement of the Neogene gabbroic rocks coincides with the late Miocene/Pliocene Andean orogenic uplift as well as with a significant pulse of hydrocarbon generation and expulsion.

ZUSAMMENFASSUNG

Die östliche Kordillere Kolumbiens besteht hauptsächlich aus sedimentären Gesteinen, die seit dem frühen Mesozoikum angelagert wurden. Magmatische Gesteine sind rar und zeigen sich nur in Form von mafischen Gängen und Lagen die in kreidezeitliches Gestein intrudierten. Diese Arbeit untersucht den kretazischen Magmatismus um die Prozesse zu verstehen, die die Bildung dieser Gesteine ermöglichte.

Die magmatischen Gesteine durchschlagen die kretazischen sedimentären Einheiten aus schwarzen Schiefern und Mergeln, die auf beiden Seiten der östlichen Kordilliere aufgeschlossen sind. Die untersuchten Gesteine wurden als Gabbros (Cáceres, Pacho, Rodrigoque), Tonalite (Cáceres, La Corona), Hornblende Gabbros (La Corona), Pyroxen-Hornblende Gabbros (Pacho, La Corona, Rodrigoque, Pajarito), und Pyroxen-Hornblendite (Pajarito) eingestuft. Die gabbroiden Proben bestehen hauptsächlich aus Plagioklas, Klinopyroxen und/ oder grüner und brauner Hornblende. Die Tonalite sind aus Plagioklas und Quarz zusammengesetzt. Die Proben sind im Bezug auf ihre Kristallgröße sehr variabel. Biotit, Titanit und Zirkon sind in Form von Akzessorien enthalten. Die Proben sind mäßig bis stark überprägt. Diese enthalten zusätzlich Epidot, Aktinolit und Chlorit.

Die Haupt- und Nebenelementzusammensetzung der Gesteine wie die Mineralassoziation an sich zeigen deutliche Unterschiede abhängig von der jeweiligen Lokalität. Das deutet auf mehrere Schmelzprozesse die zur Bildung der magmatischen Gesteine führten. Das breite Spektrum an Spurenelementen in den Intrusionen ist charakteristisch für verschiedene Grade der Mantelaufschmelzung und der Anreicherung dieser Schmelzen mit inkompatiblen Elementen. MORB und OIB Zusammensetzungen deuten auf mindestens zwei verschiedene Quellen des tholeiitischen und alkalinen Magmas hin. Im westlichen Teil des Kreidebeckens weisen höhere Ba/Nd und Sr/P Verhältnisse auf subduktionsinduzierte Fluide hin, die eventuell eine Metasomatose des Mantels nach sich zog. Die Verhältnisse der radiogenen Isotope von Sr spiegeln ebenfalls einen Fluideintrag wieder. Aufgrund der Spurenelementmuster kann davon ausgegangen werden, dass im kretazischen Becken extensionale Bewegungen zu einer Ausdünnung der kontinentalen Kruste führte.

Mikrosondenanalysen (EMPA) der Hauptelemente und Röntgenfluoreszenzanalyse mittels Synchrotonstrahlung (μ-SRXRF) der Spurenelemente von früh kristallisierten Mineralen der Intrusionen (Klinopyroxene und Amphibole) reflektieren den selben dualen Charakter wie die Gesamtgesteinsanalysen. Trotz Überprägung mancher Gesteine zeigen die Mineralkompositionen sowohl eine angereicherte als auch eine relativ verarmte Magmaquelle. Durch die Normalisierung der Spurenelemente von Klinopyroxen und Amphibol zum Gesamtgestein konnte gezeigt werden, dass die Überprägung keine Auswirkung auf die originalen Spurenelementkompositionen hatte.

Sr-Nd-Pb Daten zeigen eine große Variationsbreite in den Isotopen, trotzdem ist noch der Mantel als initiale Quelle des Magmas sichtbar. Die Proben zeigen mäßige bis hohe radiogene Mengen an $^{143}Nd/^{144}Nd$ und hohe Verhältnisse von $^{87}Sr/^{86}Sr$. Beides spricht für angereicherten Mantel als Ausgangsmaterial der mafischen Intrusiva. Sedimente, Kruste und Meerwasser kontaminieren das Gestein in variablen Anteilen. Korrigierte Pb Isotopenverhältnisse zeigen zwei unterschiedliche Probengruppen. Damit kann vermutet werden, dass die Chemie des Mantels unter den nördlichen Anden durch Interaktionen mit anderen Komponenten modifiziert wurde und so ein heterogenes Material entstand.

Frühere K/Ar Datierungen zeigen, dass die Intrusionen der mafischen Gesteine in der Kreide erfolgten. Aufgrund des hohen Fehlers in den Analysen und den Alterationen an den untersuchten

Mineralien, sollten derartige Interpretationen mit Vorsicht betrachtet werden. Diese Arbeit zeigt anhand von Ar/Ar Daten, dass sich der Zeitraum der magmatischen Ereignisse über 60Ma hinzieht. Es wurden Alter von 136 Ma bis 74 Ma ermittelt (Hauterivium/Campanium).

Extensionsprozesse traten im östlichen Teil des Kreidebeckens bereits im Paleozoikum auf, der westliche Teil wurde an der Trias-Jura-Grenze von der Entwicklung erfasst. Diese frühen Riftprozesse haben maßgeblichen Einfluss auf die Lokalität und Komposition des kretazischen Magmatismus. Daher ist die strukturelle Position und nicht das Alter ausschlaggebend, wenn es um die Art des Magmatismus und den Grad der Aufschmelzung des Mantels geht. Die Spannbreite der ermittelten Alter steht im Zusammenhang mit der Segmentierung des Beckens. Diese Subbecken zeigen eine unterschiedliche thermische Entwicklung sowie eine unabhängige Evolution in Extension und Subsidenz.

Eine erste Hypothese die zu Beginn der Arbeit formuliert wurde, ging davon aus, dass die kretazischen gabbroiden Intrusionen im nördlichen Equador mit den Intrusionen in der östlichen Kordilliere korrelierbar sind. Die mafischen Gesteine definieren ein Areal des nördlichen Südamerika, dass wohl die größte Subsidenz erfahren hat. Darum wurden die gabbroiden Gänge in den kretazischen Abfolgen des Putumayo Beckens, Süd-Kolumbien, erforscht. Diese Arbeit zeigt neue Resultate und Ergebnisse, die so nicht erwartet wurden. Der petrologische und geochemische Charakter der Magmatite zeigt subduktionsbezogenen Magmatismus. K/Ar Datierungen von Amphibolen zeigen ein spates Miozänes bis Pliozänes Alter (6.1 ± 0.7 Ma) für das Intrusionsereignis im Kreidebecken. Obwohl es keine Korrelation zwischen diesem magmatischen Ereignis und dem Kretazischen gibt, zeigen die Daten doch tektonische und ökonomische Zusammenhänge auf. Die Intrusion der neogenen Gabbroide überschneidet sich mit der späten miozänen/pliozänen andinen Hebung ebenso wie mit der signifikanten Bildung von Kohlenwasserstoffen und deren Einlagerung.

RESUMEN

La Cordillera Oriental de Colombia está compuesta principalmente por rocas sedimentarias depositadas desde el Mesozoico temprano. Las rocas magmáticas en la cordillera son muy escasas. Ellas están representadas por limitadas ocurrencias de diques y silos de composición máfica que presumiblemente fueron emplazados en el Cretácico, así como también por la presencia de rocas volcánicas de edad neogena. Este trabajo está enfocado en el estudio del magmatismo cretácico, con el fin de entender los procesos que llevaron a la formación de estas rocas y conocer su significado en el ambiente tectónico regional del norte de los Andes.

Las rocas magmáticas intruyen la sucesión sedimentaria cretácica compuesta por shales negros y margas que afloran en los flanco oriental y occidental de la Cordillera Oriental. Las rocas estudiadas fueron clasificadas como gabros, (Cáceres, Pacho, Rodrigoque), tonalitas (Cáceres, La

Corona), gabros hornbléndicos (La Corona), gabros de piroxeno y hornblenda (Pacho, La Corona, Rodrigoque, Pajarito), y hornblenditas piroxenicas (Pajarito). Las rocas gabroideas están principalmente compuestas por plagioclasa, clinopiroxeno, y/o hornblenda verde y marrón. Las rocas tonalíticas están compuestas por plagioclasa y cuarzo. Las muestras analizadas presentan una amplia variedad en el tamaño de los cristales desde grano fino a grueso. Minerales accesorios tales como biotita, titanita y circón también están presentes. Algunas de las muestras presentan alteración moderada a fuerte, lo cual se evidencia por su contenido de epidota, actinolita y clorita.

La composición de elementos mayores y traza tanto en roca total como en los minerales formadores de roca muestra diferencias significativas en las características geoquímicas y petrológicas entre las diferentes localidades estudiadas, sugiriendo que éste magmatismo no ha sido el resultado de un proceso único de fusión. El variado espectro composicional de los elementos traza en las rocas gabroideas se distingue por tener diferentes grados de fusión del manto y enriquecimiento de elementos incompatibles. La composición de los magmas que dieron origen a las rocas estudiadas es similar a MORB y OIB, lo cual sugiere que por lo menos dos fuentes diferentes de magma estuvieron involucradas en la generación de este evento magmático. Esas dos fuentes corresponden a una con afinidad toleiítica y otra con afinidad alkalina. Fueron reconocidas algunas evidencias que sugieren la presencia de fluidos derivados de una placa subducente al occidente de la cuenca cretácica, tales como valores altos en la relaciones de Ba/Nb y Sr/P. Los elementos traza indican un ambiente extensional en la cuenca cretácica, la cual llevó a la formación de un rift continental.

Los análisis de elementos mayores con la microsonda electrónica y los de elementos traza con microfluorescencia de rayos X radiación sincrotrón en los minerals que se formaron en las etapas más tempranas de la cristalización (clinopiroxenos y anfíboles), reflejan el mismo caracter dual que fue encontrado en los análisis de la roca total. A pesar de que las rocas estudiadas han sufrido evidentes procesos de alteración, la composición química de los minerales muestra evidencias de una fuente de magma enriquecida y una menos enriquecida en elementos incompatibles. Incluso la normalización de los elementos traza de los clinopiroxenos y anfíboles con respecto a la roca total de la cual hacen parte, sigue muy de cerca el patrón designado por los coeficientes de partición que se encuentran en la literatura, indicando que dicha alteración no modificó la composición original de los elementos traza en los minerales analizados.

Los datos obtenidos de isótopos de Sr-Nd-Pb revelan una amplia variación isotópica, mas sin embargo, todavía sugieren un origen inicial de los magmas en el manto. La muestras estudiadas presentan composiciones radiogénicas moderadas a altas de la relación $^{143}Nd/^{144}Nd$ y altas de $^{87}Sr/^{86}Sr$ las cuales tienden hacia composiciones de manto más enriquecidas, como por ejemplo la composición de la corteza paleozoica de Sur América. Los magmas que generaron las rocas estudiadas sufrieron diferentes grados de contaminación causado por la interacción con sedimentos, corteza continental y agua del mar. La relación isotópica de Pb, corregida por la edad de las rocas, muestra dos grupos separados de rocas. Esta separación sugiere que la composición del manto bajo los Andes del norte ha

sido modificada por la interacción con otros componentes resultando en una composición heterogenea de materiales con diversos orígenes.

Aunque las dataciones previas llevadas a cabo con el método de K/Ar mostraron que el magmatismo tuvo lugar en el Cretáceo, el error analítico de los análisis así como el estado de alteración de los minerales investigados, dan lugar a una gran incertidumbre acerca de la validez de estos datos. En este trabajo se llevaron a cabo nuevas dataciones con el método de $^{40}Ar/^{39}Ar$. Los resultados muestran una larga historia magmática que se extiende en el Cretácico por cerca de 60 Ma desde el Hauteriviano hasta el Campaniano (136 – 74 Ma).

Las fases de rifting pre-Cretácicas ocurridas en el Jura-Triásico en la parte occidental de la cuenca, y en el Paleozoico en la parte oriental, se constituyen en mecanismos decisivos que controlan la localización y composición del magmatismo cretácico. Por ello, se sugiere que es la posición estructural y no la edad de las intrusiones lo que precondiciona el tipo de magmatismo y el grado de fusión que se genera. Las diferencias encontradas en la edad son consecuencia de la segmentación de la cuenca en diversas sub-cuencas, cuyo grado de extensión, evolución termal y tasa de subsidencia se desarrolló de manera independiente.

Una de las primeras ideas formuladas al comienzo de esta investigación fue la de correlacionar las intrusiones gabroideas cretáceas identificadas al norte de Ecuador con las intrusiones encontradas en la Cordillera Oriental de Colombia. La ocurrencia de magmatismo máfico debería marcar aquellos lugares en donde la subsidencia fue mayor en la gran cuenca cretácica en el norte de Sur America. Por esta razón, fueron investigadas las rocas ígneas máficas que intruyen la sucesión sedimentaria cretácica en la Cuenca de Putumayo, al sur de Colombia. Sin embargo, los resultados del estudio fueron completamente inesperados. Las características geoquímicas y petrológicas de las rocas ígneas indican un magmatismo relacionado a una zona de subducción. La datación de anfíboles por el método K/Ar arrojó una edad Mioceno tardío a Plioceno (6.1 ± 0.7 Ma) para el evento magmático en la cuenca. A pesar de que no existe una relación entre este evento y el magmatismo cretácico en la Cordillera Oriental, los datos obtenidos tienen importantes implicaciones tanto tectónicas como económicas. El emplazamiento de las rocas gabroideas neógenas coincide con el evento andino orogénico del Mioceno tardío/Plioceno, así como también con un pulso significativo de generación y expulsión de hidrocarburos.

TABLE OF CONTENT

LIST OF FIGURES

LIST OF TABLES

ACKNOWLEDGMENTS

I am greatly indebted to my supervisor PD Dr. Uwe Altenberger for his guidance and encouragement throughout the research, and for his valuable criticism and warm guidance. I would like to express him my sincere gratitude for his friendly support in each step of my investigation, his patience and comprehension even in the most difficult times. I am deeply thankful to Prof. Manfred Strecker for his support, friendship, optimism, and good mood that helped me to overcome many downs.

I would like to express my thanks to the academic and technical staff at the Department of Geosciences of the University of Potsdam, especially, I am grateful to Dr. Max Wilke for share with me his knowledge, for his valuable comments, for his friendship, and his company during the long hours spent on experiments and measurements. To Prof. Roland Oberhänsli who showed interest on my investigation and gave me motivating input to keep on working. I also want to extend my gratitude to Dr. Andreas Möller and Dr. Beate Mocek for their helpful comments and their support at any time not only academically but also in the daily life. Dr. Masafumi Sudo and Dr. Martin Timmerman introduced me in the Ar-dating methodology; I own all my gratitude for their comments and discussions. Antje Musiol and Christine Fischer were also essential to carry on the whole work. With out you it would be very hard to finish my thesis, thank you!

Many people helped me outside of the University with the analytical procedures performed during this study. I am especially grateful to Dr. Rolf L. Romer from the GeoForschungsZentrum-Potsdam for introducing radiogenic isotopes, for his teaching and interesting discussions. At the GFZ-Potsdam, I want also to thank to Dr. Rudolf Naumann for the XRF analysis, and Ms. Oona Appelt for her support at the EMPA. Thanks to Dr. Gerald Falkenberg and particularly to Dr. Karen Rickers for their support on the experiments in HASYLAB. I also appreciate the great assistance of Juan Manuel Moreno and Dr. Ana Elena Concha from the Universidad Nacional de Colombia for fulfil the field work and for the encouragement to continue my studies and to come to Germany. I am deeply grateful to Ecopetrol S. A. and especially to the Instituto Colombiano del Petróleo and the Litoteca Nacional for permitting the publication of the data of the Putumayo Basin as well to Alberto Ortíz, Andrés Reyes, and Mercedes Álvarez who very kindly permitted me to sample the well-cores of the Orito Oil Field. I extend my gratefulness to K. Wemmer of the University of Göttingen for the K/Ar age determination for the samples of the Putumayo Basin.

For the corrections of English and the general content of the multiple versions of the manuscript I want to thank to Markus Safaricz, Ed Sobel, Uwe Baaske, and Andrés Mora. For the correction of German and multiple translations I thank to Franziska Wilke.

Many thanks to my friends and colleges Jessica Zamagni, Gabriela Marcano, Paolo Ballato, Andrea Knörich, Astrid Riemann, Katrin Rehak, Manuela Borchert, Andreas Bergner, and Dirk Rößler for your closeness and for let me know a little bit more or your countries and cultures and

make my stay in Germany more pleasant and enjoyable. To my friend Felipe Lozano, who went with me in the field and very patiently and bravely stood each inconvenience. I also want to express thanks to my friends and colleges Gaetan Rimmele and Fatma Köksal, who were once in Potsdam but now are in other latitudes, your support and comments enriched my life.

My stay in Potsdam was supported thanks to the grants from the German Academic Exchange Service (DAAD - Short-Term Research Program for 6 months) and the Graduate School Program at the University of Potsdam "Earth surface processes – Dynamics, scales, and changing environments".

Finally, I extend my gratitude to my parents for their encouragement throughout my studies and to Tilman for providing me with another view of the world.

1. INTRODUCTION

The NW corner of South America is a region considered as a large evolving triple junction between the Nazca, South America, and Caribbean plates (Ego et al., 1996). The Colombian Andes located in that convergent zone are constituted of three main ranges, the Western, Central, and Eastern Cordilleras (Fig.1.1).

The nature and composition of the three Cordilleras is substantially different, each one resulting from diverse tectonic processes undergone in the Mesozoic and Cenozoic. The Western Cordillera is composed of turbidites and ophiolites of oceanic character accreted during the Mesozoic and early Cenozoic (Barrero-Lozano, 1979). The Central Cordillera exposes a medium- to low-pressure metamorphic belt combining rocks from both oceanic and continental character which form a pre-Mesozoic basement (McCourt et al., 1984). It is intruded by several Mesozoic and Cenozoic plutons related to the subduction of oceanic lithosphere underneath the continent (Taboada et al., 2000). In contrast to these two ranges, the Eastern Cordillera is not aligned parallel to the Pacific coast, but follows a N-NE direction (Fig. 1.2). Its basement is composed of Precambrian and Palaeozoic polymetamorphic rocks. It is covered by a thick sequence of Mesozoic sedimentary rocks, strongly deformed during Neogene by thrusting and folding (Irving, 1971). Jurassic and Cretaceous sediments have been deposited within large basins whose origin is still a matter of discussion.

There exist three alternative hypotheses, that try to explain the occurrence of the rifting phase during the Cretaceous: (1) as a consequence of extensional tectonics in north-western South America a continental rift developed since Triassic, which is related to the separation between North America and South America (Geotec, 1992; Mojica et al., 1996); (2) back-arc basin extension located east of the Central Cordillera resulting from the subduction of the Farallon oceanic plate beneath the continent (McCourt et al., 1984; Fabre, 1987; Toussaint and Restrepo, 1989); (3) interruption of the subduction phase due to the change of relative motion of the oceanic plate (Caribbean plate) with respect to the South American plate producing a passive continental margin (Pindell and Erikson, 1993; Pindell and Tabbutt, 1995; Pindell et al., 2006).

The first who identified the presence of mafic intrusions in the Eastern Cordillera was Gansser (1956). However, he just briefly wrote "*Ich fand gabbroide Intrusionen in der mittleren Kreide im Gebiete der Smaragdminen von Musso und in Guaguaquifluss im mittleren Magdalenatal*". Subsequently, some authors like Pratt (1961), Campbell and Bürgl (1965) and

Hall (1973) repeatedly mentioned the presence of these rocks without questioning their origin or significance in the regional geology.

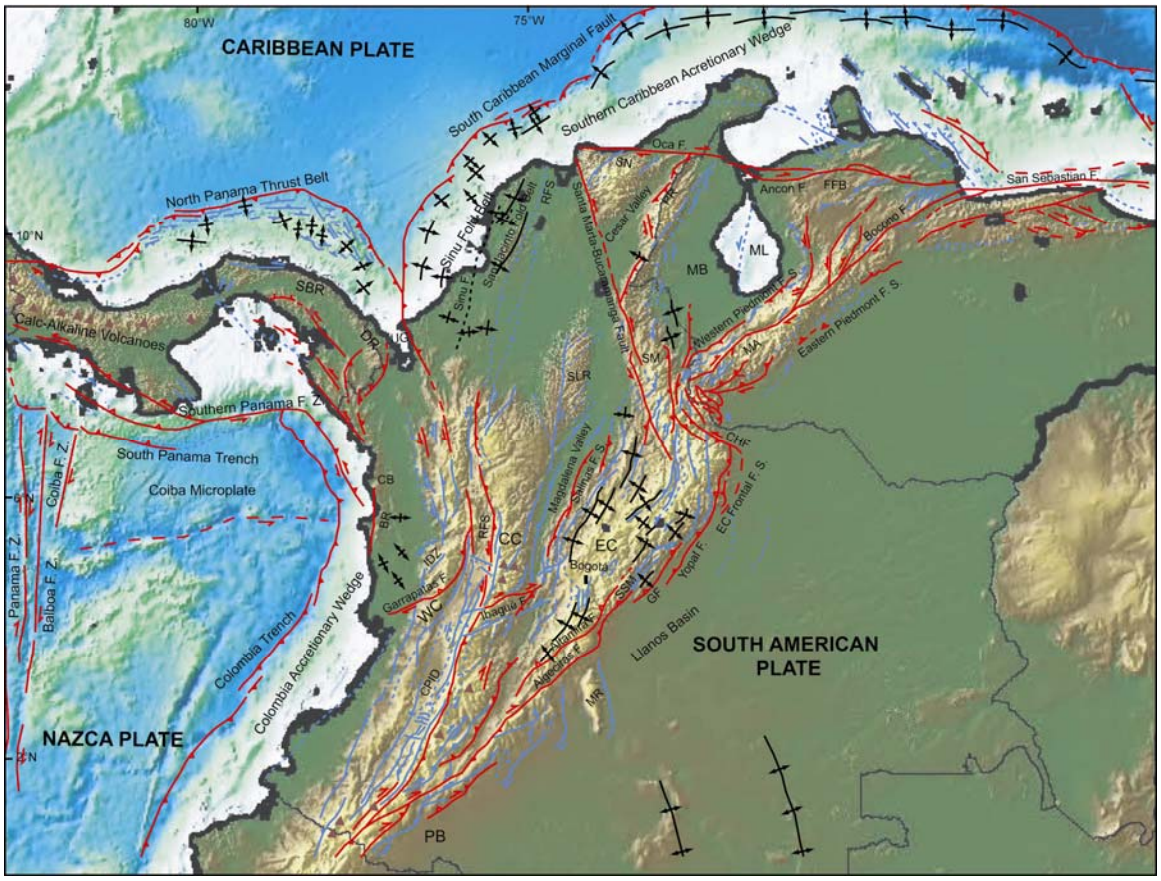

Fig. 1.1. Neotectonic map of the Northern Andes (after compilation of Taboada et al., 2000). BR: Baudó Range; CB: Chocó Block; CC: Central Cordillera; CHF: Chucarima Fault; CPID: Cauca-Patía Intermontane Depression; DR: Darién Range; EC: Eastern Cordillera; FFB: Falcón Fold Belt; GF: Guaicaramo Fault; IDZ: Istmina Deformed Zone; MA: Mérida Andes; MB: Maracaibo Block; ML: Maracaibo Lake; MR: Macarena Range; PB: Putumayo Basin; PR: Perijá Range; RFS: Romeral Fault Zone; SBR: San Blas Range; SLR: San Lucas Range; SM: Santander Massif; SN: Sierra Nevada de Santa Marta; SSM: Servitá-Santa María Fault; UG: Urabá Gulf; WC: Western Cordillera; red triangle: volcano.

In 1983 Fabre and Delaloye published a paper with quite more detailed data about the accurate places where the intrusions crop out, major-element geochemistry, K-Ar dating (Fig. 1.3), and regional significance in the Colombian Cretaceous Basin. The study included the intrusions of Cáceres, La Corona, Pajarito, and Rodrigoque. The intrusions were briefly described as small-sized dykes and sills of gabbroic composition. It was postulated that the emplacement of the intrusions is not necessarily contemporary, but represent a continuous magmatic activity from Early Cretaceous to Cenomanian. The occurrence of these plutonites in the most subsiding part of the Cretaceous basin possibly suggests a local weakness of the continental crust during the extensional phase (Fabre and Delaloye, 1983).

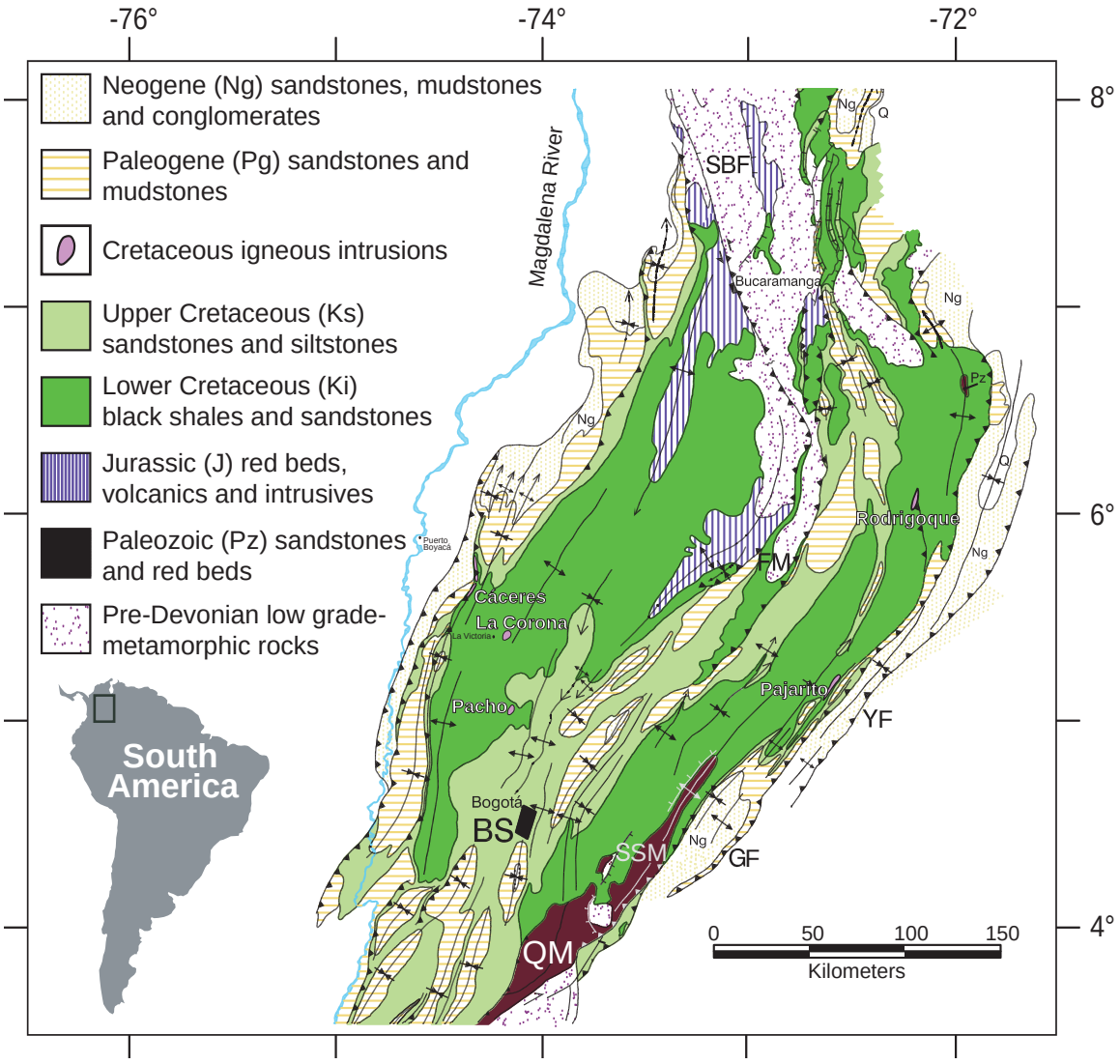

Fig. 1.2. Generalized geological map of the Eastern Cordillera after compilation and own observations made by Mora et al., (2006). BS: Bogota Savanna; SBF: Santa Marta-Bucaramanga Fault; FM: Floresta Massif; GF: Guaicaramo Fault; QM: Quetame Massif; SSF: Servitá-Santa María Fault; YF: Yopal Fault.

Ujueta (1991) used geophysical data, geomorphologic observations, and structural analysis to recognize multiple NW-SE lineaments in the Eastern Cordillera. Along those lineaments several Precambrian (?) to Early - Mid-Cretaceous intrusions, Late Pliocene-Pleistocene volcanic rocks, as well as ore deposits and hot springs are associated. He suggested that the whole magmatic event in this area is related to a set of very old deep fractures through which the magmas and mineralizing fluids raised.

Moreno and Concha (1993) described new occurrences of gabbroic rocks in the western flank of the Cordillera in the region of Puerto Romero – El Marfil (in the present study named as Cáceres) and also the intrusion of Pacho. They suggested, as well as the others above, that the

fault system identified today reflects paleo-fractures through which the magmatic bodies ascended and were emplaced in Cretaceous sedimentary rocks.

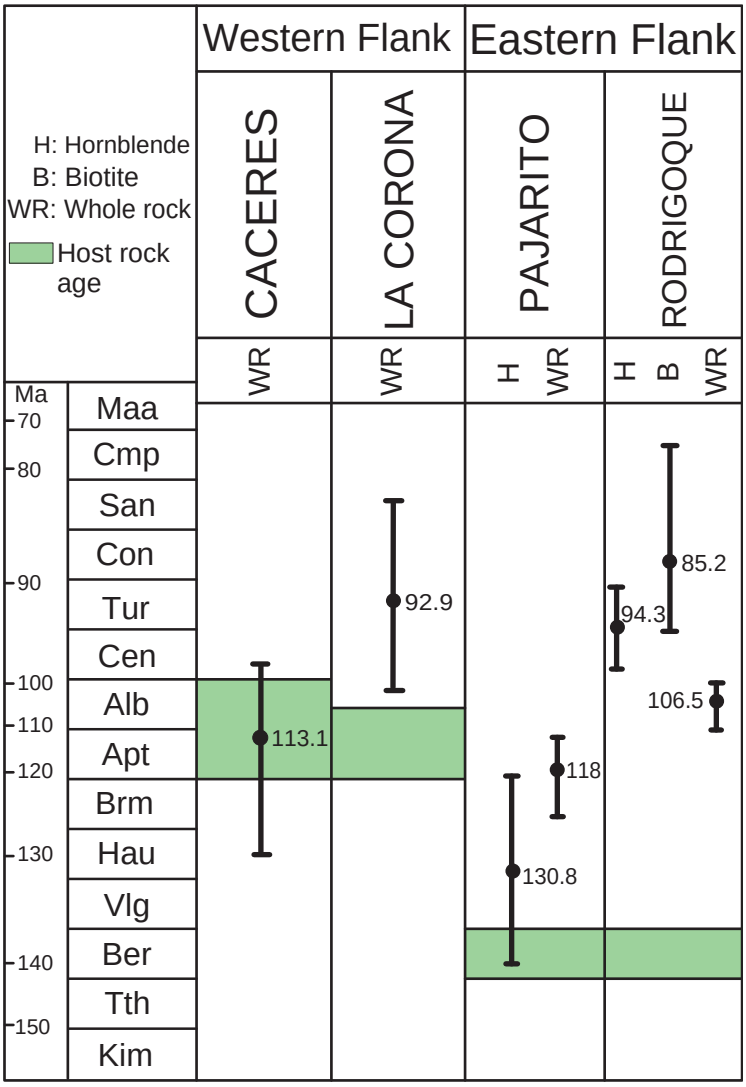

Fig. 1.3. Graphical representation showing the radiometric (Fabre and Delaloye, 1983) and stratigraphic (Fabre and Delaloye, 1983; Vásquez et al., 2000) age control.

Since the early 90's, several diploma theses have dealt with the investigation of the mafic intrusions. Some examples are Marquinez and Moreno (1993), Londoño and Mendoza (1994), and Vásquez (1999) who investigated the intrusions in the western flank of the Cordillera in the area of Cáceres; Navarrete (2002) based her investigations on the intrusion of Pacho; Tenjo (2003) investigated the intrusion of La Corona; Lozano (2005) studied the intrusion of Pajarito. Most of these theses contain petrographic descriptions and restricted major-element data, but no information about trace-elements, isotopic ratios, etc. In general, this magmatism is interpreted as

a product of thinning and weakening of the continental crust during an extensional phase in the early Cretaceous, but no more clues are given about the regional tectonic situation.

The geological setting of the Cretaceous Basin has been mainly investigated through structural, sedimentological and geophysical studies. However, large uncertainties about the Cretaceous paleogeography of the basin exist. Petrologic and geochemical investigations of the intrusions accompanying the basin evolution should be added to the actual knowledge of the basin to reveal more details of its development.

The uncertainty of the specific causes that permit the emplacement of the intrusions, as well as the lack of detailed geochemical, isotopic and geochronological information constitute the fundamental motivation for undertaking this thesis.

In order to understand the melt generating and modifying processes and their relation to the structural evolution of the Cretaceous basin, the following topics were investigated:

1. The age of the intrusions: simultaneous vs. diachronous emplacement
2. The significance of the localization of the intrusions in the evolution of the basin
3. The geochemical characterization of the crystallized melts and their variation in time and space
4. The magma sources
5. The effect of hydrothermal and low-grade metamorphic overprint on the geochemistry of the intrusions
6. Comparison of the results obtained by the study of the magmatic rocks with the existing and new structural models of the basin evolution

To unravel these topics, I used the most suitable methods available to determine contents of major, trace, and rare earth elements of the magmatic rocks. These analyses were done using techniques of X-ray fluorescence spectrometry and inductively coupled plasma-optical emission spectrometry. Furthermore, the study was supported by petrographic techniques which allow identifying the major mineral phases constituting the rocks. The major element composition of the minerals was determined using electron microprobe analyses. The results of this investigation are presented in the Chapter 2.

The uncertainty generated by the moderate to strong alteration observed in the samples and the question if that alteration has modified the primary composition of the rocks, led me to investigate the trace element composition of the first crystallized minerals in the gabbroic samples. Therefore, the trace- and light rare earth element content of clinopyroxenes and

amphiboles was quantified using synchrotron micro-XRF *in-situ* radiation. The results are described in Chapter 3.

In Chapter 4, the magma source responsible of the formation of the gabbroic rocks, Sr-Nd-Pb isotope data on bulk rock were determined using inducted couple plasma mass spectrometry. The results might show the signature for the source of the plutonites. Additionally, the age of the intrusions was defined using $^{40}Ar/^{39}Ar$ dating. The results reveal important implications on the evolution of the basin and the tectonic control on the magmatic products.

Finally, the Chapter 5 describes the mafic magmatic event that took place in the Putumayo Basin. The very first concept I had about the occurrence of these rocks, was to correlate the possible Cretaceous magmatism marking the stretching phase of the Cretaceous basin in northern South America. However, the results provided a Tertiary age for the mafic intrusions in the Putumayo Basin. The emplacement of the rocks coincides with the Andean orogenic uplift, CO_2 formation, and an important pulse of hydrocarbon generation and expulsion.

Except Chapter 1 (Introduction) and Chapter 6 (General Conclusions), each chapter of this thesis has been submitted/is in submission to peer-reviewed journals. Chapter 2 ("*Mid-Cretaceous Extension-Related Magmatism In The Eastern Colombian Andes"* by Mónica Vásquez and Uwe Altenberger) is published in the Journal of South American Earth Science, 2005, v. 20, p. 193-210. Chapter 3 ("*Trace-element content of clinopyroxenes and amphiboles in gabbros of the Colombian Andes - possible constraints for the magma source"* by Mónica Vásquez, Max Wilke, Uwe Altenberger and Karen Rickers) has been submitted to the European Journal of Mineralogy. Chapter 4 ("*Intra-plate magmatism in the Colombian Cretaceous Basin: $^{40}Ar/^{39}Ar$ ages and isotope evidence of the magmatic evolution of a segmented basin"* by Mónica Vásquez, Uwe Altenberger, Rolf L. Romer, Masafumi Sudo and Juan Manuel Moreno Murillo) is in submission to Earth and Planetary Science Letters. Chapter 5 ("*Magmatism and Hydrocarbon Generation in the Putumayo Basin, Northern Volcanic Zone, SW Colombia"* by Mónica Vásquez, Uwe Altenberger and Rolf L. Romer) has been submitted to the International Journal of Earth Sciences and is in review.

2. MID-CRETACEOUS EXTENSION-RELATED MAGMATISM IN THE EASTERN COLOMBIAN ANDES

Mónica Vásquez
Uwe Altenberger
Institut für Geowissenschaften, Universität Potsdam, Karl-Liebknecht-Str. 24 14476 Potsdam-Golm, Germany

2.1 ABSTRACT

Cretaceous magmatism in the Eastern Cordillera of Colombia is related to lithospheric stretching during the late Early–early Late Cretaceous. The small amount of preserved igneous material is represented by small mafic intrusions. This chapter focuses on three localities, from east to west: Pajarito, Pacho, and Cáceres. The investigated igneous bodies are classified as gabbros, pyroxene-hornblende-gabbros, and pyroxene-hornblendites mainly composed of plagioclase, clinopyroxene, and/or amphibole. Although their timing of emplacement and geodynamic position seem similar, significant differences in their geochemical and petrological characteristics rule out simple models of melt genesis. Clinopyroxene and bulk chemistry indicate increasing alkalinity from west to east. Trace element concentrations point to melt sources that range from a slightly enriched mantle in the west to a highly enriched one in the east. In addition, the data reflect a decreasing degree of partial melting from west to east and the decreasing importance of residual garnet in the mantle source. Probable mantle metasomatism in the source region by slab-derived fluids, as displayed by high Ba/Nb and moderate Sr_n/P_n, is clear in the west and very slight to the east. Mantle metasomatism and melt generation probably are processes of different epochs. The lack of large volumes of igneous rocks and the absence of tectonically controlled unconformities in the investigated areas indicate that a mantle plume did not affect the regional tectonics and magmatism. We favor a model of rift-related magmatism in which melt composition is modified from east to west from a highly enriched to a less enriched mantle region, the latter metasomatized by fluids derived from an older subduction phase.

2.2 INTRODUCTION

The Andean belt extends for approximately 9000 km along the western margin of the South American continent. In Colombia, the Andes split in three ranges: the Eastern (EC), Western (WC), and Central (CC) Cordilleras. The EC extends from southwestern Colombia to the

Venezuelan border following a N–NE trend. The scarcity of Cretaceous and Tertiary magmatic activity, a remarkable characteristic of the EC, has been a matter of frequent discussion.

However, few mafic plutonic bodies have been identified in the eastern and western flanks of the EC intruding Cretaceous sediments, which have been dated from biostratigraphic studies as Berriasian–Cenomanian in age. Intrusions coincide with areas in which lithospheric stretching reached its maximum during the Berriasian–Hauterivian (Sarmiento, 2001b). The plutonic rocks' stratigraphic relationship and geodynamic position of the EC in the Mid-Cretaceous enables us to assume that these widespread small intrusions record a single partial melting process of different portions of the mantle during a Cretaceous rift episode, that has been recognized in the present position of the Cordillera (Campbell and Bürgl, 1965; Fabre, 1983b; Fabre, 1983c; Colleta et al., 1990).

Despite stratigraphic and some major element geochemical investigations, the magmatic evolution of these intrusions and their response to geodynamics is not understood (Fabre and Delaloye, 1983; Vásquez et al., 2000; Navarrete et al., 2002). This chapter focuses on the petrological and geochemical features of three localities (Fig. 2.1), roughly distributed on an east–west profile, to characterize their magmatic evolution and their response to the geodynamics during melting genesis.

2.3 GEOLOGICAL SETTING

The Colombian Andean orogen north of 1°N includes, from west to east, three mountain ranges: the WC, CC, and EC. The EC is composed of a Precambrian and Paleozoic polymetamorphic basement covered by a thick sequence of Mesozoic and Cenozoic sedimentary rocks. The sedimentary rocks were strongly deformed during the Neogene by thrusting and folding (Irving, 1971). The EC rises in southwestern Colombia, with a NE-SW strike, and reaches its maximum width at approximately 6°N (up to 250 km). During Triassic and Early Jurassic times, a rifting phase affected the northern part of Colombia and Venezuela, probably as a consequence of the breakup of Pangea (Pindell and Dewey, 1982; Jaillard et al., 1990). Concomitantly, backarc extension behind a subduction-related magmatic arc occurred in the area that currently corresponds to the EC (Maze, 1984; McCourt et al., 1984; Pindell and Erikson, 1993; Toussaint, 1995). The presence of the large granitoid Ibagué Batholith (K/Ar ages 151 ± 4 to 131 ± 2 Ma; Brook, 1984; Sillitoe et al., 1982, respectively) and the Jurassic volcanoclastic Saldaña Formation in the Upper Magdalena Valley (Fig. 2.1) demonstrates the existence of a volcanic arc at the present position of the CC (Bayona et al., 1994) active until approximately

130 Ma (i.e., the lower Cretaceous; Sillitoe et al., 1982; Brook, 1984). During the Early Cretaceous, a wide system of asymmetric half-rift basins (Tablazo-Magdalena, Cocuy sub-basins) formed in response to new episodes of lithosphere stretching (Sarmiento, 2001b), which has been tentatively related to backarc extension.

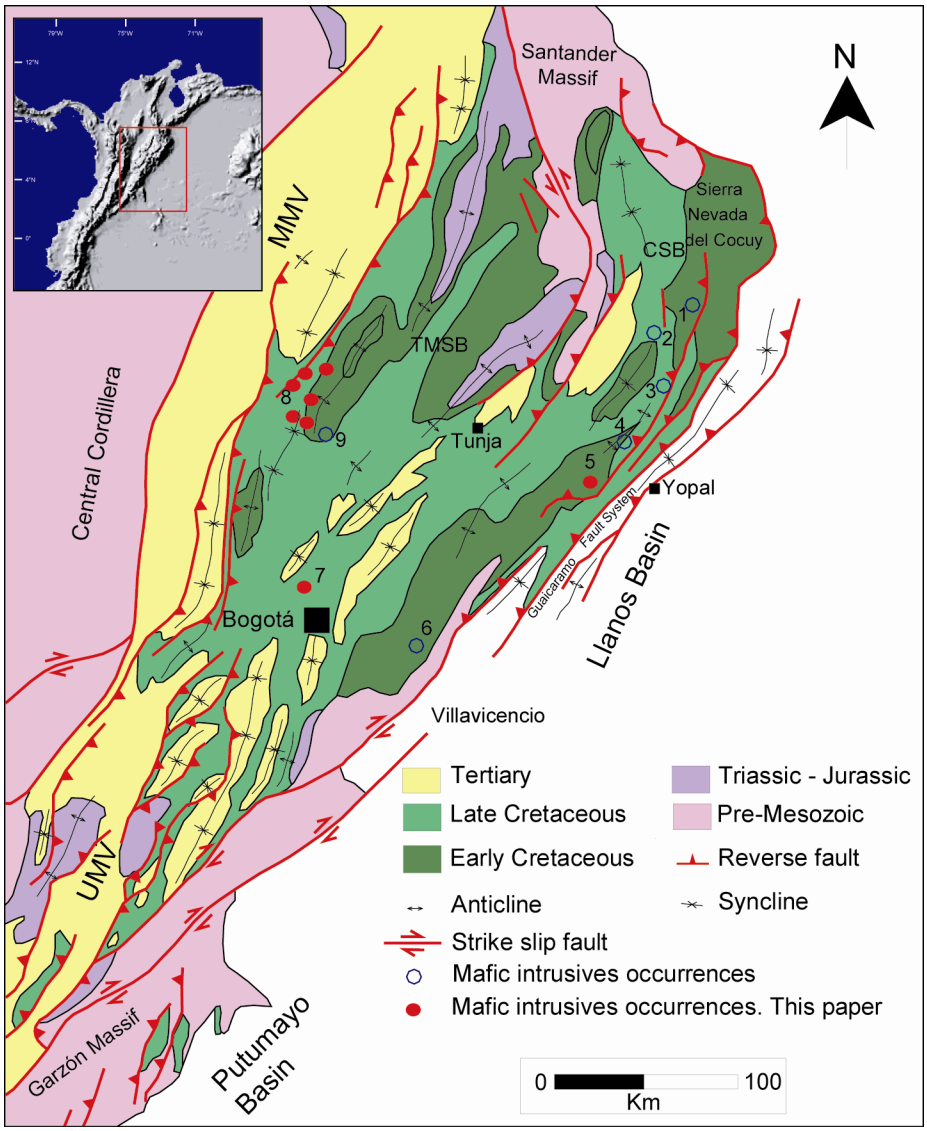

Fig. 2.1. Structural map of the Eastern Cordillera (González et al., 1988; Schamel, 1991). Distribution of mafic intrusions (1) Río Nuevo diorite; (2) Rodrigoqué microgabbro; (3) porfiritic basaltic lava; (4) Río Cravo Sur microgabbro; (5) Pajarito intrusion; (6) Río Guacavía diorite; (7) Pacho (Tragarepas gabbro); (8) Cáceres-Puerto Romero intrusion; (9) La Corona intrusion. UMV, Upper Magdalena Valley; MMV, Middle Magdalena Valley; TMSB, Tablazo-Magdalena subbasin; CSB, Cocuy subbasin.

Gansser (1956) reported mafic intrusives of the EC in the Guaguaquí River. Later, dykes and sills of gabbroic composition were reported from W to E in the localities of Cáceres-Puerto Romero (Marquinez and Moreno, 1993), La Corona, Pacho, Pajarito, and Rodrigoqué (Fig. 2.1).

Although K/Ar ages (Fabre and Delaloye, 1983) do not clearly demonstrate synchronicity for the emplacement of the bodies (see Fig. 1.3), stratigraphic observations constrained from ammonites, bivalves, and foraminifers bearing facies (Villamil and Arango, 1998; Vásquez et al., 2000) indicate ages no older than late Albian. In both western and eastern localities, the dykes strike in general N10°E, parallel to the main regional faults. Fabre and Delaloye (1983) explain the occurrence of these small mafic intrusions as a result of the most pronounced subsidence phase during the Berriasian–Cenomanian, when the Cretaceous transgression began. According to Sarmiento (2001b), intrusives are a product of the maximum crustal and lithospheric mantle stretching during the Cretaceous.

2.4 PETROGRAPHY

Mafic rocks crop out on both flanks of the EC (Fig. 2.1) and generally range from a few centimeters to tens of meters in thickness. In this study, rocks from the localities of Cáceres, Pacho, and Pajarito have been analyzed.

In the region of Cáceres-Puerto Romero, mafic melts intrude La Paja (Aptian) and Simití (Cenomanian) formations (Vásquez et al., 2000). Gabbros from five different localities in this area have been reported, emplaced as 20–50 m thick and 1–6 km long sills. The rocks are composed of plagioclase (oligoclase–labradorite, 2–4 mm) and clinopyroxene (augite and pigeonite, 1–4 mm). Minor constituents are biotite, quartz, chlorite, and ilmenite. Calcite occurs as an alteration product of plagioclase. Numerous calcite and quartz veins cut the rocks. Equigranular and ophitic to subophitic textures are the most common. A very fine-grained tonalite vein, approximately 6 cm thick and composed mainly of quartz (40%) and plagioclase-An_{17} (44%), was also observed. Simplectitic texture between quartz and plagioclase is present.

The Pacho intrusion, named by Navarrete et al. (2002) as the Tragarepas Gabbro, cuts the Pacho Formation (Late Albian). Major components are plagioclase (albite, 0.5–1.0 mm), clinopyroxene relicts (augite), and green to brown hornblende (0.6–0.9 mm), which in some samples grows up from clinopyroxene crystals. Tremolite, chlorite, and traces of biotite and epidote are present, which suggests that these rocks were affected by low-grade metamorphism or hydrothermal processes. Alteration is very strong; in most of the samples, plagioclase is replaced by calcite. The rocks are classified as pyroxene-hornblende-gabbros.

Mafic rocks from Pajarito are hosted in black silicic mudstones that correspond to the Lutitas de Macanal Formation (Berriasian–Valanginian) in the form of sills and dykes that reach up to 30 m in thickness. They are described as inequigranular, coarse-grained rocks, mainly

composed of large, brown to green hornblende crystals (up to 2 mm) occasionally overgrown by tremolite. Chlorite and subordinate clinopyroxene (diopside and augite) are also recognizable. Albite and epidote are present as minor phases, which suggest low-grade metamorphism (greenschist facies). Calcite replaces clinopyroxenes. They are classified as pyroxene-hornblendites.

Samples from all locations are olivine free. We provide a general description of each locality in Table 2.1. Fig. 2.2 shows photomicrographs of thin sections for each locality.

Locality	Rock type	Plagioclase	Clinopyroxene	Amphiboles	Quartz	Trace minerals	Observations
Cáceres	Gabbro	Oligoclase labradorite	Augite pigeonite		X	Biotite, quartz, chlorite, and ilmenite	Calcite occurs as alteration product. Numerous calcite and quartz veins cut the rocks. Textures equigranular, ophitic to subophitic
	Tonalite	Oligoclase			X		Simplectitic texture between quartz and plagioclase
Pacho	Pyroxenic hornblendic gabbro	Albite	Augite	Hornblende (green and brown)		Tremolite, chlorite, biotite, and epidote	Hornblende grows up from clinopyroxene. Plagioclase is replaced by calcite
Pajarito	Pyroxenic hornblendite		Diopside augite	X Hornblende (green and brown)		Chlorite, albite, and epidote	Hornblende occasionally overgrown with tremolite. Calcite replaces clinopyroxenes

Table 2.1. Petrographic description of the basic intrusions of the EC. Thin sections of each locality are shown in Fig. 2.2.

2.5 ANALYTICAL METHODS

Twenty-eight samples from the EC were geochemically analyzed. Major and trace element measurements were performed on a Phillips PW-2400 x-ray fluorescence (XRF) spectrometer. H_2O, and CO_2 were determined through quantitative high temperature decomposition with a Vario EL III CHN elemental analyzer. Both analyses were carried out at the GeoForschungsZentrum Potsdam (Germany). Analytical precision was determined with internationally accepted rock standards. For the XRF analysis, the estimated precision is better than 1-3% for major elements (depending on concentration levels) and better than 2-3% for trace elements.

Rare earth element (REE) analyses were performed on a Vista MPX inductively coupled plasma-optical emission spectrometer at the Geochemical Laboratory of the University of Potsdam. Sample preparation involved Na_2O_2 standard fusion and dilution techniques for dissolving rock powders into solution. Analytical precision was checked with international reference standards and found to be better than 12%. The Pb, U, and Nb in sample LAG3 from Cáceres were measured at the Institute of Geosciences, Johannes Gutenberg University, Mainz.

Mineral compositions were determined on thin sections with both Cameca SX50 and SX100 electron microprobes at GeoForschungsZentrum Potsdam. An acceleration voltage of 15

keV and beam current of 20 nA were the operating conditions. Representative results of the microprobe analyses are summarized in Tables 2.2, 2.3 and 2.5.

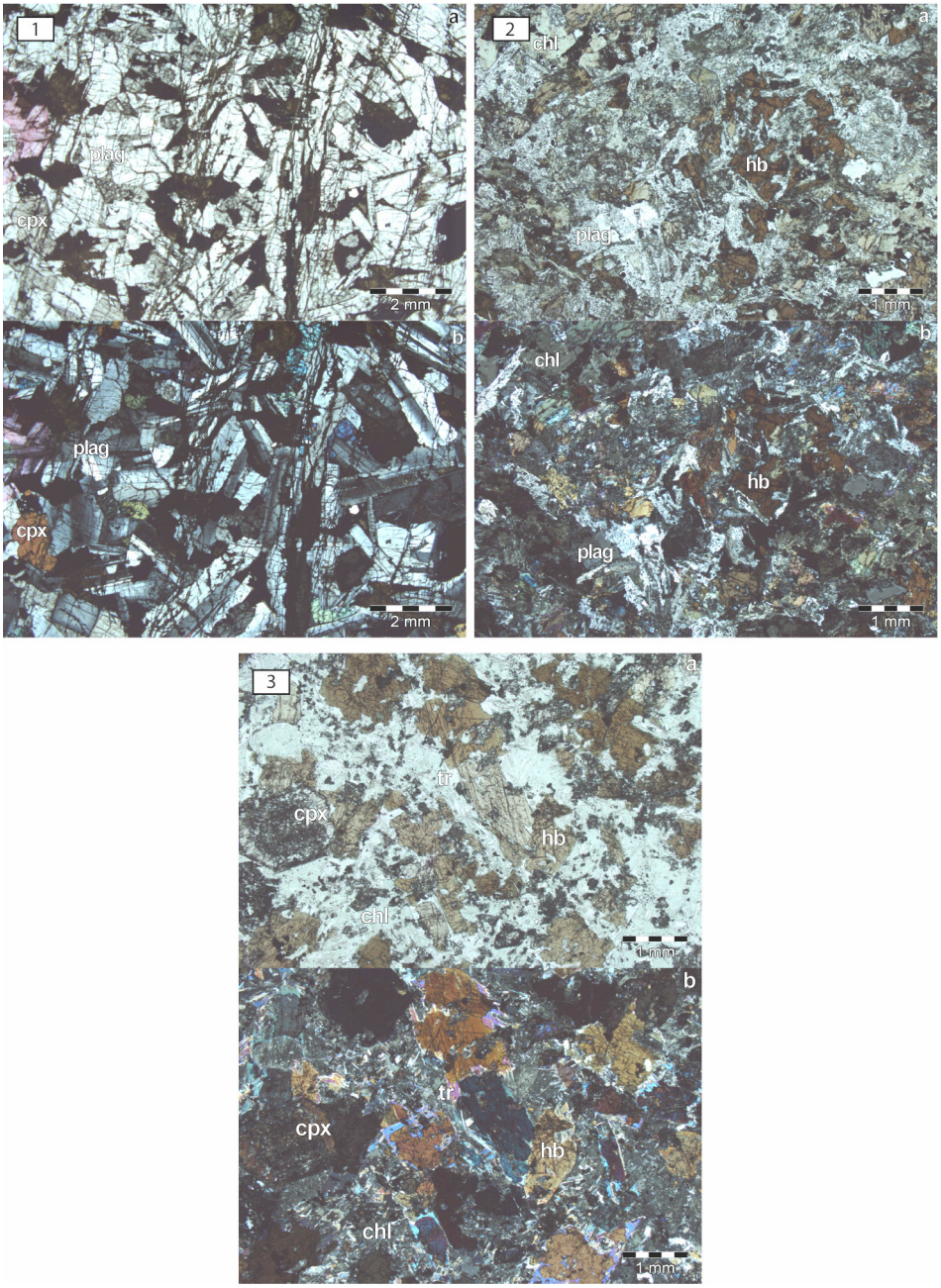

Fig. 2.2. Photomicrographs of representative thin sections: **a** plane-polarized light; **b** cross-polarized light. cpx, clinopyroxene; plag, plagioclase; chl, chlorite; hb, hornblende; tr, tremolite. **1** Cáceres, sample Ca11; **2** Pacho, sample Pa5; **3** Pajarito, sample Pj7.

2.6 MINERAL CHEMISTRY

2.6.1 Plagioclase

Plagioclase corresponds to compositions from labradorite to oligoclase (An_{54-10}) and rarely shows optical zoning, but in some cases, it presents smooth, normal zonation (Fig. 2.3).

Traces of albite are found in samples from Pajarito and Pacho, probably as products of low-grade metamorphic or hydrothermal overprints. Representative microprobe analyses appear in Table 2.2.

2.6.2 Clinopyroxene

Clinopyroxenes belong to the Ca-Mg-Fe "quadrilateral" pyroxenes (Table 2.3; Fig. 2.4a). They are classified, according to Lindsey (1983), as pigeonite (Wo_{19-7}; Fs_{53-23}; En_{68-28}), augite (Wo_{45-8}; Fs_{43-5}; En_{59-24}), and diopside (Wo_{48-45}; Fs_{15-7}; En_{48-37}), as shown in Fig. 2.4b. The latter is restricted to rocks from Pajarito, whereas augite is the only clinopyroxene in the samples from Pacho. Both augite and pigeonite appear in rocks from Cáceres, where clinopyroxenes show zonation from pigeonite in the core to augite in the rims. The Mg# [$100Mg/(Mg + Fe^{+2})$] in clinopyroxenes decreases westward from Pajarito to Cáceres, from 91.5 to 35.3, as does the Mg# of the whole rocks. The concentrations of Cr and Ti in clinopyroxene also vary with the geographic position. For example, Cr_2O_3 decreases from Pajarito (0.86 wt %) to Cáceres (under detection limits), and TiO_2 shows the same trend from 2.7 to 0.3 wt%.

According to their SiO_2–Al_2O_3 contents, clinopyroxenes from the Cáceres and Pacho intrusions indicate crystallization from a subalkaline melt; Pajarito's clinopyroxenes suggest an alkaline one (Fig. 2.5a; LeBas, 1962). In addition, the preferential alkaline character in Pajarito is confirmed in the Ti vs. Ca + Na plot (Fig. 2.5b). In the Ti + Cr vs. Ca plot (Fig. 2.5c), most clinopyroxenes fall in the non-orogenic field, as confirmed by the clinopyroxene compositional trend in the Al_z vs. TiO_2 wt% diagram (LeBas, 1962; Loucks, 1990) in Fig. 2.5d. LeBas (1962) introduced Al_z to describe the proportion of tetrahedral sites occupied by Al. The compositional trend in the gabbroic clinopyroxenes clearly matches a rift-related tendency.

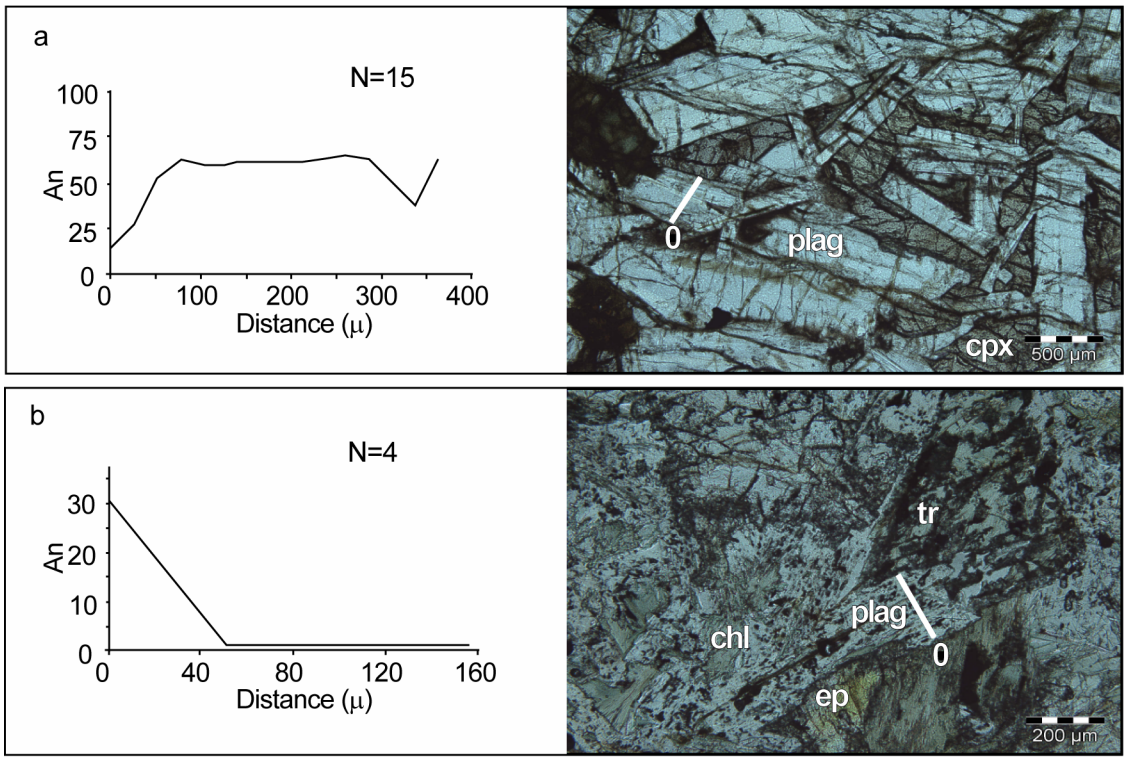

Fig. 2.3. Rim-to-rim variations in content of anortite (An). **a** Sample Ca8 from Cáceres. Plagioclase shows a very smooth normal zonation. **b** Sample Pa3 from Pacho showing albite composition. 0, starting point profile; N, number of analyses. plag, plagioclase; cpx, clinopyroxene; ep, epidote; tr, tremolite; chl, chlorite.

2.6.3 Amphibole

Amphibole occurs as brown to green individual crystals of hornblende. Colorless to green acicular tremolite/actinolite also grow around green to brown hornblendes and clinopyroxenes. In Cáceres, amphiboles are absent.

In some Pacho and Pajarito samples, tremolite has a euhedral habit. It nucleates at older brownish hornblendes, which suggests a low-grade metamorphic or hydrothermal event. For the Pacho and Pajarito samples, the amphiboles are calcic; that is, $(Ca + Na)_B \geq 1.00$, and $Na_B < 0.50$. Depending on the values of Ca_B, $(Na + K)_A$, and Ti (atoms per formula unit [apfu]) in the mineral tetrahedral positions, the amphiboles in the rocks from Pacho and Pajarito are classified (Leake et al., 1997a) as follows: Cores: kaersutite and pargasite (identified in both localities), edenite and magnesiohornblende (only in Pacho), and tschermakite (only in Pajarito); Rims: actinolite (identified in both localities) and tremolite (only in Pajarito) (Fig. 2.6, Tables 2.4 and 2.5).

	Cáceres		Pacho		Pajarito	
Sample	Ca5	Ca8	Pa3	Pa5	Pj1	Pj2
SiO_2	53.00	54.24	68.13	69.45	67.71	69.29
TiO_2	0.06	0.11	0.00	0.01	0.00	0.02
Al_2O_3	29.69	21.68	19.65	19.81	19.99	19.78
FeO	0.86	8.57	0.02	0.07	0.46	0.10
MnO	0.02	0.13	0.03	0.00	0.00	0.02
MgO	0.00	3.28	0.00	0.00	0.08	0.00
CaO	10.96	5.88	0.13	0.04	0.26	0.10
Na_2O	4.17	5.71	11.97	11.88	11.71	11.81
K_2O	1.02	0.15	0.05	0.05	0.04	0.05
Total	99.78	99.74	99.98	101.30	100.25	101.18
Cations on the basis of 8 O atoms						
Si	2.41	2.54	2.98	2.99	2.96	2.99
Ti	0.00	0.00	0.00	0.00	0.00	0.00
Al	1.59	1.20	1.01	1.01	1.03	1.01
Fe	0.03	0.34	0.00	0.00	0.02	0.00
Mn	0.00	0.01	0.00	0.00	0.00	0.00
Mg	0.00	0.23	0.00	0.00	0.01	0.00
Ca	0.53	0.29	0.01	0.00	0.01	0.00
Na	0.37	0.52	1.02	0.99	0.99	0.99
K	0.06	0.01	0.00	0.00	0.00	0.00
Cr	0.00	0.00	0.00	0.00	0.00	0.00
Sum	5.00	5.13	5.02	5.00	5.02	5.00
Ab (mol%)	44	64	99	99	97	99
An (mol%)	56	27	1	1	3	1
Or (mol%)	0	8	0	0	0	0
	Labradorite	Anortite	Albite	Albite	Albite	Albite

Table 2.2. Representative microprobe analyses of plagioclase from the EC.

	Cáceres				Pacho		Pajarito				
Sample	Ca1	Ca10	Ca11	Ca16	Pa1*	Pa5	Pj1	Pj1	Pj1	Pj2	Pj7
SiO_2	51.60	49.56	50.75	52.64	54.15	50.61	46.44	49.64	47.22	47.73	46.46
TiO_2	0.84	0.47	0.98	0.31	0.10	0.11	2.74	1.35	1.66	2.14	2.4
Al_2O_3	1.38	0.55	1.43	0.74	1.85	6.05	8.28	6.48	8.46	6.98	8.02
FeO(t)	12.76	31.31	14.67	17.62	13.28	13.57	6.03	5.19	4.96	5.17	5.12
MnO	0.38	0.50	0.28	0.25	0.11	0.21	0.06	0.06	0.09	0.11	0.07
MgO	14.12	9.57	12.47	23.75	15.28	14.02	12.76	14.26	13.51	13.63	13.15
CaO	18.48	7.98	18.82	4.03	12.73	12.48	23.15	22.34	22.29	23.38	23.18
Na_2O	0.32	0.09	0.40	0.09	0.18	0.63	0.41	0.53	0.64	0.31	0.37
K_2O	0.02	0.02	0.01	0.01	0.10	0.41	0.00	0.00	0.00	0.01	0.01
Cr_2O_3	0.11	0.06	0.00	0.06	0.05	0.17	0.08	0.25	0.63	0.27	0.86
Total	100.01	100.09	99.81	99.49	97.83	98.24	99.96	100.10	99.65	99.72	99.62
Cations on the basis of 6 O atoms											
Si	1.94	1.98	2.51	1.95	2.07	1.92	1.73	1.82	1.75	2.30	1.72
Ti	0.02	0.01	0.04	0.01	0.00	0.00	0.08	0.04	0.05	0.08	0.07
Al	0.06	0.03	0.08	0.03	0.08	0.27	0.36	0.28	0.37	0.40	0.35
Fe(t)	0.40	1.04	0.43	0.55	0.43	0.43	0.19	0.16	0.15	0.15	0.16
Mn	0.01	0.02	0.01	0.01	0.00	0.01	0.00	0.00	0.003	0.00	0.00
Mg	0.79	0.57	0.36	1.31	0.87	0.79	0.71	0.78	0.75	0.39	0.73
Ca	0.74	0.34	0.55	0.16	0.52	0.51	0.92	0.88	0.89	0.66	0.93
Na	0.02	0.01	0.02	0.01	0.01	0.05	0.03	0.04	0.05	0.02	0.03
K	0.00	0.00	0.00	0.00	0.00	0.02	0.00	0.00	0.00	0.00	0.00
Cr	0.00	0.00	0.00	0.00	0.00	0.01	0.00	0.01	0.02	0.02	0.02
Total	4.00	3.99	4.00	4.03	4.00	4.00	4.03	4.00	4.03	4.00	4.02
Mg#	68.3	35.3	45.9	73.8	67.2	64.8	86.2	86.4	91.5	72.5	89.4
Q	1.90	1.95	1.90	1.93	1.90	1.80	1.74	1.78	1.69	1.78	1.73
J	0.05	0.014	0.06	0.01	0.07	0.09	0.06	0.08	0.09	0.04	0.05
Wo%	36.58	17.45	37.93	8.18	25.45	25.10	50.76	43.52	49.58	43.96	50.98
En%	43.28	29.11	38.62	67.09	48.34	45.76	38.92	48.78	41.82	49.55	40.23
Fs%	20.14	53.44	23.46	24.73	26.21	29.15	10.33	7.70	8.60	6.49	8.79
	Augite	Pigeonite	Augite	Pigeonite	Augite	Augite	Diopside	Augite	Diopside	Augite	Diopside

Table 2.3. Representative microprobe analyses of clinopyroxenes from the EC. *High hydrotermal alteration.

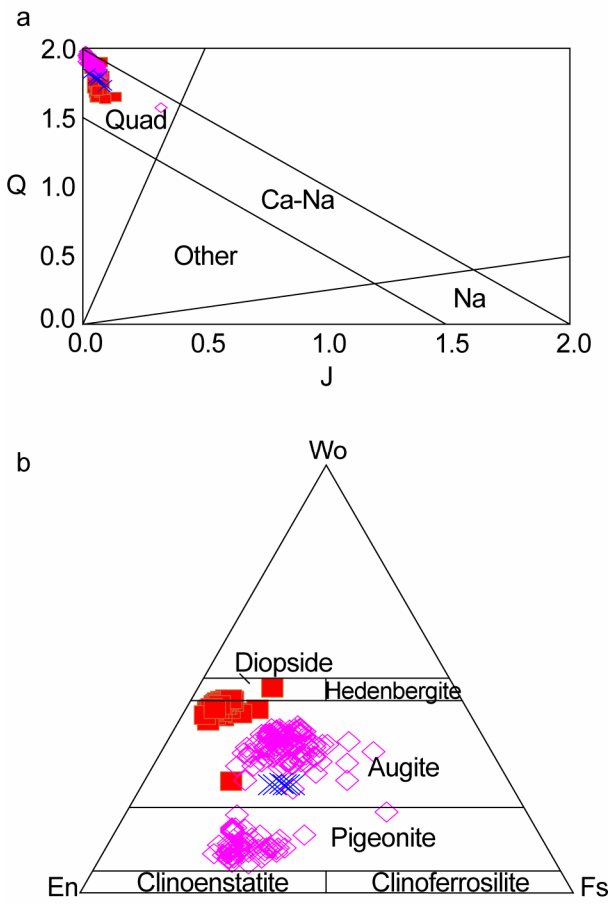

Fig. 2.4. Classification of pyroxenes according to Morimoto (1989) and Lindsey (1983). **a** Q vs. J (Q = Ca + Mg + Fe^{2+}; J = 2Na in apfu), showing that all specimens plot in the quadrilateral Ca-Mg-Fe pyroxenes. **b** Composition range of the Ca-Mg-Fe pyroxenes. Grey squares represent samples from Pajarito; crosses are from Pacho, and diamonds are from Cáceres. Symbol key serves for all other figures in this chapter.

Colour of the crystal	Pacho	Pajarito
Brown	Kaersutite Pargasite	Tschermakite Kaersutite Pargasite
Green	Edenite Magnesiohornblende Actinolite	Tremolite
Colourless	Actinolite	Tremolite Actinolite

Table 2.4. Classification of amphiboles according to their colour and location. See also figure 2.7.

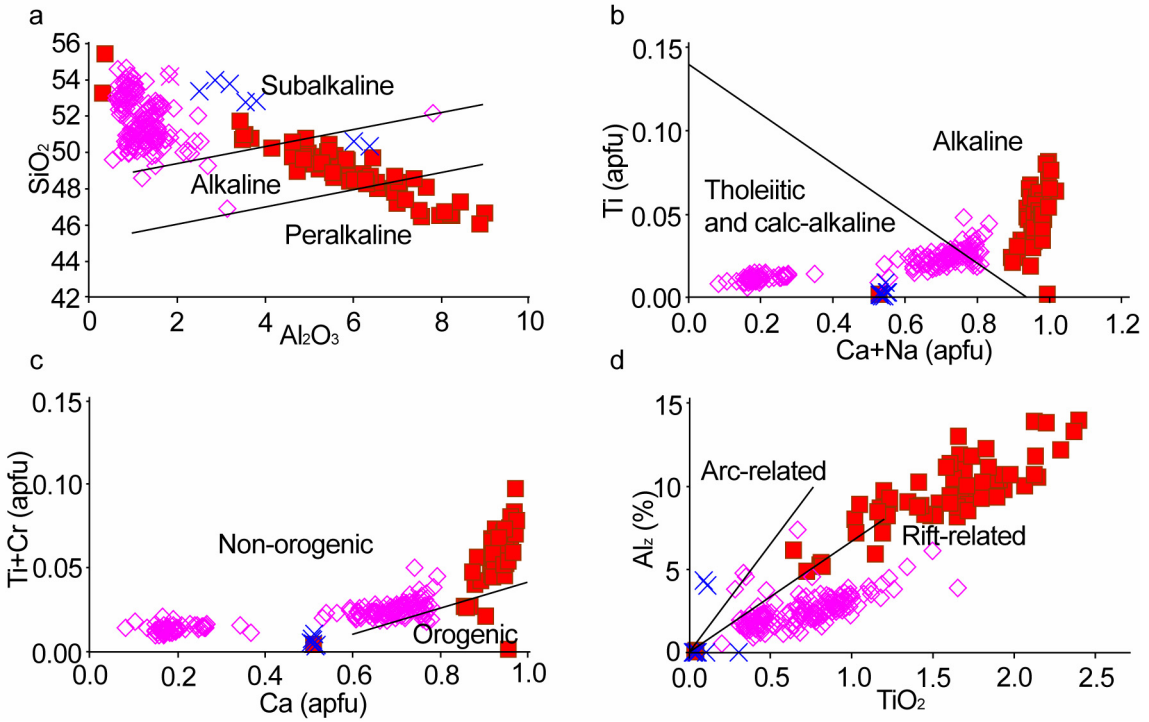

Fig. 2.5. Clinopyroxene discrimination diagrams. **a** SiO_2 vs. Al_2O_3 diagram for pyroxenes after LeBas (1962), showing the different character of the clinopyroxenes in each locality. Gabbros from Cáceres are clearly subalkaline, Pacho intrusions have a dual character between subalkaline and alkaline, and the rocks of Pajarito plot in both the alkaline and the peralkaline fields. **b** Ti vs. Ca + Na (apfu) diagram confirming the differences in character between the cpx and localities. **c** Ti + Cr vs. Ca (apfu) diagram in which, with a few exceptions, all samples plot in the nonorogenic setting. **d** Al_z (percentage of tetrahedral sites occupied by Al) vs. TiO_2 (wt%) after Loucks (1990), showing a very good defined trend related to rift magmatism products. Plots b and c after Leterrier et al. (1982). For location symbols, see Fig. 2.4.

The Al_2O_3–TiO_2 hornblende geothermometer, after Ernst and Liu (1998), though designed for metamorphic hornblende, should allow a rough estimation of the P-T conditions during crystallization. Our data show that the crystallization of the brown amphibole starts around 1000°C and 0.7 Gpa (Fig. 2.7). The rims of tremolitic composition around brown hornblende show lower crystallization temperatures (~850°C). The composition of the former amphiboles has been masked by subsequently formed euhedral tremolite, which crystallized under low-grade metamorphic conditions. In Pacho, the amphiboles crystallized at approximately 1000°C and 0.2 GPa.

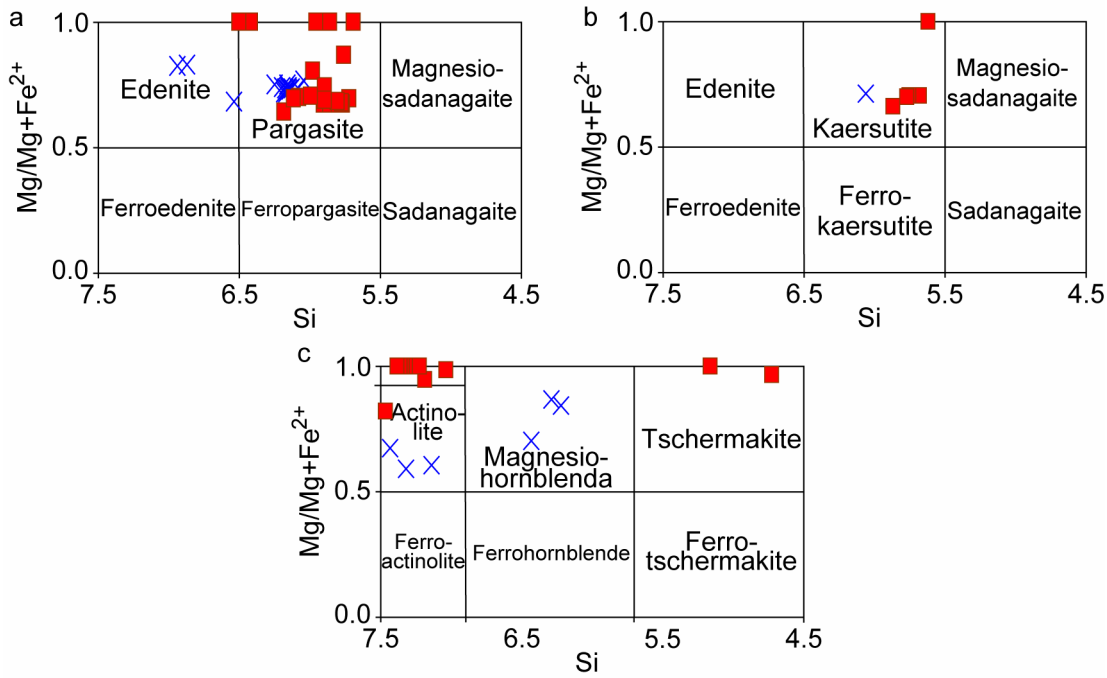

Fig. 2.6. Chemical variation of calcic amphiboles depending on the Mg/Mg + Fe^{2+} ratio and Si (apfu) content. **a, b** Diagram parameters: $Ca_B \geq 1.50$; $(Na + K)_A \geq 0.50$; **a** Ti < 0.50 or **b** Ti ≥ 0.50. **c** Diagram parameters: $Ca_B \geq 1.50$; $(Na + K)_A < 0.50$; $Ca_A < 0.50$. For location symbols, see Fig. 2.4.

	Pacho				Pajarito			
Sample	Pa5	Pa5	Pa5	Pa5	Pj7	Pj7	Pj7	Pj7
SiO_2	48.26	47.69	53.68	41.17	38.98	39.16	55.66	44.80
TiO_2	1.67	2.05	0.00	4.55	3.67	2.88	0.06	0.76
Al_2O_3	5.73	6.01	0.97	11.80	14.06	14.29	1.02	10.32
FeO	12.21	12.08	16.98	11.95	10.96	12.00	7.34	1473
MnO	0.18	0.16	0.36	0.22	0.20	0.18	0.21	0.39
MgO	16.01	15.86	13.14	13.16	12.63	14.19	20.31	12.03
CaO	9.95	9.85	12.77	11.36	12.48	11.05	12.46	11.11
Na_2O	3.13	3.41	0.09	2.98	2.23	1.95	0.07	2.85
K_2O	0.15	0.14	0.05	0.33	1.39	1.15	0.02	0.21
Total	97.37	97.32	98.04	97.71	96.77	96.99	97.19	97.26
Cations on the basis of 23 O atoms								
Si	6.93	6.87	7.85	6.06	5.86	5.69	7.74	6.42
Al^{iv}	0.97	1.02	0.15	1.94	2.14	2.31	0.17	1.58
Al^{vi}	0.00	0.00	0.02	0.11	0.35	0.13	0.00	0.16
Ti	0.18	0.22	0.00	0.50	0.42	0.32	0.01	0.08
Fe^{3+}	0.84	0.77	0.10	0.32	0.02	1.35	0.62	1.76
Fe^{2+}	0.62	0.69	1.98	1.15	1.36	0.11	0.24	0.00
Mn	0.02	0.02	0.04	0.03	0.03	0.02	0.02	0.05
Mg	3.43	3.41	2.86	2.89	2.83	3.07	4.21	2.57
Ca	1.53	1.52	2.00	1.79	2.01	1.72	1.86	1.70
Na	0.87	0.95	0.02	0.85	0.65	0.55	0.02	0.79
K	0.03	0.03	0.01	0.06	0.27	0.21	0.00	0.04
Sum	17.43	15.50	17.04	15.70	15.93	17.48	16.88	15.16
$Mg/(Mg+Fe^{2+})$	0.84	0.83	0.59	0.72	0.67	0.96	0.94	1.00
	Magnesiohornblende	Edenite	Actinolite	Kaersutite	Pargasite	Tschermakite	Tremolite	Pargasite

Table 2.5. Representative microprobe analyses of amphiboles from the EC.

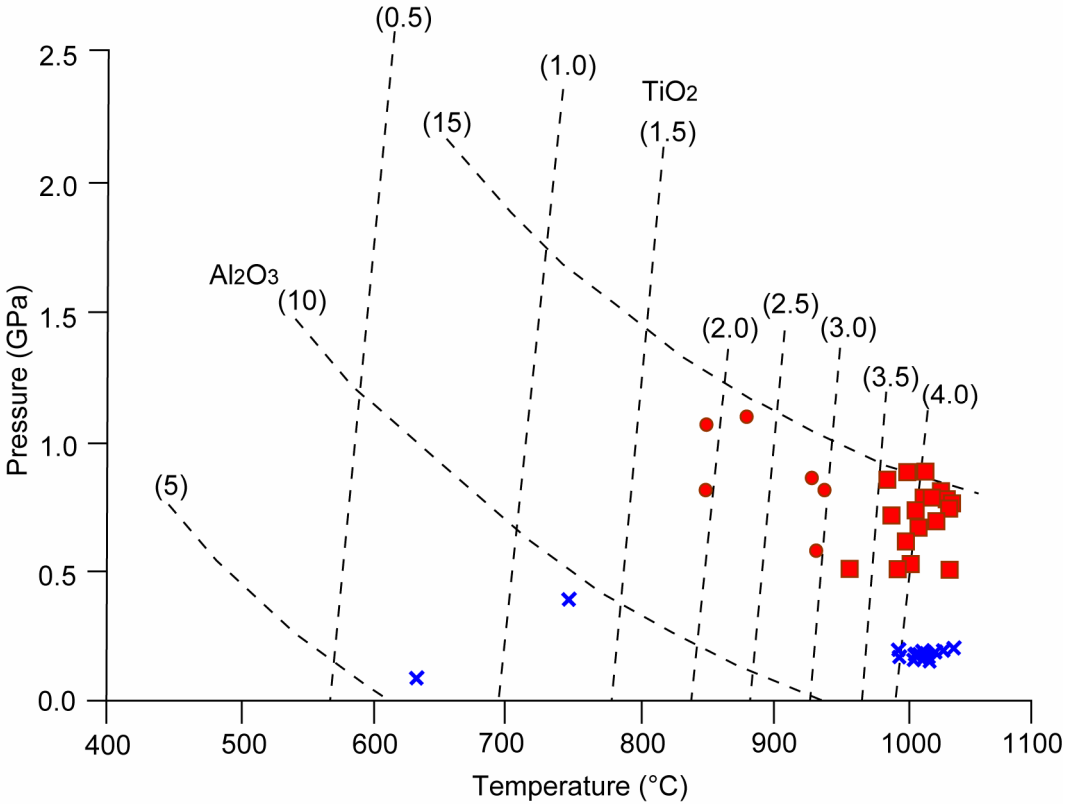

Fig. 2.7. Semiquantitative thermobarometer for hornblendes in the EC (Ernst and Liu, 1998). Circles represent crystal rims in Pajarito. For location symbols, see Fig. 2.4.

2.7 GEOCHEMISTRY

Twenty-eight gabbroic rocks from the EC were analyzed for major and trace element concentrations; 21 of these were analyzed for REE. Representative analyses appear in Tables 2.6 to 2.8.

The analyzed rocks have variable and sometimes very high H_2O and CO_2 contents and variable and sometimes very low alkali, suggesting that the major and trace element concentrations do not reflect the original magmatic compositions. In addition, in the Pacho and Pajarito localities, the rocks have been affected by a very low-grade metamorphic or hydrothermal overprint, as evidenced by the presence of epidote and euhedral tremolite. Despite their relatively high altered nature, information about magmatic genesis is preserved in early crystallized phases (Ca-Fe-Mg silicates) that were not affected by late-stage alteration processes. The concentrations of major and trace elements in clinopyroxenes display a very similar trend compared with the whole-rock chemistry. From west to east, the increasing Mg# and increasing alkalinity of the melts is a common feature in both whole-rock and mineral chemistry.

	Cáceres												
Sample	Ca1f	Ca1c	Ca2	Ca3f	Ca3c	Ca4	Ca5	Ca6*	Ca7*	Ca8	Ca9	Ca10	Ca11
wt%													
SiO_2	71.06	52.90	46.21	50.81	52.08	53.37	51.19	38.38	41.16	48.40	51.61	52.82	48.38
TiO_2	0.54	1.48	1.31	1.62	1.82	1.67	1.40	1.86	1.45	1.27	1.40	1.73	1.41
Al_2O_3	11.92	14.77	16.84	15.40	13.11	14.95	15.73	18.20	14.74	17.07	15.80	14.15	17.12
Fe_2O_3	4.65	10.38	11.89	11.25	11.85	10.74	10.71	11.24	9.19	12.13	11.01	11.63	12.46
MnO	0.06	0.16	0.13	0.14	0.17	0.15	0.14	0.17	0.17	0.14	0.14	0.16	0.17
MgO	1.95	5.99	3.02	6.68	6.81	5.19	6.63	4.26	3.31	6.54	6.74	5.23	5.60
CaO	2.32	8.26	9.62	8.59	8.43	8.36	8.64	7.74	9.08	8.02	8.22	8.51	7.99
Na_2O	5.18	3.41	3.34	3.04	3.05	3.48	3.19	0.36	1.22	3.21	3.28	3.26	3.51
K_2O	0.08	0.11	0.11	0.11	0.09	0.11	0.14	0.04	0.01	0.11	0.12	0.09	0.11
P_2O_5	0.06	0.11	0.12	0.11	0.13	0.13	0.10	0.11	0.09	0.09	0.11	0.12	0.09
H_2O	1.59	2.21	3.69	2.34	2.09	1.60	1.88	7.71	5.08	3.15	1.78	1.70	3.21
CO_2	1.22	0.87	4.26	0.42	0.67	0.58	0.88	10.52	14.81	0.40	0.33	0.74	0.45
Total	100.62	100.64	100.54	100.53	100.31	100.32	100.63	100.57	100.31	100.52	100.54	100.15	100.52
ppm													
Ba	474	638	929	153	116	283	509	154	149	355	570	208	613
Rb	10	10	10	10	10	10	10	10	10	10	10	10	10
Sr	165	219	347	190	166	227	232	115	255	174	224	199	159
Pb							1						
U							0.2						
Zr	365	74	68	67	80	73	64	79	68	60	67	78	63
Nb	11	5	9	7	7	8	6	3	6	5	4	6	6
Y	65	24	28	23	30	26	23	35	33	27	23	31	33
La	14.26	4.43	4.15	3.83	5.08		3.98	3.52		2.75		4.82	
Ce	31.74	10.62	9.61	9.23	12.34		9.37	8.78		6.88		11.77	
Pr	4.26	1.38	1.10	1.23	1.59		1.15	1.19		0.88		1.57	
Nd	20.02	7.40	6.61	6.52	8.75		6.57	6.39		5.11		8.42	
Sm	6.77	2.81	2.49	2.55	3.45		2.47	2.66		2.21		3.24	
Eu	0.88	1.12	1.03	1.10	1.33		1.06	0.69		0.97		1.31	
Gd	8.95	4.17	3.89	3.80	5.10		3.69	4.44		3.71		4.79	
Tb	1.59	0.71	0.69	0.63	0.87		0.62	0.84		0.67		0.79	
Dy	9.97	4.28	4.43	3.92	5.28		3.79	5.69		4.42		4.97	
Ho	2.06	0.82	0.87	0.79	0.98		0.71	1.24		0.91		0.96	
Er	5.96	2.35	2.74	2.19	2.93		2.12	3.86		2.87		2.76	
Tm	0.90	0.33	0.40	0.31	0.42		0.30	0.57		0.42		0.41	
Yb	5.73	2.01	2.53	1.89	2.52		1.83	3.77		2.71		2.38	
Lu	0.82	0.29	0.38	0.27	0.36		0.27	0.56		0.41		0.34	
Sc	6.71	24.31	19.59	22.53	28.18		19.58	34.62		22.59		25.00	
V	35	178	150	186	216	187	160	263	214	164	156	188	192
Cr	63	296	91	288	410	220	161	151	117	114	163	185	112
Ni	12	46	81	75	41	32	99	109	119	147	95	29	103
Zn	43	91	101	97	105	98	101	93	450	104	95	105	102
Mg#	30.11	37.36	21.71	37.99	37.31	33.19	38.97	31.80	31.17	35.92	38.56	31.70	31.89
Sr_n/P_n	2.48	1.79	2.40	1.55	1.07	1.57	1.90	0.78	2.02	1.75	1.83	1.38	1.43
Ba/Nb	43.01	120.14	108.40	20.55	16.74	34.01	87.56	49.60	26.75	66.29	129.53	35.30	108.60

Table 2.6. Whole rock analyses of plutonic rocks from Cáceres. * Highly hydrotermal altered samples. f: fine crystal-size; c: coarse crystal-size.

	Pacho					
Sample	Pa1	Pa2*	Pa3	Pa4	Pa5	Pa6
wt%						
SiO_2	44.89	44.00	48.40	47.35	45.93	46.27
TiO_2	1.64	1.70	1.90	1.51	1.73	1.75
Al_2O_3	13.61	12.93	16.53	17.93	14.66	14.59
Fe_2O_3	14.68	6.01	10.32	10.29	13.47	12.79
MnO	0.14	0.10	0.11	0.09	0.14	0.12
MgO	10.23	3.62	6.06	6.17	9.93	10.23
CaO	6.48	9.75	9.46	5.43	6.25	6.00
Na_2O	3.21	6.80	2.96	5.41	3.28	3.02
K_2O	0.04	0.16	0.06	0.01	0.14	0.13
P_2O_5	0.37	0.31	0.32	0.23	0.26	0.26
H_2O	4.61	0.82	3.70	4.32	4.56	4.89
CO_2	0.59	13.95	0.56	1.56	0.34	0.27
Total	100.50	100.16	100.38	100.30	100.68	100.33
ppm						
Ba	495	159	40	36	56	65
Rb	10	10	10	10	10	10
Sr	162	68	449	177	236	250
Zr	113	111	121	111	116	116
Nb	8	11	8	8	11	8
Y	30	37	30	21	28	31
La	12.25		12.03	8.64	11.61	11.56
Ce	31.37		30.67	21.03	29.49	29.73
Pr	4.25		4.03	2.75	4.13	4.00
Nd	19.75		19.24	12.95	18.73	18.55
Sm	5.18		5.09	3.34	4.95	4.97
Eu	1.60		2.31	1.15	1.72	1.69
Gd	5.80		5.88	3.85	5.74	5.82
Tb	0.89		0.91	0.58	0.91	0.92
Dy	5.21		5.67	3.70	5.51	5.56
Ho	0.98		1.10	0.75	1.12	1.11
Er	2.91		3.19	2.18	3.16	3.18
Tm	0.43		0.46	0.34	0.46	0.46
Yb	2.66		2.82	2.11	2.89	2.91
Lu	0.40		0.41	0.32	0.42	0.42
Sc	31.76		36.91	33.19	39.38	36.57
V	209	141	234	221	218	228
Cr	404	174	171	155	385	397
Ni	92	42	66	28	112	140
Zn	48	<10	13	<10	87	128
Mg#	42.53	33.35	38.07	39.03	43.76	45.93
Sr_n/P_n	0.37	0.16	1.19	0.66	0.76	0.80
Ba/Nb	59.84	14.67	4.74	4.47	5.12	8.31

Table 2.7. Whole rock analyses of plutonic rocks from Pacho. * Highly hydrotermal altered samples.

Furthermore, the high CO_2 concentrations of the analyzed rocks do not correlate directly with the low K_2O values (i.e., Pj7, Pj8), which indicates that the low content of the alkali is not a function of weathering in the studied samples. Moreover, those samples with high CO_2 do not necessarily have high Ba concentrations (i.e., Ca6, Ca7), so any assumption based on a non-magmatic origin of this large ion lithophile element (LILE) should be eliminated. However, calcite replaces clinopyroxene mainly at the rims, explaining the recurrent high CO_2 values, especially in samples from Pajarito.

Arbitrarily, samples whose loss on ignition (LOI = H_2O + CO_2) exceeds 14 wt% are not plotted in the diagrams to avoid any misinterpretations resulting from extreme weathered samples. Total Fe is reported as Fe_2O_3, and all major element data were normalized to 100 wt% on an LOI free basis to allow comparisons in the discrimination diagrams.

	Pajarito								
Sample	Pj1	Pj2	Pj3	Pj4*	Pj5*	Pj6	Pj7	Pj8	Pj9*
wt%									
SiO_2	42.86	40.81	39.50	41.15	43.63	43.96	41.15	42.97	39.54
TiO_2	1.75	1.81	1.70	1.52	1.74	1.56	1.68	1.98	1.83
Al_2O_3	11.59	11.75	9.99	11.93	13.49	14.58	10.32	11.15	14.82
Fe_2O_3	10.03	10.37	10.48	9.82	10.53	10.51	11.13	10.44	7.53
MnO	0.19	0.18	0.17	0.16	0.19	0.15	0.19	0.20	0.19
MgO	14.94	14.60	15.48	7.79	5.49	5.49	18.56	16.20	4.02
CaO	11.31	10.75	8.74	9.11	7.64	8.59	10.33	9.82	10.85
Na_2O	1.97	1.86	0.28	0.29	0.09	4.17	0.72	1.26	0.63
K_2O	0.32	0.46	0.10	1.14	2.34	0.04	0.40	0.05	2.56
P_2O_5	0.47	0.54	0.43	0.23	0.26	0.29	0.46	0.53	1.24
H_2O	4.11	4.66	7.43	3.87	3.71	4.31	5.11	5.75	2.81
CO_2	1.13	2.47	5.92	13.41	11.21	6.67	0.06	0.20	14.04
Total	100.69	100.24	100.12	100.43	100.31	100.32	100.11	100.55	100.06
ppm									
Ba	414	366	973	141	526	92	303	74	264
Rb	10	10	10	55	111	10	10	10	128
Sr	494	489	470	230	165	334	339	1204	114
Zr	152	148	129	125	140	143	126	162	220
Nb	70	75	55	35	39	38	60	78	122
Y	28	26	21	23	23	28	19	21	28
La	41.26	44.66			24.78	27.76	37.73	44.72	56.20
Ce	78.49	84.22			48.28	52.99	72.41	85.39	100.20
Pr	8.32	9.22			5.21	5.61	7.83	9.20	9.94
Nd	36.00	38.48			23.09	25.05	33.64	39.28	41.45
Sm	6.58	6.80			4.75	5.18	6.01	7.12	7.46
Eu	1.93	2.05			1.55	1.67	1.83	2.09	2.42
Gd	5.96	6.11			5.02	5.37	5.48	6.36	7.23
Tb	0.81	0.87			0.76	0.81	0.78	0.90	0.96
Dy	4.61	4.72			4.45	4.61	4.22	4.88	4.96
Ho	0.83	0.87			0.80	0.83	0.76	0.87	0.90
Er	2.24	2.31			2.33	2.36	2.04	2.38	2.49
Tm	0.33	0.33			0.34	0.34	0.30	0.35	0.38
Yb	1.98	2.02			2.06	2.07	1.78	2.06	2.32
Lu	0.29	0.29			0.30	0.30	0.26	0.30	0.34
Sc	36.18	26.63			24.63	23.79	26.75	35.04	12.76
V	200	195	201	181	195	196	188	205	152
Cr	584	565	572	347	201	216	563	610	45
Ni	338	320	398	165	70	77	439	363	60
Zn	151	133	76	132	559	187	167	169	<10
Mg#	61.18	60.41	63.24	56.92	38.21	37.12	63.98	62.33	39.32
Sr_n/P_n	0.89	0.70	0.85	0.75	0.48	0.91	0.62	1.94	0.07
Ba/Nb	5.88	4.91	17.54	4.04	13.33	2.44	5.04	0.95	2.16

Table 2.8. Whole rock analyses of plutonic rocks from Pajarito. * Highly hydrotermal altered samples.

The mafic samples from the EC show SiO_2 concentrations of 44–55 wt%. They are classified (Streckeisen, 1976) as gabbros, pyroxenic-hornblendic gabbros, hornblendic gabbros

and pyroxenic hornblendites on the basis of the mineralogical composition (Fig. 2.8). One sample with SiO_2 of approximately 71% is classified as a tonalite, since it does not have potassic feldspar. The Al_2O_3 contents range between 10–18 wt%.

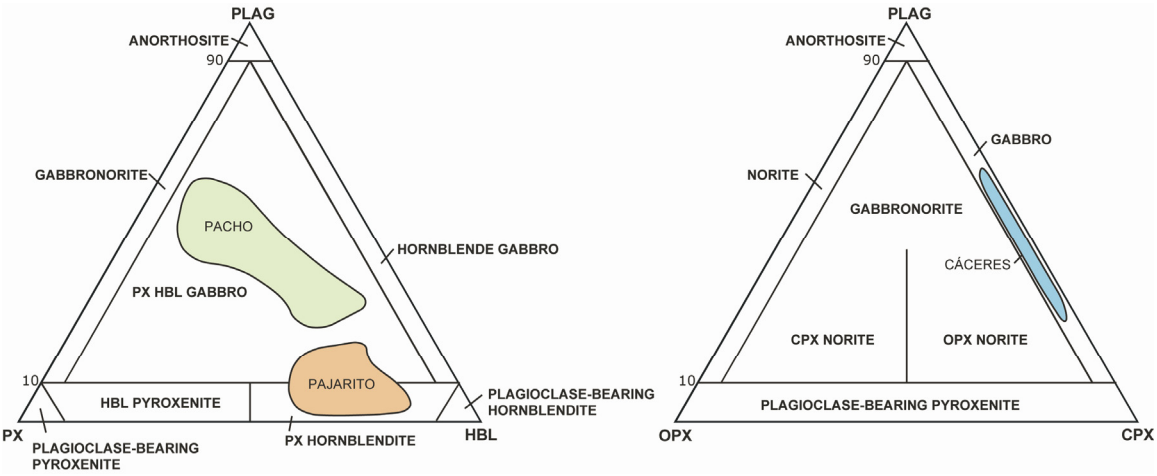

Fig. 2.8. Mineralogical classification of the plutonic rocks from the EC (Streckeisen, 1976).

MgO contents differ depending on the location. In Cáceres, these concentrations are the lowest, ranging from 2–7 wt%; in Pacho, they range between 6–14 wt%; and Pajarito samples have the highest Mg ratios, reaching contents up to 18 wt%. Nearly the same tendency is shown by the Mg# [100MgO/(MgO + FeO*) in mol. %]. The lowest Mg# corresponds to the rocks of Cáceres (22–39), intermediate values are recorded in Pacho (38–46), and the highest Mg# occurs in the rocks of Pajarito (37–64). The data indicate that the most primitive mafic melts were emplaced in Pajarito, in agreement with the high Ni (>150 ppm) and Cr (>200 ppm) concentrations (Wilson, 1993) of these samples. The variation diagrams based on Mg# vs. major elements (Fig. 2.9) show that MgO and TiO_2 have positive correlations in the Cáceres samples; there is no preferential correlation for the other oxides. In Pacho, the correlation is positive for MnO, MgO, TiO_2, and K_2O and negative for Fe_2O_3, Al_2O_3, Na_2O, and CaO. In Pajarito, these diagrams show that MgO and SiO_2 have positive correlations; Fe_2O_3, Al_2O_3, Na_2O, TiO_2, and P_2O_5 have negative correlations. If all rocks belong to one magmatic suite and were examined together, their MgO, MnO, CaO, TiO_2, K_2O, and P_2O_5 concentrations would correlate with the Mg number; whereas SiO_2, Na_2O, Fe_2O_3, and Al_2O_3 would show negative correlations. Variation diagrams of Mg# vs. trace elements (Fig. 2.10) for the rocks of Cáceres exhibit a positive correlation for Cr and negative for Y. Samples from Pacho show positive correlations in Cr, Ni, and Zn with Mg#; the correspondence is negative for Sr. Finally, the samples from Pajarito have

positive correlations with Cr, Ni, and V but negative with Y and Zr. In short, for all localities, as Mg# values decrease, Cr, Ni, Zr, and Sr decrease, and V and Y concentrations are independent.

Major and trace elements suggest a tholeiitic affinity for the Cáceres gabbroic intrusion, as shown in Figs. 2.5a, 2.5b, and 2.11a. The gabbroic rocks of Pacho fall in the subalkaline field (Fig. 2.11b), though in some diagrams, they are transitional between tholeiitic and alkaline, suggesting a heterogeneous magma source. Conversely, the Pajarito intrusions exhibit a well-defined alkaline affinity.

To evaluate melt-generating and -modifying processes in a qualitative or semi-quantitative way, the composition of the mafic rocks is normalized to chondrite (Evensen et al., 1978) and primitive mantle (Wood et al., 1979). Chondrite-normalized element concentrations show distinctive patterns for each locality (Fig. 2.12a). The Mid-Cretaceous gabbros of the EC exhibit an increase in LREE concentrations from west to east. The tholeiitic gabbros from Cáceres are 10–30 times chondritic and show a flat pattern, with La_n/Yb_n between 0.6 and 1.5, though the middle REE (Nd–Dy) display a very smooth peak. The thin tonalitic vein has a comparable flat pattern but is enriched in LREE with a La_n/Yb_n of approximately 1.7. Due to plagioclase fractionation in the magma (Powell and Bell, 1970) the REE pattern shows a negative (Eu* ~0.35) Eu anomaly.

The Pacho samples exhibit a LREE enrichment of 60–70 times chondritic and a negative slope with a La_n/Yb_n ratio of approximately 3. Eu exhibits a very smooth positive peak. All samples are REE enriched ($REE_n > 1$), and the flat pattern of the HREE suggests that residual garnet in the source region is of minor importance.

The alkaline samples from Pajarito indicate the highest LREE enrichment (up to 300 times) with a La_n/Yb_n of 8–16. This characteristic is expressed on the emphatic negative slope. The HREE also show a horizontal pattern (Fig. 2.12a) indicating that the melts of

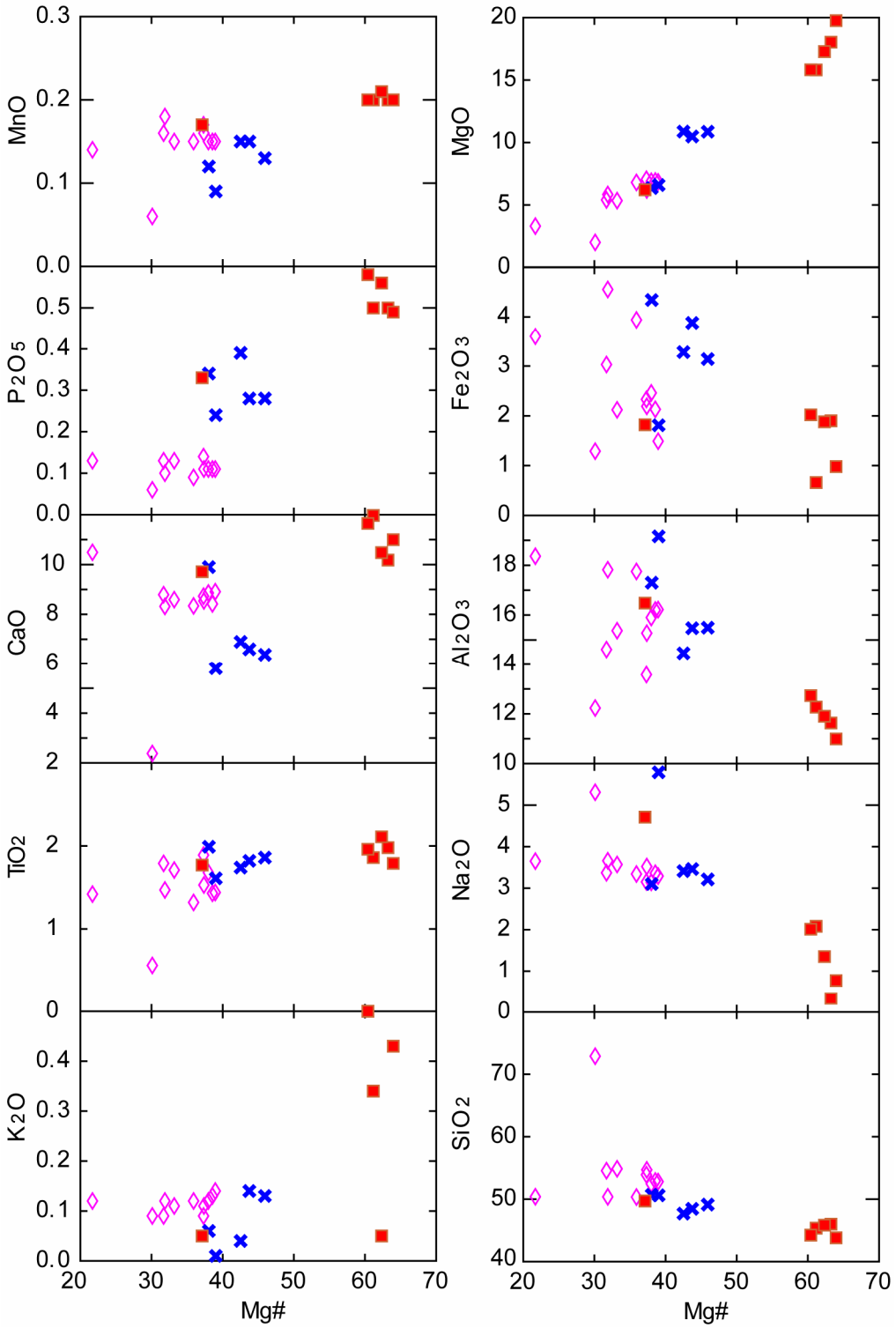

Fig. 2.9. Variation diagrams of Mg# vs. major elements for the basic intrusive bodies of the EC. For location symbols, see Fig. 2.4.

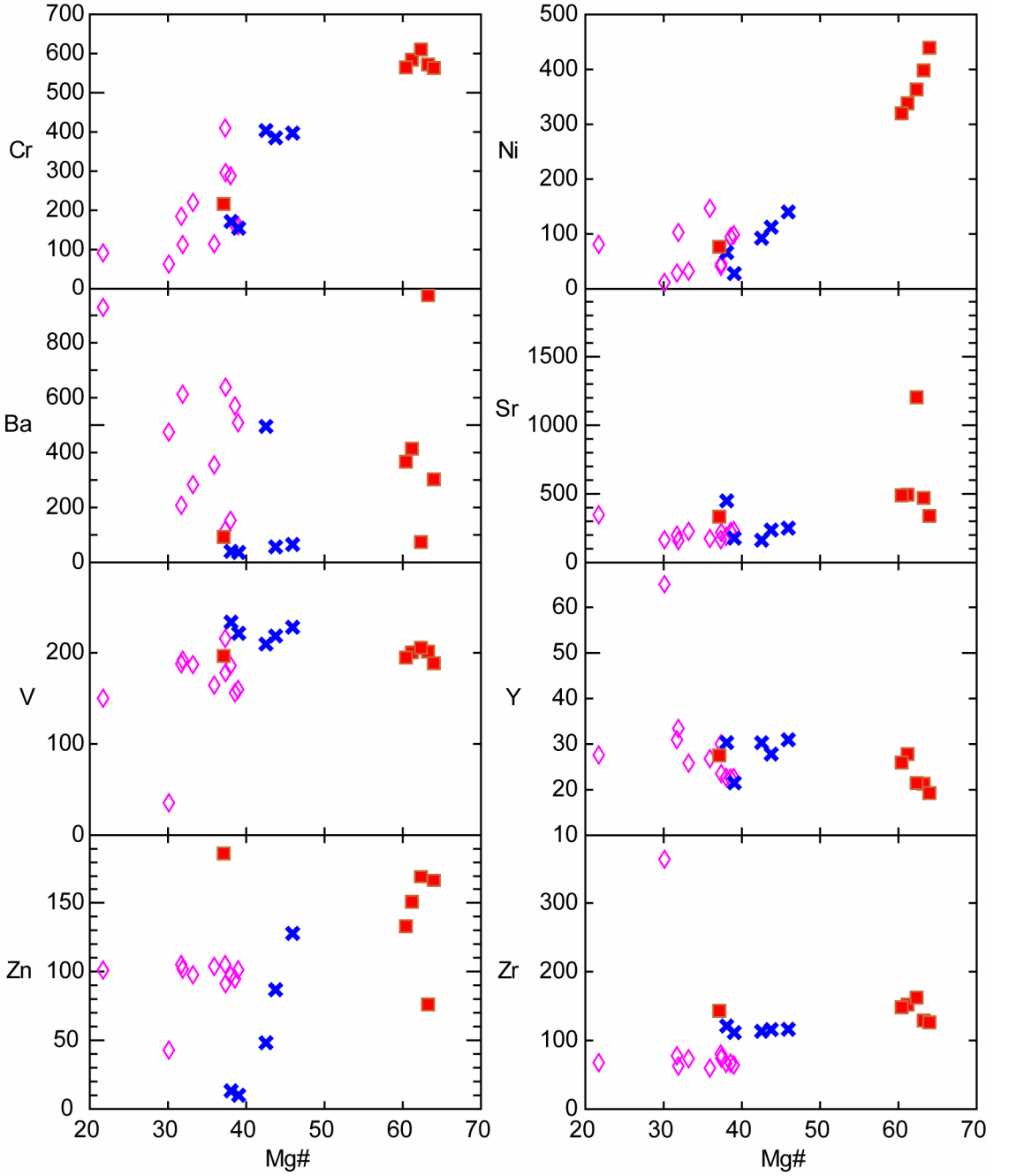

Fig. 2.10. Variation diagrams of Mg# vs. trace elements for the basic intrusive bodies of the EC. For location symbols, see Fig. 2.4.

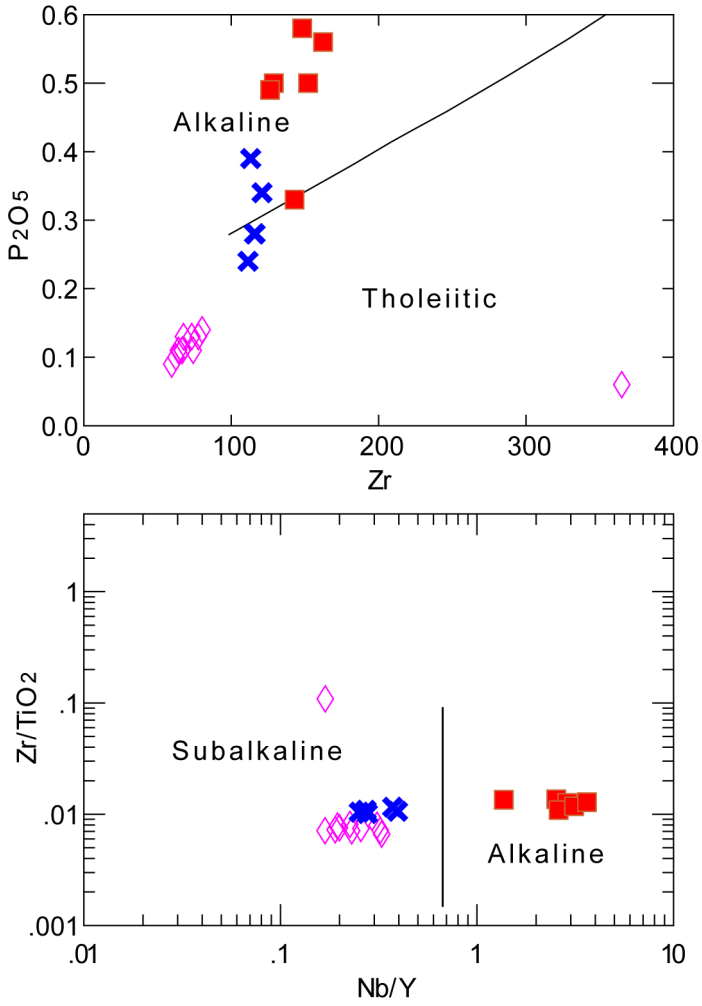

Fig. 2.11. Discrimination diagrams **a** P_2O_5 vs. Zr plot showing that the rocks of Cáceres plot in the tholeiitic field, Pajarito rocks are clearly alkaline, and Pacho rocks plot in between; **b** $(Zr/TiO_2)*0.0001$ vs. Nb/Y plot showing distinct trend between Pajarito and the Cáceres-Pacho group. Fields after Winchester and Floyd (1976). For location symbols, see Fig. 2.4.

Pajarito, and to a lesser extend those of Pacho, originated in a mantle region. In contrast, the investigated rocks of Cáceres do not show this pattern.

Samples of each locality normalized to primitive mantle composition (Wood et al., 1979) show a significant Rb and Ba enrichment (Fig. 2.12b). Whereas Rb is up to 10 times primitive mantle, Ba is around 100 times. Conversely, K is enriched in each sample compared with primitive mantle values. The samples of Cáceres have a slight but significant Sr-enrichment compared with Ce_n and P_n, whereas most samples of Pacho and Pajarito do not possess such a positive anomaly or have a very smooth one. All samples from Pajarito have high Nb concentrations, up to 100 times primitive mantle, which indicates a primitive melt composition, as described by the Mg, Ni, and Cr contents. In contrast, the intrusions from Cáceres and Pacho

have Nb values up to 10 times primitive mantle and a significant positive anomaly of this HFS element compared with K_n and La_n. Except for the tonalitic vein, Zr and Ti have very gentle positive anomalies in the primitive mantle-normalized concentrations. Therefore, significant fractionation of specific Nb-, Zr-, and Ti-bearing phases during and after melt generation did not occur. In comparison with modern analogues (Pearce, 1982), the magmas were not generated in a volcanic or magmatic arc (i.e., subduction-related environment) in a strict sense.

Most samples of Cáceres have high concentrations of Ba, which suggests a metasomatized mantle source. These fluids are known from reaction-enhanced releases during subduction and transformation of the subducting slab. Ba/Nb ratios greater than 30 are typical of melts produced in a metasomatized mantle wedge above a dehydrating subducting slab (Hildreth and Moorbath, 1988). The mafic rocks from Cáceres have Ba/Nb ratios of around 15–120; those from Pacho and Pajarito are less than 20.

Furthermore, high Sr_n/P_n (>2) may indicate slab-derived fluids (Borg et al., 1997); whereas the samples from Cáceres have a Sr_n/P_n up to 2.5, most samples of Pacho and Pajarito have values lower than 1. Therefore, the westernmost locality records a region of a mantle contaminated with fluids similar to those that result from the devolatilization of a subducting slab. The westernmost melts are clearly different from melts without or very low evidence of metasomatic fluids in the easternmost locality (Pajarito). U and Pb concentrations in Cáceres are very low, indicating that assimilation of sediment or continental material is of minor importance.

2.8 EVOLUTION OF THE MAFIC MAGMATISM IN THE EC

During Jurassic times, an active subduction zone was present to the west of the Paleo-Central Cordillera (Maze, 1984; McCourt et al., 1984; Pindell and Erikson, 1993; Toussaint, 1995), which acted as a volcanic arc. At that time, the studied area had a backarc basin position.

For Early Cretaceous times, the absence of a well-defined magmatic arc has been an obstacle to interpreting an active subduction zone (Sarmiento, 2001b). During the Early Cretaceous extension, relatively small volumes of mafic alkaline and tholeiitic magmatism affected the area that today corresponds to the EC. This magmatism shows a transition from a low to a high degree of partial melting, as well as from alkaline to tholeiitic affinity. If tholeiitic magmas are present in a continental rift, it can be assumed that the lithosphere reached the maximum amount of extension, generating tholeiitic mid-ocean ridge igneous rocks as final products (Wilson, 1993).

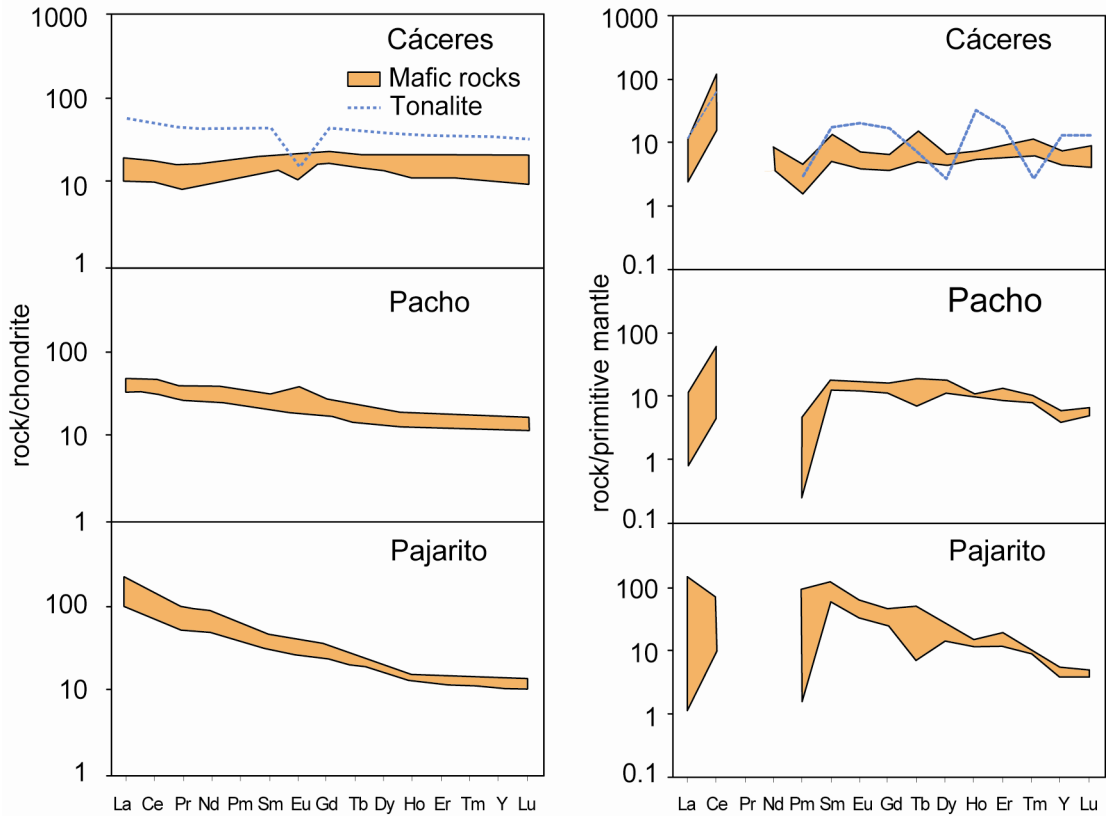

Fig. 2.12. **a** REE patterns. Chondrite-normalization after Evensen et al. (1978). **b** Spider diagram. Primitive mantle-normalization after Wood et al. (1979).

The investigated intrusions reached upper crustal levels, as displayed by amphibole barometry. In terms of the estimated pressure, the crystals formed at up to 0.7 GPa in the east, and the depth of crystallization was approximately 21 km. Sarmiento (2001b; Fig. 2.35) calculated the crustal thickness at the end of the Cretaceous using the total amount of stretching during the Mesozoic. He assumed an initial crustal thickness of 35 km before stretching and concluded that the crustal thickness ranged from 23 km in the east to 15 km in the west. This estimate suggests that the crystallization of the amphiboles took place at the Moho or the lowermost crust.

The gabbros from Cáceres show a unique geochemical signature. The chondrite and primitive mantle normalized values of the tholeiitic gabbros indicate a slightly enriched mantle source (REE_n ~ 10, T-MORB source; Schilling et al., 1983). High Ba/Nb and moderate Sr_n/P_n suggest that the mantle source probably was metasomatized by slab-derived fluids derived from an older subducted slab. In addition, the less enriched LREE reveal a higher degree of mantle melting than in the east.

The Pacho rocks, geographically between Cáceres and Pajarito, show La_n/Yb_n two times higher than those of the Cáceres rocks. The source region reflects the minor importance of residual garnet, as indicated by the normalized HREE. The influence of metasomatic fluids, suggested by the high Ba/Nb, is obvious but significantly lower than in the Cáceres samples and much higher than in Pajarito rocks.

The alkaline rocks of Pajarito in the eastern flank of the EC display the most primitive melts, as indicated by high Nb, MgO, Cr, and Ni contents. The observed high La_n/Yb_n reveal a low degree of mantle melting in the source region (Nakamura et al., 1989; Ramos and Kay, 1992) and a strongly LREE-enriched mantle source. An additional La enrichment is possible due to crystal fractionation (Haschke et al., 2002). Major and trace element signatures do not show any evidence of fluids from a subducted slab in the source region. Therefore, the Pajarito rocks can be interpreted as melts from a highly enriched mantle in an passive rift position. The ascending melt may form a magmatic reservoir at the crust–mantle boundary, as revealed by the formation of the kaersutitic amphibole (Fig. 2.6).

Hence, Mid-Cretaceous magmatism suggests the continuous evolution of mantle-derived melts. It could be interpreted as an evolutionary trend in which melts from an enriched mantle region were emplaced in the east (Pajarito). The influence of metasomatic fluids increased from east to west, which modified the mantle. The greatest influence is documented in samples from Cáceres.

Stratigraphic relations suggest that the melts were emplaced from the Hauterivian to the Cenomanian (Fabre and Delaloye, 1983). Consequently, the geochemical differences in REE shown in chondrite and primitive mantle-normalized patterns, as well as the contrast among Nb, Ti, and Zr contents and the evidence of metasomatized fluids in the western localities, could be explained by the interaction among a strongly (Pajarito) and a slightly (Cáceres) enriched mantle source. This explanation would detail the intrusion of Cáceres as the expression of a partially molten and metasomatized mantle. Pacho reflects the influence of both mantle systems, and Pajarito reveals the partial melting of "pure" enriched mantle.

2.9 DISCUSSION

During late Early-early Late Cretaceous, the area that today corresponds to the EC was affected by melts of tholeiitic–alkaline mafic composition. The stratigraphic observations indicate that the intrusions were emplaced in the Mid-Cretaceous, which coincides with the event of maximum lithospheric stretching. Although the rocks of the three different localities seem similar in age

and geodynamic position, strong diversities in their geochemical and petrological characteristics preclude simple melt genesis models. Mantle and chondrite-normalized values suggest changing melt sources from a slightly enriched mantle in the west to a highly enriched one in the east. In addition, the data reflect deeper crystallization and a lower degree of partial melting in the east than in the west. Mantle metasomatism in the source region by fluids similar to those resulting from the devolatilization of a subducting slab is significant in the west and minor in the east.

An alternative model involving a mantle plume could explain the continuous geochemical trends from east to west. Mantle plumes often have enriched parts on top of their partially molten head, followed by more depleted parts (Hofmann, 1997; Kerr et al., 2002). However, the lack of large volumes of magmatic rocks and the absence of tectonically controlled unconformities (Sarmiento, 2001b) during the Cretaceous suggest that a mantle plume did not affect the regional tectonics and magmatism.

The geochemical and petrological variation of the intrusions leads to the following model: The subcontinental mantle to the west (beneath Cáceres) was metasomatized by fluids derived from an older subducted slab. The mantle thus acted as a recorder of processes that happened in the past. The devolatilization of a subducted slab was active prior to melt generation. Maximum stretching took place when the subduction zone was situated to the west (Pindell and Tabbutt, 1995).

Another possible model proposes that convection cells in the mantle mobilized fluids released from the subducted slab and transported them to another region, far from the mantle wedge. To the east, the influence of metasomatized fluids decreased. We conclude that melts generated in the east were derived from a highly enriched mantle source, relatively unaffected by devolatilized fluids. The melts underwent the lowest degree of partial melting compared with the other intrusions. To the west, the degree of melting increased and the melts were influenced by a "contaminated" and a slightly depleted mantle region.

Consequently, a magmatic event produced as a consequence of continental rifting is proposed. That model agrees with the extensional tectonic regime assumed in northwestern South America from Triassic to Cretaceous times.

3. TRACE-ELEMENT CONTENT OF CLINOPYROXENES AND AMPHIBOLES IN GABBROS OF THE COLOMBIAN ANDES - POSSIBLE CONSTRAINTS FOR THE MAGMA SOURCE

Mónica Vásquez [a]

Max Wilke [a]

Uwe Altenberger [a]

Karen Rickers [b, c]

[a] *Institut für Geowissenschaften, Universität Potsdam, Karl-Liebknecht-Str. 24 14476 Potsdam-Golm, Germany*

[b] *Hamburger Synchrotronstrahlungslabor at Deutsches Elektronen-Synchrotron DESY, Notkestrasse 85, 22603 Hamburg, Germany*

[c] *GeoForschungsZentrum Potsdam, Division 4.1, Telegrafenberg, 14473 Potsdam, Germany*

3.1 ABSTRACT

This chapter presents a geochemical approach using major and trace element data of clinopyroxenes and amphiboles from gabbros located on both flanks of the Eastern Cordillera of the Colombian Andes in order to solve a site-specific problem: the genesis of the gabbroic rocks. The trace-element concentrations of the samples were analyzed by synchrotron radiation micro-X-ray fluorescence. The origin and original composition of the mantle melts responsible for the formation of the rocks have been evaluated on the concentrations of trace- and rare earth-elements of the studied minerals.

The characteristics of the magma source can be well distinguished between the samples coming from the eastern and western flanks of the Cordillera. Trace element patterns of clinopyroxenes and amphiboles suggest two different sources of magma, an enriched one in the east and a depleted one in the west. Based on these data we suggest divergences in the melting process between east and west.

The normalization of the trace-element concentrations of clinopyroxenes and amphiboles to whole rock values shows that the pattern follows very closely the one expected by the partition coefficients (D) between a melt and these phases. Few exceptions are the positive anomalies of Ba and Sr in the clinopyroxenes of La Corona. If we assume that the clinopyroxenes have not changed their original composition since their crystallization, then secondary processes like low grade metamorphism and/or weathering have weakly affected the bulk rock composition for these elements. The trace-elements of the first crystallized phases in these rocks, whose contents

have not been affected by secondary processes, reflect very accurately the chemical trend observed in the whole rocks. Our results document that the approach used here is a feasible alternative for investigating the magmatic origin of strongly altered magmatic rocks as long as relics of early crystallized phases are present that reflect the original composition of the rocks.

Keywords: Synchrotron radiation X-ray fluorescence analysis; Magma source; Amphiboles; Pyroxenes; Andes; Colombia

3.2 INTRODUCTION

Concentrations or normalized concentration patterns of trace elements of magmatic rocks depend on the composition and degree of melting of the magma source and the modification of the melts during transport, emplacement and cooling. Therefore, the rock composition and particularly the trace-element contents provide valuable information on melting processes, fractionation, and contamination and thus the geodynamic setting of the magmatic system (Wilson, 1989). This information can be used to better constrain models of the tectonic evolution of large parts of the earth's crust. However, hydrothermal or metasomatic processes, weathering or metamorphism may alter the initial composition of the rocks causing significant misinterpretations and uncertainties concerning the original source, particularly if bulk rock information is used.

Despite the altered nature of the analyzed samples, information about the magmatic genesis might still be preserved in the early-crystallized phases that show little to no overprinting by secondary processes. Ca-Fe-Mg-silicates (pyroxenes and amphiboles) are among the first crystallization phases of the primary magmas, and thus, they are products and expressions of the original melt composition. Therefore, patterns of trace- and rare earth-elements (REE) found in these phases should display information on the composition and degree of melting of the source region, fractionation and assimilation processes (Pearce, 1982; Hofmann, 1997; James et al., 2002).

The studied rocks come from both flanks of the central part of the EC of the Colombian Andes (Fig. 3.1). The rocks crop out in the form of dykes and sills and show gabbroic composition. They are the only known magmatic rocks of Cretaceous time in the area and therefore of big interest for the thermo-mechanical evolution of the crust during that time.

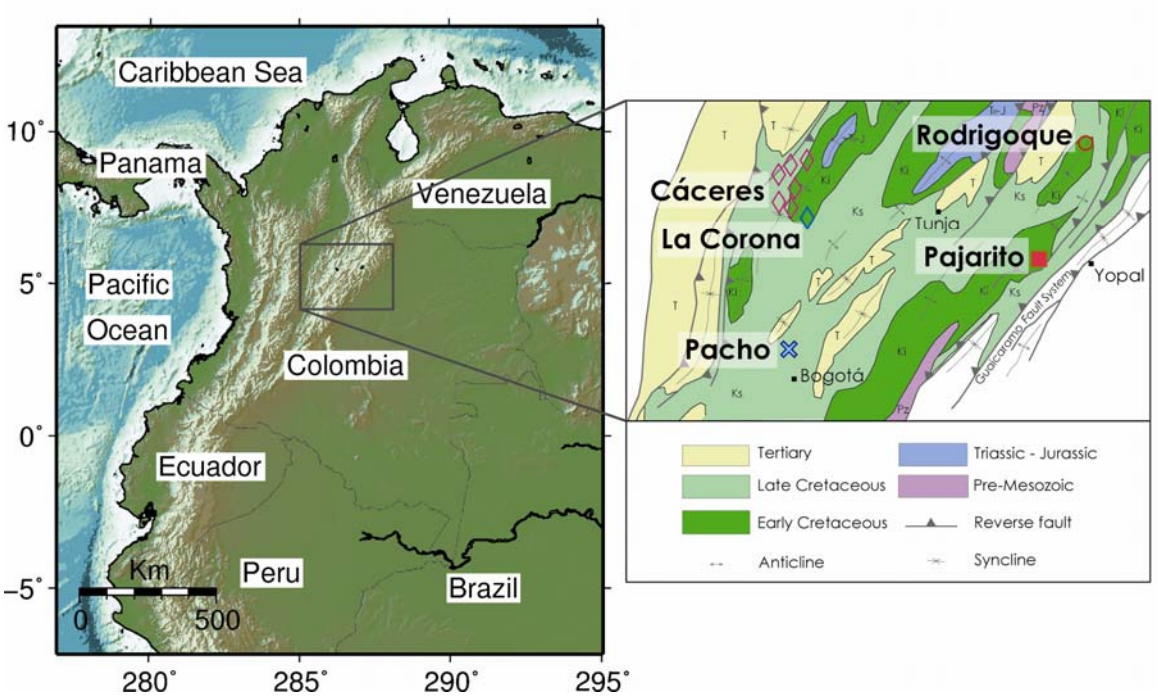

Fig. 3.1. Geological sketch map showing the studied mafic intrusions. 1. Cáceres - Puerto Romero; 2. Pacho (Tragarepas gabbro); 3. La Corona; 4. Pajarito; 5. Rodrigoque

Trace-element concentrations of the bulk rock show significant variations in the geochemical patterns of each intrusion, suggesting differences in the degree of partial melting, alkalinity, and influence of fluids i.e. from an older subducted slab (Vásquez and Altenberger, 2005). However, some of the magmatic bodies are highly altered by hydrothermal and/or low-grade metamorphism, which could have modified the original trace-element patterns of the whole rock and thus could lead to an ambiguous interpretation of the data.

Trace-element concentrations and ratios of immobile elements of early crystallized phases that are unaltered by secondary processes may still provide pristine information about the original source. A reconstruction of the magma-producing processes will contribute considerably to the understanding of the formation and development of the Northern Andean region.

The aim of this study is to chemically describe the early crystallized phases, such as clinopyroxenes and amphiboles and to verify the interpretation based on the whole rock in order to better constrain the source of magma responsible for their formation. Additionally, it is our purpose to highlight the usefulness of the applied method that may be used as a reliable alternative to other micro-analytical methods.

3.3 MAIN FEATURES OF THE MESOZOIC MAGMATISM OF THE EASTERN CORDILLERA

The Eastern Cordillera (EC) is the easternmost mountain range of the Colombian Andes, composed of a Precambrian and Palaeozoic polymetamorphic basement covered by a thick sequence of Mesozoic and Cenozoic sedimentary rocks, strongly deformed during the Neogene by thrusting and folding (Irving, 1971). The Early to Late Cretaceous magmatism consists of gabbros and hornblendites of tholeiitic to alkaline composition. Their emplacement coincides with the maximum lithospheric extension event of the former Colombian Cretaceous basin (Fabre and Delaloye, 1983; Sarmiento, 2001a). Depending on their location, these intrusions show a strong diversity in their geochemical characteristics suggesting a variety of sources from a slightly enriched mantle in the west to a highly enriched one in the east (Vásquez and Altenberger, 2005).

The data obtained by whole-rock analysis suggest a model, where the subcontinental mantle beneath the western part of the paleobasin was metasomatized by fluids derived from an older subduction phase. In addition, in the east, the rocks are the product of a highly enriched mantle source, which shows also a lower degree of partial melting than the western intrusions (Vásquez and Altenberger, 2005).

The chemical characteristics of the rocks show that the magmatic event was principally the result of continental extension. The differences in the degree of partial melting among the intrusions suggest that differences of the lithosphere from E to W were controlling their chemical features and also that such differences do not depend on the time of emplacement (Vásquez *et al.*, this volume).

3.4 ANALYTICAL TECHNIQUES

The concentrations of LREE, Cu, Zn, Ga, Rb, Sr, Y, Zr, Nb and Ba of pyroxenes and amphiboles of the mafic igneous rocks were determined by micro-synchrotron radiation-X ray fluorescence (μ-SRXRF) using the set-up at beamline L of the Hamburger Synchrotronstrahlungslabor (HASYLAB) at Deutsches Elektronen-Synchrotron (DESY) in Hamburg, Germany. The X-ray fluorescence was excited using the polychromatic beam from a bending magnet of the DORIS III positron storage ring (positron energy: 4.5 GeV; positron beam current during measurements: 80-140 mA; critical photon energy from bending magnet: 16.6 keV). The excitation spectrum was filtered using a Cu absorber of 0.2 mm thickness in order to reduce scattering background at low energies and to shift the energy maximum of the excitation spectrum to 40 keV (Rickers et al.,

2004). Collimation of the beam to the needed size was done using an adjustable cross-slit system and a straight glass capillary (Full-Width Half-Maximum of spot ca. 6.5 μm), which was measured by scanning a tungsten wire across the beam. The angle between beam and sample is 45° as well as the angle between sample and detector, resulting in a total excited area on the sample surface of around 6.5 x 9.1 μm. Fluorescence spectra were recorded using an energy-dispersive high-purity Ge detector set up at 90° to the incoming polarized beam in order to minimize the background from elastic scattering. Energy resolution measured at the energy of Mn K-alpha was 153 eV. The distance between the sample surface and the detector window was 22 mm. The accurate description of this method, as well as its fundamentals and general principles are available in Haller & Knöchel (1996), Lechtenberg *et al.*, (1996) and Koepke *et al.*, (2003).

The determination of the net peak areas of the lines of interest was performed using the AXIL software package (Analysis of X-ray spectra by Iterative Least-squares fitting) developed by Van Espen *et al.*(1977), Van Espen *et al.* (1992) and Vekemans *et al.* (1994). AXIL uses a non-linear least squares strategy in order to fit the measured spectra with suited mathematical functions.

The quantitative evaluation of spectra was performed employing the fundamental parameter quantification code "Quant" developed by L. Vincze (Vincze et al., 1993; Vincze et al., 1995a; Vincze et al., 1995b), which uses equivalent databases and is partially based on a general Monte Carlo simulation code for XRF-spectroscopy. This software allows to correct any matrix-effects on the fluorescence intensity if the composition of the major components are provided (major elements not detected by micro-XRF), i.e. the composition determined by electron-microprobe analysis. An additional correction is possible, by using one element that can be measured by both EMPA and micro-XRF, as internal standard for the quantification. We used here the Fe-content measured by electron-microprobe. The concentrations obtained from EPMA do only correspond to the composition close to the surface (a few μm in depth) of the sample. The high-intensity synchrotron beam and the K-line fluorescence radiation of elements with higher Z, however, penetrate the complete sample thickness. Therefore, the spatial resolution is governed by the sample thickness, and the excited volume will correspond to an elliptical tube. If the concentration of Fe varies with the thickness, as observed in some zoned specimens, there will be no control on that variation and the standardization to Fe data will introduce a further

	BCR-2G (N=6)				
Element	ion-probe data[1]	LIMS[2]	this study	std. dev.	Relative deviation from ion-probe data (%)
	129.5	140	135.2	2.9	4.4
Ga	22.0	22	22.0	0.7	-0.1
Rb	47.2	49	51.3	0.4	8.6
Sr	347.0	370	350.5	4.7	1.0
Y	39.0	35	24.4	1.5	-37.5
Zr	195.0	200	177.0	5.4	-9.2
Nb	14.0	13	13.4	0.2	-4.3
Sn					
Ba	698.0	660	832.6	15.9	19.3
La	25.6	25	30.9	0.5	20.6
Ce	53.7	52	62.4	0.5	16.2
Nd	30.4	32	40.7	0.9	33.8

	TB-1G (N=4)			
Element	LA-ICP-MS[3]	this study	std. dev.	Relative deviation from LA-ICP-MS (%)
Zn		68.4		
Ga		15.7		
Rb	139.0	136.2	7.0	-2.0
Sr	1298.0	1315.8	50.8	1.4
Y	24.7	17.8	7.0	-28.0
Zr	248.0	221.9	30.3	-10.5
Nb				
Sn		3.0		
Ba	931.0	1244.0	314.7	33.6
La	44.2	57.8	13.6	30.7
Ce	88.6	111.7	23.2	26.1
Nd	39.4	64.2	24.9	62.8

	NIST-612 (N=4)				Mean relative deviation of BCR-2G and NIST-612 (%)
Element	LA-ICP-MS[4]	this study	std. dev.	Relative deviation from LA-ICP-MS (%)	
Zn	39.8	34.7	2.9	-13.0	-4.3
Ga	36.9	32.2	3.2	-12.6	-6.3
Rb	31.3	29.2	2.2	-6.6	1.0
Sr	73.0	59.4	16.0	-18.6	-8.8
Y	31.5	27.8	5.5	-11.5	-24.5
Zr	35.2	31.1	3.1	-11.8	-10.5
Nb	37.2	32.8	4.6	-11.7	-8.0
Sn	36.2	40.7	21.0	12.4	12.4
Ba	38.1	50.6	32.8	33.1	26.2
La	34.0	45.3	28.4	33.2	26.9
Ce	33.9	47.6	30.8	40.6	28.4
Nd	34.7	46.6	35.0	34.2	34.0

Table 3.1. Calculation of standard deviation and relative deviation (%) of the measurements on the reference glasses BCR2G, NIST-612, and TB-1G. The obtained values were compared to recommended values from (1) Rocholl (1998), (2) Seufert and Jochum (1997), (3) Norman et al. (1998) and (4) Pearce et al. (1997). N= number of measurements.

uncertainty. Many clinopyroxene crystals of the locality of Cáceres are zoned, with variations of Fe content of about 21%. For this reason, the zoned minerals will not be used to propose hypotheses about the origin of the magmas in the discussion section. Due to the total volume of the sample, the point to be excited with the beam was carefully chosen with the aim of preventing problems related to sub-surface cracks and the presence of inclusions. The cracks might be filled with alteration phases, which may contain highly mobile elements like Ba and Sr.

The quantification procedure was checked on international geostandards. For the standard NIST-612 instead using Fe, we used Ca as internal standard since the concentration of Fe is very low. Table 3.1 shows the recommended concentration of trace elements of the reference glasses BCR-2G (Seufert and Jochum, 1997; Rocholl, 1998), TB-1G (Norman et al., 1998) and NIST-612 (Pearce et al., 1997) .

In general, the mean relative deviation shows low to intermediate values for most of the measured elements. In order to get a more particular view of the deviation observed, it is necessary to discuss each standard separately. The standard BCR-2G shows acceptable relative deviations for elements between Zn and Sr, as well as for Zr and Nb (< 10%). However, for Ba, LREE and especially Y, the deviation is much higher (between 16 and 38%). The results for the standard TB-1G presents acceptable relative deviations between 1.4 and 10.5% for Rb, Sr and Zr. Y, Ba and LREE show moderate to high relative deviations (up to 63% for Nd) with respect to the recommended values from Norman *et al.* (1998). The recommended values available for the powder TB for elements like Zn, Ga, and Sn (Govindaraju, 1994) have indicated that they cannot be taken as representative for TB-1G. The standard NIST-612 shows low to high relative deviations increasing up to ca. 41% for Ce. For the calculation of the mean relative deviation the data obtained of TB-1G were not taken into account and only average values of BCR-2G and NIST-612 were used. The highest relative deviation obtained, corresponds to Nd which reaches up to 34%. Despite the deviation observed for Ba, La, Ce, and Nd, the interpretation of chondrite-normalized patterns is not affected (see figures 4 and 6).

The major element concentrations of the analyzed phases were determined with Cameca SX50 and SX100 electron microprobes at the GeoForschungsZentrum Potsdam. The operation conditions were an acceleration voltage of 15 keV and a beam current of 20 nA.

3.4.1 Calculation of detection limits

The detection limits were determined on the reference glass standards BCR-2G and TB-1G. The calculation of the limits is given by

$$C_{MDL,i} = \frac{3\sqrt{I_{i,B}}\, C_i}{I_i}$$

where $C_{MDL,i}$ is the detection limit of element i with 99.86% confidence level in ppm, $I_{i,B}$ and I_i are the measured background and characteristic X-ray intensity of element i in counts for a given live time, and C_i is the concentration of element i in the standard sample in ppm (Haller and Knöchel, 1996). The detection limits for two different beam times (June 2004 and June 2005) are shown in Fig. 3.2. The ranges of C_{MDL} spans for the standard BCR-2G from 0.3 ppm for Nb up to 2 ppm for Zn. C_{MDL} for LREE are ca. 0.5 to 0.8 ppm. The C_{MDL} for the standard TB-1G, spans from 0.3 for Zr to 0.9 for Y and for LREE are ca. 0.5 to 0.7 ppm.

The synchrotron micro-XRF provides the possibility to determine contents of trace elements simultaneously and with high lateral resolution with an atomic number (Z) between 19 and 84, that is from K to Po by means of their K-lines. During the experimental sessions, it was proven that the chosen approach provided reliable quantitative data for trace elements with Z from 30 (Zn) to 60 (Nd) given the low concentrations encountered especially in clinopyroxenes, generally less than 150 ppm going down to 0.5 ppm.

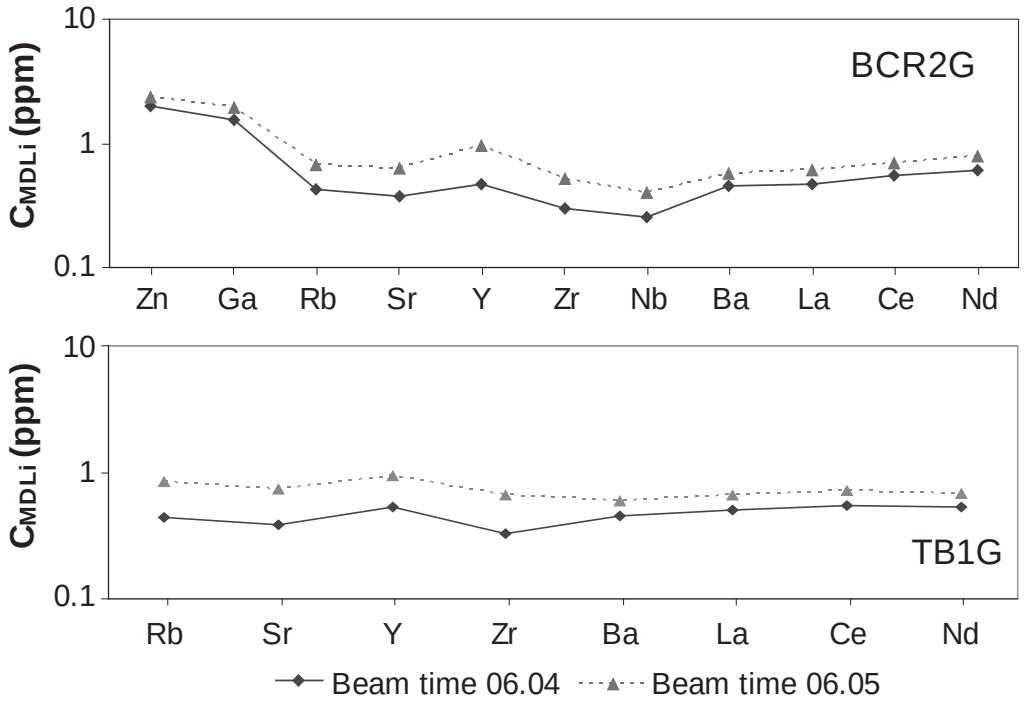

Fig. 3.2. Calculated minimum detection limits for the reference glass standards BCR-2G and TB-1G for two beam times (June 2004 and 2005)

3.4.2 Sample preparation

Sample cores of 1 inch in diameter were drilled from the rock sample, thinned to 100 μm and polished on both sides. During the analysis, the samples were separated from their glass mount in order to avoid high background from elastically scattered radiation from the glass slide and contributions to the spectra from elements of the glass. The thickness of the sample influences the quantified concentrations of the elements as the thickness affects the absorption and thus the fluorescence intensity (Koepke et al., 2003). The calculation of the element concentrations using Quant has shown that an uncertainty of ± 5 μm in the thickness of the sample results in an uncertainty between +0.5 to -0.3% for Zn and +4.1 to -3.9% for Nd.

3.5. MINERAL CHEMISTRY

3.5.1 Clinopyroxenes

Clinopyroxenes from five localities of the Eastern Cordillera have been studied. The composition of major elements from the intrusions of Cáceres, Pajarito, and Pacho have been described in Vásquez and Altenberger (2005). They belong to the Ca-Mg-Fe "quadrilateral" pyroxenes (Morimoto, 1989) and are classified as augite and pigeonite in Cáceres; augite in Pacho; and diopside and augite in Pajarito. The Mg# ($Mg/(Mg+Fe^{2+}$) decreases westward from Pajarito to Cáceres, as the Mg# of the whole rock does.

The composition of the pyroxenes from La Corona and Rodrigoque also correspond to Ca-Fe-Mg pyroxenes after the classification of Morimoto (1989) and were classified according to Lindsey (1983) as augite (Fig. 3.3a). The major element compositions of the pyroxenes are summarized in Table 3.2.

According to their SiO_2 and Al_2O_3 contents, the clinopyroxenes from Cáceres and Pacho intrusions crystallized from a subalkaline melt, whereas the clinopyroxenes from Pajarito suggest an alkaline origin (Vásquez and Altenberger, 2005). Although the intrusions of Pacho and Rodrigoque have also clinopyroxenes, the concentration of trace elements could not be determined due to the high stage of alteration of the crystals and the poor quality of the major elements obtained from EPMA. The SiO_2 (48.3% - 51.1%) and Al_2O_3 (2.8% - 5.1%) content of the clinopyroxenes in the intrusion of La Corona indicates crystallization from an alkaline melt.

Cáceres																					
Sample	Ca5											Ca10									
	1 - rim to core		2 - rim to rim			3 - rim to rim			4					1 - rim to rim						2
SiO_2	51.62	51.73	51.43	52.55	53.69	52.35	54.03	53.76	52.05	52.15		50.17	50.42	50.27	50.51	50.68	50.77	50.65	50.35		
TiO_2	0.89	0.85	0.68	0.42	0.35	0.53	0.37	0.54	0.35	0.33		0.86	0.94	1.00	0.93	0.86	0.81	0.72	0.75		
Al_2O_3	1.33	1.25	1.11	1.52	0.71	0.69	0.85	1.02	0.71	7.85		1.25	1.30	1.48	1.52	1.47	1.54	1.49	0.99		
FeO	14.90	14.27	16.02	16.72	18.83	22.38	16.93	17.16	23.05	10.76		16.46	15.75	15.22	14.04	13.70	13.15	13.51	17.93		
MnO	0.22	0.20	0.23	0.21	0.22	0.28	0.22	0.26	0.31	0.15		0.30	0.32	0.28	0.31	0.31	0.25	0.28	0.51		
MgO	13.89	14.11	13.00	21.24	22.90	19.46	23.57	22.75	18.83	16.14		13.03	13.21	13.41	13.79	14.32	14.66	14.35	12.86		
CaO	17.19	17.23	17.14	6.16	4.23	4.41	4.28	4.87	4.23	9.37		16.66	16.52	17.29	17.15	17.10	17.19	17.39	15.79		
Na_2O	0.32	0.33	0.33	0.11	0.08	0.06	0.05	0.10	0.08	2.27		0.29	0.27	0.29	0.32	0.32	0.28	0.30	0.17		
K_2O	0.01	udl	0.02	0.01	0.01	udl	udl	udl	udl	0.12		udl	udl	udl	0.03	udl	0.01	udl	0.01		
Cr_2O_3	0.02	0.02	0.04	0.13	0.05	0.01	0.09	0.17	0.09	0.10		0.03	udl	0.03	0.03	0.08	0.04	0.04	0.02		
Total	100.38	100.00	100.00	99.06	101.06	100.16	100.39	100.63	99.71	99.24		99.06	98.72	99.27	98.62	98.84	98.69	98.73	99.39		
Si	1.964	1.969	1.973	1.975	1.974	1.978	1.983	1.978	1.983	2.004		1.952	1.960	1.946	1.957	1.955	1.956	1.955	1.957		
Ti	0.025	0.024	0.020	0.012	0.010	0.015	0.010	0.015	0.010	0.010		0.025	0.027	0.029	0.027	0.025	0.023	0.021	0.022		
Al	0.060	0.056	0.050	0.067	0.031	0.031	0.037	0.044	0.032	0.356		0.058	0.060	0.067	0.069	0.067	0.070	0.068	0.045		
Fe	0.474	0.454	0.514	0.526	0.579	0.707	0.520	0.528	0.734	0.346		0.536	0.512	0.493	0.455	0.442	0.423	0.436	0.583		
Mn	0.007	0.007	0.007	0.007	0.007	0.009	0.007	0.008	0.010	0.005		0.010	0.010	0.009	0.010	0.010	0.008	0.009	0.017		
Mg	0.788	0.801	0.743	1.190	1.255	1.096	1.289	1.247	1.069	0.924		0.756	0.765	0.774	0.796	0.823	0.842	0.825	0.745		
Ca	0.701	0.703	0.704	0.248	0.167	0.178	0.168	0.192	0.173	0.386		0.694	0.688	0.717	0.712	0.707	0.709	0.719	0.658		
Na	0.024	0.024	0.025	0.008	0.005	0.005	0.004	0.007	0.006	0.169		0.022	0.020	0.022	0.024	0.024	0.021	0.022	0.013		
K	0.000	0.000	0.001	0.000	0.000	0.000	0.000	0.000	0.000	0.006		0.000	0.000	0.000	0.001	0.000	0.000	0.000	0.000		
Cr	0.001	0.001	0.001	0.004	0.001	0.000	0.003	0.005	0.003	0.003		0.001	0.000	0.001	0.001	0.002	0.001	0.001	0.001		
Total	4.043	4.039	4.039	4.037	4.028	4.019	4.020	4.025	4.020	4.207		4.053	4.043	4.058	4.052	4.055	4.054	4.058	4.042		
Mg#	0.48	0.50	0.45	0.56	0.55	0.47	0.58	0.57	0.45	0.60		0.61	0.61	0.64	0.66	0.68	0.69	0.69	0.58		
Q	1.33	1.32	1.34	1.28	1.32	1.34	1.29	1.28	1.35	0.99		1.90	1.92	1.89	1.90	1.90	1.90	1.90	1.92		
J	0.04	0.04	0.04	0.01	0.01	0.01	0.01	0.01	0.01	0.25		0.04	0.04	0.04	0.05	0.05	0.04	0.04	0.03		
Wo%	37.38	37.61	37.13	13.96	9.21	9.54	9.57	10.88	9.18	25.84		36.34	36.14	37.73	37.59	37.21	37.27	37.72	34.21		
En%	30.22	30.80	28.16	48.14	49.82	42.08	52.62	50.80	40.83	44.51		39.53	40.21	40.73	42.06	43.36	44.23	43.28	38.77		
Fs%	32.40	31.59	34.71	37.90	40.98	48.38	37.81	38.32	49.99	29.66		24.13	23.65	21.55	20.35	19.43	18.50	19.01	27.01		

Table 3.2 EPM analyses of clinopyroxenes from the Eastern Cordillera of Colombia. Cations calculated on the basis of six O atoms

Sample	Cáceres																			
	3		4 - rim to rim				5 - rim to rim				6 - rim to rim									
SiO_2	50.29	54.57	54.64	52.46	52.45	49.78	51.34	50.91	51.15	51.97	49.56	50.99	51.28	52.86	52.93	50.60	53.16	52.70		
TiO_2	0.78	0.20	0.34	0.66	0.70	0.77	0.80	0.76	0.95	0.78	0.47	0.74	0.76	0.43	0.44	0.35	0.43	0.43		
Al_2O_3	1.03	0.67	0.86	1.70	1.44	1.44	1.09	1.00	1.45	1.45	0.55	0.94	0.97	0.70	0.79	2.40	0.75	1.35		
FeO	18.55	16.66	17.52	10.39	13.42	15.33	18.55	18.84	15.93	14.51	31.31	18.31	18.24	21.74	20.43	23.21	21.71	21.68		
MnO	0.33	0.24	0.27	0.20	0.25	0.26	0.31	0.30	0.26	0.25	0.50	0.31	0.31	0.29	0.30	0.28	0.28	0.31		
MgO	11.78	23.77	24.44	16.56	16.36	13.81	13.15	11.42	13.42	14.91	9.57	12.12	13.52	20.11	21.11	19.06	20.97	19.57		
CaO	16.83	3.85	3.37	17.33	15.36	17.28	14.81	16.56	16.54	16.12	7.98	16.26	14.98	4.38	4.39	3.79	3.78	4.74		
Na_2O	0.26	0.20	0.03	0.26	0.21	0.22	0.20	0.23	0.28	0.26	0.09	0.22	0.20	0.07	0.06	0.07	0.06	0.06		
K_2O	udl	0.02	0.01	0.01	0.02	0.02	0.01	0.02	0.01	0.02	0.02	0.01	udl	udl	0.01	0.02	0.02	0.03		
Cr_2O_3	0.06	0.16	0.19	0.32	0.08	0.06	0.02	0.03	0.03	0.07	0.06	0.03	0.02	0.03	0.06	0.06	0.04	0.05		
Total	99.90	100.33	101.67	99.87	100.27	98.98	100.30	100.06	100.01	100.34	100.09	99.93	100.28	100.62	100.51	99.83	101.20	100.93		
Si	1.957	1.997	1.980	1.969	1.971	1.936	1.972	1.974	1.962	1.968	1.985	1.973	1.968	1.981	1.975	1.946	1.976	1.977		
Ti	0.023	0.006	0.009	0.019	0.020	0.023	0.023	0.022	0.027	0.022	0.014	0.022	0.022	0.012	0.012	0.010	0.012	0.012		
Al	0.047	0.029	0.037	0.075	0.064	0.066	0.049	0.046	0.066	0.065	0.026	0.043	0.044	0.031	0.035	0.109	0.033	0.060		
Fe	0.604	0.510	0.531	0.326	0.422	0.499	0.596	0.611	0.511	0.460	1.049	0.592	0.585	0.681	0.638	0.746	0.675	0.680		
Mn	0.011	0.007	0.008	0.006	0.008	0.009	0.010	0.010	0.008	0.008	0.017	0.010	0.010	0.009	0.009	0.009	0.009	0.010		
Mg	0.683	1.297	1.320	0.926	0.916	0.800	0.753	0.660	0.767	0.842	0.571	0.698	0.773	1.123	1.174	1.092	1.162	1.094		
Ca	0.701	0.151	0.131	0.697	0.618	0.720	0.609	0.688	0.680	0.654	0.342	0.674	0.616	0.176	0.175	0.156	0.151	0.190		
Na	0.020	0.014	0.002	0.019	0.015	0.017	0.015	0.017	0.020	0.019	0.007	0.016	0.015	0.005	0.005	0.005	0.004	0.004		
K	0.000	0.001	0.000	0.000	0.001	0.001	0.000	0.001	0.000	0.001	0.001	0.001	0.000	0.000	0.001	0.001	0.001	0.002		
Cr	0.002	0.005	0.006	0.009	0.002	0.002	0.001	0.001	0.001	0.002	0.002	0.001	0.000	0.001	0.002	0.002	0.001	0.001		
Total	4.048	4.016	4.024	4.048	4.037	4.072	4.029	4.029	4.043	4.041	4.014	4.030	4.033	4.019	4.026	4.076	4.024	4.031		
Mg#	0.56	0.72	0.72	0.74	0.69	0.67	0.56	0.52	0.61	0.65	0.35	0.55	0.58	0.62	0.66	0.61	0.64	0.62		
Q	1.91	1.95	1.96	1.92	1.93	1.88	1.94	1.94	1.92	1.92	1.96	1.94	1.93	1.96	1.95	1.90	1.96	1.95		
J	0.04	0.03	0.00	0.04	0.03	0.03	0.03	0.03	0.04	0.04	0.01	0.03	0.03	0.01	0.01	0.01	0.01	0.01		
Wo%	36.51	7.70	6.61	35.75	31.60	37.52	31.12	35.12	34.73	33.45	17.45	34.30	30.80	8.82	8.76	7.76	7.53	9.62		
En%	35.56	66.25	66.60	47.53	46.84	41.71	38.44	33.70	39.18	43.05	29.11	35.56	38.68	56.30	58.68	54.38	58.09	55.30		
Fs%	27.93	26.05	26.79	16.73	21.56	20.76	30.44	31.18	26.09	23.50	53.44	30.14	29.77	34.62	32.33	37.61	34.17	34.87		

Table 3.2 Continuation…

Sample	Cáceres									La Corona LC14								
					7 - rim to rim					1	2	3	4	5	6	7	8	9
SiO_2	52.36	52.58	52.40	53.88	54.21	53.72	52.05	51.39	50.57	49.80	50.47	50.73	50.80	51.11	48.82	49.18	50.87	50.82
TiO_2	0.51	0.61	0.43	0.37	0.32	0.31	0.71	0.89	0.66	1.84	1.71	1.49	1.41	1.47	2.24	1.91	1.42	1.66
Al_2O_3	0.77	1.42	1.94	1.29	1.00	0.91	1.26	1.38	0.83	3.99	3.84	3.25	3.23	2.75	4.78	5.06	3.08	3.33
FeO	22.01	12.88	12.72	17.43	15.64	17.85	14.16	16.60	23.97	7.57	7.40	7.56	7.63	7.73	8.04	8.01	7.11	7.51
MnO	0.36	0.20	0.17	0.23	0.22	0.28	0.20	0.25	0.42	0.18	0.07	0.13	0.16	0.14	0.14	0.18	0.12	0.12
MgO	19.03	17.02	18.00	22.92	25.00	23.57	15.10	14.06	10.90	15.15	15.31	15.63	15.51	15.71	14.30	15.92	16.17	15.74
CaO	5.18	15.04	13.41	4.21	3.85	3.80	16.50	15.28	12.64	20.03	20.71	20.18	20.58	20.40	20.89	18.16	19.86	20.19
Na_2O	0.08	0.24	0.24	0.10	0.08	0.06	0.25	0.26	0.15	0.46	0.45	0.45	0.47	0.43	0.56	0.64	0.44	0.44
K_2O	0.01	0.01	0.04	udl	udl	0.01	0.01	0.02	0.02	0.02	0.01	udl	udl	udl	udl	udl	0.01	udl
Cr_2O_3	0.05	0.13	0.37	0.39	0.28	0.13	0.06	0.05	0.03	0.20	0.19	0.02	udl	0.05	0.04	0.26	0.22	0.15
Total	100.36	100.12	99.72	100.80	100.60	100.63	100.30	100.17	100.19	99.24	100.15	99.42	99.80	99.78	99.79	99.31	99.30	99.94
Si	1.978	1.973	1.971	1.981	1.975	1.975	1.969	1.965	1.981	1.860	1.867	1.888	1.886	1.897	1.824	1.831	1.890	1.881
Ti	0.015	0.017	0.012	0.010	0.009	0.009	0.020	0.026	0.020	0.052	0.048	0.042	0.039	0.041	0.063	0.053	0.040	0.046
Al	0.034	0.063	0.086	0.056	0.043	0.039	0.056	0.062	0.039	0.175	0.167	0.142	0.141	0.120	0.210	0.222	0.135	0.145
Fe	0.695	0.404	0.400	0.536	0.477	0.549	0.448	0.531	0.785	0.236	0.229	0.235	0.237	0.240	0.251	0.249	0.221	0.232
Mn	0.011	0.006	0.005	0.007	0.007	0.009	0.006	0.008	0.014	0.006	0.002	0.004	0.005	0.004	0.004	0.006	0.004	0.004
Mg	1.071	0.951	1.009	1.256	1.358	1.291	0.851	0.801	0.636	0.844	0.844	0.867	0.859	0.870	0.797	0.884	0.896	0.868
Ca	0.209	0.604	0.540	0.166	0.150	0.150	0.669	0.626	0.531	0.802	0.821	0.804	0.819	0.811	0.836	0.725	0.791	0.801
Na	0.006	0.017	0.017	0.007	0.006	0.004	0.018	0.019	0.011	0.034	0.032	0.032	0.034	0.031	0.040	0.046	0.031	0.031
K	0.000	0.001	0.002	0.000	0.000	0.000	0.001	0.001	0.001	0.001	0.000	0.000	0.000	0.000	0.000	0.000	0.000	0.000
Cr	0.001	0.004	0.011	0.011	0.008	0.004	0.002	0.002	0.001	0.006	0.005	0.001	0.000	0.001	0.001	0.007	0.006	0.004
Total	4.021	4.040	4.055	4.031	4.033	4.030	4.040	4.040	4.018	4.016	4.015	4.015	4.020	4.015	4.026	4.023	4.014	4.012
Mg#	0.61	0.71	0.72	0.70	0.75	0.71	0.67	0.61	0.45	0.81	0.82	0.82	0.83	0.82	0.83	0.83	0.84	0.82
Q	1.96	1.93	1.91	1.94	1.95	1.95	1.93	1.92	1.94	1.83	1.84	1.85	1.84	1.87	1.79	1.78	1.86	1.85
J	0.01	0.03	0.03	0.01	0.01	0.01	0.04	0.04	0.02	0.07	0.06	0.06	0.07	0.06	0.08	0.09	0.06	0.06
Wo%	10.51	30.47	27.39	8.40	7.57	7.68	33.98	31.96	27.18	42.60	43.34	42.19	42.76	42.24	44.39	39.00	41.46	42.11
En%	53.76	47.97	51.17	63.70	68.42	66.22	43.27	40.93	32.60	44.84	44.57	45.47	44.85	45.27	42.28	47.57	46.96	45.67
Fs%	35.45	20.68	20.56	27.54	24.01	26.10	22.75	27.10	40.22	12.56	12.08	12.34	12.38	12.50	13.33	13.42	11.59	12.22

Table 3.2 Continuation…

	La Corona									Pajarito								
Sample										LC15						Pj2		
	10	11	12	13	14	15	16	17		1	2	3	4	5	6	1	2	3
SiO_2	50.95	50.36	48.30	50.92	50.69	50.54	50.80	48.36		49.94	50.72	50.54	49.76	50.32	51.10	48.52	49.31	47.73
TiO_2	1.32	1.68	2.42	1.33	1.30	1.36	1.34	2.35		1.80	1.50	1.62	1.96	1.71	1.46	1.89	1.72	2.14
Al_2O_3	3.00	3.49	5.12	2.95	2.93	3.00	3.10	5.04		4.45	3.61	3.28	4.57	3.75	2.98	6.34	5.16	6.98
FeO	7.91	7.45	7.65	7.97	7.98	7.71	8.29	8.07		7.20	7.22	7.46	8.20	7.34	7.52	4.92	4.95	5.17
MnO	0.19	0.13	0.14	0.21	0.16	0.12	0.11	0.16		0.16	0.15	0.17	0.16	0.18	0.17	0.07	0.10	0.11
MgO	15.72	15.56	14.25	15.21	15.38	15.47	15.39	14.16		15.22	16.04	15.62	14.16	15.43	15.47	14.05	14.50	13.63
CaO	20.05	20.43	20.84	20.39	20.20	20.32	20.19	20.87		20.51	20.13	20.81	21.41	20.86	20.76	23.24	23.18	23.38
Na_2O	0.46	0.45	0.56	0.43	0.47	0.45	0.47	0.53		0.55	0.47	0.40	0.54	0.51	0.44	0.30	0.30	0.31
K_2O	udl	0.01	0.02	udl	0.01	0.01	udl	0.01		0.01	udl	udl	udl	0.01	0.01	udl	0.01	0.01
Cr_2O_3	udl	0.24	0.17	0.01	0.02	0.03	0.03	0.06		0.27	0.27	0.05	0.01	0.22	0.02	0.28	0.26	0.27
Total	99.60	99.80	99.46	99.42	99.14	99.01	99.72	99.60		100.10	100.12	99.95	100.77	100.32	99.92	99.61	99.49	99.72
Si	1.895	1.870	1.810	1.899	1.896	1.892	1.891	1.812		1.839	1.863	1.865	1.831	1.849	1.887	1.793	1.824	1.765
Ti	0.037	0.047	0.068	0.037	0.037	0.038	0.038	0.066		0.050	0.041	0.045	0.054	0.047	0.041	0.053	0.048	0.059
Al	0.132	0.153	0.226	0.130	0.129	0.132	0.136	0.223		0.193	0.156	0.143	0.198	0.162	0.129	0.276	0.225	0.304
Fe	0.246	0.231	0.240	0.249	0.250	0.241	0.258	0.253		0.222	0.222	0.230	0.252	0.226	0.232	0.152	0.153	0.160
Mn	0.006	0.004	0.005	0.007	0.005	0.004	0.003	0.005		0.005	0.005	0.005	0.005	0.006	0.005	0.002	0.003	0.004
Mg	0.872	0.861	0.796	0.846	0.858	0.863	0.854	0.791		0.836	0.878	0.859	0.777	0.846	0.852	0.774	0.799	0.751
Ca	0.799	0.813	0.837	0.815	0.810	0.815	0.805	0.838		0.809	0.792	0.823	0.844	0.821	0.821	0.920	0.919	0.926
Na	0.033	0.033	0.041	0.031	0.034	0.033	0.034	0.039		0.039	0.034	0.029	0.039	0.036	0.032	0.022	0.021	0.022
K	0.000	0.000	0.001	0.000	0.000	0.001	0.000	0.000		0.000	0.000	0.000	0.000	0.001	0.000	0.000	0.000	0.001
Cr	0.000	0.007	0.005	0.000	0.001	0.001	0.001	0.002		0.008	0.008	0.002	0.000	0.006	0.000	0.008	0.008	0.008
Total	4.020	4.019	4.029	4.014	4.020	4.020	4.020	4.029		4.000	4.000	4.000	4.000	4.000	4.000	4.000	4.000	4.000
Mg#	0.82	0.83	0.83	0.80	0.82	0.83	0.81	0.83		0.84	0.84	0.84	0.81	0.85	0.82	0.74	0.75	0.73
Q	1.85	1.84	1.78	1.86	1.85	1.85	1.85	1.78		1.80	1.83	1.85	1.80	1.82	1.86	1.20	1.22	1.20
J	0.07	0.07	0.08	0.06	0.07	0.06	0.07	0.08		0.08	0.07	0.06	0.08	0.07	0.06	0.03	0.03	0.04
Wo%	41.69	42.66	44.69	42.67	42.23	42.45	42.01	44.53		43.35	41.87	43.03	45.06	43.40	43.11	54.96	54.25	55.43
En%	45.47	45.20	42.51	44.31	44.75	44.97	44.53	42.03		44.78	46.41	44.93	41.47	44.68	44.70	33.22	33.93	32.32
Fs%	12.84	12.14	12.80	13.02	13.02	12.58	13.46	13.44		11.88	11.72	12.04	13.47	11.92	12.19	11.82	11.82	12.25

Table 3.2 Continuation…

	Pajarito															
Sample	Pj7															
	1	2	3	4	5	6	7	8	9	10	11	12	13	14	15	16
SiO_2	49.47	48.56	48.90	48.55	49.72	46.46	49.90	49.21	48.56	48.16	49.70	49.14	49.60	49.61	49.05	49.68
TiO_2	1.68	1.95	1.73	1.77	1.02	2.40	1.52	1.54	1.91	2.15	1.66	1.67	1.49	1.52	1.61	1.51
Al_2O_3	5.32	5.99	5.78	5.85	5.38	8.02	5.03	5.36	6.26	7.08	4.91	5.68	4.84	4.82	5.25	4.66
FeO	4.59	5.07	4.56	4.44	6.39	5.12	4.43	4.60	4.79	5.70	4.68	4.55	4.44	4.54	4.55	4.65
MnO	0.04	0.09	0.08	0.08	0.14	0.07	0.06	0.06	0.06	0.12	0.08	0.05	0.09	0.08	0.10	0.08
MgO	14.36	13.81	14.25	14.07	14.36	13.15	14.71	14.38	13.92	12.22	14.64	14.21	14.75	14.65	14.42	14.73
CaO	23.16	23.12	23.30	23.23	21.34	23.18	23.28	23.23	23.27	22.68	23.01	23.19	23.06	23.31	23.18	23.28
Na_2O	0.29	0.37	0.31	0.34	0.60	0.37	0.32	0.34	0.37	0.94	0.30	0.33	0.30	0.32	0.34	0.30
K_2O	0.02	0.02	0.01	0.01	udl	0.01	udl	0.02	udl	0.01	udl	0.01	0.01	0.01	udl	0.02
Cr_2O_3	0.51	0.14	0.61	0.71	0.36	0.86	0.57	0.62	0.61	0.26	0.50	0.67	0.63	0.54	0.58	0.57
Total	99.44	99.12	99.53	99.06	99.30	99.62	99.81	99.36	99.75	99.33	99.48	99.50	99.20	99.39	99.08	99.48
Si	1.834	1.811	1.814	1.810	1.850	1.733	1.842	1.828	1.800	1.798	1.842	1.822	1.843	1.841	1.828	1.843
Ti	0.047	0.055	0.048	0.050	0.029	0.067	0.042	0.043	0.053	0.060	0.046	0.047	0.042	0.042	0.045	0.042
Al	0.233	0.263	0.253	0.257	0.236	0.352	0.219	0.235	0.273	0.312	0.215	0.248	0.212	0.211	0.231	0.204
Fe	0.142	0.158	0.142	0.138	0.199	0.160	0.137	0.143	0.148	0.178	0.145	0.141	0.138	0.141	0.142	0.144
Mn	0.001	0.003	0.002	0.002	0.004	0.002	0.002	0.002	0.002	0.004	0.002	0.002	0.003	0.003	0.003	0.003
Mg	0.793	0.768	0.788	0.782	0.797	0.731	0.809	0.796	0.769	0.680	0.809	0.785	0.817	0.810	0.801	0.815
Ca	0.920	0.924	0.926	0.928	0.851	0.926	0.921	0.925	0.924	0.907	0.914	0.921	0.918	0.927	0.925	0.925
Na	0.021	0.027	0.022	0.025	0.043	0.026	0.023	0.024	0.026	0.068	0.021	0.023	0.022	0.023	0.025	0.022
K	0.001	0.001	0.000	0.000	0.000	0.000	0.000	0.001	0.000	0.000	0.000	0.000	0.000	0.000	0.000	0.001
Cr	0.015	0.004	0.018	0.021	0.011	0.025	0.017	0.018	0.018	0.008	0.015	0.020	0.018	0.016	0.017	0.017
Total	4.007	4.014	4.014	4.014	4.020	4.024	4.010	4.015	4.014	4.016	4.008	4.009	4.012	4.015	4.016	4.016
Mg#	0.87	0.87	0.89	0.89	0.85	0.89	0.88	0.89	0.88	0.84	0.87	0.87	0.89	0.89	0.90	0.89
Q	1.83	1.80	1.81	1.80	1.78	1.73	1.83	1.81	1.79	1.71	1.84	1.82	1.83	1.83	1.81	1.83
J	0.04	0.05	0.04	0.05	0.09	0.05	0.05	0.05	0.05	0.14	0.04	0.05	0.04	0.05	0.05	0.04
Wo%	49.57	49.94	49.91	50.21	46.09	50.98	49.33	49.62	50.19	51.39	48.93	49.86	49.02	49.36	49.53	49.10
En%	42.76	41.51	42.46	42.31	43.14	40.23	43.35	42.71	41.75	38.52	43.30	42.50	43.62	43.15	42.89	43.24
Fs%	7.67	8.55	7.63	7.48	10.76	8.79	7.32	7.67	8.06	10.08	7.77	7.64	7.36	7.50	7.58	7.66

Table 3.2 Continuation…

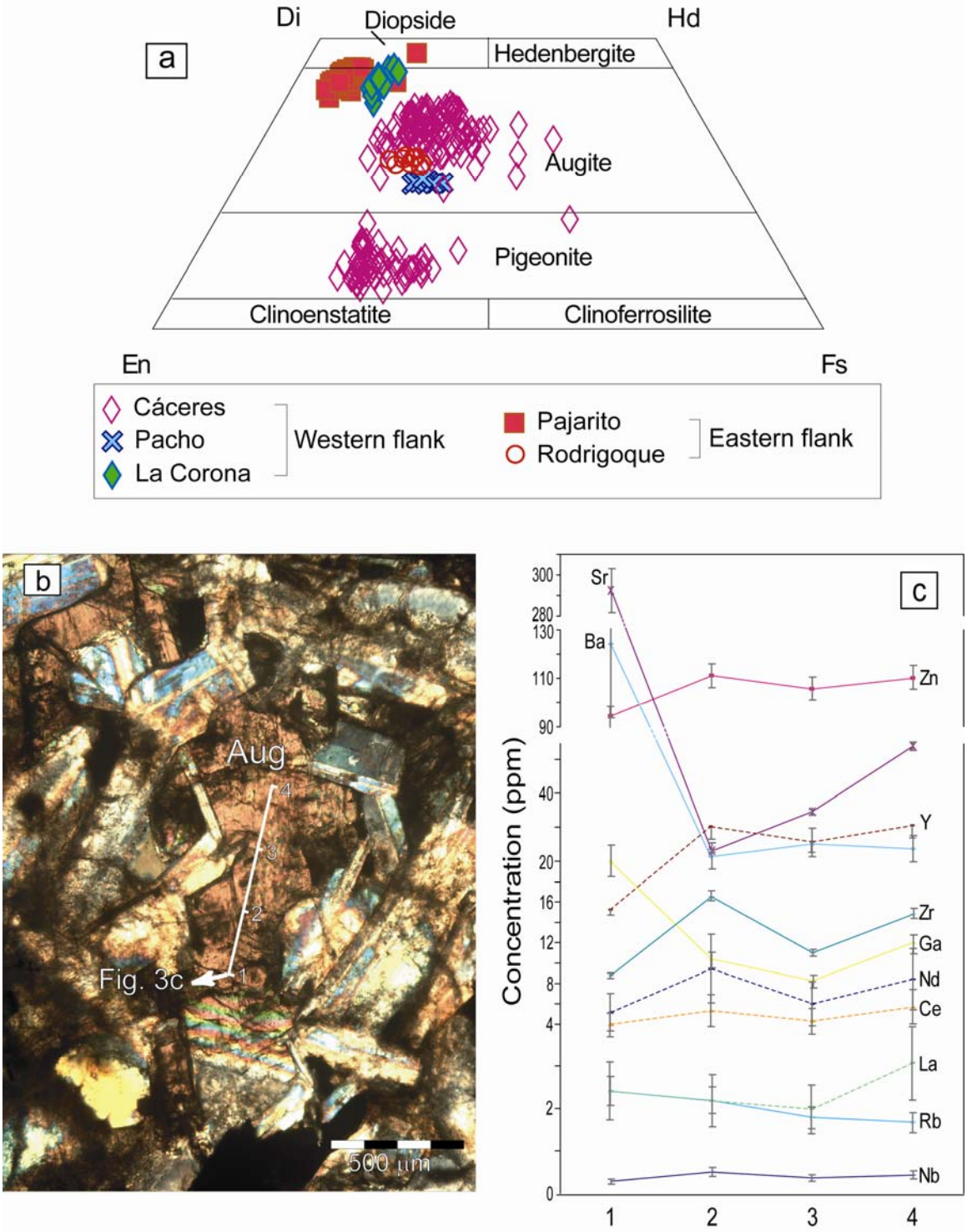

Fig. 3.3. Clinopyroxenes in the mafic intrusions of the EC in Colombia. **a**. Classification after the method from Lindsey (1983). Data from Cáceres, Pajarito and Pacho after Vásquez and Altenberger (2005). **b**. Photomicrograph of a clinopyroxene of Cáceres (sample Ca5), cross-polarized light. The white solid line indicates the profile shown in Fig. 3.3c. **c**. Rim-to-rim variations in trace elements abundances in clinopyroxenes; the concentration is given in ppm

Clinopyroxenes of Cáceres show lower concentrations of TiO_2 (<1%) and Al_2O_3 (<5%) than those of Pajarito and La Corona (1-2.4% and 2.8-8%, respectively). The tholeiitic affinity of the samples of Cáceres lead to Al- and Ti- poor concentrations (LeBas, 1962).

The concentrations of trace elements in clinopyroxenes determined by μ-SRXRF are shown in Table 3.3. An example of a clinopyroxene crystal from Cáceres (sample Ca5) with pigeonitic composition is shown in Fig. 3.3b. Figure 3.3c shows the variation of trace elements along the profile shown in Fig. 3.3b. Although the variation of FeO along the profile spans from 17 to 23% (Table 3.2), the performed calculations shown that the pattern of the curves for each element will not substantially change even if a mean value of FeO is chosen. In general, Zn, Nb, Zr, Nd and Ce do not show important modifications along the profile. A zonation can be observed in the profiles of Sr, Ba and Ga with higher concentrations at the rims of the crystal. An increasing concentration from point 1 to point 4 is suggested for Y and La, whereas it decreases for Rb.

Since the intrusion of Cáceres is the only one that has two different pyroxene phases (augite and pigeonite), we discuss some aspects of the P-T conditions of crystallization. It is well known that if pigeonite is present, the crystallization temperature should have been considerably high and the cooling rather fast (Buseck et al., 1980; Lindsey, 1980). However, pigeonite can be present even in slowly cooled plutonic rocks, because nucleation of orthopyroxene is a sluggish process in clinopyroxene and pigeonite can be metastably retained (Buseck et al., 1980). From the petrographic observations it is important to note that pigeonite and augite are not present as coexisting phases. Instead they are found as zones in pyroxene grains, so that the textural relationship cannot be ruled out. This means, that we cannot apply the methods available in the literature to better constrain the P-T conditions. We can merely assume a maximum temperature of 1250°C for the crystallization of pigeonite, whereas the augite could have reached temperatures that span from 900°C to 1100°C. With this assumption the pressure can be estimated with the concentrations of the major elements by the CpxBar software program developed by Nimis (1999). The calculated pressures of crystallization are around 1.3 kbar for augite and 1.8 kbar for pigeonite. If a mean pressure of ca. 1.5 kbar is considered, the estimate would look reasonable if a temperature of 1150˚C is assumed. The lower temperatures might probably reflect subsolidus re-equilibration or magmatic crystallization in the absence of pigeonite; in both cases, pressure might be underestimated.

Pyroxenes	Cáceres																					
Sample	Ca5p06041		Ca5p06042 rim to rim				Ca5p06045 rim to rim				Ca5p060410 rim to rim				Ca10p06041 rim to rim							
Zn	106	145	102	108	94	111	106	110	247	127	152	162	142	146	149	151	149					
Ga	5	13	9	11	20	10	8	12	6	11	8	6	8	13	12	17	15					
Rb	2	3	1	1	2	2	2	2	3	4	4	3	2	3	3	3	3					
Sr	6	20	20	23	292	23	35	54	11	17	14	10	16	25	23	34	22					
Y	5	28	27	29	15	30	26	31	11	9	9	8	34	31	28	30	21					
Zr	2	12	13	15	9	17	11	15	10	13	9	4	15	14	13	17	10					
Nb	udl	udl	udl	0.5	0.3	0.5	0.4	0.4	0.5	0.5	0.4	0.3	0.6	0.3	0.4	0.9	0.4					
Ba	14	14	13	20	124	21	25	24	20	40	27	18	5	6	9	14	8					
La	0.5	1.5	2.6	1.8	2.4	2.2	2.0	3.1	1.7	1.2	1.1	1.5	1.8	2.0	2.2	3.2	2.1					
Ce	1.0	3.8	5.1	3.8	4.0	5.3	4.3	5.7	1.8	2.3	2.0	2.0	5.0	4.3	4.7	6.1	3.1					
Nd	1.6	6.5	6.7	7.1	5.2	9.4	6.0	8.4	2.6	2.3	2.6	3.1	8.5	6.6	5.2	6.7	6.0					

Pyroxenes	La Corona																					
Sample	Ca10p06046	Ca10p06047	Ca10p10051	Ca10p10052	Ca10p10053	Ca10p10054	LC14p06041	LC14p06042	LC14p06043	LC14p06044	LC14p06045	LC14p06046	LC14p10051	LC14p10052	LC14p10053							
Zn	137	153	126	118	103	97	35	48	47	47	47	35	41	60	47							
Ga	7	21	6	7	7	8	11	10	8	9	8	8	5	6	7							
Rb	7	2	3	3	3	4	1	2	3	1	1	1	1	1	1							
Sr	14	17	9	9	10	11	103	114	91	71	89	98	72	75	80							
Y	21	25	4	4	3	9	18	16	15	12	13	12	9	11	13							
Zr	8	9	3	4	2	2	39	28	32	19	22	34	18	23	26							
Nb	udl	udl	0.4	0.4	0.4	udl	0.5	udl	0.5	0.6	0.3	1.3	0.7	1.2	0.8							
Ba	5	12	15	16	15	23	5	34	14	13	26	11	16	23	34							
La	2.4	5.6	7.0	8.1	5.4	3.8	5.3	5.4	5.1	4.0	3.7	7.8	6.9	11	7.4							
Ce	4.8	9.7	7.7	9.1	5.3	7.7	15	13	12	8.5	9.0	14	17	15	10							
Nd	4.2	17	10	4.7	6.4	8.2	18	14	14	9.9	12	23	15	18	17							

Pyroxenes	Pájarito							
Sample	Pj2p06041	Pj2p06042	Pj2p06043	Pj2p06044	Pj2p06045	Pj7p06041	Pj7p10051	Pj7p10053
Zn	136	190	126	176	74	48	40	80
Ga	8	8	13	10	9	7	5	3
Rb	1	1	1	1	1	1	1	2
Sr	64	109	76	93	108	89	35	70
Y	10	11	14	11	14	10	6	4
Zr	64	91	139	68	143	61	44	32
Nb	1.2	2	8	3	3	7	4	12
Ba	8	17	17	16	12	15	7	81
La	5.7	6.1	11	4.1	11	11	6.9	3.7
Ce	15	16	24	11	27	23	15	4.9
Nd	14	15	17	12	24	14	10	5.9

Table 3.3. Concentrations of trace elements after the μ-SRXRF analyses of clinopyroxenes from the Eastern Cordillera of Colombia. Data in ppm. udl= under detection limit

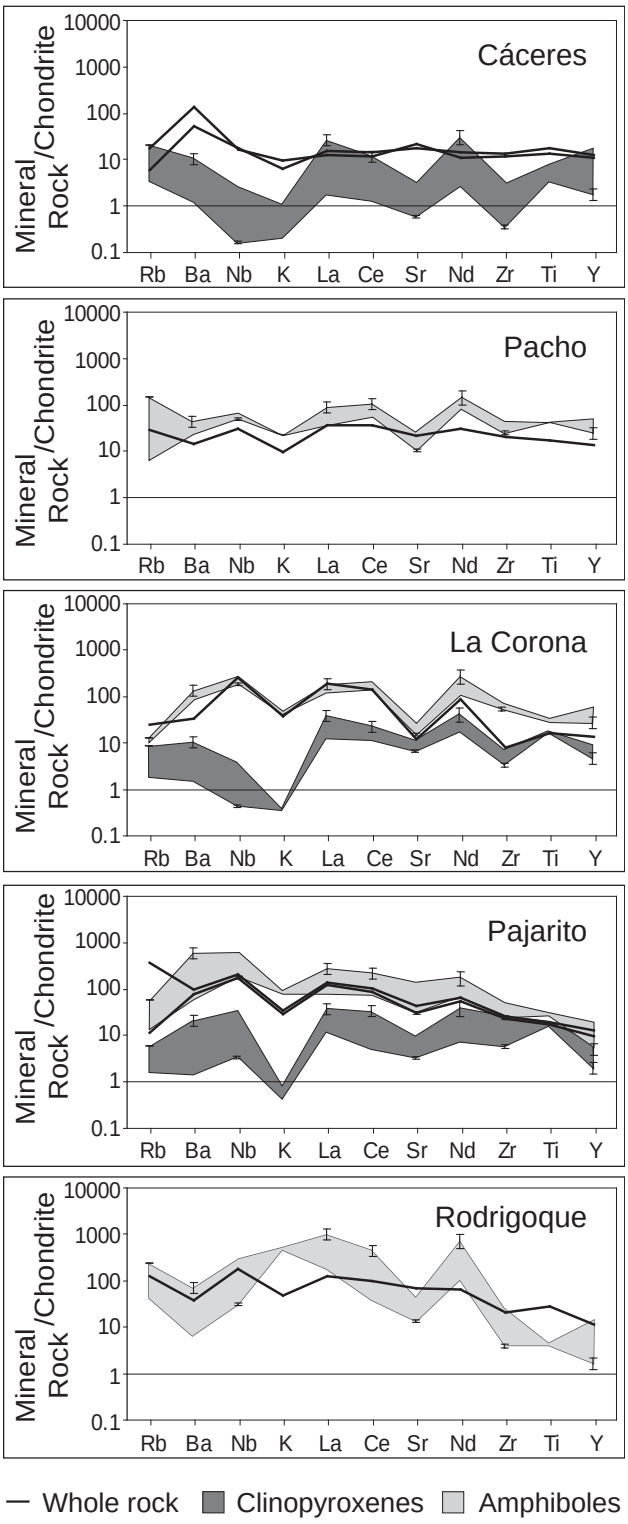

Fig. 3.4. Trace-element concentrations of minerals (clinopyroxenes and amphiboles) and whole rocks normalized to chondritic composition. Cáceres: samples Ca5 and Ca10; Pacho: sample Pa5; La Corona: sample LC14; Pajarito: samples Pj2 and Pj7; Rodrigoque: sample LS4. Normalization values after Sun (1980). Error indicator corresponds to the percentage of mean relative deviation calculated for each element as shown in Table 3.1

In order to compare trace-element patterns, the trace-element content of the clinopyroxenes and the whole rock were normalized to chondritic composition (Fig. 3.4). The clinopyroxenes of all localities show nearly consistent patterns. They exhibit negative Sr and Zr anomalies and positive for La and Nd compared to the neighbouring elements. The sharply negative anomaly observed for K is the result of the low concentrations of this element, which is a usual characteristic for clinopyroxenes. Error bars indicate the mean percentage of relative deviation determined on the reference materials as shown in table 3.1.

3.5.2 Amphiboles

Amphiboles from the intrusions of Pajarito and Pacho have been described in Vásquez & Altenberger (2005). They occur as brown to green individual crystals of hornblende. In Pacho the amphiboles are calcic and classified as: kaersutite, pargasite, edenite, and magnesiohornblende. In Pajarito the amphiboles are also calcic and classified as: kaersutite, pargasite, and tschermakite (Fig. 3.5a). Actinolite and tremolite appear to have grown around the hornblende crystals in both localities.

The amphiboles of the rocks from La Corona and Rodrigoque are brown to green individual crystals named after the classification of Leake *et al.* (1997a). A general classification of the amphiboles observed in the intrusions is presented in Fig. 3.5a. In La Corona, the amphiboles are classified as kaersutite, magnesio-hornblende, pargasite, and edenite. In Rodrigoque they correspond to ferropargasite. The concentrations of major elements in the amphiboles of the studied intrusions are shown in Table 3.4. For the calculation of amphibole formula in this paper, we have used the Probe-amph spreadsheet program developed by Tindle & Webb (1994). In that program, the formula is calculated on a water and halogen-free basis to 23 (O) and 2 (OH, F, Cl). The low total sums obtained for the amphiboles in Rodrigoque can be explained by high Cl content up to 3.4%. Each locality shows some samples of amphiboles whose TiO_2 content is much lower than the general trend. Although they can be also classified as calcic amphiboles, their compositions correspond to pargasite and ferropargasite.

	La Corona																
Sample	LC13																
	1	2 - rim to rim			3	4	5	6	7	8 - rim to rim		9	10	11	12	13	14	15	16	17
SiO_2	41.79	42.22	41.22	40.87	41.12	41.93	41.53	41.93	49.83	49.77	49.62	49.91	50.10	41.42	41.42	41.42	41.60	42.03	41.10	41.81	41.97	41.82
TiO_2	5.25	4.77	5.22	5.15	5.16	5.09	5.07	5.13	0.96	0.97	0.98	0.94	0.96	5.13	5.09	5.21	5.18	5.03	5.23	5.11	5.03	5.08
Al_2O_3	11.55	10.35	11.67	11.71	11.73	11.65	11.64	11.56	4.01	4.10	4.18	4.10	4.00	10.95	11.05	11.57	11.34	11.00	10.86	10.83	10.62	11.03
FeO	12.38	13.86	12.20	12.02	11.58	11.79	11.74	11.33	17.77	17.73	17.66	17.87	17.73	12.38	12.36	12.45	11.83	12.05	12.62	12.65	12.62	12.75
MnO	0.15	0.20	0.16	0.21	0.09	0.13	0.17	0.18	0.28	0.29	0.28	0.27	0.31	0.19	0.13	0.12	0.16	0.16	0.19	0.18	0.19	0.23
MgO	12.85	12.41	12.91	13.14	13.26	13.45	13.33	13.36	12.79	12.69	12.79	12.84	13.07	12.71	13.06	12.97	12.91	13.24	12.64	12.61	12.75	12.75
CaO	11.43	11.13	11.42	11.60	11.39	11.45	11.62	11.61	10.84	11.06	11.05	11.00	10.98	11.18	11.25	11.46	11.40	11.36	11.15	11.15	11.09	11.16
Na_2O	2.93	2.97	2.93	2.96	2.87	2.95	2.90	2.97	1.60	1.65	1.66	1.60	1.58	3.01	3.01	2.93	2.91	2.99	2.99	2.98	3.07	3.01
K_2O	0.85	0.82	0.82	0.85	0.80	0.84	0.84	0.86	0.45	0.45	0.42	0.43	0.42	0.81	0.83	0.83	0.83	0.82	0.86	0.86	0.81	0.81
Total	99.18	98.73	98.54	98.52	98.01	99.29	98.83	98.92	98.54	98.70	98.65	98.95	99.13	97.78	98.20	98.97	98.15	98.67	97.63	98.17	98.14	98.64
Si	6.104	6.218	6.057	6.012	6.049	6.088	6.073	6.126	7.240	7.244	7.217	7.227	7.226	6.143	6.105	6.061	6.136	6.157	6.115	6.181	6.200	6.144
Al^{iv}	1.896	1.782	1.943	1.988	1.951	1.912	1.927	1.874	0.687	0.703	0.717	0.700	0.680	1.857	1.895	1.939	1.864	1.843	1.885	1.819	1.800	1.856
Al^{vi}	0.092	0.013	0.078	0.043	0.082	0.078	0.117	0.000	0.000	0.000	0.000	0.000	0.000	0.057	0.026	0.057	0.108	0.058	0.018	0.067	0.050	0.053
Ti	0.577	0.528	0.577	0.570	0.571	0.556	0.558	0.564	0.105	0.106	0.107	0.102	0.104	0.573	0.565	0.573	0.575	0.554	0.585	0.568	0.559	0.561
Fe^{3+}	0.084	0.195	0.128	0.143	0.165	0.165	0.114	0.000	0.711	0.599	0.641	0.699	0.745	0.083	0.167	0.152	0.015	0.108	0.115	0.068	0.091	0.157
Fe^{2+}	1.428	1.512	1.370	1.336	1.259	1.267	1.322	1.385	1.449	1.559	1.507	1.464	1.393	1.453	1.356	1.371	1.445	1.369	1.455	1.495	1.468	1.409
Mn	0.019	0.025	0.019	0.027	0.011	0.016	0.021	0.022	0.035	0.036	0.035	0.033	0.038	0.024	0.016	0.015	0.019	0.020	0.024	0.023	0.024	0.028
Mg	2.799	2.723	2.828	2.881	2.908	2.912	2.906	2.909	2.772	2.753	2.773	2.772	2.809	2.811	2.869	2.830	2.838	2.891	2.803	2.778	2.807	2.791
Ca	1.789	1.757	1.798	1.828	1.795	1.782	1.820	1.817	1.688	1.725	1.722	1.706	1.697	1.776	1.777	1.797	1.802	1.783	1.778	1.766	1.755	1.756
Na	0.830	0.847	0.835	0.845	0.818	0.832	0.822	0.841	0.450	0.467	0.468	0.449	0.441	0.866	0.861	0.831	0.832	0.849	0.863	0.855	0.878	0.858
K	0.157	0.155	0.153	0.159	0.150	0.156	0.157	0.160	0.084	0.083	0.079	0.079	0.077	0.154	0.156	0.156	0.156	0.153	0.163	0.161	0.152	0.152
Total	15.775	15.756	15.786	15.833	15.761	15.768	15.797	15.815	15.220	15.274	15.266	15.231	15.209	15.796	15.793	15.783	15.790	15.785	15.803	15.781	15.784	15.767
Mg/(Mg+Fe^{+2})	0.66	0.64	0.67	0.68	0.70	0.70	0.69	0.68	0.66	0.64	0.65	0.65	0.67	0.66	0.68	0.67	0.66	0.68	0.66	0.65	0.66	0.66

Table 3.4. EPM analyses of amphiboles from the Eastern Cordillera of Colombia. Cations calculated on the basis of 23 O atoms

La Corona				LC14																
Sample	18	19	20	1	2	3	4	5	6	7	8	9	10	11	12	13	14	15	16	17	18
SiO_2	42.06	42.19	42.06	43.88	43.02	42.87	43.63	44.25	44.81	44.33	45.17	43.96	44.47	51.39	50.82	44.23	43.64	44.97	43.78	44.31	43.91
TiO_2	5.05	4.82	5.01	3.70	3.93	3.57	3.55	3.47	3.55	3.74	3.26	3.25	3.24	1.38	1.51	3.31	3.44	2.92	3.32	3.07	3.47
Al_2O_3	10.65	10.63	10.89	10.16	10.40	10.50	9.93	9.13	8.40	9.04	8.29	9.67	9.38	3.78	3.99	9.46	9.91	7.82	9.48	9.64	9.71
FeO	12.41	13.77	13.47	11.89	12.26	12.54	13.09	13.52	14.34	13.71	13.66	13.25	11.84	13.43	13.95	12.86	12.61	14.55	13.14	12.51	12.60
MnO	0.22	0.19	0.22	0.21	0.18	0.20	0.16	0.24	0.18	0.23	0.21	0.25	0.19	0.21	0.17	0.16	0.13	0.31	0.18	0.19	0.19
MgO	12.97	12.53	12.56	14.29	14.11	13.80	13.57	13.63	13.34	13.43	13.98	13.97	14.67	16.22	15.88	14.19	14.22	13.61	13.85	14.64	14.09
CaO	11.16	11.15	11.17	10.90	11.05	11.06	10.91	10.61	10.57	10.82	10.22	10.66	10.70	9.63	9.62	10.87	10.80	9.93	10.15	10.67	10.85
Na_2O	2.98	3.04	2.99	3.11	3.10	3.07	3.09	3.06	3.09	3.11	3.16	2.94	2.98	2.41	2.55	3.06	3.13	2.93	3.08	3.16	3.13
K_2O	0.81	0.88	0.78	0.69	0.73	0.67	0.74	0.69	0.70	0.70	0.69	0.65	0.67	0.34	0.36	0.68	0.71	0.60	0.60	0.67	0.66
Total	98.32	99.21	99.13	98.83	98.78	98.29	98.65	98.60	98.97	99.10	98.63	98.60	98.15	98.77	98.85	98.81	98.61	97.64	97.59	98.85	98.61
Si	6.189	6.183	6.154	6.333	6.237	6.250	6.350	6.432	6.514	6.441	6.536	6.355	6.430	7.223	7.170	6.393	6.320	6.561	6.377	6.370	6.365
Al^{iv}	1.811	1.817	1.846	1.667	1.763	1.750	1.650	1.563	1.439	1.547	1.413	1.645	1.570	0.627	0.664	1.607	1.680	1.344	1.623	1.630	1.635
Al^{vi}	0.037	0.018	0.031	0.061	0.013	0.054	0.053	0.000	0.000	0.000	0.000	0.003	0.029	0.000	0.000	0.005	0.012	0.000	0.005	0.003	0.025
Ti	0.559	0.532	0.551	0.402	0.429	0.392	0.388	0.379	0.388	0.408	0.355	0.353	0.353	0.146	0.160	0.360	0.375	0.321	0.364	0.332	0.378
Fe^{3+}	0.130	0.203	0.214	0.436	0.454	0.462	0.408	0.521	0.465	0.379	0.623	0.690	0.562	1.016	1.004	0.531	0.555	0.850	0.739	0.673	0.483
Fe^{2+}	1.397	1.484	1.434	0.999	1.032	1.067	1.186	1.122	1.278	1.287	1.030	0.912	0.869	0.563	0.642	1.023	0.971	0.926	0.862	0.831	1.045
Mn	0.027	0.024	0.027	0.026	0.022	0.025	0.019	0.030	0.023	0.028	0.026	0.030	0.024	0.025	0.020	0.020	0.016	0.038	0.022	0.023	0.023
Mg	2.845	2.737	2.739	3.075	3.049	2.999	2.943	2.953	2.892	2.908	3.015	3.011	3.163	3.399	3.340	3.058	3.070	2.960	3.008	3.137	3.046
Ca	1.759	1.751	1.750	1.686	1.717	1.728	1.701	1.652	1.646	1.684	1.584	1.651	1.658	1.450	1.455	1.684	1.676	1.551	1.584	1.643	1.685
Na	0.851	0.864	0.849	0.869	0.870	0.868	0.871	0.861	0.870	0.877	0.885	0.823	0.834	0.656	0.698	0.856	0.879	0.827	0.870	0.880	0.879
K	0.152	0.165	0.145	0.126	0.135	0.125	0.138	0.129	0.129	0.130	0.128	0.120	0.123	0.060	0.064	0.124	0.132	0.112	0.112	0.123	0.122
Total	15.758	15.779	15.742	15.681	15.722	15.720	15.707	15.641	15.643	15.688	15.595	15.593	15.616	15.164	15.216	15.661	15.686	15.491	15.566	15.644	15.686
$Mg/(Mg+Fe^{+2})$	0.67	0.65	0.66	0.75	0.75	0.74	0.71	0.72	0.69	0.69	0.75	0.77	0.78	0.86	0.84	0.75	0.76	0.76	0.78	0.79	0.74

Table 3.4. Continuation…

Sample			LC15																	
	19	20	1	2	3	4	5	6	7	8	9	10	11	12	13	14	15	16	17	18	19
SiO_2	43.15	43.21	42.39	42.45	41.59	42.35	43.21	41.94	42.23	42.13	42.25	42.63	42.46	42.53	41.55	41.80	42.34	41.71	41.70	41.99	42.38
TiO_2	3.84	3.90	4.60	4.52	4.92	4.73	4.75	4.96	5.00	4.87	4.80	4.69	4.77	4.69	5.11	5.01	4.82	4.76	4.68	4.63	4.50
Al_2O_3	10.06	10.04	11.22	10.82	11.69	10.75	10.37	11.23	10.95	11.29	11.28	10.62	11.00	11.21	11.64	11.46	10.72	11.70	11.89	11.72	11.15
FeO	13.42	12.92	11.67	11.78	11.85	11.95	11.94	12.21	12.37	11.89	11.17	12.79	12.21	11.69	12.10	12.55	12.30	11.87	11.75	12.06	11.18
MnO	0.17	0.17	0.19	0.09	0.12	0.16	0.17	0.16	0.11	0.16	0.17	0.16	0.15	0.17	0.11	0.16	0.14	0.16	0.18	0.10	0.14
MgO	13.46	13.55	13.84	13.87	13.38	13.47	13.57	13.32	13.25	13.71	13.94	13.60	13.75	13.76	13.45	13.21	13.40	13.40	13.77	13.63	14.01
CaO	10.74	10.99	11.23	11.19	11.34	11.26	11.04	11.23	11.23	11.41	11.25	11.27	11.38	11.48	11.43	11.49	11.21	11.58	11.40	11.34	11.30
Na_2O	3.06	3.08	3.03	3.04	3.10	3.06	3.09	3.06	2.99	3.12	3.00	3.13	3.00	3.06	2.98	3.05	3.11	3.06	2.99	3.01	3.02
K_2O	0.71	0.67	0.79	0.83	0.82	0.81	0.79	0.81	0.78	0.81	0.78	0.78	0.81	0.81	0.84	0.85	0.82	0.81	0.82	0.79	0.80
Total	98.60	98.53	98.95	98.58	98.81	98.53	98.94	98.91	98.91	99.38	98.64	99.68	99.53	99.38	99.21	99.59	98.85	99.07	99.18	99.27	98.48
Si	6.280	6.302	6.148	6.187	6.073	6.199	6.286	6.119	6.162	6.110	6.142	6.172	6.144	6.163	6.044	6.078	6.185	6.082	6.040	6.080	6.173
Al^{iv}	1.720	1.698	1.852	1.813	1.927	1.801	1.714	1.881	1.838	1.890	1.858	1.813	1.856	1.837	1.956	1.922	1.815	1.918	1.960	1.920	1.827
Al^{vi}	0.005	0.029	0.066	0.045	0.085	0.053	0.063	0.049	0.045	0.040	0.074	0.000	0.020	0.077	0.039	0.042	0.031	0.093	0.069	0.080	0.087
Ti	0.420	0.427	0.502	0.495	0.541	0.520	0.520	0.544	0.549	0.531	0.525	0.511	0.520	0.511	0.559	0.548	0.530	0.522	0.509	0.505	0.493
Fe^{3+}	0.528	0.382	0.292	0.272	0.183	0.150	0.147	0.218	0.191	0.214	0.239	0.303	0.276	0.163	0.240	0.183	0.177	0.141	0.342	0.320	0.228
Fe^{2+}	1.106	1.194	1.124	1.164	1.264	1.313	1.305	1.271	1.318	1.228	1.120	1.246	1.201	1.254	1.231	1.343	1.325	1.307	1.081	1.140	1.134
Mn	0.021	0.021	0.023	0.011	0.015	0.019	0.021	0.020	0.014	0.019	0.021	0.020	0.018	0.020	0.013	0.020	0.017	0.020	0.022	0.013	0.017
Mg	2.921	2.945	2.993	3.013	2.911	2.939	2.942	2.897	2.882	2.965	3.021	2.936	2.965	2.972	2.917	2.864	2.917	2.913	2.974	2.943	3.041
Ca	1.675	1.717	1.745	1.747	1.774	1.766	1.721	1.755	1.756	1.773	1.752	1.748	1.765	1.783	1.782	1.791	1.754	1.809	1.768	1.760	1.763
Na	0.864	0.872	0.852	0.858	0.876	0.868	0.873	0.865	0.846	0.877	0.844	0.878	0.842	0.859	0.840	0.861	0.882	0.866	0.839	0.845	0.852
K	0.133	0.124	0.145	0.154	0.153	0.151	0.147	0.150	0.146	0.149	0.145	0.144	0.149	0.149	0.155	0.158	0.152	0.151	0.152	0.146	0.149
Total	15.672	15.712	15.743	15.759	15.803	15.781	15.741	15.769	15.747	15.796	15.740	15.770	15.756	15.787	15.777	15.810	15.785	15.822	15.758	15.751	15.764
$Mg/(Mg+Fe^{+2})$	0.73	0.71	0.73	0.72	0.70	0.69	0.69	0.69	0.69	0.71	0.73	0.70	0.71	0.70	0.70	0.68	0.69	0.69	0.73	0.72	0.73

Table 3.4. Continuation…

	La Corona	Pacho																		
Sample		Pa5																		
	20	1	2	3	4	5	6	7	8	9	10	11	12	13	14	15	16	17	18	19	20
SiO_2	42.29	44.17	49.24	48.40	48.26	47.69	48.73	41.17	41.76	42.13	42.25	42.22	42.16	42.24	42.21	42.36	42.38	42.49	42.57	42.55	42.95
TiO_2	4.52	1.33	1.10	1.73	1.67	2.05	0.79	4.55	4.38	4.22	4.27	4.21	4.25	4.33	4.26	4.26	4.25	4.12	4.11	3.99	3.97
Al_2O_3	11.32	9.08	5.74	5.76	5.73	6.01	5.78	11.80	11.59	11.37	11.23	11.22	11.20	11.24	11.35	11.22	11.30	11.18	11.26	11.05	10.87
FeO	11.50	15.56	12.15	11.79	12.21	12.08	14.32	11.95	12.38	12.02	12.03	11.94	11.93	12.08	12.16	12.07	11.69	11.99	11.99	11.63	10.73
MnO	0.17	0.16	0.20	0.14	0.18	0.16	0.19	0.22	0.16	0.18	0.21	0.20	0.21	0.17	0.21	0.23	0.17	0.20	0.26	0.19	0.12
MgO	13.90	12.65	16.35	16.21	16.01	15.86	13.97	13.16	13.46	13.61	13.59	13.61	13.65	13.56	13.70	13.72	13.60	13.75	13.88	13.97	14.43
CaO	11.40	10.65	10.47	10.13	9.95	9.85	11.67	11.36	11.34	11.37	11.25	11.37	11.30	11.24	11.40	11.33	11.40	11.34	11.22	11.35	11.22
Na_2O	2.95	3.50	2.51	3.42	3.13	3.41	1.62	2.98	2.97	2.99	3.04	3.11	3.00	3.04	3.07	2.97	3.03	3.06	3.04	3.06	3.26
K_2O	0.80	0.15	0.11	0.16	0.15	0.14	0.15	0.33	0.33	0.33	0.30	0.30	0.32	0.32	0.31	0.32	0.31	0.29	0.32	0.31	0.31
Total	98.84	97.26	97.87	97.75	97.29	97.27	97.23	97.52	98.38	98.21	98.15	98.18	98.01	98.21	98.66	98.46	98.14	98.40	98.65	98.09	97.84
Si	6.141	6.534	6.993	6.942	6.932	6.873	7.110	6.061	6.081	6.141	6.159	6.163	6.155	6.157	6.128	6.151	6.185	6.175	6.158	6.196	6.251
Al^{iv}	1.859	1.466	0.960	0.973	0.970	1.021	0.890	1.939	1.919	1.859	1.841	1.837	1.845	1.843	1.872	1.849	1.815	1.825	1.842	1.804	1.749
Al^{vi}	0.079	0.118	0.000	0.000	0.000	0.000	0.103	0.109	0.071	0.093	0.088	0.094	0.081	0.087	0.069	0.071	0.127	0.089	0.078	0.092	0.115
Ti	0.493	0.148	0.118	0.186	0.181	0.222	0.087	0.504	0.480	0.463	0.468	0.462	0.467	0.475	0.465	0.465	0.467	0.450	0.447	0.437	0.435
Fe^{3+}	0.270	0.644	0.921	0.676	0.843	0.767	0.478	0.324	0.450	0.384	0.392	0.324	0.388	0.379	0.407	0.429	0.274	0.390	0.480	0.374	0.288
Fe^{2+}	1.127	1.281	0.522	0.739	0.624	0.689	1.270	1.146	1.058	1.081	1.074	1.134	1.068	1.094	1.069	1.037	1.153	1.067	0.971	1.042	1.017
Mn	0.020	0.020	0.024	0.017	0.022	0.020	0.023	0.028	0.020	0.022	0.025	0.024	0.026	0.020	0.026	0.028	0.021	0.024	0.032	0.023	0.014
Mg	3.010	2.790	3.462	3.467	3.428	3.408	3.039	2.889	2.922	2.957	2.952	2.961	2.971	2.946	2.965	2.970	2.957	2.980	2.993	3.032	3.130
Ca	1.773	1.688	1.592	1.557	1.532	1.521	1.825	1.793	1.769	1.775	1.756	1.779	1.767	1.755	1.773	1.762	1.782	1.765	1.739	1.771	1.750
Na	0.830	1.005	0.692	0.951	0.871	0.954	0.457	0.850	0.840	0.844	0.858	0.881	0.849	0.858	0.863	0.835	0.858	0.863	0.853	0.865	0.919
K	0.148	0.029	0.020	0.030	0.027	0.026	0.028	0.062	0.062	0.061	0.055	0.055	0.059	0.059	0.057	0.059	0.058	0.053	0.058	0.058	0.057
Total	15.750	15.721	15.304	15.538	15.430	15.501	15.310	15.705	15.670	15.681	15.670	15.715	15.675	15.673	15.694	15.656	15.699	15.681	15.651	15.694	15.726
$Mg/(Mg+Fe^{+2})$	0.73	0.69	0.87	0.82	0.85	0.83	0.71	0.72	0.73	0.73	0.73	0.72	0.74	0.73	0.73	0.74	0.72	0.74	0.76	0.74	0.75

Table 3.4. Continuation…

	Pajarito										Rodrigoque					
Sample	PJ7										LS7					
				1 - rim to rim							1	2	3	4	5	6
SiO_2	41.25	39.76	38.75	38.67	39.07	41.13	40.17	39.81	41.25	45.66	41.14	39.09	38.59	40.54	37.67	38.89	38.35	37.73	39.20	38.81
TiO_2	1.95	4.99	4.08	4.31	4.31	3.73	4.02	3.78	3.57	0.24	2.93	4.33	4.95	1.91	0.16	0.14	0.11	0.13	0.20	0.13
Al_2O_3	13.00	13.68	14.63	14.86	14.79	12.83	13.70	14.43	14.82	9.92	12.89	14.72	14.72	14.13	12.29	12.05	12.03	12.19	12.32	12.30
FeO	12.86	11.12	10.80	10.82	10.36	10.49	9.68	10.39	9.65	15.57	11.00	8.88	9.49	11.54	26.87	25.95	26.09	26.63	24.87	25.25
MnO	0.22	0.14	0.12	0.17	0.10	0.24	0.19	0.25	0.07	0.51	0.16	0.07	0.12	0.23	0.11	0.15	0.05	0.09	0.13	0.19
MgO	11.90	12.14	12.40	12.33	12.59	13.34	12.90	12.79	12.22	11.42	13.12	13.20	12.73	12.81	4.03	4.62	4.51	4.15	5.05	4.70
CaO	11.82	13.23	12.41	12.12	12.50	12.27	12.34	12.49	10.78	11.24	12.16	12.37	12.25	11.98	11.21	11.28	11.19	11.24	11.40	11.41
Na_2O	2.46	2.16	2.35	2.26	2.30	2.10	2.12	2.33	1.82	3.22	2.23	2.40	2.34	2.66	1.81	1.71	1.75	1.68	1.77	1.69
K_2O	1.25	1.21	1.38	1.40	1.42	1.21	1.34	1.44	2.32	0.15	1.25	1.37	1.42	1.45	1.62	1.42	1.47	1.81	1.22	1.55
Total	96.71	98.43	96.92	96.94	97.42	97.33	96.45	97.70	96.51	97.94	96.87	96.42	96.61	97.24	95.76	96.21	95.55	95.66	96.14	96.03
Si	6.180	5.868	5.799	5.776	5.802	6.078	5.989	5.891	6.110	6.504	5.952	5.687	5.619	5.859	6.058	6.171	6.140	6.076	6.190	6.175
Al^{iv}	1.820	2.132	2.201	2.224	2.198	1.922	2.011	2.109	1.890	1.496	2.048	2.313	2.381	2.141	1.942	1.829	1.860	1.924	1.810	1.825
Al^{vi}	0.475	0.246	0.379	0.393	0.390	0.313	0.397	0.408	0.697	0.169	0.149	0.210	0.144	0.266	0.387	0.424	0.411	0.390	0.482	0.481
Ti	0.219	0.554	0.459	0.485	0.481	0.414	0.451	0.421	0.398	0.026	0.318	0.474	0.542	0.207	0.019	0.017	0.014	0.016	0.024	0.016
Fe^{3+}	0.143	0.000	0.000	0.046	0.000	0.047	0.000	0.000	0.004	1.855	1.331	1.080	1.155	1.395	0.757	0.718	0.741	0.727	0.635	0.586
Fe^{2+}	1.469	1.372	1.352	1.306	1.287	1.250	1.206	1.285	1.192	0.000	0.000	0.000	0.000	0.000	2.856	2.726	2.753	2.859	2.648	2.773
Mn	0.028	0.017	0.016	0.021	0.012	0.030	0.023	0.031	0.009	0.061	0.020	0.008	0.015	0.028	0.015	0.020	0.007	0.012	0.017	0.025
Mg	2.657	2.670	2.766	2.746	2.786	2.938	2.867	2.822	2.699	2.425	2.829	2.863	2.762	2.760	0.966	1.093	1.075	0.995	1.188	1.116
Ca	1.898	2.092	1.989	1.940	1.988	1.943	1.972	1.980	1.710	1.715	1.884	1.928	1.911	1.855	1.932	1.919	1.919	1.939	1.928	1.945
Na	0.716	0.618	0.682	0.655	0.663	0.602	0.614	0.669	0.524	0.890	0.625	0.676	0.661	0.745	0.563	0.527	0.543	0.525	0.540	0.520
K	0.239	0.228	0.264	0.267	0.269	0.228	0.255	0.271	0.439	0.027	0.231	0.254	0.263	0.268	0.333	0.287	0.299	0.372	0.245	0.314
Total	15.843	15.797	15.906	15.859	15.877	15.765	15.784	15.887	15.672	15.168	15.387	15.494	15.454	15.524	15.827	15.730	15.761	15.835	15.707	15.775
$Mg/(Mg+Fe^{+2})$	0.64	0.66	0.67	0.68	0.68	0.70	0.70	0.69	0.69	1.00	1.00	1.00	1.00	1.00	0.25	0.29	0.28	0.26	0.31	0.29

Table 3.4. Continuation…

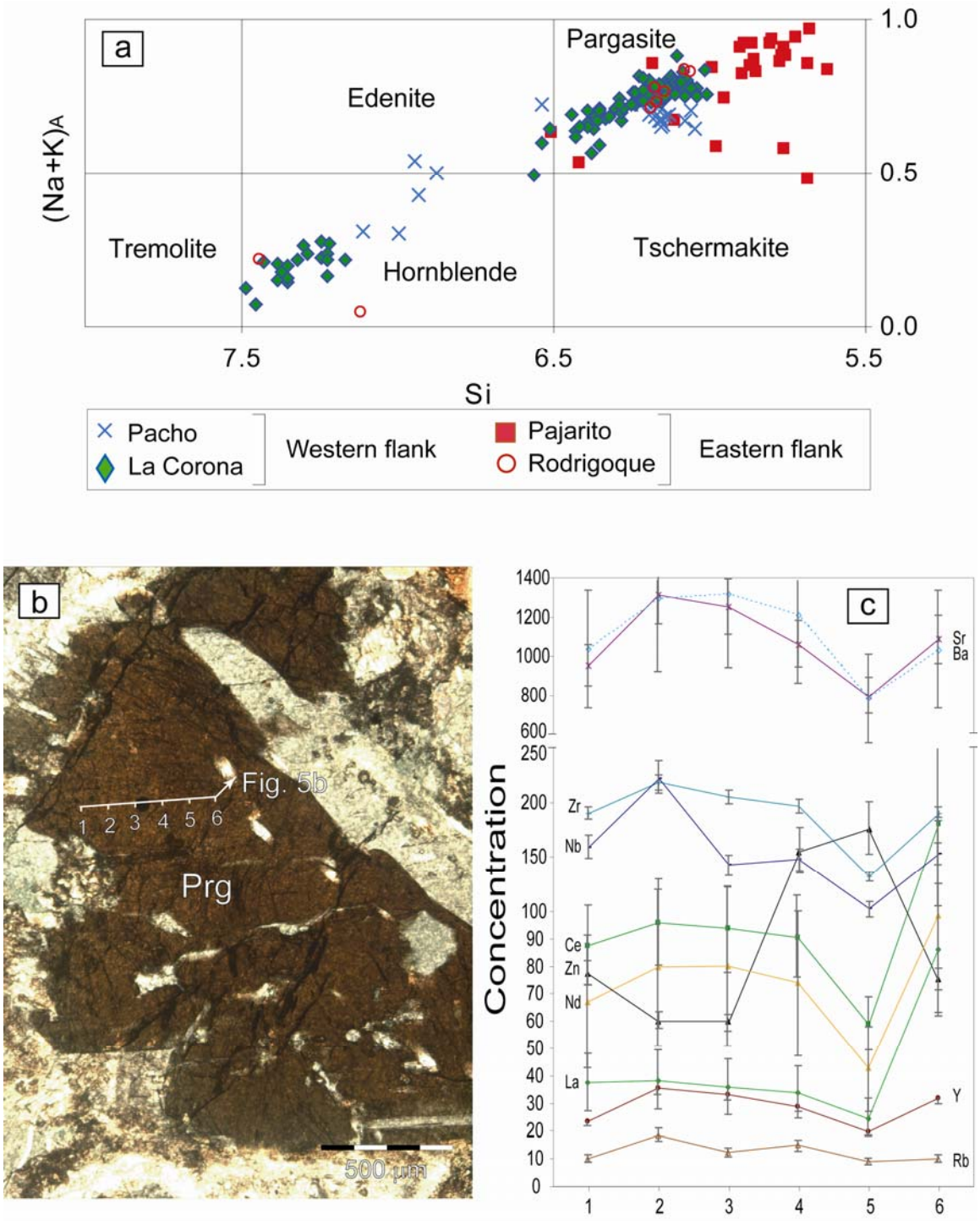

Fig. 3.5. Amphiboles of the mafic intrusions of the EC in Colombia. **a**. General classification after the method from Leake (1997). Data from Pajarito and Pacho after Vásquez and Altenberger (2005). **b**. Photomicrograph of representative amphiboles (pargasite) from Pajarito (sample Pj2); cross-polarized light. **c**. Profile measured on the amphiboles showing the variation of trace elements. Concentrations in ppm

Amphiboles

	La Corona							Pacho						
Sample	LC14a06042	LC14a10051	LC14a10052	LC14a10053	LC14a10054			Pa5a06041 rim to rim		Pa5a06044 rim to rim		Pa5a06047 rim to rim		
Zn	126	116	120	132	137			90	87	97	99	107	102	94	93
Ga	28	20	24	23	23			19	18	18	21	19	20	17	18
Rb	4	4	4	4	5			4	4	15	4	52	3	4	2
Sr	206	162	176	180	286			287	229	213	210	219	206	119	188
Y	123	50	59	56	54			79	71	65	75	101	74	50	65
Zr	390	275	348	324	300			158	140	145	175	228	176	191	154
Nb	78	65	80	84	86			19	17	17	21	22	19	20	22
Sn	7	2	3	4	3			3	3	3	4	5	3	3	3
Ba	357	299	372	378	497			183	155	147	149	174	155	97	141
La	54	36	49	37	46			11	12	15	15	27	15	14	14
Ce	171	110	132	119	128			44	44	47	51	84	55	50	50
Nd	152	65	82	85	97			61	57	56	60	88	64	49	57

	Pajarito													
Sample		Pj2a06041 rim to rim				Pj2a06045 rim to rim				Pj2a06047 rim to rim				
Zn	95	125	102	94	129	70	124	78	60	60	154	176	75	
Ga	20	13	14	20	17	20	16	21	20	19	19	15	22	
Rb	3	10	7	10	5	12	10	10	18	12	15	9	10	
Sr	221	1594	567	829	313	861	640	950	1311	1248	1057	791	1084	
Y	74	3	17	20	11	24	17	23	36	33	29	20	32	
Zr	206	135	239	241	182	187	138	190	218	204	196	132	189	
Nb	21	15	112	140	63	157	138	159	222	143	147	102	153	
Sn	3	1	2	3	1	3	2	2	2	2	2	2	2	
Ba	165	139	388	678	217	1103	839	1033	1293	1316	1208	779	1029	
La	17	81	64	72	65	37	29	38	38	36	34	24	86	
Ce	61	126	122	143	124	86	68	88	96	94	90	59	182	
Nd	72	38	43	57	40	60	49	67	80	80	74	43	99	

Table 3.5. Concentrations of trace elements after the µ-SRXRF analyses of amphiboles from the Eastern Cordillera of Colombia. Data in ppm. udl = under detection limit

Amphiboles

Sample	Pi2a060415	Pi2a060416	Pi2a060417	Pi2a060418	Pi2a060419	Pi7a10051	Pi7a10052	Pi7a10053	Pi7a10054	Pi7a10055	Pi7a10056	Pi7a10057	Pi7a10058
Zn	60	170	183	64	58	62	67	55	66	54	59	60	61	50
Ga	19	8	6	18	16	18	17	20	19	18	20	17	21	19
Rb	12	1	2	12	15	12	12	14	11	14	13	12	15	11
Sr	1002	9	18	826	1022	1014	1271	1285	794	1435	1296	1092	1022	1109
Y	24	0	10	19	24	25	24	20	19	26	27	24	21	26
Zr	182	29	70	193	192	188	188	181	202	224	260	188	166	157
Nb	168	1	88	160	173	171	149	143	166	139	162	141	157	157
Sn	2	1	3	2	2	2	2	2	1	2	2	3	2	1
Ba	1191	16	31	1100	1388	1388	1866	1903	1131	2201	1923	1659	1461	1585
La	36	2	2	38	40	42	40	38	36	51	39	35	32	36
Ce	88	1	4	91	102	105	95	82	95	111	81	93	89	89
Nd	66	0.8	4.8	59	76	74	95	89	54	101	75	73	64	56

		Rodrigoque							
Sample	Pi7a10059	LS7a10053	LS7a10054	LS7a10055	LS7a10056	LS7a10057	LS7a10058 rim to rim		
Zn	80	344	241	240	194	23	280	233	225
Ga	19	5	6	5	19	30	4	7	6
Rb	10	6	5	6	10	16	6	4	14
Sr	743	82	53	54	64	70	64	140	93
Y	17	udl	udl	udl	4	11	udl	2	2
Zr	212	20	14	13	15	13	10	11	49
Nb	166	8	5	5	8	3	4	4	21
Sn	2	3	2	2	4	7	4	3	4
Ba	1048	19	19	10	60	63	21	16	69
La	41	36	20	16	22	12	30	48	31
Ce	98	31	39	26	25	9	44	65	71
Nd	52	50	47	35	18	15	44	70	60

Table 3.5. Continuation…

The presence of pseudomorphic amphiboles (known as uralitization, predominantly tremolite and actinolite) after clinopyroxenes observed in the samples collected in La Corona, suggests that these rocks are overprinted by hydrothermal or low grade metamorphic processes at subgreenschist to greenschist facies conditions. Actinolite and tremolite grow around brown to green hornblendes and show euhedral and acicular habits varying in colours from white to pale green. For this study, the trace-elements contents were determined on those amphiboles whose texture corresponds to original magmatic products. Tremolite and actinolite were not considered as they are secondary phases.

Table 3.5 shows the concentrations of trace elements in amphiboles determined by μ-SRXRF. The variation of trace-element contents within a single grain of pargasite in the sample Pj2 from Pajarito is shown in Fig. 3.5b and 3.5c. The arrangement of the trace elements on the profile shows a persistent anomaly in point #5, which is probably caused by a mineral inclusion or imperfections of the polished section. If point #5 is discarded, the concentration of Rb, Y, Nd and Zr remains almost constant. Higher concentrations of La and Ce are observable at point 6. Nb and Zn have a very scattered distribution.

The P-T conditions determined for the amphiboles in the rocks of Pacho (Vásquez and Altenberger, 2005) show that the crystallization took place at 2 kb and 1000°C approximately.

The trace-element composition of the amphiboles and the whole rock was normalized to chondritic composition (Fig. 3.4) after Sun (1980). With only few exceptions as for instance, the negative anomaly of Ti in the minerals from Rodrigoque and La Corona vs. the positive anomaly in their rock normalization, the trend of the amphiboles reflects very precisely the whole rock data. The amphiboles as well as the rocks show a consistent chondrite-normalized positive anomaly in Nb, Nd, La and Ce, and negative in K and Sr compared to the neighbouring elements. Error bars indicate the mean percentage of relative deviation determined on the reference materials as shown in table 3.1.

3.6. DISCUSSION

The information obtained from the analysis performed on the whole rock suggests at least two different types of sources for the mafic intrusions in the Eastern Cordillera of Colombia (Vásquez and Altenberger, 2005). Although the data of that study are quite conclusive, the altered nature of some of the studied samples causes uncertainties about the original composition of the melt. Furthermore, the Sr-Nd-Pb isotopic data of these rocks indicate a strong influence of sediments, seawater and/or metasomatic fluids (Vásquez et al., 2005), which may also disturb the

original signature of the magmas. The investigation of the concentrations and patterns of trace elements in the first crystallized phases should provide a hint in order to confirm or reject the diversity of the magma source.

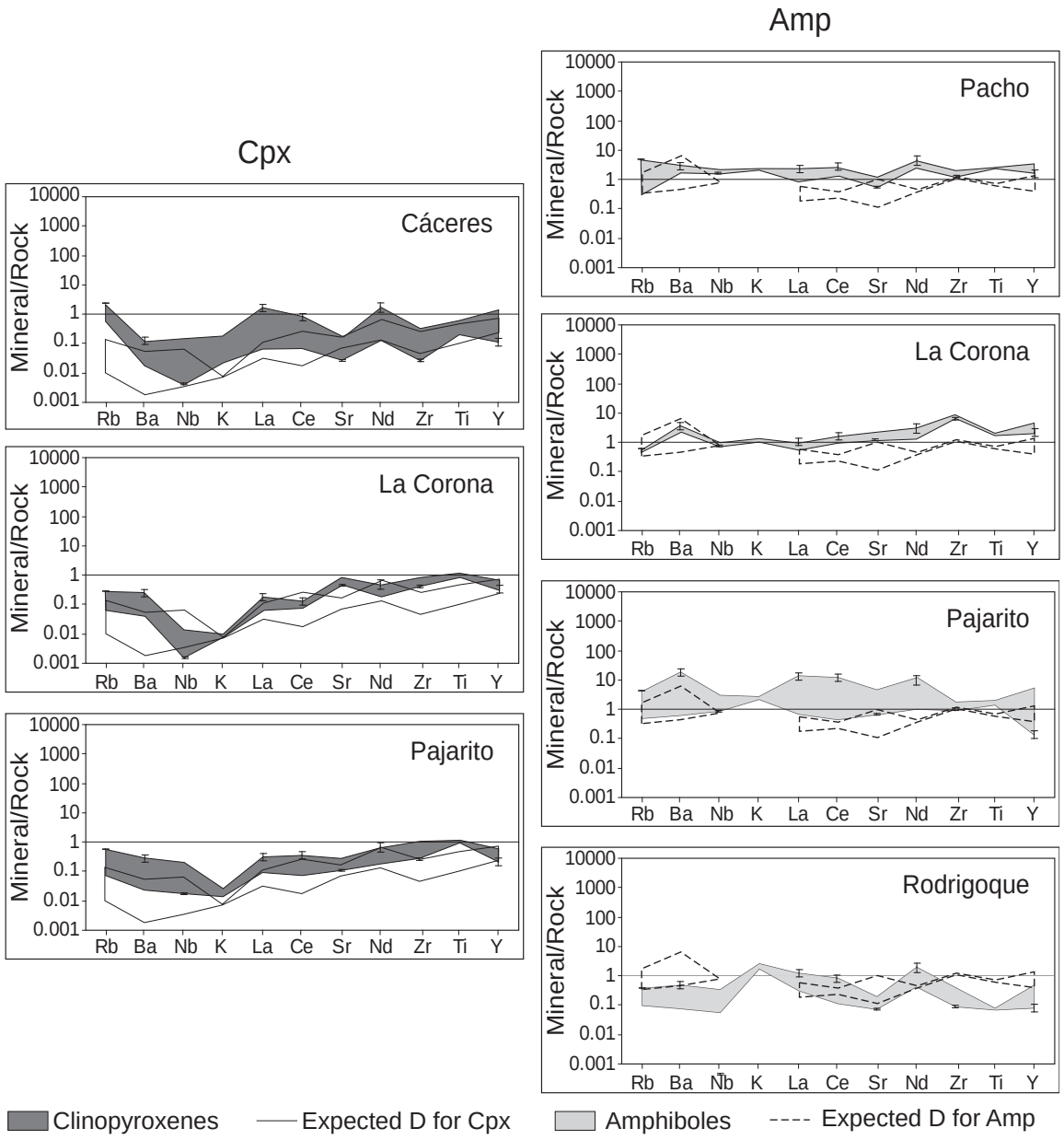

Fig. 3.6. Whole-rock normalized trace-element concentrations of clinopyroxenes and amphiboles. The D values for clinopyroxenes and amphiboles (Villemant et al., 1981; McKenzie and O'Nions, 1991; Hart and Dunn, 1993; Sobolev et al., 1996) are also plotted for comparison

In order to test a potential overprint of the whole rock, the concentrations of the trace elements of clinopyroxenes and amphiboles were normalized to the respective whole rock composition, as shown in Fig. 3.6. These values are compared to the partition coefficients (D) of clinopyroxenes and amphiboles (Villemant et al., 1981; McKenzie and O'Nions, 1991; Hart and

Dunn, 1993; Sisson, 1994; Sobolev et al., 1996; Klein et al., 1997). D can be defined as C_S/C_L , where C_S and C_L are the concentrations in ppm or wt. % of a trace element in the solid and liquid, respectively (McIntire, 1963). A similar pattern for the trace elements between the studied minerals and their corresponding whole rock composition can be expected. Thus, the comparison of whole-rock normalized trace-element values of clinopyroxenes and amphiboles to D can give us hints on secondary processes that may have altered the bulk trace-element contents of these rocks, even though the rocks may have undergone processes of fractional crystallization and are possibly the product of more than one melting phase.

As shown in Fig. 3.6, the D values for the clinopyroxenes from the literature increase from left to right. In contrast, the D for the amphiboles shows a rather flat pattern with slightly higher values for the most incompatible elements (Rb and Ba).

If compared to the D available data, the clinopyroxenes of Cáceres show positive deviations for Rb, La, and Ce. Particularly for Rb, the deviation is quite strong. Clinopyroxenes of La Corona have positive anomalies of Rb, Ba and Sr (Fig. 3.6). In Pajarito the clinopyroxenes have positive deviations for Rb, and Ba. If we consider the clinopyroxenes to be unaffected by post-magmatic processes, the positive anomalies indicate that the bulk of the rocks have lost some of the original concentration of these elements.

The whole rock normalized amphiboles show a roughly flat trend in most of the localities, except some small positive anomalies of Nd in Rodrigoque, Pajarito, and Pacho. In general, the resulting trends for the amphiboles closely follow the D pattern taken from the literature (Villemant et al., 1981; McKenzie and O'Nions, 1991; Hart and Dunn, 1993; Sobolev et al., 1996). For the samples of Pacho, La Corona and Pajarito, the rock-normalized values from La to Y are always slightly higher than D. The similarity of the rock-normalized patterns to the D patterns may be taken as indication that post-magmatic processes have not affected the whole rock. Especially the potentially mobile elements Rb and Ba of Pacho, La Corona and Pajarito do not indicate any mobilization since the normalized values are similar to D in the clinopyroxenes.

The significantly higher Rb value in Cáceres as well as the field observations (folding and deformation of the gabbroic rocks; fig. 3.7) suggest secondary alteration of the whole rock for this locality. For La Corona and Pajarito, however, the data obtained from clinopyroxenes and amphiboles imply slightly contradictory interpretations concerning any secondary alteration of the bulk rock. In comparison to Cáceres, the deviation of the mobile elements, especially Rb, from D for the clinopyroxenes is less significant. Thus, based on this procedure, a potential alteration cannot totally be ruled out for these two localities.

Fig. 3.7 Folded gabbros in the region of Cáceres (Road Puerto Romero-Otanche)

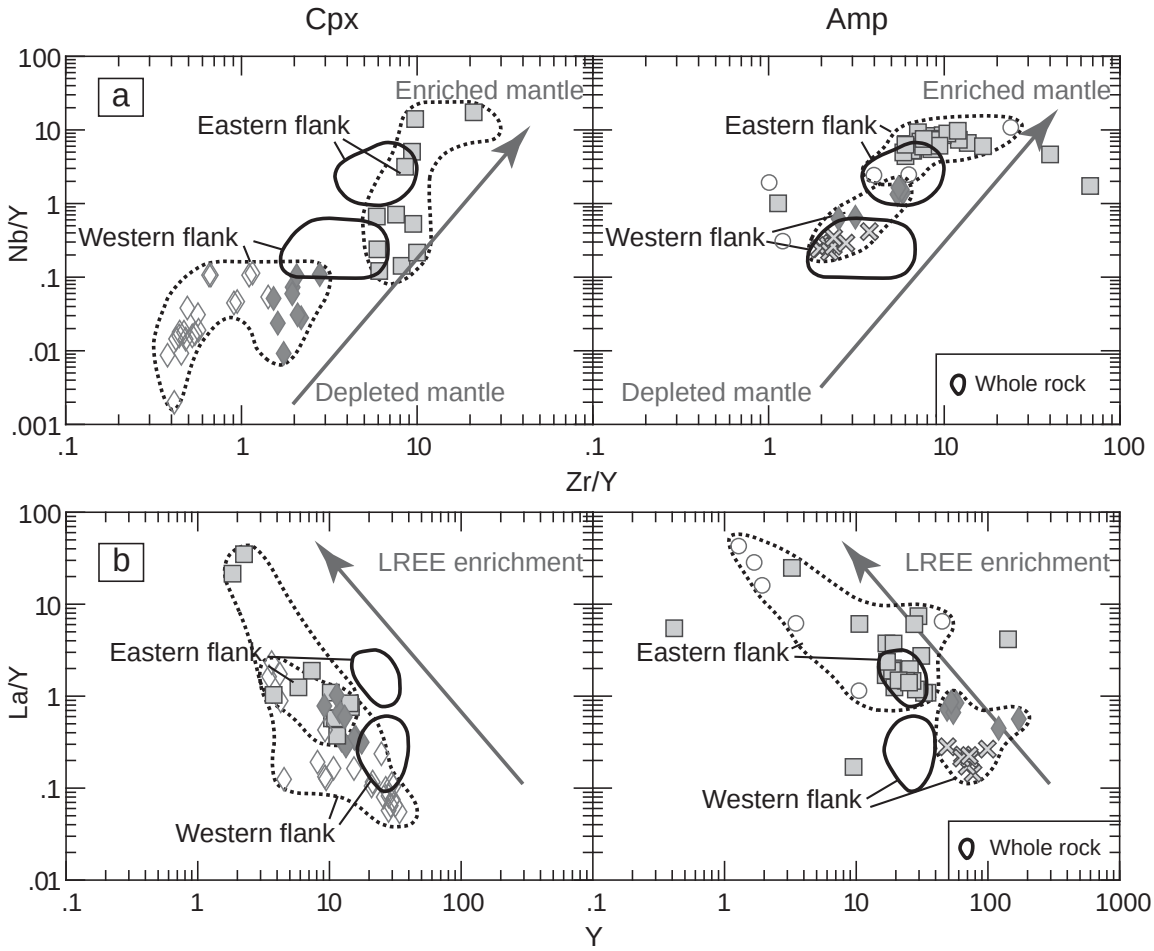

Fig. 3.8 Whole rock, clinopyroxenes and amphiboles trace element ratios. The different patterns have been grouped by the geographic location. Western flank: Cáceres, Pacho and La Corona; Eastern flank: Pajarito and Rodrigoque (see Fig. 3.1; symbols as in Fig. 3.3). **a**. Zr/Y vs. Nb/Y; the rocks from the eastern flank are more enriched in incompatible elements than those from the west. **b**. Y vs. La/Y; the degree of partial melting of the rocks has been lower for the mafic rocks in the eastern flank

For further characterization of the magma sources, the most immobile elements such as Zr, Y, Nb and La will be used. The plots Zr/Y vs. Nb/Y and Y vs. La/Y (Fig. 3.8) show that it is

possible to differentiate two groups with distinctive compositional trends. The data corresponding to the whole-rock analysis are also displayed for comparison. Both groups can also be roughly separated by their geographical location in the EC. The nearly linear trend shown in the plot Zr/Y vs. Nb/Y (Fig. 3.8a) suggests that at least two different source components were involved in the petrogenesis of the magmas. The magma sources are very well discriminated from each other, since it is possible to group the data coming from the east and from the west of the Cordillera independently; the rocks from the east are more enriched in incompatible elements than those coming from the west. Moreover, the patterns observed in the plot Y vs. La/Y (Fig. 3.8b) suggest that the rocks from the eastern flank denote lower degrees of partial melting due to the higher values of La/Y and, subsequently, an enrichment of LREE, which is not observed in the patterns of the samples from the western flank. Although the absolute positions of the whole rock data do not exactly fit the mineral data, the observed trend for both data sets is similar and thus, the interpretation based on the whole rock data (Vásquez and Altenberger, 2005) is still valid.

3.7. CONCLUSIONS

The methodology implemented in this study provides the possibility to determine *in situ* even low contents of trace elements (ca. 0.3 ppm) such as LREE. Another advantage is the simultaneous determination of elements from Zn to Nd with high lateral resolution. The calculated detection limits are particularly good from Rb to Nd (Z= 37-60).

The Cretaceous magmatic episode in the Eastern Cordillera of Colombia reflects at least two different magma sources indicated by differences in the degree of partial melting and enrichment of incompatible trace elements. The chemical pattern of the intrusions suggests an extensional regime of a continental rift (Vásquez and Altenberger, 2005). New geochronological investigations on these rocks (Vásquez et al., in preparation) show that the intrusions were not synchronously emplaced and thus record distinct times of extension for the northern Andes. The dissimilarities of the rocks in terms of degree of partial melting and enrichment/depletion of LREE can be explained by differences in the thickness of the lithosphere and the development of the sub-basins in the Cretaceous which does not necessarily implies an episodic emplacement from east to west.

Since Cáceres is the only intrusion that has two different clinopyroxene phases, it is possible to speculate about the P-T conditions of crystallization. As described by Lindsey (1980), the presence of pigeonite in rocks suggest that the beginning of crystallization took place at high

temperatures around 1100 to 1200°C and low to moderate pressures (1.3 to 1.8 kbar). Additionally, the composition of the melt should be relatively Ca-poor (Deer et al., 1966). The occurrence of pigeonite indicates either rapid cooling, otherwise demixing to orthopyroxene + augite would take place. The clinopyroxenes derived from a tholeiitic melt in Cáceres are quite evolved if we consider the low Mg# values, which confirm as well an invariably low pressure of crystallization. The P-T conditions derived from the analysis of Ti and Al content in amphiboles (Ernst and Liu, 1998) suggest also low pressure of formation (Vásquez and Altenberger, 2005).

The comparison of the whole rock and clinopyroxene-amphibole trace element data provides some insight to the alteration of the gabbroic rocks by post-magmatic processes. Such processes should mainly affect the concentration of LILE, especially Rb, Ba, and Sr. For the samples of Cáceres, alteration of the bulk rock may be indicated by the clinopyroxene/whole-rock ratio of Rb. For La Corona and Pajarito, this ratio for clinopyroxene is lower and data obtained on amphiboles for the same localities do not indicate strong overprint by alteration. The characterization of the magma sources using the most immobile elements (Zr, Y, Nb and La) has proven that the investigated minerals follow the same trend as the whole rock data. Our results document that the approach used here is a feasible alternative for investigating the magmatic origin of strongly altered magmatic rocks as long as relicts of the first crystallized minerals are present that reflect the original state of the rocks shortly after crystallization.

4. INTRA-PLATE MAGMATISM IN THE COLOMBIAN CRETACEOUS BASIN: $^{40}Ar/^{39}Ar$ AGES AND ISOTOPE EVIDENCE OF THE MAGMATIC EVOLUTION OF A SEGMENTED BASIN

Mónica Vásquez [a]

Uwe Altenberger [a]

Rolf L. Romer [b]

Masafumi Sudo [a]

Juan Manuel Moreno-Murillo [c]

[a] *Institut für Geowissenschaften, Universität Potsdam, Karl-Liebknecht-Straße 24, D-14476 Potsdam-Golm, Germany*

[b] *GeoForschungsZentrum Potsdam, Telegrafenberg, D-14473, Potsdam, Germany*

[c] *Universidad Nacional de Colombia, Departamento de Geociencias, Ciudad Universitaria Carrera 30 No 45 - 03, Edificio 224, Bogotá, Colombia*

4.1 ABSTRACT

The Eastern Cordillera of the Colombian Andes represents an inverted Cretaceous basin characterized by scarce magmatism. This magmatism is predominantly recorded by mafic dykes and sills. $^{40}Ar/^{39}Ar$, Sr-Nd-Pb isotopes as well as major and trace elements analyses of the known Cretaceous intrusions that crop out on both flanks of the Cordillera were performed. The results combined with known structural data give an insight in the complex evolution of the basin. The localization of the intrusions has to be explained as a consequence of mantle melting below the most subsiding places of each sub-basin. The mafic intrusions display at least two different magma sources: an alkaline one with OIB-like pattern and a tholeiitic one with MORB-like features. Trace-element patterns indicate that the samples were emplaced in an extensional setting. The degree of partial melting is higher for intrusions located at the western flank of the Cordillera than for intrusions located at the eastern flank.

Influence of seawater in the magmatic system and different degrees of crustal involvement/source contamination were observed in the $^{87}Sr/^{86}Sr$ and $^{143}Nd/^{144}Nd$ isotope data analyses. Furthermore, $^{206}Pb/^{204}Pb$, $^{207}Pb/^{204}Pb$ and $^{208}Pb/^{204}Pb$ isotope ratios indicate two separated groups of intrusions with contribution of different amount and composition of an old crustal source.

$^{40}Ar/^{39}Ar$ dating on primary plagioclases and hornblendes provides reliable plateaus despite some alteration of the whole rock samples. Data demonstrate a diachronous emplacement

of the Cretaceous intrusions between ~136 and ~74 Ma. The extension-related magmatism started in the Cundinamarca Sub-basin with the Pacho intrusion. Although the petrologic features suggest that all the intrusions are related to an extensional setting in the Cretaceous, the geochemical and temporal diversities show that their emplacement was tectonically controlled and correspond to a series of magmatic events. Each sub-basin has an individual subsidence evolution where thickness, structure and composition of the crust play an important role on the melting stage of the magmas.

Keywords: Intraplate magmatism; Cretaceous; extension; radiogenic isotopes; Ar-dating; Colombia.

4.2 INTRODUCTION

Age and chemical character of the magmatic products put important constraints on the reconstruction of the structural evolution of a basin in time and space. The Eastern Cordillera (EC) of Colombia (Fig. 4.1) is an example of a Mesozoic extensional basin that was inverted in the Cenozoic. Despite numerous structural analyses, detailed studies of the composition, age, and origin of the magmatic products as well as their coupling with the structural evolution of the basin is lacking. Therefore, no qualified estimates on the role of subduction-related processes as well as continental rifting or back-arc processes exist. Although magmatism in the EC is scarce several small mafic intrusions have been identified. In this chapter, we synthesize new geochemical and geochronological data and our recently published results from five key areas of the Eastern Andes. Our purpose is to establish the sources, evolution, and the temporal and spatial processes for the generation of the observed variety of magmas. The aim of this study is to investigate the geodynamic significance of the plutonic rocks on both flanks of the EC and to understand how this fits into the general kinematic framework of the Northern Andes and with the proposed tectonic interpretations. Their age of emplacement was first assumed as a minimum age, younger than the host sediments. Later on, K/Ar dating (Fabre and Delaloye, 1983) was performed on whole-rock, biotite and hornblende of the intrusions of Cáceres, La Corona, Pajarito and Rodrigoque (Fig. 4.1). The obtained results show that the intrusions were emplaced during the Cretaceous but are not necessarily synchronous. However, the analytical error of the measurements is high and even the altered nature of the analyzed samples implies many uncertainties.

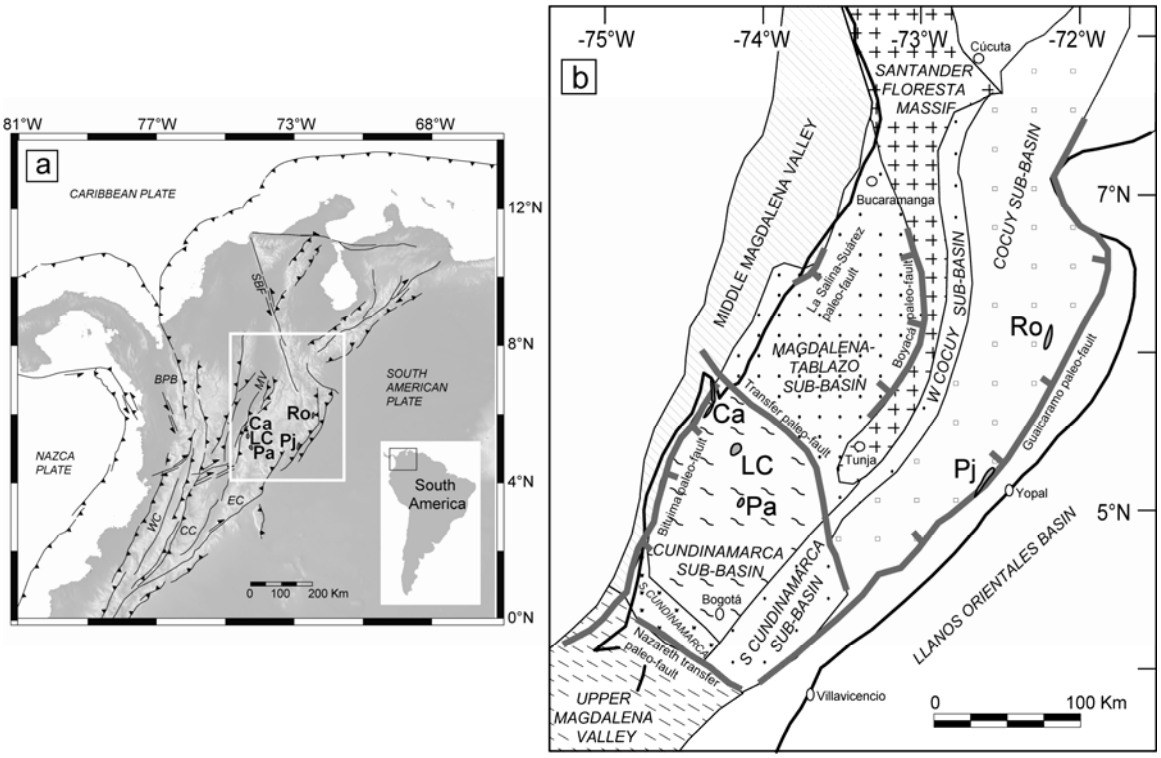

Fig. 4.1 **a** Simplified tectonic map of the Colombian Andes with locations mentioned in the text (Taboada et al., 2000). Abbreviations: BPB, Baudó-Panamá Block; CC, Central Cordillera; EC, Eastern Cordillera; MV, Magdalena Valley; SBF, Santa Marta-Bucaramanga Fault; WC, Western Cordillera. Studied intrusions: Ca, Cáceres; LC, La Corona; Pa, Pacho; Pj, Pajarito; Ro, Rodrigoque; **b** Cretaceous Colombian Basin segmented by palaeo-faults (Sarmiento, 2001). The locations of the intrusions occur in the Cundinamarca and Cocuy sub-basins that had the highest tectonic subsidence. Solid black line represents the limits of the actual Eastern Cordillera.

4.3 TECTONIC SETTING OF THE CRETACEOUS COLOMBIAN BASIN

The presence of calc-alkaline volcanoclastic strata and plutonic rocks in the northern Andes in the Upper Triassic and Lower Jurassic record suggests the existence of a subduction-related magmatic arc (Vásquez et al., 2006). Moreover, during Triassic, Jurassic, and earliest Cretaceous, the northern margin of South America was subject to significant extension as supported after the large thickness of the Mesozoic sedimentary succession.

The subsidence of the Cretaceous basin has been explained as an early rifting phase in the Early Cretaceous followed by a thermal decay after rifting in the Late Cretaceous (Fabre, 1983b; Fabre, 1983c; Fabre, 1987). Three tectonic interpretations have been formulated in order to describe the causes of the subsidence, its evolution and the deformation of the lithosphere. First, a back arc extension acting as a consequence of the subduction zone to the west (McCourt et al., 1984; Fabre, 1987; Toussaint and Restrepo, 1989; Cooper et al., 1995). It has been suggested the existence of a weakly developed Cretaceous magmatic arc in the Central Cordillera (Toussaint and Restrepo, 1994). Second, intracontinental rifting produced by the opening of the

Caribbean Sea and the break-up of Pangea (Geotec, 1992; Cediel et al., 2003). Third, a passive margin for the western continental margin has been proposed (Pindell and Erikson, 1993; Pindell and Tabbutt, 1995) whereby the Caribbean Plate was moving NE-wards and subduction under the South American plate temporary ceased. The evidence to support or refute one of the hypotheses is still very scarce, since the magmatic evolution of the former Cretaceous Basin has not been taken into account in the above mentioned studies. Although it has been proposed that the position where the magmas were emplaced corresponded to the most subsiding places from Berriasian to Cenomanian (Fabre and Delaloye, 1983) there are only few complementary studies (Vásquez and Altenberger, 2005; Vásquez et al., 2005) intending to support that hypothesis.

Stratigraphic studies, tectonic subsidence analysis (Sarmiento, 2001b), structural mapping, and sedimentary facies analysis (Mora et al., 2006) indicate that the Cretaceous Basin (Fig. 4.1b) was comprised by several sub-basins. This suggests that each sub-basin was fault-bounded and had independent subsidence histories (Sarmiento-Rojas et al., 2006). In the northern part of the EC the geometry of the basin has been described as a NNE-SSW striking wide rift system divided by the Santander-Floresta Massif into the Cocuy Sub-basin to the E, the Tablazo-Magdalena Sub-basin to the W. In the southern part, the Cundinamarca Sub-basin has been recognized (Sarmiento, 2001b). A regional tectonic subsidence increasing to the east with maximum rates in the Cocuy Sub-basin region and minimum rates in the Middle Magdalena Valley suggests a regional half-graben geometry for the whole basin (Sarmiento, 2001b; Fig. 2.18). During the Cenomanian a maximum transgression caused a rapidly increase in subsidence. The subsidence was driven by sediment/water load that affected especially the eastern flank, where the Cretaceous is thickest (Sarmiento-Rojas et al., 2006).

In the southern part of the EC, around the latitude of Bogotá, the Cundinamarca Sub-Basin formed a segmented sub-basin in which sedimentation started in the Tithonian? -Berriasian - Valanginian with turbidite deposits, prevailing up to the Hauterivian (Sarmiento, 1989; Moreno, 1991; Parra, 2000).

Pre-Andean deformation took place in the Late Cretaceous – Early Paleocene (Gómez et al., 2005), where a phase of transpression in the present Upper Magdalena Valley and the southern segment of the EC has been related to the final accretion of oceanic crustal fragments of the Western Cordillera (McCourt et al., 1984). Lately, the eastward indentation of the Baudó - Panama Block (BPB) during the Late Miocene has been considered responsible for the main phase of inversion of the Colombian Cretaceous Basin (Taboada et al., 2000).

4.4 ANALYTICAL PROCEDURES

4.4.1 Whole-rock geochemistry

Major and trace elements of gabbroic and tonalitic samples of La Corona and Rodrigoque (Fig. 4.1) were determined in order to get the chemical composition of the samples and to classify them after different criteria. The analyses were performed using a Phillips PW-2400 x-ray fluorescence (XRF) spectrometer at GeoForschungsZentrum Potsdam. Data are shown in tables 4.1 and 4.2. Major and some trace elements (Ba, Ga, Rb, Zn, and Sr) were determined using fused lithium-tetraborate disks, and Cr, Nb, Sc, V, Y, Zr using pressed powder pellets. For the XRF analysis, the estimated precision is better than 1-3% for major elements (depending on concentration levels) and better than 10% for trace elements. H_2O, and CO_2 were determined by means of quantitative high temperature decomposition with a Vario EL III CHN elemental analyzer at the GeoForschungsZentrum Potsdam (Germany). Analytical accuracy and precision was monitored using internationally accepted rock standards.

Rare earth element (REE) analyses were performed on Vista MPX inductively coupled plasma - optical emission spectrometer (ICP-OES) at the Geochemical Laboratory of the University of Potsdam. Rock powders were brought into solution using standard Na_2O_2 fusion and dilution techniques. Analytical accuracy of the appliance is <1%, and the precision for the REE ranges between 5 and 10% after comparison with international reference standards. The concentration of the REE and Rb, Sr, Y, Zr, Cs, Ba, Lu, Hf, Pb, Th, and U were determined by inductively coupled plasma – mass-spectrometry (ICP-MS; Perkin-Elmer/Sciex Elan Model 500 ICP mass-spectrometer) at the GeoForschungsZentrum Potsdam using the method of Dulski, (1994). The compositional data of Cáceres, Pacho, and Pajarito intrusions have been taken from Vásquez and Altenberger (2005).

	La Corona							
Sample	LC4	LC9	LC10	LC11	LC12	LC13	LC16	RB1
wt%								
SiO_2	50.2	60.1	54.1	44.9	44.5	59.8	56.4	70.6
TiO_2	2.58	0.60	1.63	4.14	4.55	0.83	1.44	0.24
Al_2O_3	16.7	18.0	17.4	14.0	12.3	16.0	17.8	16.3
Fe_2O_3*	10.0	0.74	7.99	12.6	12.9	5.75	5.94	0.55
MnO	0.13	0.02	0.06	0.15	0.17	0.09	0.04	0.00
MgO	3.44	0.73	2.41	5.91	8.06	4.15	1.96	1.40
CaO	6.43	5.61	3.96	9.27	9.10	4.85	3.59	2.71
Na_2O	5.04	6.93	7.54	3.06	2.86	3.98	8.09	7.09
K_2O	2.03	1.82	0.52	1.74	1.54	1.86	0.71	0.13
P_2O_5	1.07	0.24	0.62	0.91	0.74	0.27	0.51	0.14
CO_2	0.02	3.85	1.22	0.17	0.25	0.04	1.14	0.04
H_2O	2.34	1.39	2.63	2.57	2.57	2.22	2.17	1.01
LOI	2.36	5.24	3.85	2.73	2.83	2.26	3.31	1.05
Total	100.0	100.0	100.1	99.4	99.6	99.8	99.8	100.2
ppm								
Ba	1050	91	131	575	532	615	222	74
Cr	<10	<10	<10	42	157	135	<10	252
Ga	24	27	24	19	16	20	27	16
Nb	72	97	92	56	51	<10	89	<4
Rb	38	67	9	19	33	91	12	4
Sc	16	14	4	15	21	30	19	15
Sr	873	87	135	714	550	1219	142	250
V	139	10	54	240	230	110	46	<10
Y	46	18	27	27	28	47	45	3
Zn	490	73	280	542	786	74	179	25
Zr	332	75	44	148	227	169	484	5
La		69.6	59.7	39.5	38.0	49.0	88.1	2.43
Ce		145	113	80.8	72.7	98.7	156	4.38
Pr		16.9	13.1	10.2	8.78	12.4	17.2	0.53
Nd		63.3	51.8	44.3	39.5	53.5	65.4	2.25
Sm		11.2	10.9	10.3	9.19	12.7	12.7	0.60
Eu		1.83	3.74	3.34	3.09	4.19	4.08	0.31
Gd		7.19	9.54	9.57	9.25	12.6	11.0	0.64
Tb		0.89	1.35	1.33	1.44	1.76	1.51	0.10
Dy		4.37	6.99	7.00	6.78	9.41	7.79	0.59
Ho		0.71	1.11	1.14	1.22	1.63	1.29	0.11
Er		1.65	2.33	2.68	2.78	3.85	2.75	0.32
Tm		0.19	0.24	0.32	0.37	0.47	0.30	0.04
Yb		1.04	1.14	1.67	2.08	2.55	1.47	0.26
Lu		0.15	0.13	0.22	0.26	0.33	0.16	0.04
Hf		2	1	4		5	1	0.3
Pb		6	11	9		4	9	1
Th		8	7	3		4	5	1
U		2	0.5	1		1	0.5	0.1
Cs		1	0.3	1		2	0.4	0.1
Ta			5	3				
Mg#	25.5	49.7	23.2	31.9	38.4	41.9	24.8	71.7

Table 4.1 Whole rock analyses of plutonic rocks from La Corona

	Rodrigoque			
Sample	LS1	LS3	LS4	LS7
wt%				
SiO_2	44.2	45.6	45.6	43.4
TiO_2	2.43	2.77	2.71	2.74
Al_2O_3	16.5	15.6	15.0	14.4
Fe_2O_3*	8.35	11.9	12.1	12.9
MnO	0.14	0.10	0.18	0.11
MgO	4.03	6.88	8.34	8.60
CaO	10.1	9.05	6.53	9.56
Na_2O	3.72	3.60	4.07	2.73
K_2O	0.33	0.52	0.97	0.67
P_2O_5	0.59	0.61	0.74	0.62
CO_2	6.02	0.07	0.12	0.11
H_2O	3.55	3.53	3.92	3.62
LOI	9.57	3.61	4.04	3.73
Total	100.1	100.3	100.2	99.5
ppm				
Ba	683	122	240	140
Cr	174	218	287	203
Ga	19	17	18	17
Nb	52	57	86	61
Rb	13	14	39	45
Sc	30	23	38	22
Sr	718	451	347	764
V	209	235	230	220
Y	29	23	28	23
Zn	70	25	98	24
Zr	177	90	247	117
La	35.9	34.8		40.6
Ce	70.7	71.8		80.6
Pr	8.50	8.51		9.68
Nd	34.1	34.3		37.9
Sm	6.96	7.03		7.58
Eu	2.53	2.17		2.43
Gd	6.96	6.37		6.87
Tb	1.00	0.91		0.95
Dy	5.60	4.97		5.17
Ho	1.10	0.90		0.89
Er	2.87	2.13		2.15
Tm	0.37	0.24		0.25
Yb	2.36	1.31		1.24
Lu	0.35	0.16		0.14
Hf	4	3		3
Pb	1	2		2
Th	4	5		5
U	1	1		1
Cs	1	1		2
Ta		4		4
Mg#	32.5	36.5	40.9	39.9

Table 4.2 Whole-rock analyses of plutonic rocks from Rodrigoque

4.4.2 $^{40}Ar/^{39}Ar$ dating

The minimum crystallization age of the studied samples was carried out using $^{40}Ar/^{39}Ar$ dating. The analyses were performed in the $^{40}Ar/^{39}Ar$ laboratory at University of Potsdam. After initial sample selection by petrographic microscopy, fresh crystals of plagioclase and hornblende were separated by hand-picking under a binocular microscope.

Sample preparation includes crushing, sieving, washing, and drying. Later, magnetic minerals were separated first, with a hand magnet, and then with a Frantz magnetic separator. Samples with size between 315 to 200μ were selected for hand-picking. Minerals used for dating were extracted from the groundmass, except samples of Rodrigoque intrusion whose minerals correspond to plagioclase phenocrysts.

The irradiation of the samples has been performed in the reactor at Geesthacht Neutron Facility (GeNF), Germany. Samples were irradiated during 4 days (96 hours); the total fast neutron flux density was around $1x10^{12}$ neutron/cm^2/s, considering the previously performed $^{40}Ar/^{39}Ar$ dating with this reactor by the group of GEOMAR (van den Bogaard, 1995). To cut out the thermal neutron flux and prevent the production of ^{40}Ar, the sample holder was wrapped in cadmium foil of 0.5 millimetres thick. The analyzed samples have been irradiated together with a neutron flux monitoring mineral standard sample (Fish Canyon Tuff sanidine) and crystals of CaF_2 and K_2SO_4 in order to correct the interference by Ca and K in the unknown samples. The Fish Canyon Tuff sanidine had been prepared at Geological Survey of Japan (Uto et al., 1997; Ishizuka, 1998). Its age has been defined as 27.5 Ma (Ishizuka et al., 2002). During irradiation, the sample holder was rotated around its vertical axis to ensure the homogenization of a possible neutron flux gradient. After one month of cooling at room temperature, the samples were transported back to the $^{40}Ar/^{39}Ar$ geochronology laboratory of the University of Potsdam.

Two sets of samples were separately irradiated. The samples were analyzed by the method of stepwise heating until total fusion. They were incrementally heated in a Gantry Dual Wave laser ablation system fitted with a 50W CO_2 laser with a wavelength of 10.6 micrometer using a defocused continuous laser beam with a diameter of 3000 μm during 1 to 2 minutes for heating and gas extraction. The released gas was subsequently exposed for 10 minutes to a cold trap at the freezing point of ethanol and two SAES getters. Finally, the purified argon was expanded into the Micromass 5400 noble gas mass spectrometer with high sensitivity and ultra-low background operated in digital and mass-number mode between masses 36 and 40, for isotopic analysis. Final measured isotopic ratios were corrected for background contributions, mass discrimination effects, and post-irradiation decay of ^{37}Ar and ^{39}Ar, and neutron-induced interferences from Ca and K $(^{36}Ar/^{37}Ar)_{Ca}$ as follows: $(4.05\pm0.02)x10^{-4}$, $(^{39}Ar/^{37}Ar)_{Ca}$: $(9.07\pm0.17)x10^{-4}$, $(^{38}Ar/^{39}Ar)_K$: $(1.66\pm0.02)x10^{-2}$, $(^{40}Ar/^{39}Ar)_K$: $(39.3\pm7.9)x10^{-4}$ for the former irradiation and $(^{36}Ar/^{37}Ar)_{Ca}$: $(4.38\pm0.02)x10^{-4}$, $(^{39}Ar/^{37}Ar)_{Ca}$: $(9.18\pm0.15)x10^{-4}$, $(^{38}Ar/^{39}Ar)_K$: $(1.84\pm0.03)x10^{-2}$, $(^{40}Ar/^{39}Ar)_K$: $(48.8\pm8.3)x10^{-4}$ for the latter. Average blanks of the analytical system for both measurements were $1.87x10^{-12}$ to $5.49x10^{-12}$ for ccSTP for ^{40}Ar, $7.59x10^{-15}$ to

$1.16x10^{-14}$ ccSTP for ^{39}Ar, $4.88x10^{-16}$ to $8.06x10^{-15}$ ccSTP for ^{38}Ar, $6.14x10^{-15}$ to $4.80x10^{-15}$ ccSTP for ^{37}Ar and $7.14x10^{-15}$ to $3.17x10^{-14}$ ccSTP for ^{36}Ar. Total blanks were measured every third step.

J values obtained in the reactor range from $2.105x10^{-3}$ to $2.197x10^{-3}$ for the first irradiation, and from $1.691x10^{-3}$ to $1.768x10^{-3}$ for the second. Furthermore, J value errors were 0.8 % and 0.4 %, respectively. The parameters used to correct the interference are similar to those summarized from the reactors used for $^{40}Ar/^{39}Ar$ dating around the world (McDougall and Harrison, 1999). The analysis of a single step took around 30 minutes.

Age calculation follows the definition of Uto et al. (1997). Moreover, considering the definition of the plateau in McDougall and Harrison (1999) we use the following criteria to define a plateau for the dated samples: 1) it has to include at least 50% of the total ^{39}Ar released, 2) the ages of two contiguous steps in the plateau should agree with two sigma (2σ) error, excluding J value error, 3) one apparent age of the plateau should have more than 3% of the total ^{39}Ar released. Isochron ages are calculated after the parameters defined by Isoplot 3.0 (Ludwig, 2003). Chemical composition of the minerals was obtained using a Cameca SX50 electron microprobe with 15 keV and 20 nA beam current at GeoForschungsZentrum Potsdam. Table 4.3 shows a summary of the dated samples with their average content of K_2O% and the weight of each sample; however, for one analysis around half to one third of the total material separated was used.

Sample	Mineral	K_2O%	Weight (mg)
Ca10	Plag	0.17	48.42
Ca11	Plag	0.13	27.40
LC13	Hbl	0.64	27.00
RB1	Plag	0.10	53.65
Pa5	Hbl	0.25	19.18
Pj7	Hbl	1.12	24.40
LS1	Plag (phenocrysts)	0.32	24.31

Table 4.3 K_2O content and weight of the dated samples

4.4.3 Isotope geochemistry

Determination of Sr, Nd, and Pb radiogenic isotopes in gabbroic and tonalitic samples was done with the intention of characterize the source of the melts, as well as to identify secondary processes involved during their ascent and emplacement. Sr, Nd, and Pb were separated from whole-rock samples. Sr was separated using standard cation exchange techniques (Bio Rad AG50 W-X8, 100-200 mesh, 3.8 ml resin) in 2.5 N HCl medium. Before elution of the REE with 6 N HCl, Ba was washed out with 2.5 N HNO_3 (Romer et al., 2005). Nd was separated from the

other REE using standard cation exchange techniques (HDEHP-coated Teflon, 2 ml resin) in 0.18 N HCl and 0.4 N HCl medium, respectively. Pb was separated using anion exchange resin Bio Rad AG1-X8 (100-200 mesh) in 0.5 ml Teflon columns by HCl-HBr ion exchange chemistry. Pb was purified by a second pass over the column.

Sr was loaded on single Ta-filaments and its isotopic composition was determined on a VG 54-30 Sector multicollector mass-spectrometer using a triple-jump dynamic multicollection experiment. $^{87}Sr/^{86}Sr$ are normalized with $^{86}Sr/^{88}Sr=0.1194$. Nd was loaded on double Re-filaments and its isotopic composition was measured on a Finnigan MAT262 multicollector mass-spectrometer using a double-jump dynamic multicollection experiment. $^{143}Nd/^{144}Nd$ data are normalized with $^{146}Nd/^{144}Nd=0.7219$. Pb was loaded, together with H_3PO_4 and silica-gel, on single Re-filaments (Gerstenberger and Haase, 1997). The isotopic composition of Pb was determined at 1200-1250°C on a Finnigan MAT262 multicollector mass-spectrometer using static multicollection. Lead isotope data were recalculated to the $^{40}Ar/^{39}Ar$ age using the contents of Pb, Th, and U (Tables 4.1 and 4.2) and the constants recommended by IUGS (Steiger and Jager, 1977).

4.5 GEOCHEMISTRY AND PETROGENETIC PROCESSES

The geochemistry of the Cáceres, Pacho and Pajarito intrusions was presented in Vásquez and Altenberger (2005) and are also summarized in figures 4.2b to 4.5. The mineralogical classification of the rocks is presented in the figure 4.2a. The rocks are compositionally diverse, ranging from tholeiitic to alkaline. This compositional range suggests changing melt sources, different depths of melting and/or crystallization, mantle metasomatism and differing degrees of partial melting.

In the present study twelve samples of the intrusions of La Corona and Rodrigoque were analyzed and were integrated with previous analyses of the of the Cretaceous intrusions (Vásquez and Altenberger, 2005). Ten samples were analyzed for REE; the analytical data are shown in Tables 4.1 and 4.2. Petrographically, the rocks of both localities demonstrate effects of low grade metamorphism as is suggested from the presence of secondary epidote, chlorite, actinolite, and tremolite. In addition, weathering may have caused changes in composition, affecting especially the mobile elements (e.g. Cs, Rb, U) modifying the concentration of those elements and elevating the content of H_2O and CO_2. However, the results show no correlation between these elements, which suggests that the alteration did not play an important role and did not substantially affect the bulk composition of the rocks. The intrusions are composed by

clinopyroxene hornblendites, hornblenditic gabbros, and gabbros. A subordinate group can be defined, namely, the Cretaceous tonalites from La Corona intrusion, whose petrogenetic characteristics differ from the first group.

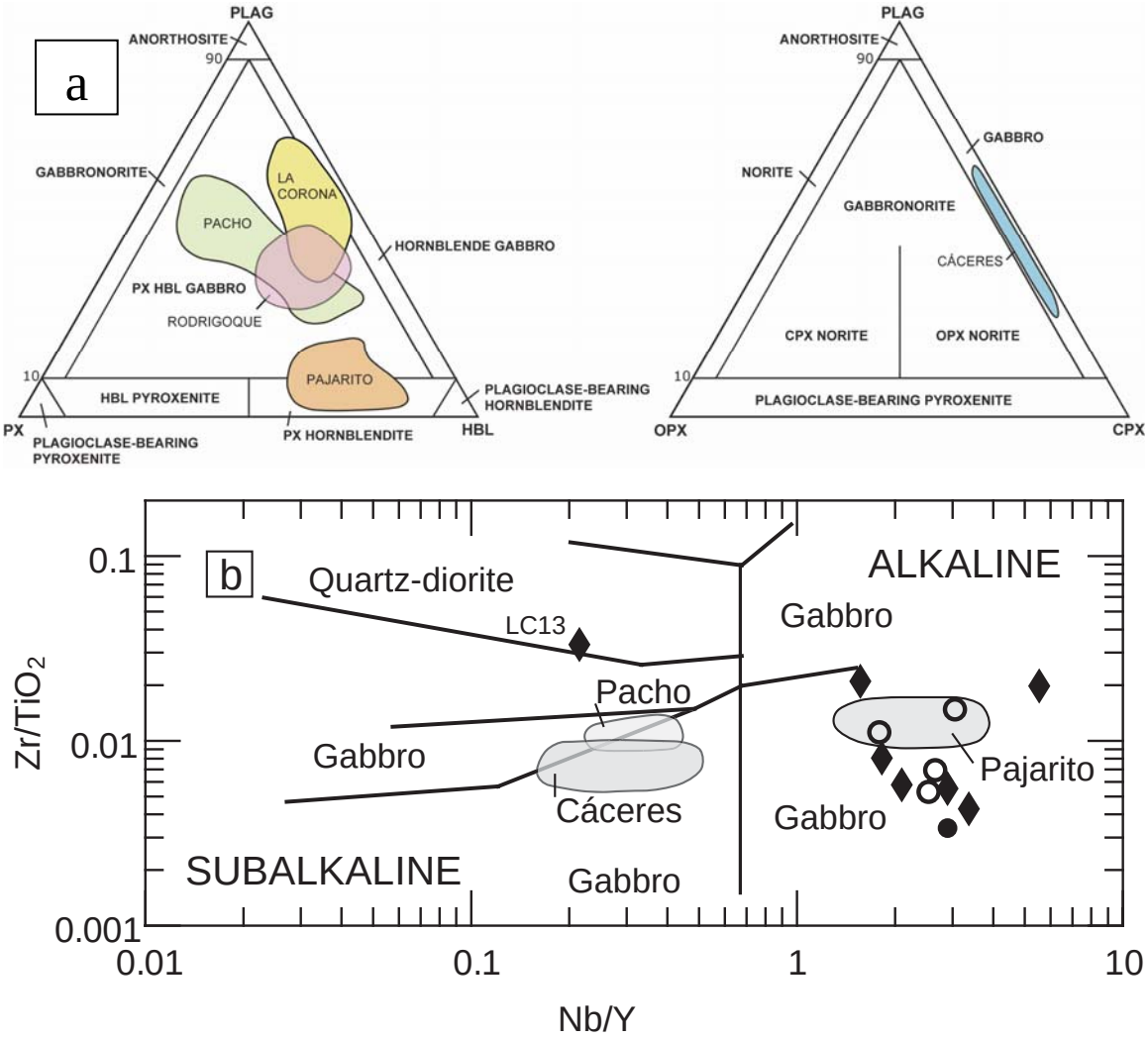

Fig. 4.2 **a** Mineralogical classification of the five studied localities (Streckeisen, 1976); **b** Nb/Y vs. Zr/TiO_2 diagram showing the alkali affinity of the intrusions of La Corona and Rodrigoque. The deviation of the sample LC13 from the other samples of La Corona, plotting on the subalkaline field, will be discussed on the text.

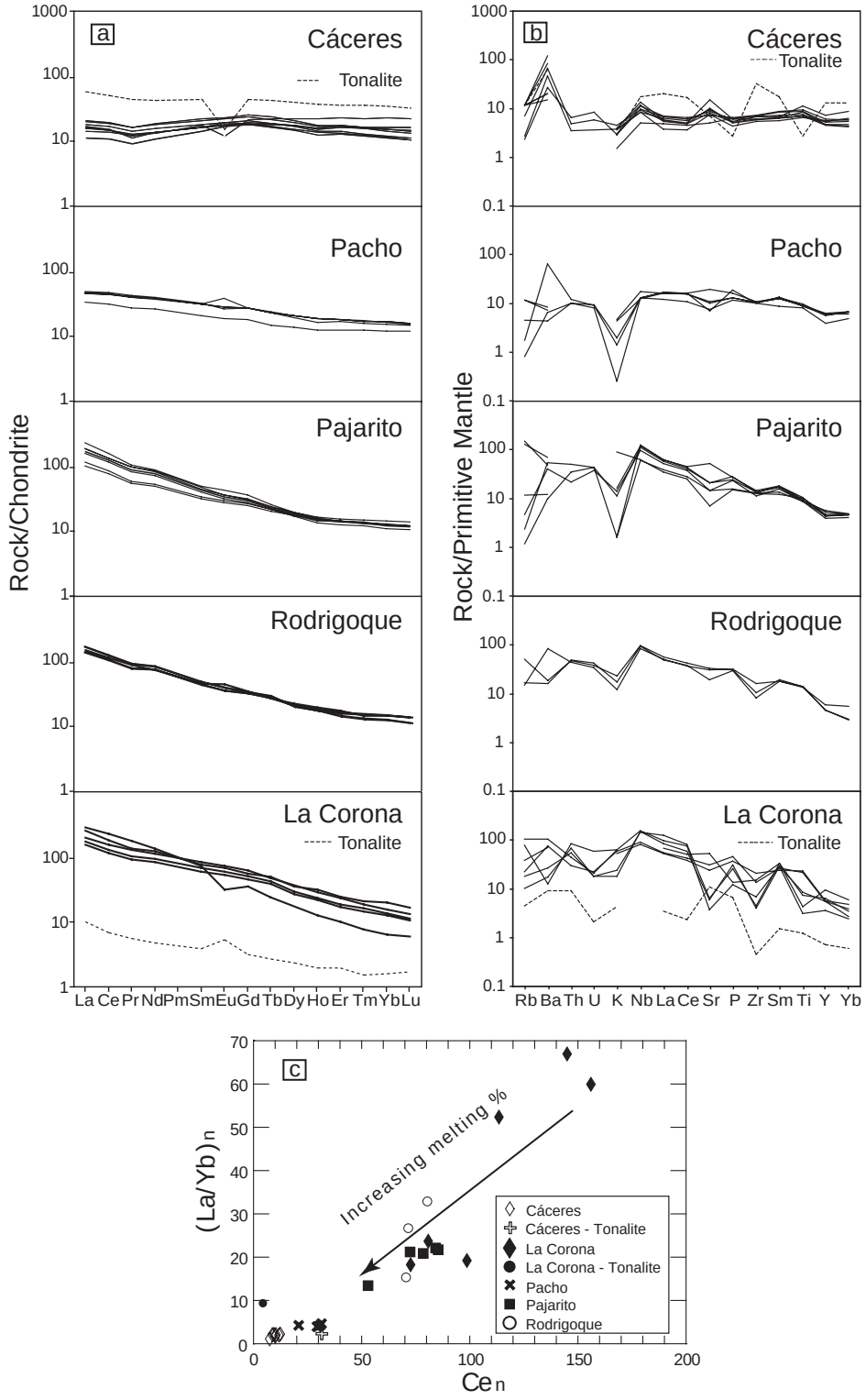

Fig. 4.3 **a** Chondrite-normalized REE patterns (normalization after Evensen et al., 1978) and **b** primitive mantle-normalized trace element patterns (normalization values of Wood et al., 1979); **c** Ce_n vs. $(La/Yb)_n$. with degree of melting (%) using chondrite normalization values of Evensen et al., 1978.

The rocks of the La Corona intrusion are characterized by a wide range of SiO_2 (45-71 *wt*%), Al_2O_3 (12-18 *wt*%), and MgO (0.7-8 *wt*%). Sample RB1 has 71 *wt*% SiO_2 and according to its mineral composition (quartz and plagioclase) is classified as tonalite. The calculated Mg# (magnesium-number) [100*MgO/(MgO+Fe_2O_3*)] ranges from 23 to 50 for gabbroic rocks and up to 72 for tonalites. Total Fe is reported as Fe_2O_3* and the major element data were normalized to 100% on a LOI-free basis.

Generally, the Rodrigoque samples exhibit a more restricted range of major and trace element composition (Table 4.2). The SiO_2 contents vary between 44-46 *wt*%, whereas Al_2O_3 and MgO are between 14-16.5 *wt*% and 4-8.6 *wt*%, respectively. Mg# ranges from 32 to 41.

The mineral classification (Streckeisen, 1976) shows that the La Corona and Rodrigoque samples can be classified as hornblendic gabbros, and pyroxenic hornblendic gabbros (Fig. 4.2a). Some tonalites were also recognized (sample RB1). Trace element compositions suggest an alkaline affinity, except for sample LC13 which plots in the subalkaline field (Fig. 4.2b).

The trace element concentrations were normalized to chondrite (Evensen et al., 1978) and primitive mantle values (Wood et al., 1979) as shown in Fig. 4.3. For comparison, plots of Cáceres, Pacho, and Pajarito intrusions are also presented. The chondrite-normalized element concentrations (Fig. 4.3a) show similar patterns for samples from La Corona and Rodrigoque localities. The light rare earth elements (LREE) exhibit negative slopes and show an enrichment of more than 200 times chondrite values. In the Rodrigoque samples, the heavy rare earth elements (HREE) present a slightly flattened pattern. A negative Eu anomaly was observed in the sample LC9 (Eu* 0.62). On the other hand, La Corona tonalite has a similar pattern as the other samples but is less enriched and has a slightly positive (Eu* 1.51) Eu anomaly due to the high plagioclase content.

The primitive mantle-normalized multi-element patterns show negative K and Zr and positive Nb and P anomalies (Fig. 4.3b). The La Corona tonalite shows generally lower trace element concentrations but have a comparable trend with the more mafic rocks of the same intrusion.

The plot Ce_n vs. $(La/Yb)_n$ suggests different degrees of partial melting (Fig. 4.3c). Samples of the eastern flank of the EC (Pajarito and Rodrigoque) have a lower degree of partial melting than those from the western flank (Cáceres and Pacho). Exceptions to this geographic arrangement are the rocks from La Corona whose relative partial melting varies from the lowest

in the gabbroic rocks to the highest in the tonalite. However, a continuous melting is still a matter of discussion.

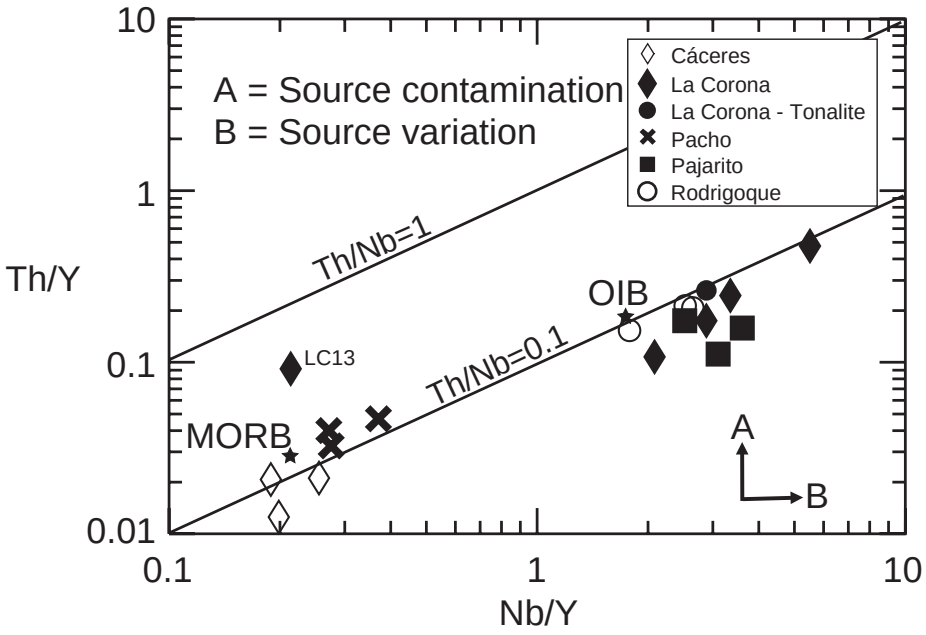

Fig. 4.4 Nb/Y vs. Th/Y diagram for the mafic intrusions of the EC. MORB and OIB after Sun and McDonough (1989).

In terms of source composition, the intrusive rocks can be subdivided into two groups as shown in Fig. 4.4. The plot Nb/Y vs. Th/Y shows two well defined groups that have MORB- (middle oceanic ridge basalts) and OIB-like (oceanic island basalts) character (Sun and McDonough, 1989). This indicates that the respective parent melts were derived from different mantle depths, since the upper mantle (the source of MORB) is generally depleted in incompatible elements (MORB) whereas the lower mantle is not (the source of OIB).

Own field observations and published literature concerning the geological evolution of the Cretaceous basin point to an extensional regime (Etayo-Serna et al., 1976; Fabre, 1983b; Fabre, 1983c; Fabre and Delaloye, 1983; Fabre, 1985; Cooper et al., 1995; Sarmiento, 2001b; Gómez et al., 2005). Furthermore, the tectonic setting was tested using the trace element concentration in the magmatic rocks (Fig. 4.5). The La/10-Y/15-Nb/8 discrimination diagram of Cabanis and Lecolle (1989) shows that most samples of Pacho plot in continental field and the samples of Cáceres, La Corona, Pajarito, and Rodrigoque plot in the oceanic field suggesting a within plate setting interpreted as a continental rift (Fig. 4.5a). The diagram Ti/1000 vs. V of (Shervais, 1982) confirms magma emplacement in an extensional setting (i.e. continental rift) and does not support a magmatic arc setting (Fig. 4.5b).

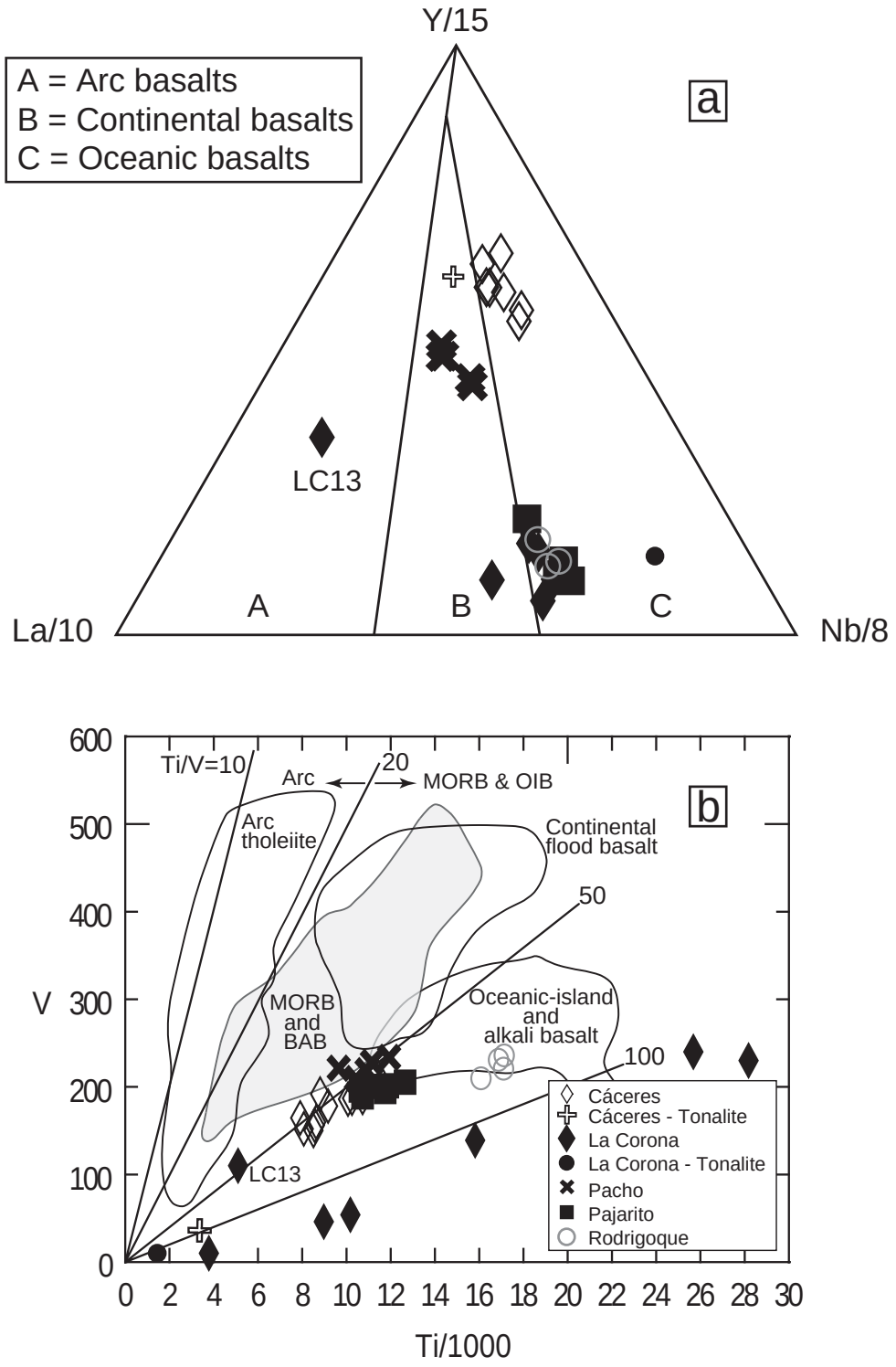

Fig. 4.5 Discrimination diagrams for the Cretaceous intrusions in the Easten Cordillera. **a** La/10-Y/15-Nb/8 ternary diagram after Cabanis and Lecolle (1989). This diagram indicates within plate (Continental rift) setting for the studied rocks. **b** Ti/1000 vs. V diagram after (Shervais, 1982) confirms the continental rift setting.

Sample LC13 from the La Corona intrusion has a trace element composition very different than those of the other samples of the same intrusion (Figs. 4.2b, 4.4 and 4.5). The figure 4.3c suggest a fractionation of the melt of La Corona which point to a successive fusion of a parental magma and furthermore an apparent heterogeneity of the magmatic products.

Summarizing, it is possible to differentiate two main groups in these rocks. The first group comprises the subalkaline rocks of Cáceres and Pacho intrusions that reflect a relatively high degree of partial melting. The gabbros have a MORB-like composition and the subordinate tonalites show a similar flat trend. The second group is represented by the alkaline rocks from La Corona, Pajarito and Rodrigoque intrusions revealing an OIB-like composition and lower degree of partial melting.

4.6 GEOCHRONOLOGY

4.6.1 Previous work

The Cáceres intrusion is hosted in Aptian to Cenomanian black shales and marlstones of Paja, Hiló, and Simití formations (Morales et al., 1958); the Pacho intrusion cuts the Upper Albian to Lower Cenomanian Pacho Formation (Navarrete et al., 2002). Thus, the field relations indicate that the parent melts of these rocks must have crystallization and cooling ages younger than 93.5±0.8 Ma, the age of the Cenomanian-Turonian boundary (Gradstein et al., 2004). The La Corona diorites and tonalites intruded Albian black shales of the Simití Formation (Tenjo, 2003), and should therefore be younger than 99.6±0.9 Ma (Gradstein et al., 2004). The Pajarito hornblende-gabbros and hornblendites intrusion cuts the black shales of the Berriasian to Valanginian Lutitas de Macanal Formation (136.4±2.0 Ma) (Gradstein et al., 2004). The Rodrigoque gabbroic intrusion was described as of up to 2 m thick dykes cutting siltstones and black shales (Fabre, 1983a) of the Berriasian to Valanginian Lutitas de Macanal Formation (136.4±2.0 Ma) (Gradstein et al., 2004).

4.6.2 New results

A total of seven samples from the five localities were analyzed. The step heating $^{40}Ar/^{39}Ar$ spectra and analytical data for the intrusions of the EC are presented in Fig. 4.6 and Table 4.4, respectively. $^{40}Ar/^{39}Ar$ step-heating experiments were performed on groundmass plagioclase (Cáceres, La Corona) and hornblende separates (La Corona, Pacho, Pajarito) and phenocrysts of plagioclase for the intrusion of Rodrigoque. It should be noticed that, due to their

plutonic nature, the studied rocks have presumably cooled slowly. Therefore, the plateau ages do not necessarily represent their crystallization age but the timing of cooling of the respective minerals through the closure temperature for argon diffusion. Moreover, the shape of the step-heating spectrum can give us some hints about the thermal evolution of the samples, even in the absence of a valid, calculated plateau. Details for each intrusion are given below.

4.6.2.1 Cáceres

Two samples of groundmass plagioclase separated from gabbro samples Ca10 and Ca11 were analyzed in order to constrain the minimum crystallization ages (Fig. 4.6a). Sample Ca10 was analyzed in duplicate. It yielded irregular gas release spectra that provide an idea about the thermal history but is open to interpretation. Notable characteristics are: 1) the anomalously old apparent ages of the gas fractions released during the lowest temperature steps, 2) the younger ages (~62-67 Ma) recorded just before the apparent plateau is reached and 3) a gradually increasing of ages to the higher temperature steps at the end of the spectrum (evident in the duplicate analysis, Fig. 4.6a, Table 4.4). The total ages of 79.8 and 81.4 Ma obtained from the duplicate analysis of the sample Ca10 agree within 2σ error. Additionally, the last step of the analysis number 1 includes a large fraction of ^{39}Ar (62%) yielding an age of 78.4 Ma. Although spectra of the sample Ca10 show relatively complex patterns, it is possible to assume a geologically meaningful age between 78 and 82 Ma.

On the other hand, a 74.1±0.4 Ma plateau age (steps 4 to 11, comprising 77% of total ^{39}Ar released) was calculated for sample Ca11. Sample Ca11 yielded inverse and normal isochron ages of 73.7±2.6 Ma and 73.6±2.6 Ma, respectively, which support the plateau age.

4.6.2.2 La Corona

Groundmass hornblende of the dioritic sample LC13, and groundmass plagioclase from sample RB1 (tonalite) were dated. The intrusion of La Corona is hosted in the Albian (99 – 112 Ma) black shales of the Simití Formation (Tenjo, 2003).

Sample LC13 was analyzed in duplicates and both analysis yielded similar results (Fig. 4.6b). The spectrum reveals the presence of excess Ar at low temperature steps, but in the duplicate the higher temperature steps define a 96.7±0.2 Ma plateau age (heating steps 9 to 12, comprising 68% of the total ^{39}Ar released; Fig. 4.6b). We calculated a 95.4±3.4 Ma inverse isochron age and a 95.5±2.9 Ma normal isochron age.

Analysis number	Sample	Analyzed mineral	Heating %	39Ar/40Ar measured	±	39Ar%	Ar cum%	Age	±	Total gas age (Ma)	Identified plateau	Plateau age (Ma)	Inverse age (Ma)	Normal age (Ma)
1	Cáceres													
	Ca10	Plagioclase	0.8	2.80E-03	14.00	0.00	0.00	16136.72	547536.69	**79.8 ± 0.9**	nd	nd	nd	nd
			1.0	2.22E-03	4.10	-0.01	-0.01	858.53	645.07					
			1.2	2.81E-04	9.30	0.01	0.00	444.56	933.64					
			1.4	1.63E-04	7.10	0.07	0.07	1116.01	267.59					
			1.6	2.57E-04	3.90	0.16	0.24	42.84	174.68					
			1.8	5.07E-04	2.80	0.50	0.73	296.74	42.73					
			2.0	1.01E-03	1.50	1.12	1.85	190.75	25.91					
			2.2	2.70E-03	1.10	2.46	4.31	72.07	10.59					
			2.4	7.48E-03	0.48	6.14	10.45	77.47	6.54					
			2.6	2.02E-02	0.70	6.25	16.69	70.57	3.25					
			2.8	2.26E-02	1.10	7.70	24.39	76.73	3.03					
			3.0	1.60E-02	0.65	6.94	31.33	71.47	2.22					
			3.2	2.25E-02	0.91	6.71	38.04	67.53	2.19					
			3.4-6.0	2.05E-02	0.33	61.96	100.00	78.37	0.87					
2	Ca10 (duplicated)	Plagioclase	1.4	1.22E-04	5.20	0.06	0.06	413.03	139.47	**81.4 ± 0.9**	yes	**81.7 ± 0.8**	**31.2 ± 3.6**	**27 ± 190**
			1.8	2.41E-04	1.50	0.43	0.49	406.49	54.08					
			2.2	1.33E-03	0.66	2.96	3.45	135.35	9.16					
			2.6	4.03E-03	0.34	5.46	8.91	72.20	3.55					
			3.0	9.70E-03	0.23	6.21	15.12	80.37	3.29					
			3.4	1.61E-02	0.33	9.47	24.59	70.30	1.47					
			3.8	2.54E-02	0.50	11.12	35.71	68.39	1.33					
			4.2	2.43E-02	0.35	9.60	45.31	62.20	1.01					
			4.6	1.95E-02	0.64	7.14	52.45	77.91	1.87					
			5.0	1.93E-02	0.52	6.77	59.22	78.36	1.46					
			5.4	1.78E-02	0.39	5.34	64.56	83.80	1.77					
			5.8	1.90E-02	0.63	2.99	67.55	86.18	2.31					
			6.4-8.2	1.91E-02	0.87	32.45	100.00	86.69	2.12					
3	Ca11	Plagioclase	1.4	3.35E-04	2.4	0.11	0.11	-377.25	-97.98	**74.03 ± 0.4**	yes	**74.1 ± 0.4**	**73.7 ± 2.6**	**73.6 ± 2.6**
			2.0	2.10E-03	0.35	3.30	3.41	70.69	5.58					
			2.6	6.41E-03	0.2	9.28	12.69	69.78	1.45					
			3.2	1.26E-02	0.39	12.31	25.00	73.94	0.87					
			3.8	2.52E-02	0.18	22.60	47.61	72.75	0.78					
			4.4	2.39E-02	0.46	13.81	61.41	73.54	1.49					
			5.0	2.44E-02	0.3	8.69	70.11	76.95	1.30					
			5.6	2.49E-02	0.32	5.49	75.59	75.92	1.23					
			6.2	2.49E-02	0.29	2.72	78.31	73.18	1.82					

Table 4.4 Analytical data of $^{40}Ar/^{39}Ar$ step-heating results for the plutonic rocks in the Eastern Cordillera, Colombia. nd: no determined

Analysis number	Sample	Analyzed mineral	Heating %	39Ar/40Ar measured	±	39Ar%	Ar cum%	Age	±	Total gas age (Ma)	Identified plateau	Plateau age (Ma)	Inverse age (Ma)	Normal age (Ma)
			6.8	2.52E-02	0.46	4.55	82.86	74.21	1.64					
			7.4	2.12E-02	0.33	6.13	88.99	73.96	1.13					
			8.0-8.4	2.53E-02	0.24	11.01	100.00	79.53	1.21					
	La Corona													
4	LC13	Hornblende	1.4	6.71E-04	1.3	9.86	9.86	324.56	27.21	**97.5±0.2**	**yes**	**96.7 ± 0.4**	**nd**	**nd**
			2.0	1.96E-03	1.4	14.08	23.94	83.95	17.01					
			2.6	5.13E-03	0.5	18.31	42.25	76.40	7.61					
			3.2	2.29E-02	0.2	22.54	64.79	96.35	0.68					
			3.6	2.88E-02	0.2	25.35	90.14	96.81	0.46					
			3.8	2.93E-02	0.14	25.35	115.49	98.17	0.51					
			4.0	2.91E-02	0.06	26.76	142.25	98.49	0.49					
				2.87E-02	0.2	28.17	170.42	96.39	0.51					
5	LC13 (duplicated)	Hornblende	1.4	2.66E-04	1.5	0.05	0.05	711.89	64.642	**97.8±0.1**	**yes**	**96.7 ± 0.2**	**95.4 ± 3.4**	**95.5 ± 2.9**
			2.0	1.98E-03	1.6	0.28	0.33	163.41	9.23					
			2.6	5.84E-03	1.2	0.66	0.99	93.32	3.75					
			3.0	1.56E-02	0.5	2.07	3.05	114.26	1.22					
			3.2	2.15E-02	0.3	4.66	7.72	101.73	1.02					
			3.4	2.72E-02	0.32	7.23	14.95	96.75	0.68					
			3.6	2.78E-02	0.25	12.78	27.73	97.93	0.53					
			3.6	2.82E-02	0.48	4.79	32.52	93.86	1.13					
			3.8	2.98E-02	0.13	14.60	47.12	97.21	0.46					
			3.8	2.93E-02	0.26	7.60	54.71	96.71	0.56					
			4.0	3.05E-02	0.2	15.05	69.76	96.26	0.47					
			4.2	3.03E-02	0.07	30.24	100.00	96.60	0.39					
6	RB1	Plagioclase	2.0	9.63E-04	0.36	1.51	1.51	46.08	8.592	**73.1 ± 0.5**	**yes**	**66.5 ± 0.5**	**64.3 ± 2.3**	**64.3 ± 2.3**
			2.6	3.38E-03	0.28	3.99	5.49	69.08	1.40					
			3.0	7.14E-03	0.19	21.78	27.27	66.19	0.74					
			3.4	7.34E-03	0.14	14.48	41.75	65.37	1.82					
			3.4	9.86E-03	0.17	13.96	55.72	64.89	1.27					
			3.6	8.34E-03	0.38	9.90	65.62	67.34	1.04					
			3.8	7.16E-03	0.12	16.02	81.64	75.07	1.05					
			4.0	4.35E-03	0.07	6.78	88.42	90.21	1.55					
			4.2	4.41E-03	0.34	4.26	92.68	94.26	1.90					
			4.4-5.8	4.32E-03	0.12	7.32	100.00	107.52	1.79					
	Pacho													
7	Pa5	Hornblende	1.4	3.28E-04	1.98	0.10	0.10	215.89	48.429	**131.01± 0.2**	**yes**	**136.0± 0.4**	**136.9± 4.6**	**136.9± 3.9**

Table 4.4 Continuation…

Analysis number	Sample	Analyzed mineral	Heating %	39Ar/40Ar measured	±	39Ar%	Ar cum%	Age	±	Total gas age (Ma)	Identified plateau	Plateau age (Ma)	Inverse age (Ma)	Normal age (Ma)
			2.0	1.56E-03	0.24	0.88	0.98	67.15	6.84					
			2.4	2.25E-03	0.4	1.07	2.05	70.93	6.87					
			2.8	7.95E-03	0.81	2.28	4.33	75.03	1.66					
			3.0	1.00E-02	0.2	3.53	7.86	103.23	1.57					
			3.2	1.66E-02	0.4	6.75	14.61	126.55	1.15					
			3.4	1.90E-02	0.28	10.62	25.23	132.66	0.81					
			3.6	1.95E-02	0.25	9.87	35.11	134.84	0.70					
			3.6	2.01E-02	0.28	6.08	41.19	133.04	0.80					
			3.8	2.04E-02	0.3	13.68	54.88	135.92	0.71					
			3.8	2.05E-02	0.24	7.51	62.39	135.43	0.92					
			4.0	2.07E-02	0.27	10.82	73.20	136.21	0.73					
			4.2-4.6	2.10E-02	0.03	26.80	100.00	136.16	0.57					
	Pajarito													
8	Pj7	Hornblende	1.4	3.30E-04	3.8	0.03	0.03	413.40	89.55	**119.7±0.1**	**nd**	**120.5± 0.6**	**nd**	**nd**
			2.0	6.65E-03	1.2	0.29	0.32	93.21	6.48					
			2.6	6.74E-03	0.4	0.46	0.78	79.71	5.13					
			3.2	1.45E-02	0.7	0.87	1.65	89.09	1.95					
			3.8	2.72E-02	0.14	14.17	15.83	122.47	1.05					
			4.4	3.06E-02	0.06	57.17	73.00	120.03	1.01					
			5.0	3.14E-02	0.1	27.00	100.00	119.20	1.00					
	Rodrigoque													
9	LS1	Plagioclase	2.0	9.04E-03	0.32	9.84	9.84	22.31	0.96	**49.9 ± 0.2**	**nd**	**nd**	**nd**	**nd**
			2.6	5.60E-02	0.07	29.60	39.45	28.83	0.37					
			3.0	4.88E-02	0.13	13.52	52.97	45.29	0.39					
			3.2	3.66E-02	0.29	7.31	60.28	60.22	0.58					
			3.4	3.68E-02	0.38	5.83	66.11	59.82	0.66					
			3.6	3.85E-02	0.41	4.86	70.98	50.71	0.95					
			3.8	3.72E-02	0.25	6.98	77.95	57.60	0.79					
			4.2	3.19E-02	0.32	3.80	81.75	62.77	1.24					
			4.8-6.2	2.97E-02	0.21	18.25	100.00	88.24	0.53					

Table 4.4 Continuation…

Plagioclases of the tonalite sample RB1 (Fig. 4.6b) yielded an unusual shaped spectrum. The apparent ages increase from low apparent ages at low temperatures to high apparent ages at high temperatures, forming a plateau in the middle temperature steps. The calculated plateau age is 66.5±0.5 Ma, but the higher temperature gas fractions have apparent ages up to ~107 Ma.

The plateau age and the shape of the spectrum suggest that the age of 66 Ma does not correspond to a magmatic event. The gentle increment in age that reaches up to 107.5±1.8 Ma, indicates that the plagioclase crystals have older cores. The 66 Ma plateau is indicating presumably a later sericitization process where the plagioclases assimilated fluids that modified the potassium content. Both, inferred Ca/K ratios (Fig. 4.6b) and electron microprobe compositional data (not shown) present Ca enrichment towards the center, indicating a normal magmatic zoning of the plagioclase crystals. Only the rims of the crystals may have been affected by the pervasive alteration on the studied samples.

Moreover, the low to middle temperature steps of the Cáceres and Pacho samples (see below) show anomalously younger steps, Late Cretaceous-Early Paleogene (around 69 to 62 Ma) ages (Table 4.4). These young ages may be due to a regional alteration process presumably linked to the deformation phase recognized in the Upper Magdalena Valley and the southern segment of the EC (Gómez et al., 2005). This deformation has been related to the final accretion of oceanic crustal fragments of the Western Cordillera (Taboada et al., 2000) and the eastward progressing uplift and tectonic quiescence of the Central Cordillera (Gómez et al., 2005). In this sense, the tonalites of La Corona would reflect the melting of lower crustal rocks with similar composition as the La Corona mafic rocks.

4.6.2.3 Pacho

The lowest temperature steps in the step-heating spectrum of groundmass hornblendes display Ar loss from sample Pa5 (gabbro) (Fig. 4.6c). Gas fractions 10 to 13 (total ^{39}Ar fraction = 60%) define a plateau age. The calculated plateau age is 136.0±0.4 Ma and the inverse and normal isochron ages are 136.9±4.6 and 136.9±3.9, respectively. Steps 2 and 3 show younger ages (67 to 71 Ma) that are supposed to be related with the regional deformation and alteration process.

The age obtained for the rocks of Pacho seems to contradict the Upper Albian to Lower Cenomanian age of the host rocks (Navarrete et al., 2002). The Tragarepas intrusion crops out in the core of the Tragarepas Anticline and is lined up along a N-S trending fault (Navarrete et al., 2002). This suggests that the contact of the Pacho intrusion and the surrounding rocks is tectonic, and not intrusive. Therefore, the biostratigraphic age of the surrounding rocks cannot be used as

a youngest age limit for the Pacho intrusion, and for this reason we propose the new argon age to be more reliable.

4.6.2.4 Pajarito

$^{40}Ar/^{39}Ar$ step-heating dating of hornblende separated from sample Pj7 from the Pajarito intrusion of gabbroic major element composition indicates a 120.5±0.6 Ma weighted mean age (steps 5 to 7, Table 4.4, Fig. 4.6d). Although the last three steps do not agree with the 2σ error, they cover 99% of the total ^{39}Ar fraction and show similar ages from 119.2 to 122.5 Ma. Besides, if J value errors are introduced into the errors of the three fractions, they will agree within 2σ error. The weighted mean age of 120.5 will be treated as a "plateau age".

4.6.2.5 Rodrigoque

Plagioclase phenocrysts from the gabbroic sample LS1 yielded a disturbed gas release spectrum with apparent ages fluctuating between ca. ~ 22 and 88 Ma; a reasonable plateau cannot be defined (Fig. 4.6e). The 49.8±0.1 Ma total gas age is probable geologically meaningless.

4.7 RADIOGENIC ISOTOPE DATA

Corrections for in situ growth were calculated for the $^{40}Ar/^{39}Ar$ age determined for each intrusion. The Sr-Nd-Pb isotopic compositions are listed in Table 4.5. Their ranges are as follows: $^{86}Sr/^{87}Sr$ 0.70329-0.70972; $^{143}Nd/^{144}Nd$ 0.512749-0.512942; $^{206}Pb/^{204}Pb$ 18.33-19.27; $^{207}Pb/^{204}Pb$ 15.59-15.71; $^{208}Pb/^{204}Pb$ 38.23-39.22.

The $^{86}Sr/^{87}Sr$ vs. $^{143}Nd/^{144}Nd$ diagram (Fig. 4.7) reveals a short isotopic variation. In general the samples tend to have relatively homogen compositions of $^{143}Nd/^{144}Nd$ similar to the sub-arc mantle signature found in the South Andes in Argentina (Becchio et al., 1999; Lucassen et al., 1999; Lucassen et al., 2001). The Mercaderes mantle xenoliths representing the deep crust and the upper mantle of the Northern Andes (Weber et al., 2002) are plotted for comparison. The Pacific MORB data are based on the compilation of Lucassen et al. (2002). Except for sample Pj-8, which has a significantly different initial Sr isotope composition, the studied samples have very similar Nd and Sr isotope compositions, considering the variation in composition and age. The Pacho samples have higher initial Sr ratios and plot slightly towards the isotopic composition of the local Andean Palaeozoic rocks.

The corrected $^{207}Pb/^{204}Pb$ isotope ratios show two groups: the less radiogenic Cáceres samples and the more radiogenic samples from the other four intrusions (Fig. 4.8). Fields

corresponding to basalts, andesites, and trachytes from continental margin and Central Rift (Argentina ~26°S) are taken from Lucassen et al. (2002). The samples from Cáceres form a small cluster that overlaps with the continental margin field. Samples from the other localities plot very close to average local Palaeozoic crust (Lucassen et al., 2001), average subducted sediments (Plank and Langmuir, 1998), and the Mercaderes xenoliths field (Weber et al., 2002). The $^{207}Pb/^{204}Pb$ ratios of the samples from all intrusions are higher than the ratio of average Pacific MORB, but most of them, except those from Cáceres, are more radiogenic than the local Paleozoic crust average and the average subducted sediment. The field corresponding to Nazca Plate sediments (Hamelin et al., 1984) is also shown for comparison.

The $^{208}Pb/^{204}Pb$ vs. $^{206}Pb/^{204}Pb$ ratios show two different well defined suites. Except for Cáceres, the isotope ratios correlate and define a single, quite well constrained array (Fig. 4.8). The Pb isotope ratios of sample Pj8, which has an anomalous Sr isotope composition, plot within the array defined by most of the samples.

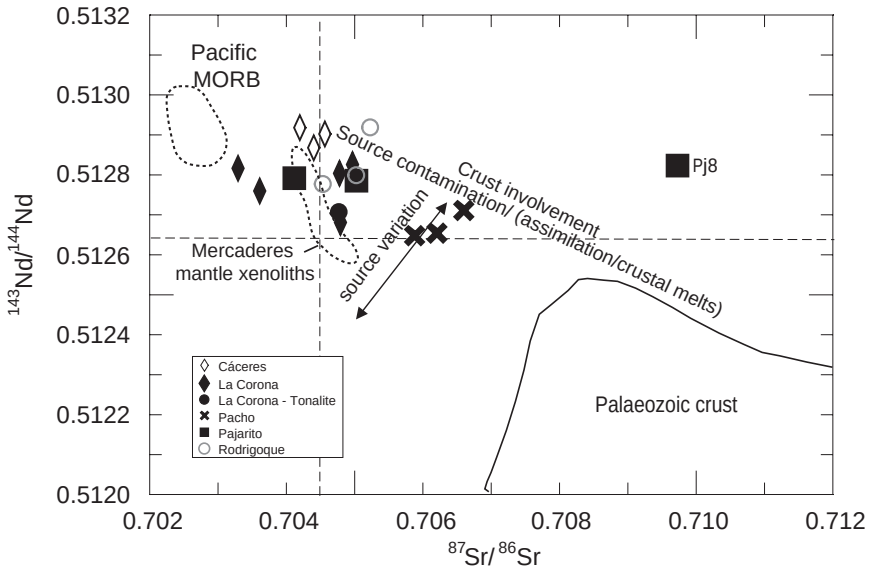

Fig. 4.7 $^{87}Sr/^{86}Sr$ vs. $^{143}Nd/^{144}Nd$ initial isotope ratios of the studied intrusions compared with those of South American Palaeozoic crust and Pacific MORB. The ratios were corrected for in situ decay using the ages in Table 4.4. The field of Mercaderes xenoliths represents the deep crust and upper mantle of the Northern Andes (Weber et al., 2002) and the values for the Palaeozoic crust are taken from (Becchio et al., 1999; Lucassen et al., 1999; Lucassen et al., 2001)

Sample[a]	Rb (ppm)	Sr (ppm)	$^{87}Sr/^{86}Sr$ [b]	$^{87}Sr_{(T)}/^{86}Sr$ [c]	Sm (ppm)	Nd (ppm)	$^{143}Nd/^{144}Nd$ [b]	$\varepsilon_{Nd(T)}$ [c]	Pb (ppm)	Th (ppm)	U (ppm)	$^{206}Pb/^{204}Pb$ [d]	$^{207}Pb/^{204}Pb$ [d]	$^{208}Pb/^{204}Pb$ [d]	$^{206}Pb/^{204}Pb$ [e]	$^{207}Pb/^{204}Pb$ [e]	$^{208}Pb/^{204}Pb$ [e]
Cáceres																	
Ca5	2	241	0.704616±10	0.70459	2.42	6.89	0.512927±7	5.5	1.01	0.47	0.16	18.547	15.605	38.413	18.42	15.60	38.30
Ca8	2	178	0.704466±10	0.70442	2.29	5.77	0.512904±5	4.8	1.33	0.33	0.10	18.392	15.591	38.295	18.33	15.59	38.23
Ca10	2	209	0.704244±10	0.70421	3.22	9.12	0.512942±6	5.8	1.46	0.63	0.23	18.555	15.599	38.405	18.43	15.59	38.30
La Corona																	
LC9	67	87	0.707801±7	0.70481	11.2	63.3	0.512772±4	3.7	6.34	8.18	1.57	19.285	15.708	39.014	19.04	15.70	38.60
LC10	9	135	0.705250±7	0.70499	10.9	51.7	0.512870±7	5.4	10.9	6.57	0.49	19.136	15.679	39.189	19.09	15.68	39.00
LC11	19	714	0.703735±8	0.70363	10.3	44.3	0.512828±7	4.4	8.71	2.84	0.60	19.146	15.688	39.132	19.08	15.69	39.03
LC13	91	1219	0.703574±6	0.70329	12.7	53.5	0.512868±6	5.1	4.21	4.19	0.57	19.063	15.654	39.07	18.93	15.65	38.75
LC16	15	148	0.705196±11	0.70480	12.7	65.4	0.512860±5	5.3	8.64	5.27	0.49	19.155	15.697	39.199	19.10	15.69	39.00
Tonalite																	
RB1	4	250	0.704834±7	0.70479	0.60	2.25	0.512783±7	3.1	1.39	0.89	0.06	18.731	15.634	38.81	18.70	15.63	38.67
Pacho																	
Pa1	2	167	0.706658±8	0.70661	5.17	21.7	0.512790±4	3.9	9.30	1.19	0.25	19.209	15.713	39.169	19.17	15.71	39.11
Pa3	4	473	0.705950±10	0.70590	5.11	20.9	0.512750±8	3.0	0.60	0.97	0.25	19.309	15.681	39.415	18.73	15.65	38.69
Pa4	<0.7	179	0.706235±10	0.70621	3.29	13.4	0.512749±5	3.0	0.56	0.99	0.22	19.613	15.701	39.72	19.07	15.67	38.92
Pajarito																	
Pj1	2	479	0.705048±10	0.70503	6.36	33.7	0.512845±6	5.3	21.4	4.78	1.19	18.996	15.681	39.119	18.93	15.68	39.03
Pj7	4	359	0.704189±10	0.70413	5.57	30.0	0.512849±5	5.4	24.8	2.11	1.03	19.007	15.709	39.215	18.96	15.71	39.18
Pj8	1	1280	0.709726±10	0.70972	6.74	36.1	0.512870±6	5.8	9.41	3.34	1.18	19.041	15.694	39.217	18.89	15.69	39.08
Rodrigoque																	
LS1	13	718	0.705308±5	0.70524	6.96	34.1	0.512939±9	6.8	1.45	4.31	0.93	19.679	15.638	39.609	19.02	15.61	38.61
LS3	14	451	0.704687±8	0.70456	7.03	34.3	0.512837±6	4.8	1.76	4.68	1.16	19.708	15.733	39.946	19.03	15.70	39.05
LS7	45	764	0.705241±7	0.70501	7.58	37.9	0.512856±4	5.2	1.82	4.63	1.05	19.864	15.738	40.08	19.27	15.71	39.22

a Samples were dissolved with 52% HF for four days at 160°C on the hot plate. Digested samples were dried and taken up in 6N HCl. Sr and Nd were separated and purified using ion-exchange chromatography as described in Romer et al. (2005). Pb was separted using a HBr-HCl ion-exchange procedure.

b $^{87}Sr/^{86}Sr$ and $^{143}Nd/^{144}Nd$, normalized to $^{86}Sr/^{88}Sr = 0.1194$ and $^{146}Nd/^{144}Nd = 0.7219$, respectively, were obtained on a Finnigan MAT262 multi-collector mass-spectrometer using static multicollection. Analytical uncertainties are given at $2\sigma_m$ level.

c $^{87}Sr/^{86}Sr_{(T)}$ and $\varepsilon Nd_{(T)}$ were calculated for the $^{40}Ar/^{39}Ar$ age using $\lambda^{87}Rb = 1.42E\text{-}11$ y-1 and $\lambda^{147}Sm = 6.54E\text{-}12$ y-1, $(^{147}Sm/^{144}Nd)_{0CHUR} = 0.1967$, and $(^{143}Nd/^{144}Nd)_{0CHUR} = 0.512638$, respectively, and the concentration data.

d Lead isotope data corrected for mass discrimination with 0.1% / A.M.U. Reproducibility at 2σ level is better than 0.1%.

e Lead isotope data recalculated to the $^{40}Ar/^{39}Ar$ age using the contents of Pb, Th, and U (Tables 4.1 and 4.2) and the constants recommended by IUGS (Steiger and Jager, 1977)

Table 4.5 Whole-rock Sr, Nd, and Pb isotope data of the plutonic rocks of the Eastern Cordillera, Colombia.

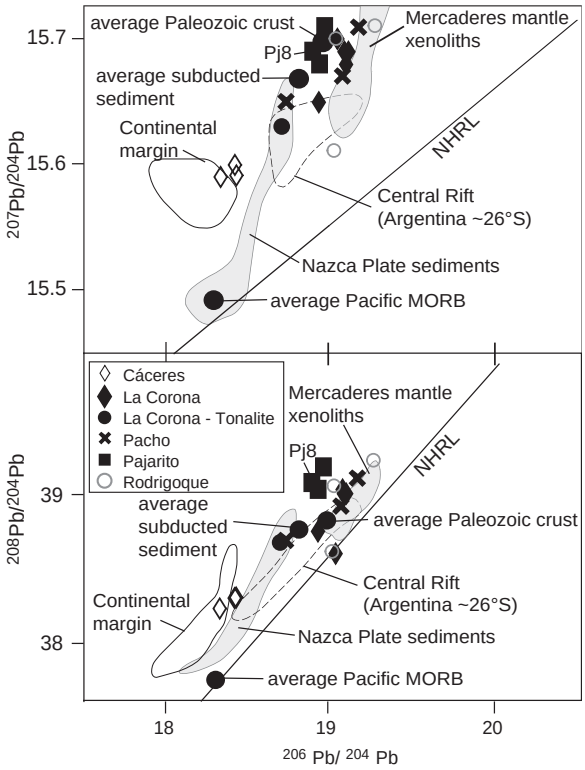

Fig. 4.8 Initial $^{207}Pb/^{204}Pb$ vs. $^{206}Pb/^{204}Pb$ and $^{208}Pb/^{204}Pb$ vs. $^{206}Pb/^{204}Pb$ isotopic ratios of the studied intrusions compared with other rocks of central South America and the Northern Andes. Sample Pj8, which has an anomalous Sr isotope ratio, plots on the general trend of the Pajarito samples. Data sources: Average Pacific MORB, continental margin and Central Rift (Lucassen et al., 2002); average Palaeozoic rocks (Lucassen et al., 2001); average subducted sediment (Plank and Langmuir, 1998); Mercaderes mantle xenoliths (Weber et al., 2002; and Nazca Plate sediments (Hamelin et al., 1984).

4.8 IMPLICATIONS OF GEOCHEMICAL AND GEOCHRONOLOGIC DATA FOR THE GEODYNAMIC EVOLUTION OF THE REGION

4.8.1 Geodynamic setting based on trace element data

The present day exposed mafic intrusions in the EC of Colombia are compositionally heterogeneous comprising alkaline and tholeiitic mafic rocks and local tonalites, with varying degrees of LREE enrichment. The intrusions can be correlated to different stages of extension in the Cretaceous. If we assume that the mafic intrusions in the EC had been emplaced within a single basin during a single magmatic episode (Vásquez and Altenberger, 2005), then the first magmas generated during relatively low degrees of mantle melting should be expected to have alkaline compositions and later melts generated during higher degrees of mantle melting should be expected to have tholeiitic (subalkaline) compositions. Furthermore, a geographic trend of

older magmatism in the east towards younger magmatism in the west could be proposed. However, the new geochemical and geochronologic data do not present a geographical correlation and such a trend cannot be defined.

The sub-continental mantle to the west (beneath Cáceres, i.e. beneath the Tablazo-Magdalena and Cundinamarca sub-basins) was presumably metasomatized by fluids derived from an older or reactivated subducted slab as can be observed in some slab-sensitive trace-element ratios like Ba/Nb and Sr/P (Vásquez and Altenberger, 2005). In this case, the mantle acted as a recorder of past processes, since the devolatilization of the subducted slab happened prior to melt generation. The tholeiitic affinity of the Cáceres and Pacho samples (Vásquez and Altenberger, 2005) suggests a maximum crustal extension in the Tablazo-Magdalena and Cundinamarca sub-basins and also, an uppermost mantle origin (Wilson, 1993).

Moreover, Fig. 4.5a shows a very interesting attribute for the samples of Pacho. They plot only in the field of continental basalts, since the other intrusions are plotting mostly in the field of oceanic basalts. It is important to correlate its age (136 Ma), which is the oldest of the investigated rocks, with the earliest stage of the Cretaceous rifting phase and the continental character of the crust. Since the extension took place contemporaneously in each sub-basin, and the magmatic rocks were produced at different times, it is possible to assume that the extension reached evolved stages that even generated an oceanic-like crust in places where the other intrusions were emplaced before.

West of Bogotá in the Cundinamarca and Tablazo-Magdalena sub-basins, pre-Cretaceous deposits (i.e. Saldaña, Bocas, and Montebel formations) have been recognized, and most of them have been identified as syn-rift events (Pindell and Erikson, 1993; Bayona et al., 1994; Pindell and Tabbutt, 1995; Vásquez et al., 2006). On the other hand, east of Bogotá in the Cocuy Sub-basin, pre-Cretaceous sediments have not been recorded at all. Furthermore, the evidences of a syn-rift character of the Late Paleozoic record (Sarmiento, 2001b) in the eastern sub-basin are still insufficient. The sedimentary record suggests that even if the Late Paleozoic deposits of the east do indicate a syn-rift event, the rifting phase had ended long time before the starting of deposition of Cretaceous sediments in the Berriasian. That means that the lithosphere at the east has had time enough to recover an early stage before the new Cretaceous rifting phase begins. In contrast, in the west, the Jurassic and Triassic extension was a continuous process followed by the Cretaceous extension. These sedimentary evidences suggest that the differences in the degree of mantle melting of the mafic intrusions are the result of the influence of the Mesozoic extension before the Cretaceous. The continuous rifting phase in the west produced a thinner

weaker lithosphere where the melting products have tholeiitic affinity because the uppermost mantle could be sampled. In the east, the Cretaceous lithosphere is thicker and the degree of mantle melting of the magmatic products is low with a markedly alkaline affinity.

4.8.2 Isotope constrains

The isotope ratios are not affected by processes such as degree of melting or fractional crystallization. For this reason the source type and contamination by crustal material can be constrained using the Nd-Sr-Pb isotope ratios. Fig. 4.7 shows the variation of Sr - Nd initial ratios of the samples. The Pacho samples plot towards the field of Central Andean Palaeozoic crust. The samples have slightly lower $^{86}Sr/^{87}Sr$ and slightly higher $^{143}Nd/^{144}Nd$ than undepleted mantle. The horizontal $^{86}Sr/^{87}Sr$ trend towards sample Pj8 of the Pajarito intrusion (Fig. 4.7; Table 4.5) can be explained by assimilation of high-Sr crust (Worner et al., 1986), sediments whose Sr isotope composition has been modified by seawater (Lucassen et al., 2002) at some stage of their genesis and a direct interaction with seawater in the marine basin. The La Corona and Pacho samples deviate from the mantle array towards lower $^{86}Sr/^{87}Sr$ and $^{143}Nd/^{144}Nd$ ratios, and the variation in source composition is again a matter of discussion. The La Corona tonalite shows almost the same mantle signature and crustal contamination signature as the other samples from the same locality.

The Mercaderes mantle xenoliths that represent the lower crust and upper mantle of the Northern Andes (Weber et al., 2002) were also plotted for comparison. They indicate that the lower crust underlying the Northern Andes is isotopically heterogeneous, the mantle is dominated by hornblende-bearing assemblages, and furthermore, the analyzed samples reflect the isotopic signature of the local mantle. A positive $^{207}Pb/^{204}Pb$ vs. $^{206}Pb/^{204}Pb$ correlation defined by samples from the Pacho, La Corona, Pajarito, and Rodrigoque intrusions indicates the contribution of old crustal material to their parent melts (Fig. 4.8a). A positive correlation can be also observed in the $^{208}Pb/^{204}Pb$ vs. $^{206}Pb/^{204}Pb$ diagram (Fig. 4.8b). Nevertheless, assimilation of the contaminants is not uniform and for this reason the scatter of the Pb isotope ratios may have been caused by random sampling of a heterogeneous crust.

The Pb isotopic ratios of the Cáceres samples have radiogenic ratios lower than those of the other intrusions. This suggests that assimilation of one of the crustal sources was minimal, although the $^{208}Pb/^{204}Pb$ vs. $^{206}Pb/^{204}Pb$ diagram shows the Cáceres rocks plotting next to the field of Nazca Plate sediments. In other words, it is possible that crustal contamination was minimal and that the Cáceres samples basically reflect the Pb isotope composition of their mantle source.

Finally, the differences in Pb isotope composition are caused by different amounts of crustal contamination.

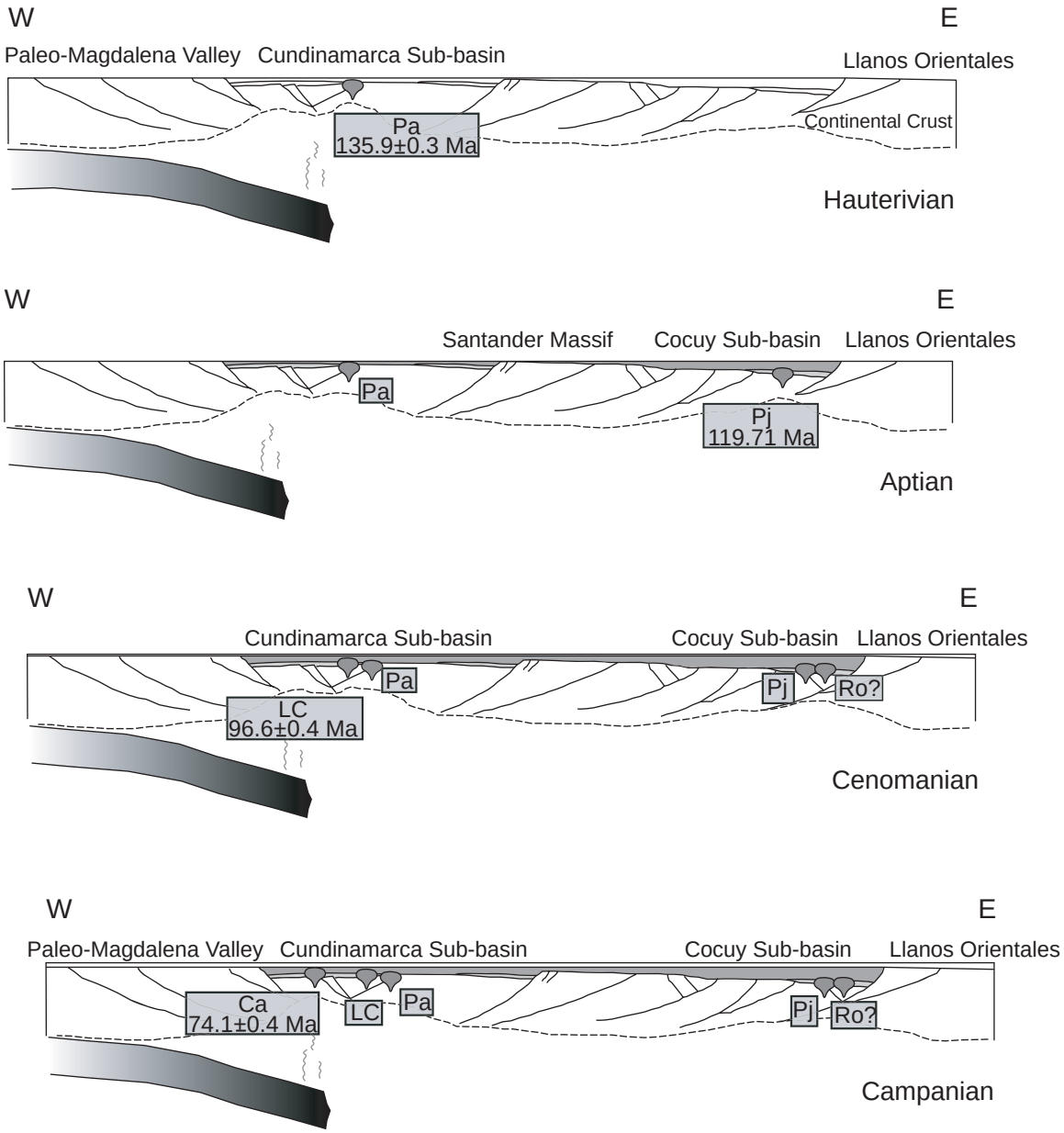

Fig. 4.9 W-E projected schematic profile across the Colombian Cretaceous Basin. The chronological evolution of the magmatism shows the position of the intrusions and the differences of crustal thickness in each sub-basin.

4.8.3 Consequences on the structure of the crust based on the age of the magmatism

The $^{40}Ar/^{39}Ar$ data show that the five studied intrusions were not emplaced synchronously. The determined ages range between 135 Ma and 74 Ma (Hauterivian to Campanian) and provide time constraints for the tectonic evolution of the region. Dykes emplacement occurred in several distinct phases associated with the extension of a segmented basin, and presumably with an episode of alteration linked to the first pre-Andean deformation within the basin.

We assume the obtained ages, except that of the tonalite of La Corona, to be minimum crystallization ages. The plagioclase samples are affected by sericitization that may have disturbed the original age of some steps. The significance of the geochemical and geochronologic heterogeneities is explained in terms of structure of the crust and different stages of stretching as follows.

The development of the Cretaceous basin began during the Triassic as a response to back arc rifting (Pindell and Erikson, 1993; Bayona et al., 1994; Pindell and Tabbutt, 1995; Vásquez et al., 2006). Subsequently, the arc magmatism ceased when the regional compressional setting changed to rift-related setting and the opening of the Proto-Caribbean Ocean took place (Bayona et al., 2005; Vásquez et al., 2006).

Sedimentation in the basin continued in Jurassic and Early Cretaceous time on the western side, the Tablazo-Magdalena sub-basin (Fig. 4.1b,) without tectonic-related angular unconformities. The stretching of the Tablazo-Magdalena sub-basin affected previously weakened lithosphere during earlier rifting episodes (Sarmiento, 2001b). Later during the Aptian and even during the Cenomanian, the western margin of Colombia became a passive margin without major changes in its plate tectonic configuration (Pindell and Erikson, 1993).

The development of the eastern side of the basin has been explained by Berriasian-Hauterivian reactivation of pre-existing crustal discontinuities related to an older Palaeozoic rift system situated along the Guaicaramo palaeo-fault (Sarmiento, 2001b).

Correlating published Mesozoic subsidence analysis of the basin using backstripping techniques (Gómez et al., 2005; Fig. 5; Sarmiento-Rojas et al., 2006; Fig. 10) and the minimum crystallization ages (this study), it is possible to observe that: 1) the Pacho intrusion (~135 Ma) is associated with a fast synrift subsidence event; 2) the mafic rocks from Pajarito (~120 Ma) intruded during the transition between rifting and thermal subsidence; 3) the gabbros from La Corona (~97 Ma) can be related to the end of the synrift subsidence; and 4) the Cáceres intrusion (~74 Ma) marks the thermal subsidence event.

The pre-existent Jura-Triassic rifting phase in the west has a strong influence in the crustal and lithospheric structure in the Cretaceous. For this reason, the degree of mantle melting in Cáceres and Pacho is similar, although the age of crystallization differs from each other. So, the partial melting of these samples does not depend on the Cretaceous rifting phase but on the previous rifting phases. The pre-Cretaceous extension was the conditioning factor for the magmatism at the west, whereas at the east this is not observed because there was not previous extension since the Paleozoic. The alkaline character of the samples of La Corona is still a matter of discussion. Local changes in the thickness and structure of the lithosphere could be argued. However, this argument does not seem convincing and detailed geophysic and stratigraphic studies should be done. Fig. 4.9 shows a sequence in the Cretaceous where the position of the intrusions is inferred and the ages are posted. Note the change on the thickness of the crust in the eastern and western sub-basins. The influence of slab-derived fluids is suggested in the western flank by an inactive subduction zone.

The development of the Cretaceous basin as described above implies that the pre-existing rifting phases conditioned the magmatic processes in each sub-basin. Consequently, the structure of the crust and lithosphere was heterogeneous, and the heat flux and stretching were varying among the sub-basins. It has been proposed that the generation of tholeiitic magmas within a continental rift setting, as in the western flank (Cáceres and Pacho areas), occurred at lithospheric mantle depths (Keller and Hoover, 1988) where the stretching was the strongest, whereas the alkalic magmas (La Corona, Pajarito, and Rodrigoque intrusions) indicate melting of deeper mantle sources. The intrusions are associated with major faults which could have served as conduits along the magmas reached uppermost crustal levels. It can be assumed that each intrusion represent the most subsiding place of each sub-basin at the time of emplacement.

The continental rifting and the generation of associated magmas are influenced by many factors, such as the effect of pre-tectonic events that affected the lithosphere and/or sublithospheric mantle. For this reason, type and quantity of rift-related magmatism may be unique, sharing only few fundamental similarities with other examples around the world.

4.9 CONCLUSIONS

The magmatic evolution of the EC during the Cretaceous documents the heterogeneity of the subcontinental mantle beneath the Northern Andes as well as the influence of previous tectonic processes that affected the lithosphere.

The basin evolution was controlled by main palaeo-faults creating sub-basins that developed in different times and styles. Consequently, the ascending melts have sampled different parts of the mantle at different times in the Cretaceous (136 to 74 Ma).

Geochemistry and petrogenesis of the Cretaceous intrusive rocks differentiate at least two main groups in terms of mantle source and source contamination. This chemical difference among each intrusion suggests a very inhomogeneous mantle where the isotope ratios reflect contamination coming from different sources. There are many factors governing the development of a continental rift, as for instance the effect of previous tectonic events. Such events affect the nature of the lithosphere and/or sublithospheric mantle and control the localization and composition of the magmatism.

5. MAGMATISM AND HYDROCARBON GENERATION IN THE PUTUMAYO BASIN, NORTHEN VOLCANIC ZONE, SW COLOMBIA

Mónica Vásquez [a]

Uwe Altenberger [a]

Rolf L. Romer [b]

[a] *Institut für Geowissenschaften, Universität Potsdam, Karl-Liebknecht-Str. 24 14476 Potsdam-Golm, Germany*

[b] *GeoForschungsZentrum Potsdam, Division 4.1, Telegrafenberg, 14473 Potsdam, Germany*

5.1 ABSTRACT

The Cretaceous oil-bearing source and reservoir sedimentary succession in the Putumayo Basin, SW Colombia, was intruded by gabbroic dykes and sills. The petrological and geochemical character of the magmatic rocks points to a subduction-related magmatic event. K/Ar dating of amphibole indicates a Late Miocene to Pliocene age (6.1 ± 0.7 Ma) for the igneous episode in the basin. Therefore, we assume the intrusions to be part of the Andean magmatism of the Northern Volcanic Zone (NVZ). The age of the intrusions has significant tectonic and economic implications because it coincides with two regional events: 1) the late Miocene/Pliocene Andean orogenic uplift of most of the sub-Andean regions in Peru, Ecuador and Colombia, and 2) a pulse of hydrocarbon generation and expulsion that has reached the gas window. Therefore, the latter one is thermally more evolved than a previous one (Late Oligocene - Miocene) that reached only the peak of oil generation. We discuss the possibility that a magmatic chamber west of the basin, below the Cordillera, did increase the heat flow in the basin prompting generation and expulsion of hydrocarbons and CO_2.

Keywords: Colombia; K/Ar dating; magmatism; Putumayo Basin; radiogenic isotopes; oil generation; oil expulsion.

5.2 INTRODUCTION

Hydrocarbons related to the presence of igneous rocks have become considered an additional exploration strategy. Maturation and migration of the hydrocarbons, as well as traps and reservoirs can be modified by the interaction with a magmatic event. There are numerous

examples around the world that document the interaction between magmatic heat and convection, migration, and maturation of oil (Kontorovich et al., 1997; Chen et al., 1999; Polyanskii et al., 2002).

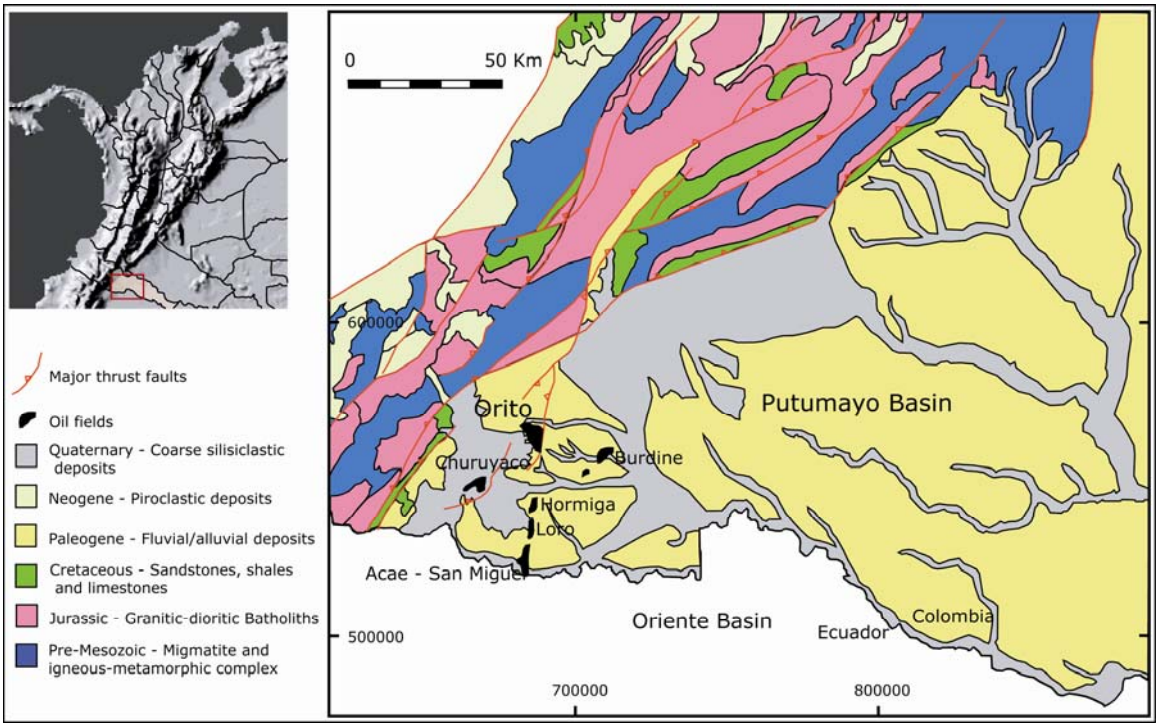

Fig. 5.1 Simplified geologic map of the Putumayo Basin in SW Colombia (González et al., 1988). The mafic rocks were sampled from wells of the Orito Oil Field

The Putumayo Basin is the Colombian part of the vast Putumayo-Oriente-Marañón province at the eastern flank of the Andes (Fig. 5.1). With an approximate area of 30,000 km^2, it is bounded to the west by the sub-Andean belt including the Garzón Massif and the Main Andean Cordillera (Central Cordillera and Real Cordillera). This basin is one of the most important oil regions in Colombia, where large hydrocarbon accumulations (i.e. Orito Field) have been discovered since the early 1940's (Higley, 2000). Some wells revealed that mafic sills and dykes truncate the sedimentary succession. Gonçalves et al. (2002) and Kairuz (1993) suggested that these magmatic pulses played a significant role on the paleoheat flow of the basin and prompted higher maturity of the oil-prone source and reservoir rocks westwards of the basin, below the Cordillera.

Whereas the thermal and burial reconstruction of a pseudo-well (Gonçalves et al., 2002) have been used to constrain the starting of petroleum generation and expulsion, there are no geochronological or geochemical studies of the magmatic event and also no data available to test a possible coupling of magmatism and oil generation. Therefore, the aim of this study is to

geochemically characterize the mafic rocks, to determine the age of the intrusion and to discuss the geodynamic setting of the magmatic episode and its relationship to the generation of hydrocarbons in the basin.

5.3 GEOLOGIC DEVELOPMENT OF THE BASIN

The Pre-Mesozoic basement of the Putumayo Basin, composed of migmatites and the Garzón Igneous - Metamorphic Complex (Fig. 5.1), is overlain by a Triassic-Jurassic sequence of volcanic deposits and shallow marine to continental siltstones and sandstones (Fig. 5.2) of the Santiago and Motema Formation (Córdoba et al., 1997). Coastal to shallow marine sandstones and black shales (Caballos Formation); marine limestones, shales and sandstones (Villeta Group), and shallow marine to continental siliciclastic sediments (Rumiyaco Formation) were deposited during the Cretaceous to Paleocene. Pyroclastic deposits and andesitic-basaltic volcanic rocks form the Neogene succession. During late Pliocene and Quaternary times the deposition of coarse siliciclastic sediments completed the sequence.

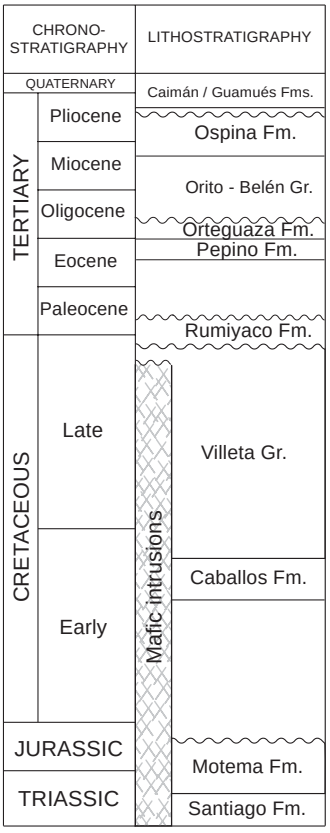

Fig. 5.2 Stratigraphic column of the Putumayo Basin (Córdoba et al., 1997). The mafic intrusions cut the sedimentary succession

A regionally pervasive late Miocene to early Pliocene uplift event, known as Quechua III (Sébrier and Soler, 1991; Mathalone and Montoya, 1995; Higley, 2000), has been well documented and expressed by thrusting and compressional folding over most of the sub-Andean region in Peru, Ecuador and Colombia (Mathalone and Montoya, 1995). This episode has been widely recognized as the main Andean orogenic uplift causing the present-day relief and assessed to the westward drift of South America and the progressive decrease in the age of crust entering the trench along the mountain belt (Pindell and Tabbutt, 1995).

The main petroleum source rocks of the Putumayo Basin are th e marine calcareous shales and marls of the Villeta Group, whose sandy and carbonatic facies - together with the Caballos and the Eocene Pepino formations - also form the main reservoirs rocks. Two pulses of hydrocarbon generation and expulsion have been recognized within the basin during Tertiary times (1. late Oligocene – Miocene, 28 - 20 Ma; and 2. Late Miocene – Pliocene, 13 - 3 Ma) (Gonçalves et al., 2002). The first pulse is characterized by low to moderate gravity less than 30° API and relatively high sulphur content up to 1.5% (Gonçalves et al., 2002). The latter pulse has been described as to be thermally more evolved than the former, as some processes involved in the generation of the second (i.e. magmatism, uplift) were not acting on the first one. It is characterized by higher API gravity values (~40°) and lower sulphur contents (<0.75%) (Gonçalves et al., 2002). The thermal evolution has been suggested after burial reconstruction based on geochemical data of oil and gas samples, vitrinite reflectance and basin modelling showing that the first migration phase corresponds to the peak of oil generation, whereas the second corresponds to the gas window (lighter oil and gas). Some wells in the Orito Oil Field show that sediments of the Motema, Caballos and Villeta formations are cut by fine- to medium grained mafic dykes of few meters of thickness.

5.4 ANALYTICAL PROCEDURES

Six samples of hornblendic micro-gabbros from three wells of the Orito Oil Field (Orito-3, Orito-4, and Orito-10), were selected for whole-rock geochemistry (Table 5.1). Major elements were determined by wavelength-dispersive X-ray fluorescence spectrometry using fused lithium-tetraborate discs. Pressed powder pellets were used for trace element determinations by XRF. All XRF analyses were made with a Phillips PW-2400 spectrometer at the GeoForschungsZentrum GFZ in Potsdam, Germany.

Well	Orito 3		Orito 4			Orito 10
Depth (m)	1908.25	1909.5	1769.97	1770.33	1770.58	1999.74
Sample ID	1	2	3	4	5	6*
wt%						
SiO_2	50.9	49.8	50.3	50.5	48.3	39.7
TiO_2	1.18	1.18	1.41	1.38	1.36	1.55
Al_2O_3	15.0	14.7	16.0	16.5	14.1	27.9
Fe_2O_3	8.1	8.1	8.2	7.9	10.0	10.8
MnO	0.10	0.10	0.12	0.11	0.13	0.39
MgO	6.25	6.74	4.75	4.28	9.30	0.74
CaO	5.34	5.18	8.49	7.81	7.62	1.45
Na_2O	5.09	5.01	3.62	3.49	3.88	0.01
K_2O	0.71	0.69	1.39	2.29	1.53	1.12
P_2O_5	0.37	0.35	0.32	0.35	0.32	0.60
H_2O	4.35	4.48	5.26	4.77	2.71	10.07
CO_2	3.22	4.13	0.75	0.68	1.18	6.35
Total	100.6	100.4	100.6	100.0	100.5	100.6
ppm						
Rb	15	10	17	40	22	20
Sr	464	463	772	912	867	89
Ba	523	570	779	1010	835	89
Cs	0.41			0.59	0.21	
V	199	201	235	226	232	349
Cr	215	251	126	58	437	36
Ni	107	114	32	17	191	47
Sc	17			20	25	
Zn	74	88	68	77	94	20
Y	11	14	17	13	16	35
Zr	117	118	117	120	113	163
Nb	11	12	12	10	12	9
Hf	4			3	3	
La	22.2			22.0	20.6	
Ce	47.6			46.0	43.1	
Pr	5.8			5.6	5.2	
Nd	25.2			24.4	22.8	
Sm	4.9			4.9	4.6	
Eu	1.5			1.5	1.4	
Gd	4.1			4.2	4.0	
Tb	0.5			0.6	0.5	
Dy	2.7			2.9	2.8	
Ho	0.4			0.5	0.5	
Er	1.1			1.4	1.3	
Tm	0.2			0.2	0.2	
Yb	0.9			1.2	1.1	
Lu	0.1			0.2	0.2	
Pb	7			5	4	
Th	4			3	2	
U	1			1	1	
Na_2O/K_2O	7.2	7.2	2.6	1.5	2.5	
$(La/Yb)_N$	15.9			12.5	12.5	
Ba/Nb	47.1	47.6	67.7	106.5	67.1	

Table 5.1 Geochemical data of gabbroic rocks from the Orito Oil Field, Putumayo Basin, Colombia. (*) Sample 6 shows strong alteration

The REE, Rb, Sr, Y, Zr, Cs, Ba, Lu, Hf, Pb, Th and U were analyzed by inductively coupled plasma-mass-spectrometry (ICP-MS) with a Perkin - Elmer/Sciex Elan Model 500 ICP mass-spectrometer using the method outlined by Dulski (1994). The analyses were carried on at the GeoForschungsZentrum Potsdam on a subset of three samples. The subset of three samples was analyzed as well by inductively coupled plasma-optical emission spectrometer (ICP-OES, Vista MPX) at the Laboratory of Geochemistry in the University of Potsdam. Sample preparation

involved Na_2O_2 standard fusion and dilution techniques for dissolving rock powders. Analytical precision was checked against international reference standards. For the XRF analysis, the estimated precision is better than 1-3% for major elements (depending on concentration levels) and better than 10% for trace elements.

The major element concentrations of the analyzed phases were determined with a Cameca SX50 electron microprobe at the GeoForschungsZentrum Potsdam. The operation conditions were an acceleration voltage of 15 keV and a beam current of 20 nA.

K-Ar age was obtained of fresh hornblende in the Geowissenschaftliches Zentrum at the University of Göttingen. After extraction and purification of the released gases from the samples the argon isotopic composition was measured on-line with a VG 1200 C noble gas mass spectrometer operating in static mode. The amount of radiogenic ^{40}Ar was determined by isotope dilution method using a highly enriched ^{38}Ar spike from Schumacher (1975). The spike was calibrated against the biotite standard HD-B1 (Fuhrmann et al., 1987). The age calculations are based on the constants recommended by the IUGS quoted in Steiger and Jager (1977).

Potassium was determined in duplicate by flame photometry using an Eppendorf Elex 63/61. The samples were dissolved in a mixture of HF and HNO_3 according to the technique of Heinrichs and Herrmann (1990). CsCl and LiCl were added as an ionization buffer and internal standard respectively. The analytical error for the K/Ar age calculations is given on a 95% confidence level (2σ). Details of argon and potassium analyses for the laboratory in Göttingen are given in Wemmer (1991).

5.5 PETROGRAPHIC DESCRIPTION

The dark-green gabbroic rocks are composed of plagioclase, hornblende, and minor amounts of biotite. Their texture can be described as holocrystalline microphyric.

Plagioclase is commonly replaced by calcite, which masks the initial feldspar composition of the crystals. Fresh plagioclase shows a composition from oligoclase to labradorite (An_{22-54}) and is characterized by normal zonation. The crystal size reaches up to 0.5 mm.

The amphiboles are not altered at microscopic scale. They have been classified as pargasite and tschermakite, using the classification of Leake et al. (1997b). The crystal size ranges from 0.75 to 1 mm.

Some relicts of pyroxenes have been observed. However, due to their nearly complete replacement by calcite, they can not be classified. Biotite is commonly fresh with brown to green pleocroism. In addition, epidote and prehnite are present as secondary products.

Based on the petrographic description, the studied samples are classified according to Streckeisen (1976) as olivine-free hornblende gabbros.

5.6 WHOLE ROCK GEOCHEMISTRY

The composition of the analyzed samples is shown in Table 5.1. All samples show some degree of alteration. Sample 6, however, is particularly strongly altered with volatile contents as high as 16% and higher Al_2O_3 concentrations. This sample was not used in the diagrams. Alteration typically results in the loss or gain of alkali earth elements and LILE, some of which are used as distinctive geochemical fingerprints to establish magma provenance. To check whether alteration

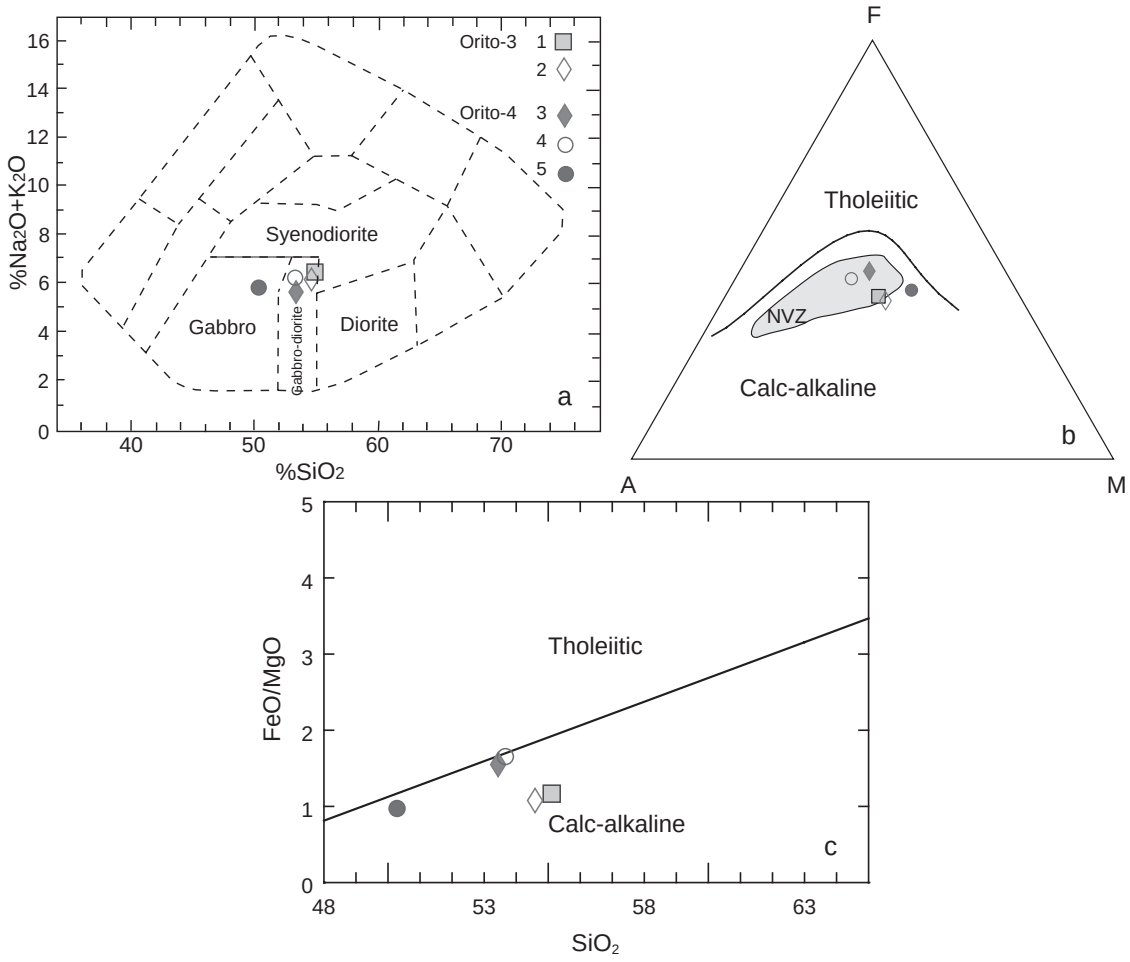

Fig. 5.3 **a**. Diagram of total alkali vs. silica, showing the classification of the plutonic rocks from the Putumayo Basin (after Middlemost, 1994); **b**. AFM (alkali-FeO-MgO) diagram (Irvine and Baragar, 1971) showing the calc-alkaline affinity of the rocks and comparing the NVZ with the mafic rocks. The coincidence between the two groups of rocks is undeniable; **c**. SiO_2 vs. FeO/MgO plot corroborating the calc-alkaline character of the rocks.

resulted in significant modifications of the trace-element pattern, elements tending to be mobile (Sr, Ba, K, Na, and Ca) were compared with immobile elements (Al, Ti; not shown). The

samples show good correlation as would be expected for geochemically related rocks that have not been affected by significant secondary element mobilization. Moreover, the concentration of the elements Rb, Cs, and K_2O is very low, which precludes significant contamination by fluids or melts derived from the crust. In addition, there is no clear correlation between the mobile elements and the H_2O and CO_2 contents.

The rocks show a restricted range of SiO_2 content (50 - 55 wt.% after normalization to a volatile-free basis) and fall in the SiO_2 vs. alkali (K_2O + Na_2O) diagram (Middlemost, 1994) in the field of gabbros and gabbro-diorites (Fig. 5.3a). The studied samples plot in the field alkaline gabbros in the diagram Nb/Y vs. Zr/TiO_2 (not shown). The rocks have medium to high K_2O contents ranging from 0.7 to 2.3 wt. % and show a calc-alkaline tendency (Fig. 5.3b and c).

The compositional patterns of the northern, central and southern subduction-related South American volcanic zones (Thorpe and Francis, 1979) were plotted in Fig. 5.4 for comparison with the Orito samples. The pattern of the three zones correlate very well with the studied rocks, showing the same trends for K, Sr, and Ba enrichment as well as the conspicuous through at Nb.

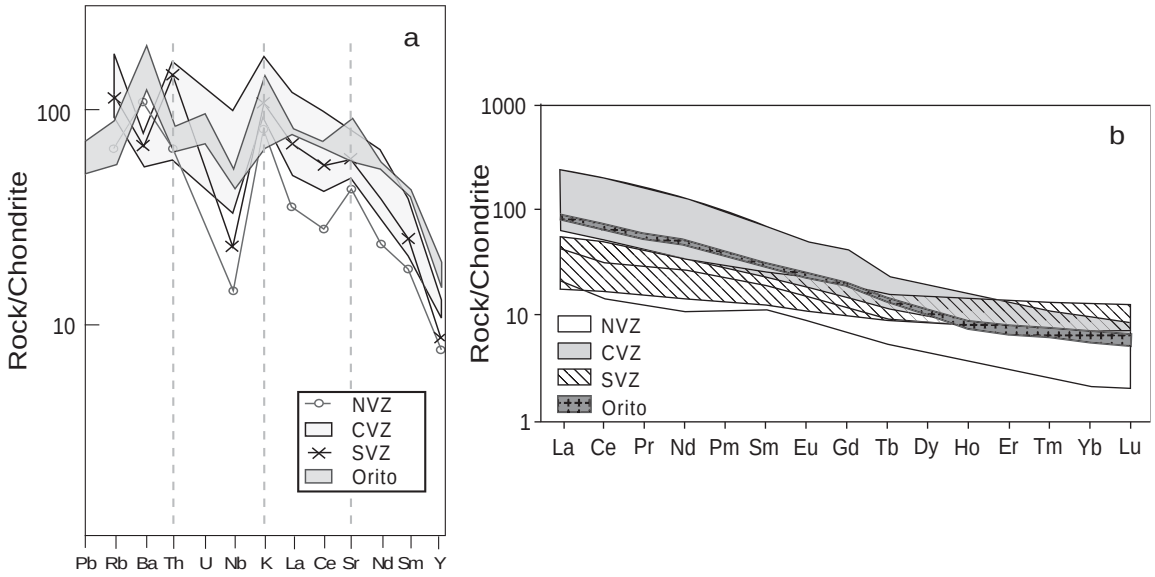

Fig. 5.4 Chondrite normalization shows the significant enrichment of large ion lithophile elements (LILE) as Rb, Ba, K and Sr and light rare earth elements (LREE). **a**. Normalization factors after Sun (1980); **b**. Normalization factors after Evensen et al. (1978).

The trace elements and REE patterns of the gabbroic Orito Field rocks are characterized by a significant enrichment of large ion lithophile elements as Rb, Ba, K, and Sr and a depletion of Nb compared to chondritic composition (Fig. 5.4a). In addition, the rocks have high Ba/Nb ratios (47-107). The limited geochemical data indicate that the Orito intrusive rocks may be more enriched in LREE (Fig. 5.4b) than the average subduction-related volcanic rocks of the northern

Andes (Northern Volcanic Zone, NVZ). LREE concentration are up to 100-fold chondritic whereas the heavy rare earth elements (HREE) are up to 20-fold chondritic. La/Yb_n ratios span from 12 to 15.

5.7 K/Ar AGE DETERMINATION

K-Ar age was determined of fresh hornblende separated from sample 3 (Table 5.2). The age determination resulted in a value of 6.1 ± 0.7 Ma, which suggests that the crystallization of the sills and dykes of gabbroic composition occurred in the late Miocene and was contemporaneous to the second hydrocarbon generation (Gonçalves et al., 2002) in the Putumayo Basin and the Late Miocene-Pliocene Andean uplift event, called Quechua III (Sébrier and Soler, 1991; Mathalone and Montoya, 1995; Higley, 2000).

K/Ar - Age Determination					
Sample	**K_2O** (Wt. %)	**^{40}Ar *** (nl/g) STP	**^{40}Ar *** (%)	**Age** (Ma)	**2σ-Error** (Ma)
3 (hornblende)	0.69	0.14	16.49	6.1	0.7

Table 5.2 K/Ar age determined on hornblendes from sample 3.

5.8 Sr-Nd-Pb ISOTOPE GEOCHEMISTRY

The Sr-Nd-Pb isotopic compositions for three samples are listed in table 3. Corrections for in situ growth of Sr, Nd, and Pb over the last 6.1 Ma are very small. The corrected data are within analytical uncertainties of the measured data.

Sample[a]	Age (Ma)	$^{87}Sr/^{86}Sr$ [b]	$^{87}Sr_{(T)}/^{86}Sr$ [c]	$^{143}Nd/^{144}Nd$ [b]	$\varepsilon Nd_{(T)}$ [c]	$^{206}Pb/^{204}Pb$ [d]	$^{207}Pb/^{204}Pb$ [d]	$^{208}Pb/^{204}Pb$ [d]	$^{206}Pb/^{204}Pb$ [e]	$^{207}Pb/^{204}Pb$ [e]	$^{208}Pb/^{204}Pb$ [e]
1	6.1	0.706172±10	0.70617	0.512723±7	1.7	19.362	15.700	39.169	19.352	15.700	39.158
4	6.1	0.705369±7	0.70536	0.512731±4	1.9	19.126	15.663	38.888	19.116	15.663	38.878
5	6.1	0.704997±9	0.70499	0.512736±6	2.0	19.073	15.653	38.835	19.062	15.652	38.823

a Samples were dissolved with 52% HF for four days at 160°C on the hot plate. Digested samples were dried and taken up in 6N HCl. Sr and Nd were separated and purified using ion-exchange chromatography as described in Romer et al. (2005). Pb was separted using the HBr-HCl ion-exchange procedure of Tilton (1973) and Manhès et al. (1978). Samples are listed in Table 5.1.

b $^{87}Sr/^{86}Sr$ and $^{143}Nd/^{144}Nd$, normalized to $^{86}Sr/^{88}Sr = 0.1194$ and $^{146}Nd/^{144}Nd = 0.7219$, respectively, were obtained on a Finnigan MAT262 multi-collector mass-spectrometer using static multicollection. Analytical uncertainties are given at $2\sigma_m$ level.

c $^{87}Sr/^{86}Sr_{(T)}$ and $\varepsilon Nd_{(T)}$ were calculated for the radiogenic age using $\lambda^{87}Rb = 1.42E\text{-}11$ y-1 and $\lambda^{147}Sm = 6.54E\text{-}12$ y-1, $(^{147}Sm/^{144}Nd)0_{CHUR} = 0.1967$, and $(^{143}Nd/^{144}Nd)0_{CHUR} = 0.512638$, respectively, and the concentration data given in Table 5.1.

d Lead isotope data corrected for mass discrimination with 0.1% / A.M.U. Reproducibility at 2 σlevel is better than 0.1%.

e Lead isotope data recalculated to the radiogenic age using the contents of Pb, Th, and U (Table 5.1) and the constants of Jaffey et al (1971) recommended by IUGS (Steiger and Jäger, 1977).

Table 5.3 Whole-rock Sr, Nd, and Pb isotope data of gabbroic rocks in Orito Oil Field, Putumayo, Colombia

The variation of $^{87}Sr/^{86}Sr$ vs. $^{143}Nd/^{144}Nd$ compared to volcanic rocks from the Northern, Central, and Southern Volcanic Zones of the Andes and to MORB (mid-ocean ridge basalts), OIB (oceanic-islands basalts), and OIA (oceanic-island arcs) fields (Hawkesworth et al., 1982; James, 1982; Thorpe et al., 1984; Hickey et al., 1986) is shown in figure 5.5. The low-grade alteration of plagioclase to secondary calcite is unlikely to be responsible for the shift to higher $^{87}Sr/^{86}Sr$ values (Fig. 5.5) as the alteration seemed to have resulted in a Sr loss rather than a Sr gain (Table 5.1).

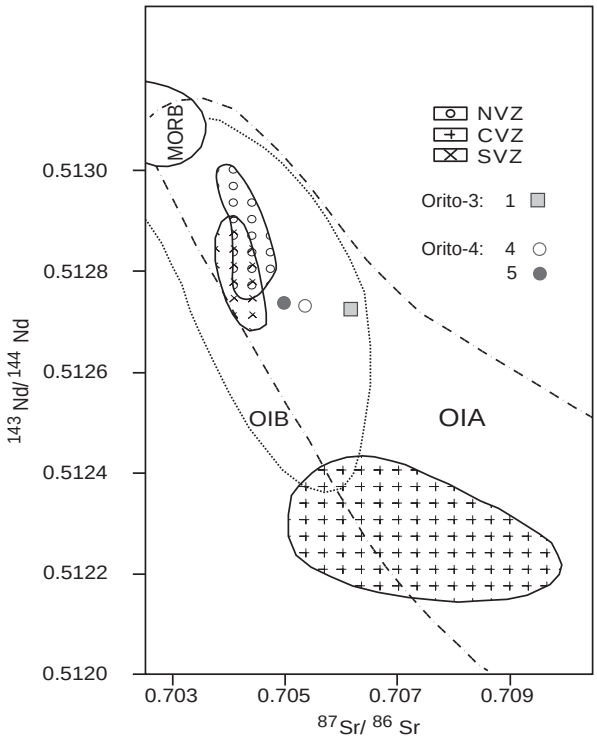

Fig. 5.5 Correlation of $^{87}Sr/^{86}Sr$ vs. $^{143}Nd/^{144}Nd$ showing fields of volcanic rocks from the Northern, Central, and Southern Volcanic Zones of the Andes and to the MORB (mid-ocean ridge basalts), OIB (oceanic-islands basalts), and OIA (oceanic-island alkali basalts). Fields after Hawkesworth et al. (1982); Hickey et al. (1986); James (1982) and Thorpe et al. (1984).

The Orito gabbros have a restricted range of $^{206}Pb/^{204}Pb$, $^{207}Pb/^{204}Pb$, and $^{208}Pb/^{204}Pb$ values (see table 5.3, Fig. 5.6). The Pb isotopic ratios form an array that extends from the field of rocks from the NVZ and from the Central Rift (Fig. 5.6) to more radiogenic compositions and that show the offset to higher $^{207}Pb/^{204}Pb$ values (in comparison to the northern hemisphere reference line) which is typical for subduction and rift related rocks of South America.

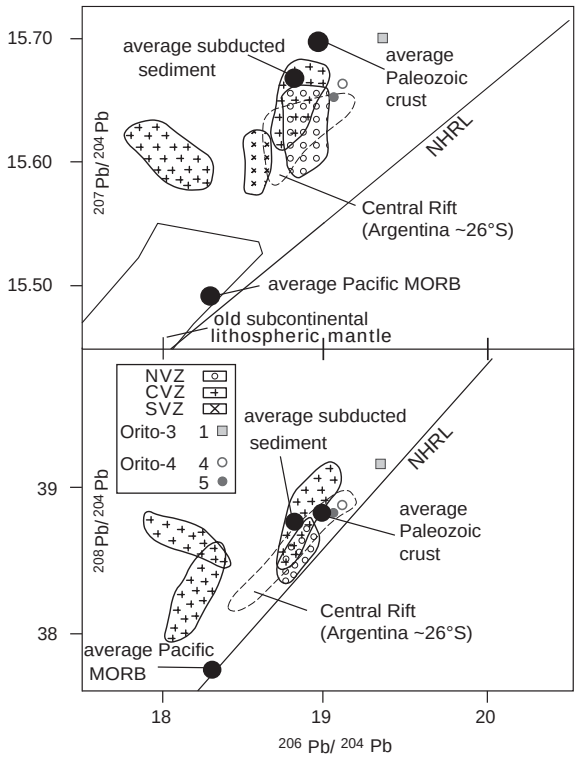

Fig. 5.6 Initial $^{206}Pb/^{204}Pb$ - $^{207}Pb/^{204}Pb$ and $^{208}Pb/^{204}Pb$ - $^{207}Pb/^{204}Pb$ isotopic ratios of the Putumayo Basin plutonic rocks compared with other zones related to the Andes. Fields: average Pacific MORB and Central rift (Lucassen et al., 2002); average Paleozoic crust (Lucassen et al., 2001); average subducted sediment (Planck and Langmuir, 1998); NVZ, CVZ and SVZ (Harmon et al., 1984; Hickey et al., 1986; James, 1982); CVZ in $^{208}Pb/^{204}Pb$ vs. $^{207}Pb/^{204}Pb$ diagram after Wörner et al. (1992). Northern hemisphere reference line (NHRL) after Hart (1984)

5.9 DISCUSSION

Late Miocene evolution of South America was characterized by a high spreading rate in the Equatorial Atlantic Ocean, a high westward drift of South America, which prompted shortening in a roughly E-W direction, and the climax of voluminous magmatic activity in its western edge. In the Putumayo Basin, there are some geological events that coincide with this large scale evolution during the late Miocene to early Pliocene (13 - 3 Ma): regional orogenic uplift, persistent igneous intrusions, CO_2 formation, and a second pulse of hydrocarbon generation and expulsion. The Late Miocene - Pliocene age of the intrusion determined by K/Ar (6.1±0.7 Ma) and its relation with the second pulse of hydrocarbon generation and expulsion is the key to formulate a hypothesis where the four events listed above are causally related.

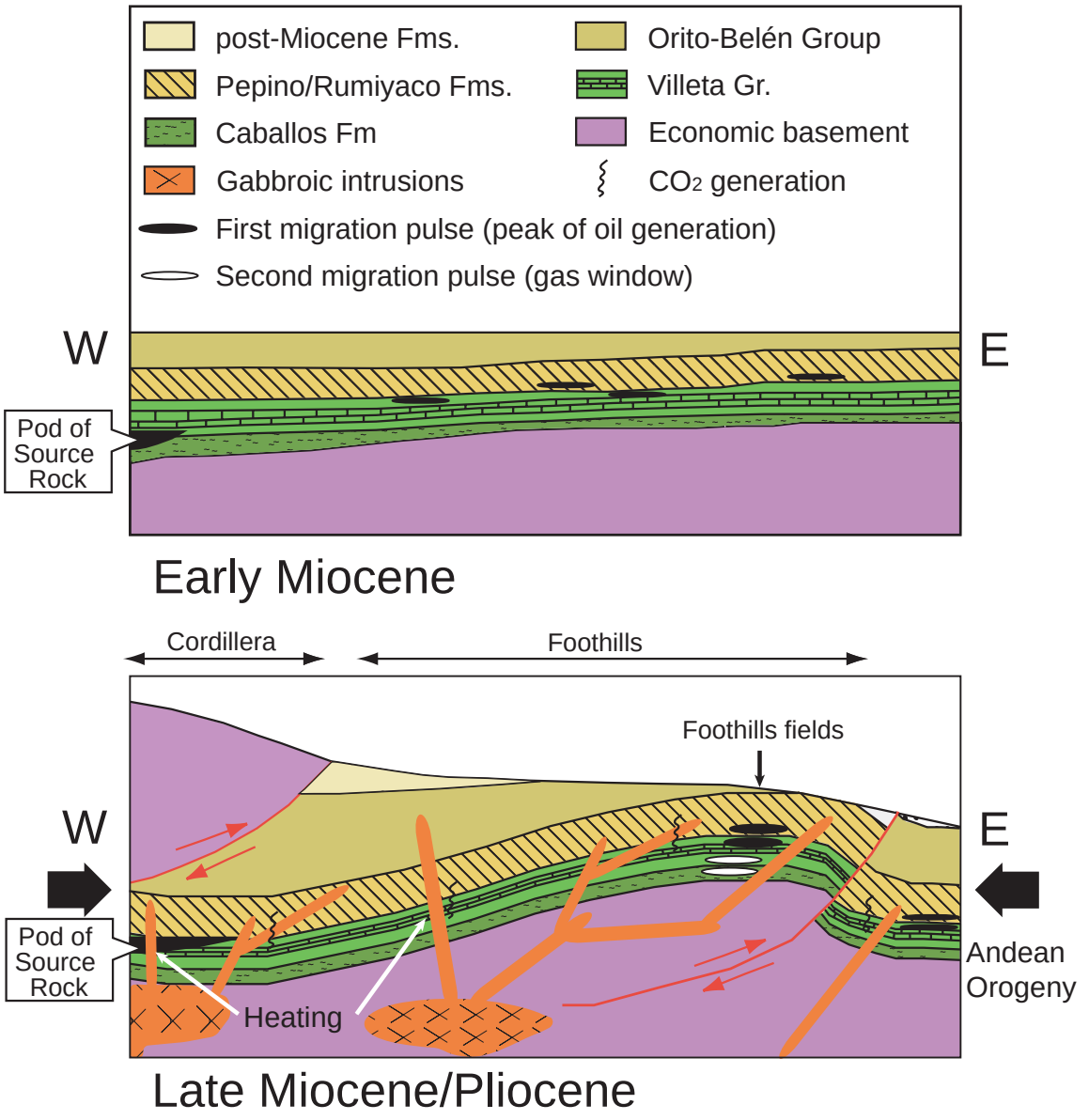

Fig. 5.7 Schematic W-E cross-section in the Putumayo Basin from the Cordillera to the foreland area. Hydrocarbons mobilized during the first, early Miocene migration were mainly stored in sedimentary traps and locally also in minor extensional structural traps. The late Miocene/Pliocene was marked by the beginning of the Andean orogenic uplift and the onset of the magmatic event that heated the sediments in the basin. The generated heat was the crucial factor to trigger the second generation of hydrocarbons in the gas window. The breakdown of carbonates in the rocks intruded by the mafic rocks may be the source of the CO_2.

5.9.1 Regional uplift vs. intrusions

The studied mafic rocks of the Orito Oil Field are derived from the mantle wedge below the western edge of the South American continent and record the subduction phase and the starting of the last pervasive uplift episode that took place during the Late Neogene. Their chemical signature suggests melting from a mantle source enriched in slab-derived fluids, as indicated by the higher Ba/Nb ratios (Hildreth and Moorbath, 1988) and a significant negative Nb anomaly

(Fig. 5.4a). The Sr-Nd-Pb isotopic data suggest assimilation of oceanic crust and crustal material affected by seawater. The trend observed could reflect derivation of the primary magmas from a subduction-modified source mantle with a continental crustal component (Zindler and Hart, 1986). The higher $^{87}Sr/^{86}Sr$ values of the Orito rocks (0.70499 – 0.70617) in comparison to the NVZ rocks produce a flat trend that might suggest assimilation of oceanic crust and sediments whose Sr isotopic composition had been affected by seawater (e.g. Lucassen et al., 2002). A high $^{207}Pb/^{204}Pb$ signature is commonly taken as an indication for the involvement of old crustal material. Such an explanation may readily apply for rocks of the Andean magmatic arc, which are located above an old craton and show Pb provinces along the orogen that correspond to basement domains of contrasting geological and metamorphic evolution (cf. Worner et al., 1992), but is little compatible with mantle-derived rocks of the Central Rift in Argentina (~26°S) as even mantle xenoliths carry this Pb signature (Lucassen et al., 2005). The rocks of the Central Rift indicate that the mantle beneath large parts of South America may have been modified by Pb derived from subducted continentally derived terrigenous sediments. Thus, the Pb isotopic composition of the Orito gabbros does not necessarily have to reflect crustal assimilation but could equally well reflect a mantle source that has been altered by subducted material.

Moreover, the resulting high (La/Yb) normalized ratios (around 12 to 15) reveal a low degree of partial melting and enrichment of LREE in the mantle source. The geochemical signature of these rocks that form part of the called NVZ reflects subduction-related magmatism.

The age data obtained suggests that the emplacement of the dykes can be correlated with the Quechua III uplift phase. Figure 5.7 suggests that the second pulse of hydrocarbon generation and migration is accompanied by exhumation of the foreland structures. An increased burial rate due to a flexural load of a rising Cordillera could be an additional mechanism that prompted the generation of oil. The influence of a magmatic chamber and the additional tectonic burial on the source rocks below the uplifting Cordillera triggered a heat anomaly that produced the second migration of thermally more evolved hydrocarbons (gas window).

5.9.2 Intrusions vs. second migration phase

The Late Miocene pulse of hydrocarbon generation and migration coincides closely with the determined age of the intrusions; therefore, there may be a causal link with the geothermal anomaly induced by the magma chamber west of the basin. The temperature of a mafic magma reaching 1000 to 1200°C is sufficient to heat the host rocks near to the magma chamber. Since the host rocks within the basin have not reached the oil window and are therefore immature, we

assume that the heat produced by the dykes was not high enough to increase the maturity of the rocks. The thickness of the dykes spans from less than 5 up to 25 m which apparently is still very low to produce a regional thermal anomaly that could lead to the maturation of the rocks. That would suggest the presence of a huge magma source to the west of the basin, which heated the oil-prone rocks and also generated dykes that were emplaced into the basin. The confidentiality of the data and the actual published state of the investigation does not permit to determine the size of the magma chamber, the volumes of magma emplaced, to what degree was the surrounding country rock heated or how much hydrocarbon was generated through the influence of the magmatic event.

5.9.3 Intrusions vs. CO_2

The presence of carbonates in the sedimentary succession is a key to generate CO_2. The carbon isotopic ratios determined by Gonçalves *et al.* (2002) ranging from -1.3 to -7.1‰ can be explained as the result of carbonate breakdown associated with igneous intrusions in carbonate sequences (Kairuz, 1993). Moreover, the carbonates are part of the source and reservoir formation of the basin, which makes the gas a fundamental factor to take into account when assessing the risk during various exploration phases. The understanding of the origin and presence of CO_2 should help to evaluate properly the petroleum system in the Putumayo Basin and to reduce the risk on further exploration. The figure 5.7 illustrates the sequence of events that affected the basin during the Quechua III event.

5.10 CONCLUSIONS

The gabbroic intrusions cutting the Cretaceous sedimentary succession in the Putumayo Basin correspond to a subduction-related magmatic event. They were emplaced during the Late Miocene – Pliocene (6.1± 0.7 Ma) and can be assigned to the Northern Volcanic Zone of the Andean magmatism. The trace elements and REE patterns of the studied samples show enrichment of K, Rb, Sr, and Ba and depletion of Nb compared to chondritic composition.

These calc-alkaline plutonic rocks were emplaced after the deposition of the Orito - Belén Group. We suggest that these rocks played a decisive role in the paleo-heat flow scenario increasing the maturity of the source rock and becoming an essential part in the petroleum system of the basin. The combination of the elements mentioned above modified the thermal gradient from middle Miocene to Pliocene creating the conditions to form thermally more evolved hydrocarbons.

6. GENERAL CONCLUSIONS

The Cretaceous plutonic rocks from the Eastern Cordillera of Colombia document the development of a segmented extensional basin. The composition of the intrusions shows tholeiitic to alkaline melts with strong diversities in their petrologic and geochemical characteristics. This suggests different degrees of partial melting and variable enrichment of incompatible elements. The gabbroic rocks document sampling of different parts of the mantle. At least two different magma sources characterize the Cretaceous magmatic episode.

Major element data obtained from clinopyroxenes and trace element data from whole rock point to an extensional setting during the Cretaceous and reject any assumption of a magmatic arc related origin. Further investigations on the chemical composition of the rock-forming minerals reflect at least two different magma sources characterized by the distinct enrichment of incompatible trace elements and the degree of partial melting.

Alteration processes like hydrothermal, low grade metamorphism or weathering affecting the studied rocks were identified. Secondary minerals such as chlorite, sericite, actinolite/tremolite, epidote and calcite document the occurrence of non-primary magmatic minerals. Although the studied samples have been moderate to strongly altered, the acquired data show that alteration did not affected substantially the trace element patterns of clinopyroxenes and amphiboles. Therefore, the trace element patterns of the whole rock still show the chemical features of the original melts that formed the early crystallized phases.

The Sr-Nd-Pb isotope ratios suggest that the melts that originated the gabbroic rocks have their source in a heterogeneous mantle. The local mantle has been affected in different levels by fluids coming from an ancient subducted slab, by seawater, and by sediments that were incorporated in the system mainly during an early subduction phase.

$^{40}Ar/^{39}Ar$ ages obtained from separated minerals of the studied rocks show a spectrum of ages in the Cretaceous that span from 136 to 74 Ma. The wide range of ages recording almost the whole Cretaceous Period indicates the important role played by previous rifting phases in different times in the basin. The Triassic-Jurassic rifting phase in the west and the Paleozoic rifting phases in the east conditioned the thickness and structure of the lithosphere. In this sense, the degree of partial melting for each intrusion was controlled by the structure of the crust and lithosphere (E – W control) and not by the magmatic system itself. In the places where the crust was thinnest, the magmatic products correspond to tholeiitic depleted magmas; where the crust was thickest, the products corresponded to enriched alkaline melts. The segmentation by main

paleo-faults along the Cretaceous basin created sub-basins that controlled separately the timing of the magmatic event.

The obtained data suggest that the regional tectonic setting for the Cretaceous corresponds with the passive margin model for the western continental margin proposed by Pindell and Erikson (1993) and Pindell and Tabbutt (1995). The development of the Cretaceous basin began during the Triassic as a response to back arc rifting (Pindell and Erikson, 1993; Bayona et al., 1994; Pindell and Tabbutt, 1995; Vásquez et al., 2006). Subsequently, the arc magmatism ceased when the regional compressional setting changed to rift-related setting and the opening of the Proto-Caribbean Ocean took place (Bayona et al., 2005; Vásquez et al., 2006).

Sedimentation in the basin continued in Jurassic and Early Cretaceous time on the western side, the Tablazo-Magdalena sub-basin without tectonic-related angular unconformities. Later, during the Aptian and even during the Cenomanian, the western margin of Colombia became a passive margin without major changes in its plate tectonic configuration. The development of the eastern side of the basin has been explained by Berriasian-Hauterivian reactivation of pre-existing crustal discontinuities related to an older Palaeozoic rift system situated along the Guaicaramo palaeo-fault (Sarmiento, 2001b).

The intrusions are related to regional normal faults reactivated during the basin inversion. The faults have presumably acted as conduits that permitted the raising of the magmas, forming the gabbroic rocks near to the surface. Additionally, the places where the intrusions are located probably indicate the most subsiding places for each sub-basin at the time of emplacement.

The gabbroic intrusions that cut the Cretaceous sedimentary succession in the Putumayo Basin were geochronological and petrological characterized. The data obtained show that this magmatism corresponds to a subduction-related event. They were emplaced during the Late Miocene – Pliocene (6.1± 0.7 Ma) and can be assigned to the Northern Volcanic Zone of the Andean magmatism. The paleo-heat scenario of the basin was presumably influenced by these igneous occurrences increasing the maturity of the oil-bearing rocks and consequently yielding the generation and migration of significant amounts of petroleum in the basin. Moreover, the heating of the host rocks through the gabbroic intrusions might have induced the carbonate breakdown of the adjacent carbonates and the formation of CO_2 in the basin. The study of magmatism linked to petroleum systems is a topic of economic relevance when assessing the risk during exploration phases.

7. REFERENCES

Barrero-Lozano, D. (1979). "Geology of the central Western Cordillera, west of Buga and Roldanillo, Colombia." Publicaciones Geológicas Especiales del INGEOMINAS **4**: 1-75.

Bayona, G., D. F. García and G. Mora (1994). La Formación Saldaña: producto de la actividad de estratovolcanes continentales en un dominio de retroarco. Estudios geológicos del Valle Superior del Magdalena. In: F. Etayo-Serna, Universidad Nacional de Colombia**:** I1-I21.

Bayona, G., A. E. Rapalini, V. Constanzo-Alvarez, C. Montes, G. Veloza, R. C. Ayala-Calvo, M. Gómez-Casallas and C. Silva (2005). Mesozoic terrane translations and crustal block rotations in the Eastern Cordillera and Magdalena Valley of Colombia, as inferred from paleomagnetism. 6th ISAG - Barcelona. Paris, IRD Éditions.

Becchio, R., F. Lucassen, S. Kasemann, G. Franz and J. G. Viramonte (1999). "Geoquímica y sistemática isotópica del basamento metamórfico, Paleozoico inferior, noroeste de Argentina y norte de Chile (21°-27°S)." Acta Geológica Hispana **34**: 273-299.

Borg, L. E., M. A. Clynne and T. D. Bullen (1997). "The variable role of slab-derived fluids in the generation of a suite of primitive calc-alkaline lavas from the southernmost Cascades, California." Canadian Mineralogist **35**: 425-452.

Brook, M. (1984). New radiometric age data from SW Colombia. Technical report INGEOMINAS, 10: 1-25

Buseck, P. R., G. L. Nord Jr. and D. R. Veblen (1980). Subsolidus phenomena in pyroxenes. Pyroxenes. In: C. T. Prewitt, Mineralogical Society of America.Reviews in Mineralogy 7, **Reviews in Mineralogy 7:** 117-212.

Cabanis, B. and M. Lecolle (1989). "Le diagramme La/10-Y/15-Nb/8: un outil pour la discrimination des séries volcaniques et la mise en évidence des processus de mélange et/ou de contamination crustale." Comptes rendus de l'Académie des sciences **309**: 2023-2029.

Campbell, C. J. and H. Bürgl (1965). "Section through the Eastern Cordillera of Colombia, South America." Geological Society of America Bulletin **76**: 567-589.

Cediel, F., R. P. Shaw and C. Cáceres (2003). Tectonic assembly of the Northern Andean Block. The Circum-Gulf of Mexico and the Caribbean: Hydrocarbon habitats, basin formation, and plate tectonics. In: C. Bartolini, R. T. Buffler and J. Blickwede.AAPG Memoir, **79:** 697-734.

Chen, Z., H. Yan, J. Li, Z. Ge, Z. Zhang and B. Liu (1999). "Relationship between Tertiary volcanic rocks and hydrocarbons in the Liaohe Basin, People's Republic of China." AAPG Bulletin **83**(6): 1004-1014.

Colleta, B., F. Hebrard, J. Letouzey, P. Werner and J. L. Rudkiewicz (1990). Tectonic and crustal structure of the Eastern Cordillera (Colombia) from a balance cross-section. Petroleum and Tectonics in Mobile Belts. In: J. Letouzey. Paris**:** 80-100.

Cooper, M. A., F. T. Addison, R. Alvarez, M. Coral, R. H. Graham, A. B. Hayward, S. Howe, J. Martinez, J. Naar, R. Peñas, A. J. Pulham and A. Taborda (1995). "Basin development and tectonic history of the Llanos Basin, Eastern Cordillera, and Middle Magdalena Valley, Colombia." AAPG Bulletin **79**(10): 1421-1443.

Córdoba, F., F. Buchelli, J. Moros, W. Calderón, C. Guerrero, E. C. Kairuz and L. Magoon (1997). Proyecto evaluación regional Cuenca del Putumayo - Definición de los sistemas petrolíferos. Bogotá, ECOPETROL**:** 140 p.

Deer, W. A., R. A. Howie and J. Zussman (1966). An introduction to the rock-forming minerals.

Dulski, P. (1994). "Interferences of oxide, hydroxide, and chloride analyte species in the determination of rare earth elements in geological samples by inductively coupled plasma-mass spectrometry." Fresenius Journal of Analytical Chemistry **350**: 194-203.

Ego, F., M. Sébrier, A. Lavenu, H. Yepes and A. Egues (1996). "Quaternary state of stress in the northern Andes and the restraining bend model of the Ecuadorian Andes." Tectonophysics **259**: 101-116.

Ernst, W. G. and J. Liu (1998). "Experimental phase-equilibrium study of Al- and Ti-contents of calcic amphibole in MORB - a semiquantitative thermobarometer." American Mineralogist **83**: 952-969.

Etayo-Serna, F., G. Renzoni and D. Barrero-Lozano (1976). Contornos sucesivos del Mar Cretáceo en Colombia. Memorias del Primer Congreso Colombiano de Geología 1969. 217-252.

Evensen, N. M., P. J. Hamilton and R. K. O'Nions (1978). "Rare earth abundances in chondritic meteorites." Geochimica et Cosmochimica Acta **42**: 1199-1212.

Fabre, A. (1983a). Geología de la extremidad sur de la Sierra Nevada del Cocuy y los alrededores de La Salina y Sacama: Plancha 153, Chita, Boyacá - Arauca y Casanare-. Bogotá, INGEOMINAS**:** 42 p.

Fabre, A. (1983b). "La subsidencia de la Cuenca del Cocuy (Cordillera Oriental de Colombia) durante el Cretaceo y el Terciario Inferior. Primera parte: Estudio cuantitativo de la subsidencia." Geología Norandina **8**: 49-61.

Fabre, A. (1983c). "La subsidencia de la Cuenca del Cocuy (Cordillera Oriental de Colombia) durante el Cretaceo y el Terciario Inferior. Segunda parte: Esquema de evolución tectónica." Geología Norandina **8**: 21-27.

Fabre, A. (1985). Dinámica de la sedimentación Cretácica en la región de la Sierra Nevada del Cocuy, Cordillera Oriental de Colombia. Proyecto Cretácico - Contribuciones. In: F. Etayo-Serna and F. Laverde-Montaño.Publicación Geológica Especial, **16:** XIX1-20.

Fabre, A. (1987). "Tectonique et géneration d'hydrocarbures: Un modèle de l'évolution de la Cordillère Orientale de Colombie et du Bassin des Llanos pendant le Crétacé et le Tertiaire." Archives des Sciences Genève **40**(2): 145-190.

Fabre, A. and M. Delaloye (1983). "Intrusiones básicas en las sedimentitas de la parte central de la Cordillera Oriental." Geología Norandina **6**: 19-28.

Fuhrmann, U., H. J. Lippolt and J. C. Hess (1987). "Examination of some proposed K-Ar standards: 40Ar/39Ar analyses and conventional K-Ar-Data." Chemical Geology **66**: 41-51.

Gansser, A. (1956). "Ein Beitrag zur Geologie und Petrographie der Sierra Nevada de Santa Marta (Kolumbien, Südamerika)." Mineralogische und Petrologische Mitteilung **35**(2): 209-279.

Geotec (1992). Facies distribution and tectonic setting through the Phanerozoic of Colombia. A regional synthesis combining outcrop and subsurface data presented in 17 consecutive rock-time slices. Bogota**:** 100 p.

Gerstenberger, H. and G. Haase (1997). "A highly effective emitter substance for mass spectrometric Pb isotope ratio determinations." Chemical Geology **136**: 309-312.

Gómez, E., T. E. Jordan, R. W. Allmendiger and N. Cardozo (2005). "Developmen of the Colombian foreland-basin system as a consequence of diachronous exhumation of the northern Andes." GSA Bulletin **117**: 1272-1292.

Gonçalves, F. T. T., C. A. Mora, F. Cordoba, E. C. Kairuz and B. N. Giraldo (2002). "Petroleum generation and migration in the Putumayo Basin, Colombia: insights from an organic geochemistry and basin modeling study in the foothills." Marine and Petroleum Geology **19**(6): 711-725.

González, H., A. Núñez and G. Paris (1988). Mapa geológico de Colombia, scale 1:1’500.000. 2 sheets, INGEOMINAS.

Govindaraju, K. (1994). "1994 Compilation of working values and sample description for 383 geostandards." Geostandards newsletter **18**(Special issue): 1-158.

Gradstein, F. M., J. G. Ogg, A. G. Smith, W. Bleeker and L. J. Lourens (2004). "A new geologic time scale, with special reference to Precambrian and Neogene." Episodes **27**: 33-100.

Hall, M. L. (1973). The mineralogy and geochemistry of the Muzo emeralds veins. Inedito.

Haller, M. and A. Knöchel (1996). "X-ray fluorescence analysis using synchrotron radiation (SYXRF)." Journal of Trace Microprobe Techniques **14**: 461-488.

Hamelin, B., B. Dupre and C. J. Allegre (1984). "Lead-strontium isotopic variations along the East Pacific Rise and the Mid-Atlantic Ridge: a comparative study." Earth & Planetary Science Letters **67**(3): 340.

Hart, S. R. and T. Dunn (1993). "Experimental cpx/melt partitioning of 24 trace elements." Contribution to Mineralogy and Petrology **113**: 1-8.

Haschke, M., W. Siebel, A. Günther and E. Scheuber (2002). "Repeated crustal thickening and recycling during the Andean orogeny in north Chile (21°-26°S)." Journal of Geophysical Research **107**(B1): 1-18.

Hawkesworth, C. J., M. Hammill, A. R. Gledhill, P. Van Calsteren and G. Rogers (1982). "Isotope and trace element evidence for late-stage intra-crustal melting in the high Andes." Earth and Planetary Science Letters **58**: 240-254.

Heinrichs, H. and A. G. Herrmann (1990). Praktikum der analytischen Geochemie, Springer Verlag.
Hickey, R. L., F. A. Frey and D. C. Gerlach (1986). "Multiple sources for basaltic arc rocks from the southern volcanic zone of the Andes (34-41°S): trace element and isotopic evidence for contributions from subducted oceanic crust." Journal of Geophysical Research **91**: 5963-5983.
Higley, D. K. (2000). The Putumayo-Oriente-Maranon Province of Colombia, Ecuador, and Peru, Mesozoic-Cenozoic and Paleozoic petroleum systems. U. S. Geological Survey Digital Data Series, 63: 35 p.
Hildreth, W. and S. Moorbath (1988). "Crustal contributions to arc magmatism in the Andes of Central Chile." Contribution to Mineralogy and Petrology **98**(4): 455-489.
Hofmann, A. W. (1997). "Mantle geochemistry: the message from oceanic volcanism." Nature **385**: 219-229.
Irving, E. (1971). "La evolución estructural de los Andes más septentrionales de Colombia." Boletín Geológico de Colombia INGEOMINAS **19**(2): 90 p.
Ishizuka, O. (1998). "Vertical and horizontal variations of the fast neutron flux in a single irradiation capsule and their significance in the laser-heating $^{40}Ar/^{39}Ar$ analysis: Case study for the hydraulic rabbit facility of the JMTR reactor, Japan." Geochemical Journal **32**: 243-252.
Ishizuka, O., M. Yuasa and K. Uto (2002). "Evidence of porphyry copper-type hydrothermal activity from a submerged remnant back-arc volcano of the Izu-Bonin arc. Implications for the volcanotectonic history of back-arc seamounts." Earth & Planetary Science Letters **198**: 381-399.
Jaffey, A. H., K. F. Flynn, Glendeni.Le, W. C. Bentley and A. M. Essling (1971). "Precision measurement of half-lives and specific activities of U-235 and U-238." Physical Review C **4**(5): 1889.
Jaillard, E. P., P. Solar, G. Carlier and T. Mourier (1990). "Geodynamic evolution of the northern and Central Andes during early to middle Mesozoic times: a Tethyan model." Journal of the Geological Society of London **147**: 1009-1022.
James, D. E. (1982). "A combined O, Sr, Nd and Pb isotopic and trace element study of crustal contamination in central Andean lavas." Earth and Planetary Science Letters **57**: 47-62.
James, O. B., C. Floss and J. J. McGee (2002). "Rare earth element variations resulting from inversion of pigeonite and subsolidus reequilibration in lunar ferroan anorthosites." Geochimica et Cosmochimica Acta **65**(7): 1269-1284.
Kairuz, E. C. (1993). Origen del CO_2 en la Cuenca del Putumayo y su riesgo exploratorio asociado. VI Congreso Colombiano de Geología, Medellín, Colombia**:** 210-214.
Keller, G. R. and J. D. Hoover (1988). A comparison of the Newark and Rio Grande rift systems and associated magmatism. Triassic - Jurassic rifting. Continental breakup and the origin of the Atlantic Ocean and passive margins. Part B. In: W. Manspeizer, Elsevier.Developments in Geotectonics 22**:** 911-932.
Kerr, A. C., J. Tarney, P. D. Kempton, P. Spadea, A. Nivia, G. F. Marriner and R. A. Duncan (2002). "Pervasive mantle plume head heterogeneity: Evidence from the late Cretaceous Caribbean-Colombian oceanic plateau." Journal of Geophysical Research **107**(B7): 2140, doi:10.1029/2001JB000790.
Klein, M., H. G. Stosch and H. A. Seck (1997). "Partitioning of high field-strength and rare-earth elements between amphibole and quartz-dioritic to tonalitic melts: An experimental study." Chemical Geology **138**(3-4): 257-271.
Koepke, J., G. Falkenberg, K. Rickers and O. Diedrich (2003). "Trace element diffusion and element partitioning between garnet and andesite melt using synchrotron X-ray fluorescence microanalysis (μ-SRXRF)." European Journal of Mineralogy **15**: 883-892.
Kontorovich, A. E., A. V. Khomenko, L. M. Burshtein, I. I. Likhanov, A. L. Pavlov, V. S. Staroseltsev and A. A. Ten (1997). "Intense basic magmatism in the Tunguska petroleum basin, eastern Siberia, Russia." Petroleum Geoscience **3**(4): 359.
Leake, B. E., A. R. Woolley, C. E. S. Arps, W. D. Birch, M. C. Gilbert, J. D. Grice, F. C. Hawthorne, A. Kato, H. J. Kisch, V. G. Krivovichev, K. Linthout, J. Laird, J. Mandarino, W. V. Maresch, E. H. Nickel, J. C. Schumachr, D. C. Smith, N. C. N. Stephenson, L. Ungaretti, E. J. W. Whittaker and G. Youzhi (1997a). "Nomenclature of amphiboles. Report of the subcommittee on amphiboles of the International Mineralogical Association Commission on new minerals and mineral names." European Journal of Mineralogy **9**(3): 623.

Leake, B. E., A. R. Woolley, C. E. S. Arps, W. D. Birch, M. C. Gilbert, J. D. Grice, F. C. Hawthorne, A. Kato, H. J. Kisch, V. G. Krivovichev, K. Linthout, J. Laird, J. A. Mandarino, W. V. Maresch, E. H. Nickel, N. M. S. Rock, J. C. Schumacher, D. C. Smith, N. C. N. Stephenson, L. Ungaretti, E. J. W. Whittaker and Y. Z. Guo (1997b). "Nomenclature of amphiboles: Report of the subcommittee on amphiboles of the International Mineralogical Association, Commission on New Minerals and Mineral Names." Canadian Mineralogist **35**: 219-246.

LeBas, M. J. (1962). "The role of aluminium in igneous clinopyroxenes with relation to their parentage." American Journal of Science **260**: 267-288.

Lechtenberg, F., S. Garbe, J. Bauch, D. B. Dingwell, J. Freitag, M. Haller, T. H. Hansteen, P. Ippach, A. Knöchel, M. Radtke, C. Romano, P. M. Sachs, H.-U. Schmincke and H.-J. Ullrich (1996). "The X-ray fluorescence measurement place at beamline L of HASYLAB." Journal of Trace Microprobe Techniques **14**(3): 561-587.

Leterrier, J., R. C. Maury, P. Thonon, D. Girard and M. Marchal (1982). "Clinopyroxene compositions as a method of identification of the magmatic affinities of paleo-volcanic series." Earth and Planetary Science Letters **59**: 139-154.

Lindsey, D. H. (1980). Phase equilibria of pyroxenes at pressures > 1 atmosphere. Pyroxenes. In: C. T. Prewitt, Mineralogical Society of America.Reviews in Mineralogy 7, **Reviews in Mineralogy 7:** 289-308.

Lindsey, D. H. (1983). "Pyroxene thermometry." American Mineralogist **68**: 477-493.

Londoño, J. and R. Mendoza (1994). Evaluación geológica de un área en los alrededores del municipio de Puerto Romero (Boyacá). Departamento de Geociencias. Bogotá, Universidad Nacional de Colombia**:** 112 p.

Loucks, R. R. (1990). "Discrimination of ophiolitic from non-ophiolitic ultramafic allochtonous in orogenic belts by the Al/Ti ratio in clinopyroxene." Geology **18**: 346-349.

Lozano, E. L. (2005). Petrografía detallada y geoquímica de las rocas ígneas aflorantes en los alrededores de Pajarito, Boyacá - Colombia. Departamento de Geociencias. Bogotá, Universidad Nacional de Colombia**:** 77 p.

Lucassen, F., R. Becchio, R. S. Harmon, S. Kasemann, G. Franz, R. Trumbull, H. G. Wilke, R. L. Romer and P. Dulski (2001). "Composition and density model of the continental crust in an active continental margin - the central Andes between 18° and 27°S." Tectonophysics **341**: 195-223.

Lucassen, F., M. Escayola, G. Franz, R. L. Romer and K. Koch (2002). "Isotopic composition of Late Mesozoic basic and ultrabasic rocks from the Andes (23-32°S) - implications for the Andean mantle." Contributions to Mineralogy and Petrology **143**: 336-349.

Lucassen, F., G. Franz, M. F. Thirlwall and K. Mezger (1999). "Crustal recycling of metamorphic basement: Late Paleozoic granites of the Chilean Coast Range and Precordillera at ~22°S." Journal of Petrology **40**: 1527-1551.

Lucassen, F., G. Franz, J. Viramonte, R. L. Romer, P. Dulski and A. Lang (2005). "The late Cretaceous lithospheric mantle beneath the Central Andes: Evidence from phase equilibria and composition of mantle xenoliths." Lithos **82**: 379-406.

Ludwig, K. (2003). "Isoplot 3.0 - A Geochronological Toolkit for Microsoft Excel." Berkeley Geochronology Center Special Publication **4**: 70 p.

Manhès, G., J. F. Minster and C. J. Allegre (1978). "Comparative uranium-thorium-lead and rubidium-strontium study of Saint-Severin amphoterite - Consequences for early solar-system chronology." Earth and Planetary Science Letters **39**(1): 14-24.

Marquinez, G. and L. Moreno (1993). Cartografía geológica y análisis petrográfico de las rocas ígneas básicas aflorantes en el extremo sur-este de la plancha169 Puerto Boyacá (Departamentos de Cundinamarca y Boyacá). Departamentos de Geociencias, Universidad Nacional de Colombia**:** 81 p.

Mathalone, J. M. P. and R. M. Montoya (1995). Petroleum geology of the sub-Andean basins of Peru. Petroleum basins of South America. In: A. J. Tankard, R. Suárez Soruco and H. J. Welsink.AAPG Memoir, **62:** 423-444.

Maze, W.B. (1984). Jurassic La Quinta Formation in the Sierra de Perijá, northwestern Venezuela: geology and tectonic environment of red beds and volcanic rocks. The Caribbean - South American Plate

Boundary and Regional Tectonics. In: W. E. Bonini, R. E. Hardgraves and R. Shagam.Geological Society of America Memory, **162:** 263-282.

McCourt, W. J., T. Feininger and M. Brook (1984). "New geological and geochronological data from the Colombian Andes: continental growth by multiple accretions." Jounal of the Geological Society of London **141**: 831-845.

McDougall, I. and T. M. Harrison (1999). Geochronology and thermochronology by the $^{40}Ar/^{39}Ar$ method, Oxford University Press.

McIntire, W. L. (1963). "Trace element partition coefficients - a review of theory and applications to geology." Geochimica et Cosmochimica Acta **27**: 1209-1264.

McKenzie, D. and R. K. O'Nions (1991). "Partial melt distributions from inversion of rare Earth element concentrations." Journal of Petrology **32**: 1021-1091.

Middlemost, E. A. K. (1994). "Naming materials in the magma/igneous rock system." Earth Science Review **37**: 215-224.

Mojica, J., A. Kammer and G. Ujueta (1996). "El jurásico del sector noroccidental de Suramérica y guía de la excursión al Valle Superior del Magdalena (Nov. 1-4/95), Regiones de Payandé y Prado, Departamento del Tolima, Colombia." Geología Colombiana **21**: 3-40.

Mora, A., M. Parra, M. R. Strecker, A. Kammer, C. Dimaté and F. Rodríguez (2006). "Cenozoic contractional reactivation of Mesozoic extensional structures in the Eastern Cordillera of Colombia." Tectonics **25**(TC2010): doi:10.1029/2005TC001854.

Morales, L. G., D. J. Podesta, W. C. Hatfield, H. Tanner, S. H. Jones, N. H. S. Barker, D. J. O'Donoghue, C. E. Mohler, E. P. Dubois, C. Jacobs and C. R. Gross (1958). General geology and oil ocurrences of Middle Magdalena Valley, Colombia. Symposium American Association of Petroleum Geologist, Tulsa, Oklahoma.

Moreno, J. M. (1991). "Provenance of the Lower Cretaceous sedimentary sequences, central part, Eastern Cordillera, Colombia." Revista Academia Colombiana de Ciencias Exactas, Físicas y Naturales **18**(69): 159-173.

Moreno, J. M. and A. E. Concha (1993). "Nuevas manifestaciones ígneas básicas en el flanco occidental de la Cordillera Oriental, Colombia." Geología Colombiana **18**: 143-150.

Morimoto, N. (1989). "Nomenclature of pyroxenes." Canadian Mineralogist **27**: 77-90.

Nakamura, E., I. H. Campbell, M. T. McCulloch and S. S. Sun (1989). "Geochemical geodynamics in a back arc region around the Sea of Japan: implications for the genesis of alkaline basalts in Japan, Korea and China." Journal of Geophysical Research **94**: 4634-4654.

Navarrete, A. T. (2002). Evaluación geológica y petrográfica del cuerpo ígneo aflorante en el Cerro Tragarepas, al norte de la población de Pacho, Cundinamarca. Departamento de Geociencias. Bogotá, Universidad Nacional de Colombia**:** 122 p.

Navarrete, A. T., J. M. Moreno, A. E. Concha and P. Patarroyo (2002). "Interpretación petrogenética del Gabro de Tragarepas al norte de Pacho, Cundinamarca, Colombia." Geología Colombiana **27**: 109-120.

Nimis, P. (1999). "Clinopyroxene geobarometry of magmatic rocks. Part 2. Structural geobarometers for basic to acid, tholeiitic and mildly alkaline magmatic systems." Contribution to Mineralogy and Petrology **135**: 62-74.

Norman, M. D., W. L. Griffin, N. J. Pearson, M. O. Garcia and S. Y. O'Reilly (1998). "Quantitative analysis of trace element abundances in glasses and minerals: A comparison of laser ablation ICPMS, solution ICPMS, proton microprobe, and electron microprobe data." J. Anal. Atom. Spec. **13**: 477-482.

Parra, M. (2000). Estratigrafía y petrografía del Cretácico inferior en el Parque Natural Chingaza y la Cuenca Alta del Río Guatiquía, Cundinamarca y Meta, Colombia. Departamento de Geociencias. Bogotá, D.C, Universidad Nacional de Colombia**:** 71 p.

Pearce, J. A. (1982). Trace element characteristics of lavas from destructive plate boundaries. Andesites: Orogenic Andesites and Related Rocks. In: R. S. Thorpe**:** 525-548.

Pearce, N. G. J., W. T. Perkins, J. A. Westgate, M. P. Gorton, S. E. Jackson, C. R. Neal and S. P. Chenery (1997). "A compilation of new and published major and trace element data for NIST SRM 610 and NIST SRM 612 glass reference materials." Geostandards newsletter **21**(1): 115-144.

Pindell, J. L. and J. F. Dewey (1982). "Permo-Triassic reconstruction of western Pangaea and the evolution of the Gulf of Mexico - Caribbean region." Tectonics **1**: 179-211.

Pindell, J. L. and J. Erikson (1993). The Mesozoic margin of northern South America. Cretaceous Tectonics of the Andes. In: J. Salfity**:** 1-60.

Pindell, J. L., L. Kennan, K. P. Stanek, W. V. Maresch and G. Draper (2006). "Foundations of Gulf of Mexico and Caribbean evolution: eight controversies resolved." Geologica Acta **4**(1-2): 303-341.

Pindell, J. L. and K. D. Tabbutt (1995). Mesozoic-Cenozoic Anden paleogeography and regional controls on hydrocarbon systems. Petroleum basins of South America. In: A. J. Tankard, R. Suárez and H. J. Welsink.AAPG Memoir, **62:** 101-128.

Plank, T. and C. H. Langmuir (1998). "The chemical composition of subducting sediment and its consequences for the crust and mantle." Chemical Geology **145**: 325-394.

Polyanskii, O. P., V. V. Reverdatto and V. G. Sverdlova (2002). "Convection of two-phase fluid in a layered porous medium driven by the heat of magmatic dikes and sills." Geochemistry International **40**(SUPPL. 1): S69-S81.

Powell, J. L. and K. Bell (1970). "Strontium isotopic studies of alkalic rocks - localities from Australia, Spain, and western United States." Contribution to Mineralogy and Petrology **27**(1): 1-10.

Pratt, S. (1961). The Muzo emerald mine. Geological field trip Colombia, 1959-1978. Colombian Society of Petroleum Geologists and Geophysicist**:** 33-63.

Ramos, V. A. and S. M. Kay (1992). Southern Patagonian plateau basalts and deformation: back arc testimony of ridge collisions. Andean Geodynamics. In: R. A. Oliver, N. Vatin-Perignon and G. Laubacher, **205:** 261-282.

Rickers, K., R. Thomas and W. Heinrich (2004). "Trace-element analysis of individual synthetic and natural fluid inclusions with synchrotron radiation XRF using Monte Carlo simulations for quantification." European Journal of Mineralogy **16**(1): 23-35.

Rocholl, A. (1998). "Major and trace element composition and homogeneity of microbeam reference material: basalt glass USGS BCR-2G." Geostandards newsletter **22**(1): 33-45.

Romer, R. L., H. W., B. Schröder-Smeibidl, A. Meixner, C.-O. Fischer and C. Schulz (2005). "Elemental dispersion and stable isotope fractionation during reactive fluid-flow and fluid immiscibility in the Bufa del Diente aureole, NE-Mexico: Evidence from radiographies and Li, B, Sr, Nd, and Pb isotope systematics." Contribution to Mineralogy and Petrology **149**: 400-429.

Sarmiento-Rojas, L. F., J. D. Van Wess and S. Cloetingh (2006). "Mesozoic transtensional basin history of the Eastern Cordillera, Colombian Andes: Inferences from tectonic models." Journal of South American Earth Sciences **21**(4): 383-411.

Sarmiento, L. F. (1989). Stratigraphy o the Cordillera Oriental west of Bogotá, Colombia. Columbia, SC., University of South Carolina. **M.Sc.:** 102 p.

Sarmiento, L. F. (2001a). Mesozoic rifting and Cenozoic basin inversion history of the Eastern Cordillera, Colombian Andes - Inferences from tectonic models. Faculty of Earth and Life Sciences. Amsterdam, Vrije Universiteit. **PhD:** 295.

Sarmiento, L. F. (2001b). Mesozoic rifting and Cenozoic basin inversion history of the Eastern Cordillera, Colombian Andes - Inferences from tectonic models. Faculty of Earth and Life Sciences. Amsterdam, Vrije Universiteit**:** 295.

Schamel, S. (1991). "Middle and upper Magdalena basins." American Association of Petroleum Geologists **Memoir 52**: 283–303.

Schilling, J. G., M. Thompson, M. Zajec, R. Evans, T. Johnson, W. White, J. D. Devine and R. Kingsley (1983). "Petrologic and geochemical variations along the Mid-Atlantic Ridge from 27°N to 73°N." American Journal of Science **283**: 510-586.

Schumacher, E. (1975). "Herstellung von 99.9997% ^{38}Ar für die ^{40}K/^{40}Ar Geochronologie." Geochron. Chimia **24**: 441-442.

Sébrier, M. and P. Soler (1991). Tectonics and magmatism in the Peruvian Andes from Late Oligocene time to the present. Andean magmatism and its tectonic setting. In: R. S. Harmon and C. W. Rapela, Geological Society of America.Special paper, **265:** 259-278.

Seufert, H. M. and K. P. Jochum (1997). "Trace element analysis of geological glasses by laser plasma ionization mass spectrometry (LIMS): A comparison with other multielement and microanalytical methods." Fresenius Journal of Analytical Chemistry **359**: 454-457.

Shervais, J. W. (1982). "Ti-V plots and the petrogenesis of modern and ophiolitic lavas." Earth & Planetary Science Letters **59**: 101-118.

Sillitoe, R., L. Jaramillo, P. Damon, M. Shafiqullah and R. Escobar (1982). "Setting, characteristics, and age of the Andean porphyry copper belt in Colombia." Economic Geology **77**: 1837-1850.

Sisson, T. W. (1994). "Hornblende-Melt Trace-Element Partitioning Measured by Ion Microprobe." Chemical Geology **117**(1-4): 331-344.

Sobolev, A. V., A. A. Migdisov and M. V. Portnyagin (1996). " Incompatible element partitioning between clinopyroxene and basalt liquid revealed by the study of melt inclusions in minerals from Troodos lavas, Cyprus." Petrology **4**(3): 307-317.

Steiger, R. H. and E. Jager (1977). "Subcommission on geochronology - Convention on use of decay constants in geochronology and cosmochronology." Earth and Planetary Science Letters **36**(3): 359-362.

Streckeisen, A. L. (1976). "To each plutonic rock its proper name." Earth-Science Reviews **12**: 1-33.

Sun, S. S. (1980). "Lead isotopic study of young volcanic rocks from mid-ocean ridges, ocean islands and island arcs." Philosofical Transactions of the Royal Society of London **A297**: 409-445.

Sun, S. S. and W. F. McDonough (1989). Chemical and isotopic systematics of oceanic basalts: implications for mantle compositions and processes. Magmatism in the ocean basins. In: A. D. Saunders and M. Norry, **Special publication of the Geological Society 42:** 313-345.

Taboada, A., L. A. Rivera, A. Fuenzalida, A. Cisternas, H. Philip, H. Bijwaard, J. Olaya and C. Rivera (2000). "Geodynamics of the northern Andes: Subductions and intracontinental deformation (Colombia)." Tectonics **19**(5): 787-813.

Tenjo, N. C. (2003). Reconocimiento geológico de rocas ígneas básicas aflorantes en los alrededores de La Victoria, Boyacá - Colombia. Departamento de Geociencias. Bogotá, Universidad Nacional de Colombia**:** 119 p.

Thorpe, R. S. and P. W. Francis (1979). "Variations in Andean andesite compositions and their petrogenetic significance." Tectonophysics **57**: 53-70.

Thorpe, R. S., P. W. Francis and L. O'Callaghan (1984). "Relative roles of source composition, fractional crystallization and crustal contamination in the petrogenesis of Andean volcanic rocks." Philosophical Transactions of the Royal Society of London **A310**: 675-692.

Tindle, A. G. and P. C. Webb (1994). "Probe-amph - a spreadsheet program to classify microprobe-derived amphibole analysis." Computers and Geosciences **20**(7/8): 1201-1228.

Toussaint, J. F. (1995). "Hipótesis sobre el marco geodinámico de Colombia durante el Mesozoico temprano. Contribution to IGCP 322, Jurassic events in South America." Geología Colombiana **20**: 150-155.

Toussaint, J. F. and J. J. Restrepo (1989). Acreciones sucesivas en Colombia; un nuevo modelo de evolución geológica. V Congreso Colombiano de Geología, Bucaramanga**:** 127-142.

Toussaint, J. F. and J. J. Restrepo, Eds. (1994). The Colombian Andes during Cretaceous times. Cretaceous tectonics of the Andes, Views Brunwick, Germany.

Ujueta, G. (1991). Tectónica y actividad ígnea en la Cordillera Oriental de Colombia. Simposio sobre magmatismo Andino y su marco tectónico, Manizales, Universidad de Caldas**:** 151-192.

Uto, K., O. Ishizuka, A. Matsumoto, H. Kamioka and S. Togashi (1997). "Laser-heating $^{40}Ar/^{39}Ar$ dating system of the Geological Survey of Japan: System outline and preliminary results." Bulletin of the Geological Survey of Japan **48**(1): 23-46.

van den Bogaard, P. (1995). "$^{40}Ar/^{39}Ar$ ages of sanidine phenocryst from Laacher See Tephra (12,900 yr BP): Chronostratigraphic and petrological significance." Earth & Planetary Science Letters **133**: 163-174.

Van Espen, P., K. Janssens and I. Swenters (1992). "AXIL X-ray analysis software." Manual of Computer program **University of Antwerp**(Belgium).

Van Espen, P., H. Nullens and F. Adams (1977). "Method for the accurate description of the full-energy peaks in non-linear least-squares analysis of X-ray spectra." Nucl Instrum Methods **145**(3): 579.

Vásquez, M. (1999). Evaluación Petrográfica y Caracterización Geoquímica de los cuerpos intrusivos básicos aflorantes en la región de Cáceres y Puerto Romero, departamentos de Cundinamarca y Boyacá. Departamento de Geociencias. Bogotá, Universidad Nacional de Colombia**:** 74 p.

Vásquez, M. and U. Altenberger (2005). "Mid-Cretaceous extension-related magmatism in the eastern Colombian Andes." Journal of South American Earth Sciences **20**: 193-210.

Vásquez, M., U. Altenberger, R. L. Romer and J. M. Moreno (2005). Extension-related magmatism during mid-Cretaceous times in the Eastern Cordillera, Colombia. 6th ISAG - Barcelona. Paris, IRD Éditions.

Vásquez, M., G. Bayona and R. L. Romer (2006). Geochemistry of Jurassic volcanic rocks of the northern Andes: Insights for the Mesozoic evolution of Northwestern Gondwana. Backbone of Americas - Patagonia to Alaska, Mendoza, Argentina.**:** 62.

Vásquez, M., A. E. Concha, J. M. Moreno and P. Patarroyo (2000). "Caracterización geoquímica y petrografía de los cuerpos intrusivos básicos aflorantes en la región de Cáceres y Puerto Romero, departamentos de Cundinamarca y Boyacá, Colombia." Geología Colombiana **25**: 185-198.

Vekemans, B., K. Janssens, L. Vincze, F. Adams and P. Van Espen (1994). "Analysis of X-ray spectra by iterative least squares (AXIL): New developments." X-Ray Spectrometry **23**(6): 278-285.

Villamil, T. and C. Arango (1998). Integrated stratigraphy of latest Cenomanian and early Turonian facies of Colombia. Paleogeographic Evolution and Non-Glacial Eustasy, Northern South America. In: J. L. Pindell and C. L. Drake.SEPM Special Publication, **58:** 129-159.

Villemant, B., H. Jaffrezic, J. L. Joron and M. Treuil (1981). "Distribution Coefficients of Major and Trace-Elements - Fractional Crystallization in the Alkali Basalt Series of Chaine-Des-Puys (Massif Central, France)." Geochimica et Cosmochimica Acta **45**(11): 1997-2016.

Vincze, L., K. Janssens and F. Adams (1993). "A general Monte Carlo simulation of energy-dispersive X-Ray fluorescence spectrometers - Part I." Spectrochim. Acta **48**(B): 553-573.

Vincze, L., K. Janssens, F. Adams and K. W. Jones (1995a). "A general Monte Carlo simulation of energy-dispersive X-Ray fluorescence spectrometers - Part III." Spectrochim. Acta **50**(B): 1481-1500.

Vincze, L., K. Janssens, F. Adams, M. L. Rivers and K. W. Jones (1995b). "A general Monte Carlo simulation of energy-dispersive X-Ray fluorescence spectrometers - Part II." Spectrochim. Acta **50**(B): 127-148.

Weber, M. B. I., J. Tarney, P. D. Kempton and R. W. Kent (2002). "Crustal make-up of the Northern Andes: Evidence based on deep crustal xenolith suites, Mercaderes, SW Colombia." Tectonophysics **345**(1-4): 49.

Wemmer, K. (1991). "K/Ar Altersdatierungsmöglichkeiten für retrograde Deformationsprozesse im spröden und duktilen Bereich - Beispiele aus der KTB-Vorbohrung (Oberpfalz) und dem Bereich der Insubrischen Linie (N- Italien)." Göttinger Arb. Geol. Paläont. **51**: 1-61.

Wilson, M. (1989). Igneous petrogenesis, Springer Netherlands.

Wilson, M. (1993). "Magmatism and the geodynamics of basin formation." Sedimentary Geology **86**: 5-29.

Winchester, J. A. and P. A. Floyd (1976). "Geochemical magma type discrimination; application to altered and metamorphosed basic igneous rocks." Earth and Planetary Science Letters **28**: 459-469.

Wood, D. A., J. L. Joron, M. Treuil, M. Norry and J. Tarney (1979). "Elemental and Sr isotope variations in basic lavas from Iceland and the surrounding ocean floor." Contribution to Mineralogy and Petrology **70**: 319-339.

Worner, G., S. Moorbath and R. S. Harmon (1992). "Andean Cenozoic volcanic centers reflect basement isotopic domains." Geology **20**: 1103-1106.

Worner, G., A. Zindler, H. Staudigel and H. U. Schmincke (1986). "Sr, Nd and Pb isotope geochemistry of Tertiary and Quaternary alkaline volcanics from West Germany." Earth & Planetary Science Letters **79**(1-2): 107.

Zindler, A. and S. Hart (1986). "Chemical geodynamics." Annual Review of Earth and Planetary Sciences **14**: 493-571.